SIMULATING WHOLE-EARTH CYCLES USING
HIERARCHIES AND OTHER GENERAL SYSTEMS CONCEPTS

By

GUY MCGRANE

ACKNOWLEDGMENTS

TABLE OF CONTENTS

LIST OF TABLES

LIST OF FIGURES

SIMULATING WHOLE-EARTH CYCLES USING
HIERARCHIES AND OTHER GENERAL SYSTEMS CONCEPTS

By

Guy McGrane

May, 1998

Main features of the Earth system and industrial civilization were
modeled with a new general systems overview, according to the natural
hierarchy of energy transformations. Structures and processes were organized
by a scale of value based on energy and work, the emergy concept (spelled
with an "m"; the available energy of one kind, solar in this study, required to
make a product, with units of solar emjoules, abbreviated sej). Calculations of
emergy per unit mass helped identify the position of marine rocks, mountains,
and continental platforms in the Earth hierarchy: 0.94, 1.8, and 10 sej/gram,
respectively.

Computer simulations of the aggregated models, calibrated with modern
values, showed temporal patterns consistent with this hierarchical view of the
Earth. Extrapolations suggested the sedimentary system has yet to achieve
steady state. In Earth models, pulsing was generated by combining linear and
higher order connections between levels, which may help explain how large
scale surges occurred in Earth history. Generic models of hierarchical energy

transformation produced independent oscillations on two scales. There was an optimal material distribution for maximum power.

A model including coupling of surface and deep energies suggested that total material processed by the sedimentary cycle depends on deep energies, and surface energies have only transient influence.

A model of convective precipitation displayed strong buffering of surface water storage, related to the distribution of solar energy between latent and sensible heating. Simulations showed a 20% increase in drainage rate caused more sensible heating and storms, and surface water changed by only 2%. A global hydrologic model suggested hydrology alone could account for a 40% buffering of surface temperature if solar input changed by 30%.

The pulse of the human economy, when energetically connected to the sedimentary system, simulated peaks in fuel use and continental denudation (30 E15 g/yr), and a minimum in planetary biomass (60% the pre-industrial level), early in the next century.

Results provide a new, quantitative, top-down approach to understanding the Earth as a whole.

CHAPTER 1
INTRODUCTION

General systems theory is by definition founded on generalities and
principles drawn from many different fields of inquiry. In this study, general
systems theory is used to help address questions about whole-earth systems
whose dynamics are too slow to directly observe. Conversely, studies of the
Earth system may help establish and verify general principles, thereby
contributing to the broader field.

Purpose of this Study

Understanding the global system of the geobiosphere and its
relationship to human civilization is a major goal of science. The long range
future of society depends on fitting the global economy with the complex
relationships of air, water, chemical cycles, rocks, and life. In this study,
aggregated models are developed and simulated to examine the structure and
workings of global systems of geology and man with special emphasis on the
sedimentary cycle.

Here the sedimentary cycle is defined as the overall cycle that changes
hard rock and volatiles at the Earth's surface into salts, sediments, and soil.
Also included is the reverse process that proceeds at shallow to deep Earth
levels, without which there would be no true "cycle". The overall cycle also
includes processes at the Earth's surface that shape the way material is

processed, including human economics, the hydrologic cycle, and biological processing.

Models are developed using general systems theory and diagrammatic energy language. These tools use principles from ecological, chemical, social, mechanical, astronomical, and other diverse types of systems to help understand phenomena in all fields, on all scales of size and time. The energy systems diagrams explicitly define mathematical properties and their relation to energy. Hence, models are hypotheses about components and relationships. Hypotheses in models are tested by comparing simulation results with historical geologic evidence, especially the relationship of pulsing and performance. Included are atmospheric, oceanic, and economic process models on the scale of hundreds of years, and the main cycles of the Earth's crust over periods of millions of years.

Specific Issues Concerning Earth Systems

A main focus of this study is the investigation of the structure and configuration of the whole system of sedimentary processes. Equally important is the role of human society in the sedimentary cycle. The following questions formed a basis for the investigations:

Structure and configuration

- How do the driving energies of the Earth interact? What are their respective roles in driving material cycles of air, land, and water?
- How do the fast cycling Earth units of hydrology and biomass affect the larger scale units of tectonics and continents?
- What are likely hierarchical divisions of the sedimentary system?
- What are the main self-organized units of structure in the whole-earth system of material cycling?

- What is the role of the hydrologic cycle in the sedimentary system? What are the roles of plants and soil?
- What homeostatic mechanisms are present in the hydrologic cycle? What is the magnitude of their effect?

Human influence

- What geological components drive human industry? Agriculture?
- How have agriculture and industry developed? What historical patterns might suggest future behavior of the systems of agriculture and industry?
- What is the likely time scale of industrial dynamics, and how might those dynamics affect large-scale Earth systems?
- How might large-scale human induced changes affect the hydrologic cycle? What are likely consequences of those changes?

General Issues

In addition to understanding the general aspects of the Earth system and the relationships among its materials and driving energies, an important goal of this study was to contribute to the broader field of systems theory. This included examining the appropriate relationship between systems studies and individual fields like Earth sciences, and looking at how Earth science can illustrate and complement various aspects of systems study. For example, the following questions guided the evolution of this paper.

- What can general systems theory contribute to the understanding of the Earth and geological sciences?
- What general phenomena can be likened to the surge in human influence and economic power of the industrial age?
- What systems configurations lead to stability and homeostasis?
- What configurations lead to pulsing and oscillations?

- What are the consequences of pulsing behavior in geologic and general systems?
- How do models developed with the general systems view of the energy systems hierarchies in the Earth, compare with previous overview models?

Background

General systems theory considers many different types of systems to find out what general principles they share, and what general characteristics and patterns are found repeatedly at all scales of observation. This information from various sources is a tool for understanding new areas and problems. Application to large scale systems like those of the Earth has special promise where dynamics are too slow for direct observation.

A summary of general systems concepts is given in later in this chapter under the heading "Systems Concepts Summary". Also later in this chapter, the section "How to Read Models" defines energy circuit language, the diagrammatic language used throughout this study. That section also defines some commonly used systems terms.

Top-down Modeling

In this study a top-down approach is used to model Earth systems. This approach emphasizes overview configurations rather than individual mechanisms, and so reduces complexity. Main units are those that reinforce their own growth, and therefore are the most obvious manifestations of system workings. Connections between these units are drawn by assuming that lower hierarchical levels contribute to the higher levels, and that each level is self-reinforcing.

In the sedimentary cycle, for example, the main self-organized units were chosen as submerged sediments (marine rocks), uplifted sediments (mountain belts), and cratons (continental basement). In increasing hierarchical level (determined as outlined later in this introduction), sediments support mountains, which in turn support cratons. The supporters feed into the production of the next level, and dispersed materials recycle to the lowest level, completing the material loop.

Thus, a simplified view of total system function is obtained. This view features only the essential pathways expected for any self organizing system. Each unit may represents many mechanisms collected in aggregate. In this way complexity of real systems is reduced on a logical basis, in order to make realistic, understandable models whose results may be interpreted with confidence.

Related Work and This Study's Contributions

To facilitate comparisons of this work to similar studies, and for general information on the state of global simulation attempts, a general literature review is provided later in this chapter. There are described important sources of worldwide data on geochemical, geothermal, tectonic, hydrologic, and meteorological parameters. Then a summary is given of significant work on synthesis and interpretation of the data. Finally, previous simulation models of global processes are briefly presented, and illustrated by translations into energy circuit language.

How to Read the Models

To properly and quickly read general systems models, the following procedure is suggested:

1. Note the box surrounding the model's main features. This box is the system boundary. The boundary selected by the modeler separates parts and processes inside from those outside. Influences from the outside features are sources for the systems defined by the boundary. In simulations, external sources are not influenced by internal model workings.

2. Note interior subsystems and descriptive components. These are shown by boxes, rounded bullets, or hexagons. These symbols (described in the background section of this Introduction) usually have dark, thick lines to show that they are the main items of system structure.

3. Note storage tanks and their description, numerical value, and units. Their numerical values give an idea of their relation to other components.

4. Each line in the diagram is a flow of material or energy. Flows on all lines (including inputs and outputs) connected an interaction (pointed bullet), are in the same proportion, differing only in their individual coefficient, the k value. Follow the connections to the interaction symbols to see which elements influence which flows. Flows not connected to an interaction depend only on the upstream storage or source.

5. Note the arrangement of components in order from left to right. Components increase in quality, transformity, concentration, and potential effect per unit, as the diagram proceeds from left to right. Lines pointing right represent upgrading energy quality and productive processes, while those heading left are controlling flows and dispersal pathways.

6. Finally, view the diagram from a distance, and note its general configuration related to the above items. This gives a holistic perspective which de-emphasizes mechanisms and parts. This is the hardest step in understanding general systems diagrams, and may take much practice.

7.   Each symbol and its configurations with the other symbols define energetic and mathematical relationships. The equations that result are the basis for the computer simulation programs.

8.   For ease of reference, definitions of energy language symbols, energy concepts, energy hierarchy, and related items are assembled as follows:

General systems symbols, terms, and notation

In this section, definitions of the common symbols are given in Figure 1-1. Common terms are explained in Table 1-1, diagram notations and unit of measure abbreviations are given in Table 1-2.

Energy Hierarchy and the Sedimentary Cycle

The focus of this study is the sedimentary cycle of the Earth, viewed as part of an energy hierarchy. The sedimentary cycle was defined as the movement of material at the Earth's surface, the cycles which sustain the movement, and the energies which drive the cycles.

In this cycle, as in many processes, energy transformations convert available energy at one level into smaller amounts of energy in a new product. Emergy is the available energy of one kind, previously used up, directly and indirectly, to make a product. A product's emergy per unit (of mass or energy) determines its position in the energy hierarchy (Odum, 1987, 1996). The emergy required to generate a unit of energy at any level is called its transformity, a number that increases with successive energy transformations.

When Earth components and processes are arranged in order of their position in the energy hierarchy, a new view of the Earth system is attained. In this study the position of main Earth components, which are part of the sedimentary cycle, was evaluated by calculating the emergy per unit weight, in

Source: the circle provides energy or materials from outside the system, and is effectively independent of changes going on inside the system.

Storage: the tank is an accumulation of matter or energy in a contiguous fashion.

Flow: the line is the symbol for any movement of matter or energy, or simply its incorporation into some other item of the system.

Interaction: the pointed bullet is the junction where two entities work together to manufacture something new and different.

Producer: the bullet is a converter of a raw energy or material source into a refined product.

Consumer: the hexagon is a module that further converts low grade products into ones that have higher quality and ability to feed back to help the system capture more energy.

Heat Sink: the ground symbol is the pathway for any matter or energy that has lost concentration, quality, or ability. It is the second law depreciation inherent in all systems.

Sensor: the small box symbol indicates a force provided in proportion to the attached storage or flow; however, little energy is tapped in the process.

Unspecified system: the large box represents some unspecified process, the workings of which may or may not be included inside in the diagram.

Figure 1-1. Summary of the energy circuit language symbols used extensively in the diagrams of this study.

Table 1-1. Common terms used in this study.

Term	Meaning
Available Energy	Energy available to do work, units of Joules (Calories, Btu's, or joules).
Donor Value	A value of a product determined by the production process and not by what a person is willing to pay.
EMERGY	(spelled with an "M") All the available energy that was used in the work of making a product expressed in units of one form of energy, units of solar emjoules (sej).
Emjoule	The unit of EMERGY which has the dimensions of the energy previously used (grams-cm squared per second squared).
Empower	Flow of EMERGY per unit time (units of sej/s, sej/day, sej/yr, etc.).
Energy	A property of all systems which can be turned into heat and measured in heat units (Calories, Btu's, or joules).
Energy Hierarchy	The convergence and transformation of energy from many small units into smaller amounts of higher-level types of energy (often in units of larger size) with greater ability to interact with and control smaller units.
Energy Circuit Language	A general systems language for representing units and connections for processing materials, energy and information of any system; diagrammatic representation of systems with a set of symbols that have precise mathematical and energetic meanings.
Maximum Power Principle	An explanation for the designs observed in self organizing systems (energy transformations, hierarchical patterns, feedback controls, amplifier actions, etc.). Designs prevail because they draw in more available energy and use it with more efficiency than alternatives.
Next Larger Scale	Larger territorial areas occupied by units with longer replacement times which must be considered in determining system behavior because of the controls

Table 1-1--continued

	larger units exert on smaller scale units and processes. (See Energy Hierarchy)
Reinforce	The action of a unit or process to enhance production and survival of a contributing unit or process, thereby enhancing itself; a loop of mutually enhancing interactions.
Self Organization	The process by which systems use energy to develop structure and organization.
Maximizing EMERGY	The process by which the maximum power principle operates within a system to select from among the available component and interactions the combinations that results in production of the most EMERGY.
Second Law	(of Thermodynamics) Principle that energy concentrations disperse spontaneously and in all energy transformations some of the available energy is dispersed in the process.
Solar Transformity	Solar EMERGY per unit energy, expressed in solar emjoules per joule (sej/J).
Systems Ecology	The field which came from the union of systems theory and ecology and provides a world view for energy analysis.
Transformity	The EMERGY of one form required to make a unit of energy of another type. For example, since three coal joules and one coal emjoule of services are required to generate one joule of electricity, the coal transformity of electricity is four coal emjoules per joule.
Turnover Time	(or Replacement Time) The time for a flow to replace a stored quantity. For example, a flow of 10 gallons of water per day will replace a 1000 gallon tank of water in 100 days.
Wealth	Usable products and services however produced.

* After Odum and Arding (1991).

Table 1-2. Abbreviations for notations and units commonly used in this study

| Abbr. | Explanation |

Notations

E	Capital E denotes a number raised to a power of ten. For example 6E21 means 6 times ten to the 21st power, or 6 with 21 zeroes following.
k	A small k with a following integer denotes pathway coefficients for each flow required in the simulation. These k's correspond to similar numbered J's, the flow variables, in the calibration tables of Appendix A.
J	Variable, usually with a following descriptor, such as J1, Jr, etc., denoting a flow used in the difference equations.
R	Variable, usually followed by a descriptor, such as R1, Rr, etc., denoting a flow remaining after some is pumped away. This remainder provides the force for the pumping interaction.

Units

g	Grams.
yr	Years.
d	Days
J	Joules
sej	Solar emjoules
sej/g	Solar emjoules per gram
sej/J	Solar emjoules per joule
Ma	Million years
Ga	Billion years

units of solar emjoules per gram (sej/g). Then, models were developed and organized according to the energy hierarchy. Systems diagrams were arranged from left to right, in order of increasing transformity and hierarchical position.

According to the hierarchy concept (see section "Systems Concepts Summary" later in this chapter"), cycling materials grow in quality, transformity, and potential work per unit, during successive, productive transformations (shown proceeding left to right on the diagrams). Cycling materials that lose quality and transformity are the result of dispersing pathways, which flow leftwards on the diagrams.

Emergy per Mass in The Sedimentary Cycle

As explained under the later heading "Systems concepts Summary", hierarchical relationships in systems are thought to be correlated with turnover time and with spatial properties (Odum, 1983, 1996). For the sedimentary cycle, Veizer (1988a) used population theory and observed age distributions of many different rock types to classify Earth materials into eight major tectonic realms listed here with his calculated half life in million years : 1. Active margin basins-27; 2. Oceanic intraplate basins-51; 3. Oceanic crust-59; 4. Passive margin basins-75; 5. Immature orogenic belts-78; 6. Mature orogenic belts (roots)-355; 7. Platforms-361; 8. Continental basement-673 to 1728. The half lives conveniently fell into three groupings: Realms 1-4 had similar times and were all marine in nature. Realms 5, 6 and 7 all were associated with mountain belts. Although immature orogenic belts (realm 5) had a much shorter half life than the other two, it was included because of the logical association between young and old mountains, and because this realm was really a developmental stage for the mature mountain realm. Realm 8 was the continental basement,

which Veizer also termed cratons. The wide range of half lives for this realm reflected three possible definitions of age: time to low grade metamorphism, time to high grade metamorphism, and time to melting or absorption into the mantle.

In order to study the position in the hierarchical order of aggregated, whole-earth parameters such as rain, soil, and the tectonic realms derived from Veizer as defined above, the emergy per unit mass of each was evaluated independently (Table 1-3) and compared with previous work (Odum, 1996). This information facilitates use of the diagrammatic language, because components are customarily arranged from left to right in order of emergy concentration (transformity or emergy per mass). This arrangement suggests the most appropriate connections of the main storages, as interactions between disparate hierarchical levels are usually of minor significance (Odum, 1983, 1996). Geologic transformations may concentrate and converge energy and mass to spatial hierarchical centers.

Table 1-3 lists some aggregated hydrologic, biotic, and geologic parameters related to whole-earth processes, along with the following information for each item: turnover time, total amount stored, annual production rate, and finally, emergy per gram. The items are listed in order of increasing solar emergy per gram, so that the more diffuse forms with lower ability to do real work are on top, while the hierarchical centers appear at the bottom. The table was divided into three sections, the first listing storages at background concentration, the second structural storages, and the third showing messenger storages and simple flows. Background storages were defined as those at background concentration, which lack available energy, the ability to do work, and emergy; these storages are energized by external sources into forms that can do work, as when ocean water is transformed into waves, tides, and vapor.

Table 1-3. Turnover times, storages, flows, and emergy per mass of global components on geological scale of time. See Appendix Table A-1 for literature sources, calculations, and assumptions.

Item Description	Turnover time Ma	Earth Storage E21g	Production E21 g/Ma	Emergy/gram E9 sej/g
A Background concentration (no available energy or emergy)				
1 Ocean water	3.38E-02	1350	40000	Set to 0
2 Ocean ions	10.5	47.25	4.5	Set to 0
3 Suspended seds.	2.41E-06	4.94E-05	20.5	Set to 0
B Essential structures (large storages)				
4 Marine sediments	60	600	10.0	0.94
5 Mountains	250	1850	7.40	1.28
6 Cratons	2496	20100	0.81	11.74
C Controlling flows (and free storages)				
7 Vapor	3.07E-08	0.013	1050000	8.99E-06
8 Clouds	5.71E-11	5.61E-05	1000000	9.44E-06
9 Rainstorms	7.48E-12	5.61E-06	750000	1.26E-05
10 Plant production	1.45E-05	2.50E-03	172	5.49E-02
11 Soil	1.39E-02	0.16	11.55	0.82
12 Acid volatiles	1.59E-03	1.67E-03	1.05	8.99

Notes for Table 1-3
i. For calculations, literature sources, and assumptions, see Appendix Table A-1.
ii. Items at background concentration (section A) are dispersed and lack available energy, emergy, and the ability to do work. Essential structures (section B) are storages which have special ability to feedback and grab more energy. Small storages (part C of the table) are non-essential storages that act as messengers produced by the essential storages and flowing through the system providing mechanisms of control.
iii. For hydrologic cycle components, total earth emergy is assumed to be required for present system operation; i.e., tides and deep heat via continents provide impetus to the hydrologic system. Also, the production rate of a component is its total throughflow; i.e., vapor production rate = ocean evaporation + land evaporation + cloud evaporation + sublimation.
iv. The division between oceanic and continental rocks follows that of Ronov and Yaroshevskiy (1976), where the boundary is a particular crustal thickness, approximately 25 km, so that much of the shelf area and very thick marginal sequences belong with the continents.
v. Total earth emergy= 9.44E+24 sej/yr   Odum, 1996
    This value was used to calculate the emergy per gram for all items.

Structural storages were defined as key elements of system structure. Each feeds back high quality, autocatalytic, controlling functions, while the messenger storages and simple flows are those intermediate parameters that carry material or energy between the structural and background storages. These messenger storages could well be the main structural storages in smaller scale systems, such as clouds in the hydrologic cycle.

As an example of how to read Table 1-3, water vapor (item 7) had a turnover time in the atmosphere of 3.07E-8 Ma (about 11 days), a total Earth storage of 0.013E21g, a production rate of 1,050,000 E15g/yr, and its emergy per gram was calculated as 1.25E-3 sej/gram. Vapor is a principal circulating part of the hydrologic cycle which carries energy(latent heat) and materials (water) to storms. In the table notes (Appendix Table A-9), which explain calculations, sources, and assumptions, the production of vapor was defined as total conversions from liquid water or ice to vapor, by any method including surface water evaporation, sublimation, evapotranspiration, cloud evaporation, and rain evaporation. Also, the emergy required to make the vapor was defined as the total solar emergy that goes into latent heating and into free energy, and total storage was according to Berner and Berner (1987).

Odum (1983) showed a general trend of increasing turnover time with emergy concentration. For structural elements in Table 1-3, solar emergy per gram increases with turnover time from oceanic sediments to continental sediments and to continental cratons.

Among the controlling flows, soil cycles very slowly, with a turnover time of about 14000 years (See Appendix Table A-1, item 11), and its emergy concentration is slightly less than uplifted sediments. Because it acts by exposed surface, and exists as a thin shell, soil may exert considerable controlling influence despite its small size. In contrast, rocks in cratons(item 6

in the essential storages category) cycle slowly, possibly because of their small exposed surface area per unit mass. Acid volatiles may be used up quickly because of their gaseous state; thus their turnover time and stored amount is low despite their high transformity.

Most of the Earth products listed in Table 1-3 have similar transformities to those evaluated previously. Odum (1996) found average rock to have an emergy per gram of 1E9 sej/g, very close to the value for uplifted sediments found in this study, despite different data sources. For this study, sediment half life (Veizer, 1988a) and total sedimentary mass (Ronov and Yaroshevskiy, 1976) were used to estimate production of average land, while Odum used a land uplift rate of 9.36E15 g/yr, calculated by Garrels and MacKenzie (1971) from runoff data and an assumption of steady state for the cycle.

Overview of the Sedimentary Cycle

The sedimentary cycle consists of material transportation and transformation from land storages with chemical and potential energies to sediment storages in the sea, and to a lesser extent on marginal basins and in interior continental basins. Completing the cycle is lithification, metamorphism, and uplift of the material to its original position and form. The process is coupled to energy of the deep Earth and that of the hydrologic cycle.

Incorporating the concepts of essential storages, transformity, and hierarchy discussed in the previous section, Figure 1-2 is an aggregated block diagram of the sedimentary cycle and its interaction with the human economy. Numerical values are shown for flows of energy, fluids, and solids, which link the main compartments. Values of the total mass, turnover time, and transformity are shown for each box. All items are arranged from left to right in

17
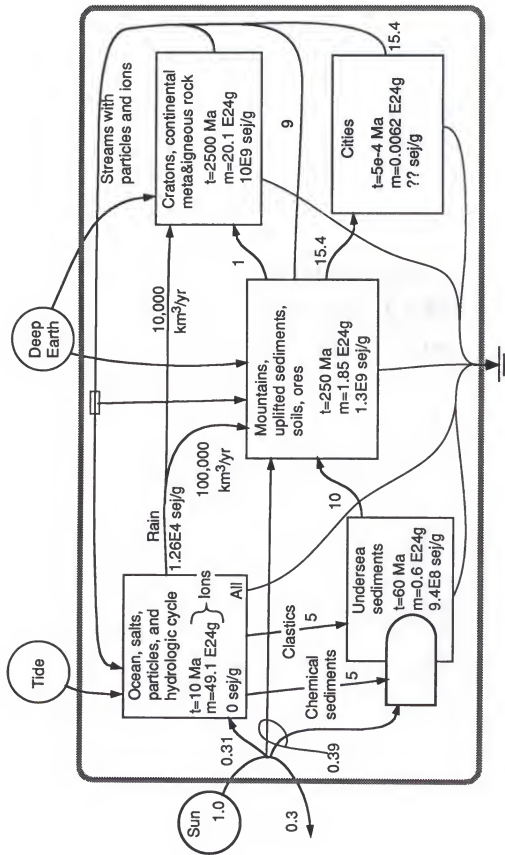
Figure 1-2. Block diagram of the sedimentary cycle, arranged hierarchically from left to right, showing main flows of energy, fluids, and solids. Turnover time, t, and total storage, m, and emergy per mass are given for the main compartments. Flows given in units of E21 g/million yrs of energy (units as shown) and sun, standardized to one unit of inflow.

increasing order of energy quality, area of influence, and time scale of operation of the units.

At the far left, diffuse solar radiation crosses the system boundary, energizing the hydrologic and biotic systems of the Earth's surface. Seawater's ionic composition is a base state for chemical potential and sea level is a base state for gravitational potential. Proceeding to the right from seawater, solar energy is used to energize the hydrologic cycle. Also, dispersed particles and ions are concentrated by biotic and settling action into the aggregated ocean sediment compartment. Then these sediments interact with Earth heat and surface cycles of weather and material transport, to create uplift and build mountain ranges. At the far right is the slower, higher transformity process of continent building, which is supported by the intermediate-level mountain subsystem, by as yet unspecified mechanisms. Throughout the diagram, the main connections between blocks were made to conform to the hierarchical order of the system, rather than representing specific processes.

Because of their similar transformities, soil processes and ores were aggregated with mountains. Cities were shown at far right because they use soils and ores from the mountain block, and must have higher transformity due to losses inherent in chains of support. All feedbacks and dispersing flows are shown circling back leftwards, reflecting the dispersal of solids to wetlands, the continental shelves, the deep sea floor, and to sea water as dilute ionic constituents.

Human economies impact the sedimentary cycle by direct mechanisms such as mining, diversion of waters, and altering biotic activity. Human agriculture increases the drain on soils and plants, altering the terrestrial weathering process. Agriculture also competes with the natural consumers, but

uses the subsidies of fossil fuels and ores that are unavailable to the animal consumers.

The turnover time shown for cities is comparatively low at 500 years, which represents the turnover time of individual civilizations such as Rome, the Mongol Empire, the Incas, etc. The long-term information retained by civilizations, however, lasts longer than any one society. This information includes systems of language and writing, mathematics and science, culture, religion, successful technologies, and even human genetics. Thus, the time required to make civilizations starting from nothing may be on the order of the age of the Earth. This scale is very similar to the cratons, which are the longest lasting unit of the sedimentary cycle. This reasoning may justify the placement of civilization in the highest hierarchical level of the sedimentary cycle.

The aggregated block diagram of the sedimentary cycle serves as an organizing structure for understanding issues involved in the overall process and human influence on it. It shows an integrated picture of the proposed important components and flows of the system. Filling in details can facilitate further study of particular aspects of the cycle such as ore formation, differentiation of rock types, and human impact on weathering.

<u>Systems Concepts Summary</u>

This section gives a short introduction to the concepts used throughout the study to shed light on whole-earth systems. General systems theory is a synthesis of thermodynamic, evolutionary, and energetic principles derived from the study of commonality among all systems.

Energy Circuit Language

Conceptual models of any real world process or component require the aggregation of parts into definite lumps with similar characteristics. Identifying the parts and understanding their normal properties are necessary to make valid predictions about future behavior.

Energy circuit language is a shorthand diagramming notation which facilitates the construction of general systems models. The language consists of a set of symbols (defined under the later heading "How to Read Models") which represent the essential elements of all systems (See Odum, 1972 and Odum, 1983, for extensive explanation of these symbols and their use). Specific systems may be modeled by assigning energy circuit language symbols to parts of the real system, and connecting them to form a working hypothesis about the important parts and processes of the real-world system. To accomplish this, a system boundary must be defined, and the contained system must be aggregated into parts with similar properties that can be evaluated. Any items entering through the boundary are treated as external sources, which are unchanged by variations within the model.

Energy circuit language is formulated to enable the construction of holistic models, that are consistent with thermodynamic and general systems principles, as outlined below. Differential equations for model simulation are implied by the diagram, so that the system configuration comes before the mathematical equations. Thus, general systems principles and overview system configurations are the primary consideration, as opposed to the practice of assembling physical and/or empirical equations from small-scale disparate disciplines. This emphasis facilitates a top-down approach to modeling, which may help focus attention on important aspects of the system under study.

Energy and available energy

The concept of energy embraces phenomena such as electricity, heat, gravity, etc., in which physical objects (e.g. molecules, photons, planets) can be displaced from their equilibrium state. Available energy is the ability to do work, such as lifting a weight, moving an object against friction, and making chemical transformations. It is different from dispersed energy at background concentration, which lacks ability to do work locally.

For example: two electrically charged plates have available energy which causes electrons to flow; gravitational available energy accelerates meteorites toward the Earth; and chemical available energy releases concentrated heat when gasoline burns, pushing pistons that drive an automobile. After the work (arranging electrons, attracting meteorites, and moving a vehicle against friction in the above examples) is done, some of the available energy is used up. In the case of the meteorite, the gravitational potential energy is mostly converted into heat initially, some of which goes into chemically transforming the impacted material, and some of which is dissipated at a temperature practically indistinguishable from the ambient.

The first law of thermodynamics states that energy and matter can be neither created nor destroyed. Used, dissipated energy is not destroyed, only converted into a form that no longer can drive work processes. Dissipated energy is usually waste heat, and on energy systems diagrams, waste heat is shown leaving the system via the heat sink (See the Key to Symbols).

Depreciation

Stored forms of available energy always have a loss associated with the storage. For example, stored electrical energy in a capacitor leaks out in proportion to the amount stored; stored heat in the Earth flows to the surface and surface heat radiates away; chemical energy of paper in books is

degraded over time by acid dissolution and insects. It is a general systems principle that all stored available energy tends to dissipate over time. This principle is implied by the second law of thermodynamics.

<u>Conservation of materials and energy</u>

In real systems, conservation requires that the total storage in the system account for the difference between what is coming in and what is leaving. Therefore the system under study is not forced to conserve total internal storage, but overall conservation still holds. Material cycles are important components of general systems models, often being driven by inflowing energies.

<u>Energy transformation hierarchy, emergy, and transformity</u>

Various forms of energy include kinetic, gravitational, chemical, electrical, thermal, radiation, mechanical, and energy of macro-scale concentration. According to energy conservation, energy cannot be created or destroyed, but its form changes. However, no form change of energy can be accomplished with 100% efficiency, except transforming to heat. As implied by the second law of thermodynamics, transformations between any other forms always involve the loss of some ability to do work as dispersed heat.

In nature real processes transform energy. Thus plants convert sunlight into sugar (chemical energy), people convert fossil fuels into mechanical work, and stars transform gravitational energy into light. In all cases some available energy is dispersed as heat in the process, and in energy circuit language this heat is shown as a pathway to the heat sink from interactions.

Because no energy transformation is 100 percent efficient (except for the ultimate transformation to dispersed heat), successive energy transformations carry smaller and smaller amounts of available energy. The ultimate amount of initial energy resource required to make the product of a chain of

transformations is a property of the product, and has been termed emergy (Odum, 1976; 1996). In order to assess the position of any product in a chain of energy transformations, the measure transformity has been applied (Odum, 1976, 1996). Transformity is the ratio of the emergy of the product as defined above, to the actual available energy associated with the product. Products at the end of a long chain of energy conversions carry small amounts of actual energy and large amounts of emergy, so their transformity is large. For example, a volcano may represent the end of a long chain of energy conversions, from diffuse heat of chemical conversion during subduction, to more concentrated pools of magma working toward the Earth's surface, to high energy surface magma reservoirs with great volatile concentration that may contain enough concentrated energy to cause eruptions. The volcano may release a huge amount of energy during short time periods, but its long-term average energy release is small compared to the energy receipt of its entire support area over the same time period. The volcano is a high transformity item that represents the convergence and concentration of dilute energy resources, and is thus a hierarchical center. Like many other hierarchical centers, they have great potential to do work per unit of energy.

Hierarchical organization is the orderly progression of support and influence that is seen in many systems of various types. In this scheme, a large number of dispersed, low quality units provide support to a smaller number of more influential units with larger territory and higher transformity. These more influential units in turn support units of even higher quality and larger territory. Hierarchical organization is very evident in human systems, where political, social, military, and family ranks are well established in almost all societies. Food chains and food webs are excellent examples of hierarchical organization in ecological systems. Even astronomical systems show evidence of hierarchy:

stars, clusters, and galaxies each have their own territory and requirement of support from the lower level. Proper hierarchical ordering facilitates the development of meaningful systems models of the real world.

<u>Autocatalysis</u>

A prevalent design that results in self organization and more power is autocatalysis (Figure 1-3), which is the ability of any stored quantity to actively acquire more resources. In the figure, the heavy round rectangle is the system boundary, through which energy flows in, and degraded heat passes out. The pointed bullet interaction symbol is the work junction where the stored quantity Q interacts with the energy source in a pumping action. Each pathway connected to this interaction carries a flow in proportion to the product of the energy source E and the storage Q, but each pathway has its own coefficient. The stored quantity Q also is connected to its depreciation pathway, which is proportional to the amount stored. Thus, the difference equation for the storage is determined by the diagram, and is written below it.

An autocatalytic component exhibits positive feedback, because more stored energy can lead to further increases due its active resource acquisition strategy. Simple examples of autocatalytic processes include the way a fire entrains oxygen through convective flow, enhancing its own burning; the action of an ocean wave, which grows taller and therefore catches more wind; growing stars that, by increasing their mass, gain more gravitational pull with which to sweep up more material; and forests that build leaf area to capture more sun to build more leaf area. In fact, most observable phenomena with energy inflow above a threshold, are autocatalytic. In the real world, limited energy and material resources prevent runaway growth by these units.

The ubiquitous existence of autocatalytic configurations has important implications for general systems studies. Proper aggregation of models and
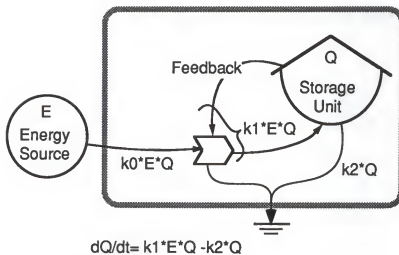
Figure 1-3. Energy language illustration of a typical autocatalytic configuration, which can grow exponentially without bound because of unlimited energy source. Variables are shown for the energy source E, storage Q, and pathway coefficients (k's). Flow equations are shown for each pathway. Typical units: joules and joules per day for storage and flows, respectively.

diagrams requires finding those structural storages that perform active resource acquisition. Moreover, each scale of inquiry is thought to have a most appropriate aggregation scheme corresponding to natural organization of autocatalytic units (Odum, 1983).

Maximum power and maximum empower

The concept that system evolution proceeds so as to maximize power (energy per unit time) has been postulated many times (See Boltzmann, 1905; Lotka, 1922; Odum, 1955). Odum (1983) formally stated the Maximum Power Principle as follows: "systems prevail that develop designs to maximize the flow of useful energy." Furthermore, useful energy was defined as that which develops structure capable of producing feedback which amplifies energy inflow. In this sense, power maximization is a standard against which all systems can be measured to evaluate their performance. Higher average power over the time period of interest defines the optimum system.

In terms of whole-earth systems, the maximum power principle predicts that the whole Earth should be organized to maximize the amount of energy used to create useful functions. Considering solar energy, maximum power use is equivalent to minimum albedo, because that is the case where the greatest average solar energy is incorporated per unit time. The Earth's 30% albedo may represent a compromise between the energy capturing ability of land with surface water and the energy reflecting properties of clouds that produce surface water.

Some confusion has arisen due to the seeming contradiction of the maximum power principle with the thermodynamic principle of entropy, in which lower energy states are preferred. Maximization of power requires dissipating energy faster, which simply implies that systems evolve to reach low energy

states the fastest. Faster dissipation toward a lower energy state is simply another way of stating the maximum power principle.

The maximum power principle is a goal function similar to the concept of survival of the fittest population, except it explicitly defines the goal of system self organization, and what "the fittest" is. The principle, therefore, supplements evolutionary theory in biology, as well as giving a firm basis to the study of evolution and dynamics of systems of all types.

Maximum power might imply organizing so as to maximize energy flows at lower levels, such as solar and atmospheric processes, where total energy is greater. Empower is the rate of flow of emergy, which is weighted to account for the different values of various forms of energy. Accordingly, Odum (1987, 1996), and Scienceman (1987) theorized that systems which maximize empower, rather than simple power, are actually optimizing performance. They refined the principle of maximum power into the maximum empower concept.

Pulsing and scale

Volcanoes erupt, storms rain, lightning strikes, the Earth quakes, supernovae explode, and the economy booms. These examples of pulsing behavior have long been a source of mystery, wonder, and scientific exploration. Pulsing is a special form of oscillation, which involves slow growth and storage of resources, followed by autocatalytic, frenzied consumption, which resets the state of the system to the slow growth mode. In ecological systems, material cycles are quickened by the release of nutrients, for example, in a fire. This nutrient return function may enable continued growth, adaptation, and flexibility, so that the ecosystem can respond to contingencies and continue processing maximum power in the long term.

The observed generality of pulsing requires explanation. Is there something intrinsic to the cycle of production and consumption that favors

pulsing behavior? What characteristics of real systems must be included in models to reproduce observed pulsing? Perhaps systems that pulse have been selected for, while non-pulsing systems are not competitive.

Odum (1983) proposed that pulsing is very general on all scales of space and time. These two types of scale are linked by transformity, in that high transformity quantities tend to have both a large area of influence, and a long turnover time (Note: in this study, turnover time is defined for a storage as amount divided by through-flow for steady systems, that value averaged over a period for oscillating systems, and storage divided by outflow for transient systems), as shown in Figure 1-4. Small scale, low transformity pulsing may look like random high frequency noise at the higher level. Pulsing from the larger scale can have disastrous consequences to the smaller scale systems if they are not adapted. For example, a hurricane ripping through South Florida is a large scale pulse on small scale housing.

Literature Review

Possibly because their scale is so much larger than that of everyday human experience, aggregated global simulation models have received scant attention from scientists in the past. The increasingly global scope of human influence, however, has drawn attention to global processes and human impact on them, and a very large amount of work has documented rates and magnitudes of the relevant parameters.

This section is a short review of data on global cycles, some theories of overall Earth operation relevant to this study, and numerical models and simulation studies in the areas of geochemistry, climate, and their interaction with global economics.
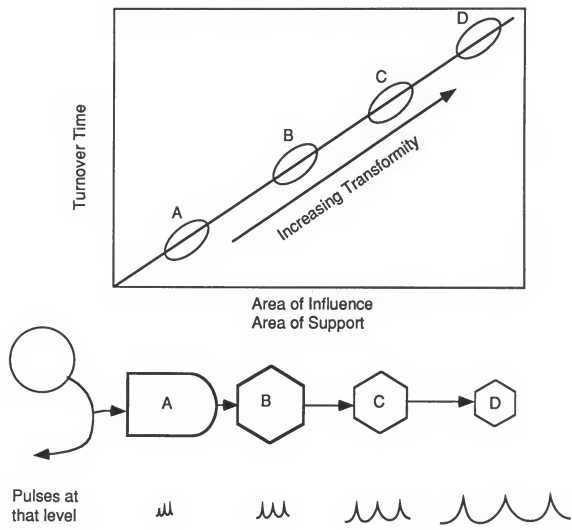
Figure 1-4. Theoretical relationship between scales of space and time, transformity of products, and pulsing patterns in chains of energy transformations.

Work Facilitating Global Simulations

Increased attention to global scale phenomena has spurred many estimates of global hydrologic, geologic, economic, biotic, and energetic parameters. In addition many authors have used this data to suggest significant properties of the overall Earth system, including such things as steady state cycles, causes of continental differentiation, and major feedbacks responsible for Earth regulation. The following is a brief discussion of some of the major work on whole-earth data and interpretation.

Geochemical data

Early global geochemical data were assembled by Clarke (1908), who reviewed and synthesized then available information on the geochemistry of rocks and elements, especially their abundances and locations. Goldschmidt (1933) proposed an overall Earth surface differentiation reaction, where initial igneous rocks and acid volatiles combine to form water, salts, sediments, and soils. This work was followed up more quantitatively by Rubey (1951), and Li (1972). Goldschmidt (1937) also summarized work on the affinity of particular chemical elements for various types of rock, outlining atomic reasons for the observed affinities. Rankama and Sahama (1950) extended the work of Goldschmidt and Clarke in an exhaustive review of geochemistry. Their work focused on the manner of occurrence of particular elements, and they discussed the linkages between the minor (surface) and major (deep) parts of the sedimentary cycle, which term included surficial and deep processes.

Global interpretation of geochemical data

Odum (1951) calculated fluxes of strontium and other elements involved in the sedimentary cycle, finding that many of them are close to steady state. He

proposed that the Earth's overall sedimentary cycle was likewise in a steady condition, implying that the mass of continents is also in steady state. Barth (1962) covered the descriptions and formation processes of sedimentary, metamorphic, and igneous rocks, and their relevance to overall geochemical cycles. He proposed that the observed strong differentiation of igneous rocks is related to the surface process of selective weathering and transport of basic rock components, different from the prevailing view that igneous differentiation is responsible for continental layering.

Garrels and MacKenzie (1971), in a student oriented text, discussed whole-earth cycling of materials. They provided perhaps the first semi-quantitative overview of the whole-earth process, and included much explanation of the geochemical and geophysical evidence for their understanding of the Earth system processes. Their work emphasized the feedbacks and interconnections in the complex system that determines surface environmental conditions and rates.

Goldberg (1972) compared the rates of material processing by the natural sedimentary system and those associated with human industry alone, for such substances as petroleum, metal ores, and various atmospheric gases. He found that overall rates are comparable within an order of magnitude for most substances, and proposed that this equivalence of rates indicates humans significantly impact the overall sedimentary cycle.

Ronov (1982) summarized data gathered primarily by Soviet scientists on the quantitative aspects of the Earth's sedimentary shell. He calculated numerical values for volumes and masses of material in the sedimentary cycle, and percentage of continental area as platforms over geologic time. From his studies, he stated a geochemical principle for the preservation of life, as follows: "Life on Earth and other planets, other things being equal, is possible only as

long as these planets are active and exchange of energy and material takes place between their interiors and surfaces. With the energy demise of the planets, life must also inevitably cease."

Lerman and Meybeck (1988) edited a collection of papers on weathering as a factor in geochemical cycles. The chapter by Garrels used models of the carbonate-silicate-sulfur linked geochemical cycles to suggest operation of the principle of uniformitarianism in the long term. Stallard's (1988) contribution pointed out that the vegetation influences weathering rates by roots holding soil and by soil creating an intimate contact between acids, water, and rocks, thereby promoting further weathering. Veizer's (1988b) chapter (See also Veizer, 1988a, and Veizer et al., 1989b) used concepts from population dynamics to examine histories of continental and oceanic crust, mineral bodies, and sediments. He concluded that both evolutionary and cyclical processes are operating in Earth systems, and that the time scale of observation determines which is the more significant.

Schlesinger (1992) also summarized recent estimates of global parameters in the Earth's biogeochemical cycle, and their changes due to human influence. He cited numerous examples of large changes in the Earth's surface environment as a result of economic activity, including decreased net primary production, increased chemicals in surface waters, and increased atmospheric carbon dioxide and methane.

Dobrovolsky (1994) reviewed estimates of the total mass in Earth reservoirs and mass flows for global systems. He included both biological and geochemical cycles, and human alteration of those systems. Dobrovolsky summarized the overall land net primary production of the biota, the average compositions and total dry weight of elements and, therefore, the rates of cycling of elements through the biota. He related these compositions and rates

of uptake to the average concentrations of the same elements in the Earth's surface rocks and its atmosphere, waters, and soils. He then looked at the individual cycles of volatile elements and those normally found in solid rock, and evaluated each with respect to their biological contribution. His results suggested that biological processes are significant in all of the major cycles of elements at the Earth's surface.

Rea and Ruff (1996) compiled knowledge of ocean rock assemblages with known rates of ocean plate movement to estimate present and past mantle recycle rates for solids and water. They concluded that over geologic time instantaneous rates of sediment exit from the oceans (by any and all processes) are normally much lower than those of sediment accumulation. They thus implied that pulsing phenomena are important in the removal of sedimentary material from the world's ocean basins.

Earth heat data

Sclater et al. (1980) used simple thermal models of oceanic crust and continental crust to study mechanisms of internal Earth heat production and dissipation. They estimated the heat flow attributable to ancient deep heat, that due to radioactive processes, and the relative proportions of heat dissipated through oceans and continents. They also found that heat lost due to convective processes of plate creation and orogeny is about two thirds of the total Earth heat loss, and conductive heat loss accounts for the rest.

Odum (1996) included many data on the energy and energy quality of items crossing the boundary of the total Earth system, and of those cycling at the surface. He calculated that on an Emergy basis, the Earth's surface receives approximately 42.5% of its total contribution from sunlight, an equal amount from deep geologic heat, and about 15 percent from gravitational energy transmitted from the moon and sun.

Kiehl and Trenberth (1997) summarized the state of information regarding whole-earth solar energy receipt and radiative losses as determined by satellite information and detailed radiative models. They computed the so-called "forcing", the average net longwave heat retention in clear and cloudy conditions to be 125 and 155 Watts per square meter, respectively. They also found that the heat retained under clear sky conditions by water vapor and carbon dioxide was 60 percent and 25 percent of the total, respectively, emphasizing the importance of water in the radiation trapping and the heat balance of the surface.

Oceanic, hydrologic and biological data

Holland et al. (1986), discussing historical patterns, suggested that the chemical content of the oceans has changed little over the past five hundred million years. They also reasoned that the Archean atmospheric mass of carbon dioxide was much higher, and that of oxygen much lower, changing later due to the development of land plants.

Colinvaux (1986) gave quantitative overviews of the geochemical cycles of phosphorus, nitrogen, sulfur, and carbon, which are important to ecological processes. He also summarized energy flows for the biosphere, including gross and net production and consumption.

Berner and Berner (1987) summarized significant parameters of the global hydrologic cycle, including rates of precipitation, evaporation, evapotranspiration, and streamflow. They also discussed the controls on these rates, and the implications of water and its cycling for the Earth's living and inorganic systems.

Numerical Models of Large Scale Processes

The studies cited and many more have supplied a wealth of numerical estimates of Earth circulation. Using this information with physical laws and principles, models of the way our world works have been offered by previous authors, including some that concentrate on the scale of the whole Earth. Because this study concerns the general circulation of the Earth's geobiosphere and the global biogeochemical role of human society, this review includes large scale calculations and numerical models of the Earth systems and people. The relevant time scales are the multi-million year periods required for operation of the main sedimentary-continental cycle and the several hundred year period involved in the global geochemical impact of the human economy. Models of components and processes with faster turnover times were not included.

Glaciers, oceans, and atmospheres

Because of strong scientific interest in understanding historic patterns of glaciation and the implications of rising carbon dioxide levels in the atmosphere, many numerical models have been proposed for the interconnected system of atmospheres, oceans, and glaciers. For example, Raymo et al. (1990) proposed tectonic and thermal processes to explain variations in the correlation of ice with oceanic circulation rate from isotope studies. Later, Raymo and Ruddiman (1992) compared climatic data with timing of Tibetan uplift, and suggested that, because continental collision can expose large quantities of rock to weathering and subsequently uptake large amounts of carbon dioxide, these processes may decrease greenhouse forcing and therefore greatly influence global climate patterns. They cited cooling after Himalayan uplift to support their argument.

Kerrick and Caldeira (1996) used data on metamorphic rocks in the Himalayas to estimate the rate and duration of collision-related metamorphism, and by proxy CO_2 release, during Himalayan uplift. They used chemical kinetics of overall weathering reactions to calculate global uptake rates for the released CO_2, and computed probable carbon dioxide levels in the atmosphere of about double the present day amount. They suggested that warm climate during the early Cenozoic and subsequent cooling are due to the initial release of carbon dioxide during collision-related metamorphism, and later weathering of uplifted rock.

Broecker and Denton (1990) and Broecker (1991) analyzed present and past ocean circulation in relation to glacial activity. Their models of ocean circulation included thermohaline overturn. They concluded that net salt transport between ocean basins may control vertical circulation, and that orbital variations, by affecting precipitation, alter salt transport and, therefore, deep ocean circulation. Thus, chemical potential gradients driven by the hydrologic cycle may drive vertical ocean currents and glacial cycles.

Crust and continental formation

The large scale operation of Earth systems that produce crust, oceans, continents, and mountains has been the subject of many investigations. Moorbath and Windley (1981) edited a collection of articles on geochemical and geophysical evidence for crust formation and evolution. The overall shape of the crustal growth curve was sigmoidal, with fast early growth rates becoming much slower at present. In addition, crust building was cyclic in character, with preferential preservation of some minerals and rocks in average crust. These two traits of self-reinforcing growth reaching a limit, and material cycling, two key parts of general systems modeling, are applicable to very large scale geologic systems.

In the Moorbath and Windley collection, Armstrong (1981) observed that average continental height above sea level has been constant because of the coinciding erosion and base levels of ancient and modern cratons. Because of the constant thickness of continents of various ages (See Cummings and Schiller, 1971; Condie, 1973; Davies, 1979), he reasoned that total continental volume must have been constant since about 3 Ga. He also showed how the isotopic evolution of lead, strontium, and neodymium can be consistent with that interpretation. Also in that collection, however, Taylor and McLennan (1981) interpreted rare Earth element geochemical patterns as consistent with fast early growth of continents, and slow but constant growth of continents in the Phanerozoic.

Reymer and Schubert (1984) and Schubert and Reymer (1985) proposed that constant freeboard over post-Archean time suggests the continental volume has been increasing, because of their assumption that ocean basins have deepened as mantle heat production declined. They argued that because ocean basins have deepened, sea level should have fallen, other things being equal. The fact that freeboard has been constant, however, indicates sea level has not fallen. Thus, the continents must have grown, and pushed in the sides of the ocean basins, in order to keep sea level up. Reymer and Schubert's model ignored the influence of surface processes and gravity on erosion rates, and the resulting negative feedback from freeboard to erosion, that could act as a regulator of sea level relative to the continents.

Veizer and Veizer et al. (1979, 1985, 1988a, 1988b, 1989b) used population dynamics theory to analyze mass age distribution of many different rocks and minerals. They demonstrated that most of the components of the Earth's crust are in balance between rates of formation (analogous to birth) and

destruction (analogous to death). From the rates of disappearance in the geologic record, they evaluated characteristic turnover times for mineral bodies and large features of the crust, and grouped the Earth system into several distinct tectonic realms, such as marginal basins, cratons, and mountain ranges. They suggested that those realms with larger decay and replacement times are more important to overall function of the Earth system. They further proposed that geologic realms with slower characteristic times are more important controlling elements than biotic and other surface processes with faster characteristic times.

Arndt and Goldstein (1989) proposed that hotspots and volcanic arcs are parallel pathways bringing mantle material to the continents, via underplating (coating from below) and volcanic overplating. They suggested that differentiation processes operating on continental blocks tend to isolate very heavy continental constituents at the lowest levels of the crust, and that these become unstable and spontaneously break off, returning to the mantle. They calculated that between 20 and 50 percent of the present continents have returned to mantle by this method over Earth history.

Evidence from other planets and bodies in the solar system has been used to speculate on general aspects of planetary crust formation. Anderson, (1989) suggested that, opposed to prevailing theory, Earth's mantle is irreversibly stratified, and the crust is prone to delamination if its thickness grows greater than 60 km. Using the moon as an analogy, Lowman (1989) argued for early Earth continent differentiation, followed by formation of ocean basins via meteorite impacts.

Kroner and Layer (1992), after examining ancient orogenic belts and their deformation characteristics, suggested that ancient tectonics were probably similar in style and rate to those occurring today. They concluded

large continental blocks existed 3.5 billion years ago, and that continental additions seem to have occurred mostly in short intense pulses about once every billion years, possibly linked to Wilson cycles of continental closure. Thus they supported the concept of uniformitarianism in the long term, and also hinted that short term deviations from uniformitarianism, of a pulsed nature, may be expected.

Short term changes. CO_2 increase

Many more conceptual models have been developed to analyze specific problems facing our global economic system, such as the increase of carbon dioxide. For example, Decker (1988) combined predictions generated by global circulation models for a doubling of atmospheric carbon dioxide with statistics for the response of individual crops, such as corn, wheat, and soybeans, to changes in rainfall and temperature, and estimated likely changes in U.S. agricultural productivity. He found that average yields could drop by as much as 20%. When he then combined those results with experimentally predicted gains in crop production due to enhanced carbon dioxide fertilization (i.e. growth gains due solely to increased CO_2 in the air) he predicted a net gain in U.S. crop production.

Ozone

Ozone systematics have also been the subject of many conceptual models of whole-earth scale. For example, Bekki et al. (1993) studied the interaction of sulfur, insolation, and volcanoes to explain observed stratospheric ozone dynamics after the eruption of Mt. Pinatubo. Using a chemical dynamic model developed by Harwood and Pyle (1975), they closely reproduced an ozone anomaly in the stratosphere attributed to two effects of sulfur: ozone production catalysis by SO_2 and ozone production hindrance due to sunlight absorption by SO_2.

Fisher et al. (1990) modeled the system of stratospheric ozone and its impacts by anthropogenically released chemicals. They simulated the ozone depletion caused by the use of chlorofluorocarbon refrigerants, using equations for atmospheric chemical kinetics. Their results suggested that, if 5E12 g of refrigerant is released in a one time event, the proposed substitute chemicals (hydrohalocarbons) will bring about a peak magnitude and duration of ozone depletion of about 10% of that caused by the standard halocarbon refrigerants. They did not simulate the effect on the ozone layer of a global economic switching to the new refrigerants.

Previous Simulations of Global Scale Models

Simulation models are often implied by conceptual models, and are good tests of those ideas. In spite of the many whole-earth numerical models, there are few aggregated global-scale simulation models. This section summarizes some of the global simulations that have been carried out on overview models of geochemistry, climate, glaciers, and global economics. To help comparisons, sets of equations were translated into energy circuit diagrams.

Geochemical systems

Geochemical processes have left many clues to the workings of large-scale Earth systems, including variations over time and space of chemical and isotopic compositions of rocks and minerals. The following are some simulation models that seek to explain Earth behavior while meeting observational constraints in the geochemical record.

BLAG: silicate-carbonate model: Berner, Lasaga, and Garrels (1983) simulated the interactions of carbonate and silicate geochemical cycles to gauge their influence on CO_2 in the atmosphere. Their findings suggested that

rates of geologic activity and deep Earth processes can have substantial effects on atmospheric gases, and thus climate. An energy circuit language translation of the BLAG model, as it is called in the literature, is shown in Figure 1-5: the legend lists the original equations used by Berner, Lasaga, and Garrels. The diagram shows how the driving forces of sun, rain, and deep processes affect the circulation of chemicals among compartments of seawater, sediments, rock, and air. The main processes of weathering, metamorphism, sedimentation, and hydrothermal exchange, and their relations to one another, can be seen at a glance. Sources implied, but not explicitly shown by the authors, were added as dashed lines.

The BLAG model aggregated all Earth geochemical cycles into a simple system of transformations among reservoirs of dolomite, calcite, silicates, air CO_2, and sea salts. Fluxes from one reservoir to another were by means of weathering, metamorphism, hydrothermal reaction, and precipitation of calcite. These fluxes were made linear and donor-controlled, but also dependent on temperature, land area, and sea floor spreading rate. Land area and spreading rate were made independent of the model, but temperature was allowed to vary based on CO_2 levels generated by the model.

The model was simulated from 100 million years ago to the present, and tested for sensitivity to varied spreading rate, continental land area, and masses of dolomite and calcite. It generated temperature trends consistent with isotopic evidence, and suggested that independently controlled parameters of seafloor spreading and land area are major controls of world climate. Reciprocal effects of world climate on geologic parameters were excluded because of the assumption that land area and spreading rate were independently controlled. To simulate future trends, models should include feedbacks from existing system elements to control spreading rates and land area.

BLAG-83

Legend on facing page
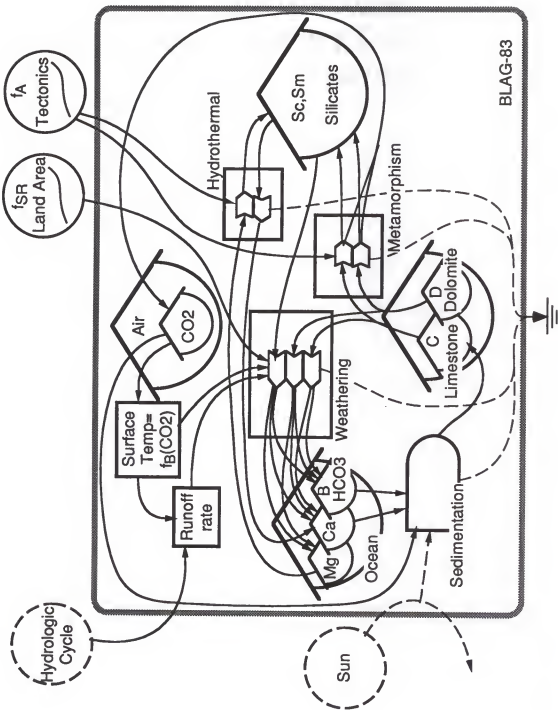
Figure 1-5. Energy circuit language translation of BLAG-83, the carbonate-silicate transfer model of Berner, Lasaga, and Garrels (1983), with dashed lines indicating inferred elements. Author's equations shown below.

$$dD = -k1*f_A*f_B*D -k2*D*f_{SR}$$

$$dC = -k3*C*f_A*f_B -k4*C*f_{SR} +k5*(Ca*B -k6*CO2)$$

$$dSc = -k7*C*f_{SR} +k8*D*f_{SR} -k9*Sc*f_{SR} -k10*Mg*f_{SR}$$

$$dSm = k11*D*f_{SR} -k12*Sm*f_{SR} +k10*f_{SR}*Mg$$

$$dMg = k14*D*f_A*f_B -k15*Sm -k10*f_{SR}*Mg$$

$$dCa = k14*D*f_A*f_B +k3*C*f_A*f_B +k9*Sc*f_{SR} +k10*f_{SR}*Mg -k15*(Ca*B -k16*CO2)$$

$$dB = k14*4*D*f_A*f_B +k3*2*C*f_A*f_B +k9*2*Sc*f_{SR} +k15*2*Sm*f_{SR} -2*k15*(Ca*B -k16*CO2)$$

$$dCO2 = k11*2*D*f_{SR} -k14*2*D*f_A*f_B -k15*2*Sm*f_A*f_B -k9*2*Sc*f_A*f_B +k4*C*f_{SR} -k3*C*f_A*f_B +k15*(Ca*B -k16*CO2)$$

$$f_B = 1 +0.252*[\ln(CO2/0.055) +0.0156*\{\ln[CO2/0.055]\}]2$$

where:

k's are constant coefficient values; f's are correction factors as given in notes 9 to 11.

D= mass of dolomite rock

C= mass of calcite rock

Sc= mass of calcium silicate rock

Sm= mass of magnesium silicate rock

Mg= concentration of magnesium in seawater

Ca=concentration of calcium in seawater

B=concentration of bicarbonate in seawater

CO2=mass of carbon dioxide in the atmosphere

f_g=combined CO2 and temperature correction factor (function of CO2 as given above.)

f_{SR}=spreading rate factor (determined from geologic record)

f_A=land area factor (determined from geologic record)

Some of the interesting assumptions used in the BLAG model were 1) that temperature was a function of atmospheric CO_2 (function based on previous global weather models), 2) that organic carbon cycling was unimportant to the global carbon balance, 3) that runoff was constant throughout the simulation, and 4) that increased CO_2 in the air does not affect weathering rates, except by its effect on temperature.

Volatile production and recycling: Zhang and Zindler (1993) developed a highly aggregated model of volatile circulation between mantle and surface (crust and atmosphere), in which material was conserved in a cycle. For gases, including carbon dioxide and nitrogen, mantle degassing was proportional to the amount present in the mantle, and to a factor exponentially decreasing with time (analogous to deep heat production). Recycling of gases into the mantle from the surface was proportional to the amount of gas in the aggregated surface storage (crust and atmosphere).

Figure 1-6 is a general systems version of Zhang and Zindler's model, with the author's original equations in the legend. The diagram resembles Benard type models presented in chapter 4, except that none of the pathways are autocatalytic.

Simulation of Zhang and Zindler's model showed an initial peak of gas in the surface compartment during early Archean time, followed by exponential decline to the present. Computed bulk mantle recycling rates agreed with those independently calculated by Taylor and McLennan (1985). Because of their reactivity and tendency to form solid compounds, carbon and nitrogen recycled to the mantle at much greater rates than noble gases.

Zhang and Zindler further proposed that the early peak in atmospheric carbon dioxide might have led to more dolomite formation in ancient times. High carbon dioxide levels may have led to fast rates of carbonate precipitation,
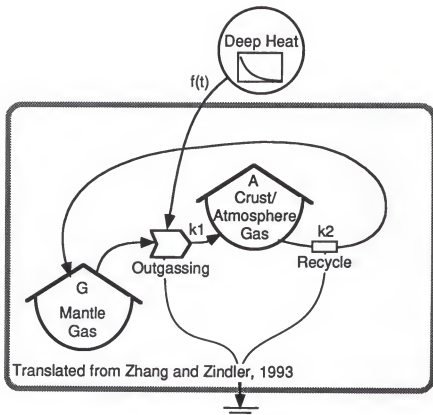
Figure 1-6. Energy circuit language translation of Zhang and Zindler's (1993) model of volatile circulation between deep earth to the surface, with author's equations shown below.

$dG = -k1*G*f(t)+k2*A$

$A = TG-G$

$f(t) = e^{-k3*t} / (1+k4*(1-e^{-k5*t})$

where:

k's are constant coefficient values.

G= mass degassable gas in mantle

A= mass of gas in crust and atmosphere

TG= total mass of gas in crust, atmosphere and mantle.

f(t) is a somewhat complicated exponential function whose end result is very similar to a simple negative exponential. It is meant to represent interior earth heat declining over earth history.

first depleting calcium to make calcite and then using magnesium for dolomite. They did not address the problem of increased carbonate dissolution due to increased acidity of oceans under a high carbon dioxide atmosphere.

Continent growth and thermal evolution: Spohn and Breuer (1993) simulated a model of crustal growth, Earth heat flow, and mantle convection to study radioactive heat generation and its decline over geologic time. Their results suggested that mantle radiogenic heat production comprises about half of Earth's total heat outflow, and that initial mantle radiogenic heat production was approximately five times the present rate.

Spohn and Breuer assumed that continent production was proportional to ocean area and to speed of mantle convection, and that continent loss (recycle into the mantle) was proportional to continent area and to mantle convection speed. Thus, they aggregated all continental loss mechanisms into a single process. They made mantle convection speed proportional to the temperature difference across the whole mantle, and also influenced by the viscosity of the mantle, which depended upon absolute temperature of the upper mantle. Their original equations are shown in Table 1-4. The intricate and complex nature of the model made it not amenable to translation into energy circuit language.

The authors simulated relative continental surface area, crust production rate, mantle heat flow, and temperatures in the lower and upper mantle over historical time, and found good agreement with observational constraints when U (the Urey ratio of radiogenic heat production to total heat flow) was set to 0.4 for the present Earth and when Σ (the ratio of initial Earth radiogenic heat production to present radiogenic heat production) was set to 5. Simulation results indicated quick initial growth of continents followed by a leveling at about 3 billion years ago, when close to 90 percent of the continental volume

Table 1-4. Original equations for the simulation model of Spohn and Breuer (1993)

$$dV/dt = dV_p.dt - dV_r/dt$$
$$dV_p/dt = [A_o/4\Pi R_p^2]^{1/2} (V_{max} - V_c)/R_p x_p u$$
$$dV_r/dt = A_c x_r u$$
$$u = u_0 Ra^{2\beta}$$
$$Ra = [\alpha g(\Delta T_s + \Delta T_c)(R_p - R_c)^3]/kv$$
$$v = v_0 e^{(A/Tu)}$$
$$dTu/dt = [-(A_0 q_{os} + A_c q_{mc}) + A_{co} q_{co} + V_m Q_m] / \rho_m C_m V_m n_m$$
$$q_{os} = k (Tu - T_s)/\partial_s$$
$$q_{mc} = q_{cs} - Q_c D_c$$
$$q_{co} = k(T_{cm} - eT_u))/d_c$$
$$Q_m = Q0e^{(-\lambda t)} - Q_c V_c/V_m$$

where:

V=continent volume
Vp=continent production
Vr=continent recycle into mantle
A0=Ocean area
u = speed of mantle convection
Ra=rayleigh number for convection determination
ΔTs=temperature difference across the crust
ΔTc=temperature difference across the core/mantle boundary
v=mantle viscosity
Tu=upper mantle absolute temperature
Ts=surface temperature of Earth
qos=oceanic surface heat flow
qco = heat flow from core into mantle
All other parameters are system constants.

was present. They also showed an approximately exponential decline in temperature of the upper and lower mantle over Earth history.

Punctuated tectonic evolution: Davies (1995) developed a simulation model of the thermal evolution of upper and lower mantle to study stratification and overturn in the mantle. His results suggested periodic ancient mantle overturns have been replaced by modern style plate tectonics as the main mechanism of mantle heat dissipation. He proposed that catastrophic ancient overturns affected surface conditions and frustrated the development of life.

Davies' model included radiogenic heat production, heat transfer between lower mantle, upper mantle, and the surface, and mantle layering breakdown criteria. The thermal evolution equations (Table 1-5) were simulated until one of two mantle overturn conditions were met. Then, convection was assumed to immediately equalize reservoir temperatures, after which thermal evolution was again allowed to proceed.

Model of global biological metabolism and carbon dioxide: Odum (1995) modeled the world system of surface carbon exchange in an aggregated overview shown in Figure 1-7. His minimodel included total biospheric production, carbonate precipitation, and fuel burning to study possible future changes in atmospheric carbon dioxide. The diagram illustrates at a glance the main system interactions that build organic matter and carbonate from carbon dioxide and sunlight. The simplified equation for limestone production suggests carbonate precipitation is a function of bicarbonate and sunlight (primary and secondary production were aggregated together to simplify the treatment of plants and animals precipitating carbonate), as ocean organisms produce organic matter and shells, and that high atmospheric carbon dioxide turns the limestone into bicarbonate.

Table 1-5. Original equations for the simulation model of Davies (1995)

$$dT_u/dt = H/C_m + (Q_{tz}-Q_s) / M_uC_m$$
$$dT_l/dt = H/Cm + Q_{tz} / M_lC_m$$
$$Q_s = [a_s(T_u-T_s)^{1+ns}] / n_u^{ns}$$
$$Q_{tz} = [B_za_z\Delta T_d^{(1+n_c)}] / n_l^{n_z}$$
$$\Delta Td = T / [E / R_gT -1]$$

where:

T_u = Temperature, upper mantle
T_l = Temperature, lower mantle
T_s = Temperature, surface
Q_s = Heat flow, mantle to surface
Q_{tz} = Heat flow, lower to upper mantle
ΔT_d = temperature difference, across boundary of upper/lower mantle
All other symbols are constants in the model.

WORLDCO2
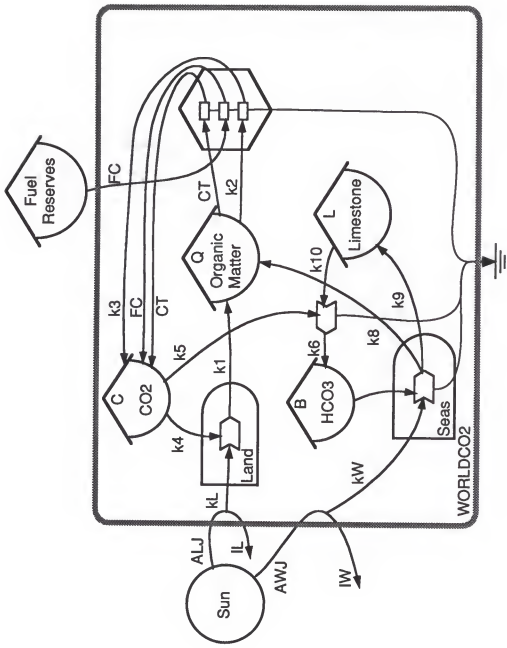
Figure 1-7. System of carbon cycling and exchange at the surface after Odum (1995), with author's equations shown below.

IL = ALJ/(1+ kL*C)
IW = AWJ/(1 +kW*B)
TC = B + C + Q + L + FC
dQ/dt = k1*IL*C +k8*IW*B -k2*Q -CT
dB/dt = k6*C*L -k7*IW*B
dL/dt = k9*IW*B -k10*C*L
dC/dt = CT +FC +k3*Q -k4*IL*C -k5*L*C
where:

IL = unused land insolation
IW = unused sea insolation
ALJ = land insolation
ALW = sea insolation
TC = total carbon in system
B = bicarbonate
C = atmospheric CO2
Q = organic matter
L = limestone reserve
FC = fuel consumption
CT = forest clearing and combustion

Simulations closely reproduced observed seasonal variations in carbon dioxide concentration, and suggested that forest regrowth could effectively counterbalance atmospheric additions from fuel burning. Results also indicated that CO_2 fertilization was more important than forest clearing to the overall carbon balance. Further, the simulations indicated that carbon dioxide concentration could stabilize at about 410 parts per million, even if present rates of fuel burning continued indefinitely. Increased organic production and higher bicarbonate formation rates helped hold down atmospheric CO_2.

Carbon cycle with human inputs: Walker and Kasting (1992) developed a carbon cycle model that examined the effects of fuel use and forest clearing on atmospheric carbon dioxide. Their simulation model aggregated Earth carbon into eight storages, six in the ocean, one in the biota, and one in the atmosphere. Carbon transfers between these reservoirs were functions of mixing and of diffusion. Average surface temperature depended on a simple heat balance, with heat loss a linear function of the temperature. Carbon emissions from fuels and forests were based on exogenously determined scenarios, including a "business as usual" case, a no-forest-clearing case, and a case of limited fuel burning.

The model consisted of 97 differential equations, which covered phosphorus, three isotopes of carbon, and alkalinity in each of the ocean reservoirs, and carbon dioxide and surface temperature for the aggregated surface compartment. Simulation results indicated carbon dioxide levels would peak at 5 to 7 times the pre-industrial level near 2400 A.D. Also, to keep atmospheric carbon dioxide under 500 parts per million, fuel burning would have to be immediately and permanently reduced to one fifth of its present level. Finally the results were much more affected by changes in fuel use than by

altered forest clearing practices. Because of the very large number of
equations, no energy translation was attempted.

Atmosphere, climate, and temperature

Many authors have proposed models to explain empirically observed
secular oscillations in northern hemisphere glacial activity and to study its
possible relation to greenhouse warming of the planet resulting from industrial
carbon emissions (See for Example Milankovitch, 1941; Hays et al., 1976;
Sergin, 1979; Broecker, 1991). In addition, astronomical calculations of long-
term changes in solar output have raised questions about Earth's temperature
regulation. Simulation models of atmospheres, glaciers, and oceans have
been developed to explain observed patterns and predict those in the future.

Sergin's model of glaciers, oceans, and atmosphere: A model
describing the global process of glacier formation was developed and
simulated by Sergin (1979). He used complex differential equations for two
aggregated Earth compartments (ocean heat and glacial mass), and produced
an internally oscillating glacial mass very similar to the empirical record of Plio-
Pleistocene glaciation. The simulation initiated glacial oscillations in the late
Cenozoic, reproduced climate in the southern hemisphere, and reproduced
global sea levels and mean hemispheric temperatures. All of these results
were in reasonable agreement with historical trends from isotopic and
paleontological records.

An energy circuit language version of the simplest case of Sergin's
model is shown in Figure 1-8, with the author's original equations and their
expanded form listed in the legend. The diagram illustrates the multiple
pathways of many powers (i.e. linear, autocatalytic, quadratic) by which ice
accumulates. Although not shown in the diagram, Sergin's ablation function for
ice loss also included an autocatalytic accumulation. Thus, the model was

Sergin's GOA Model
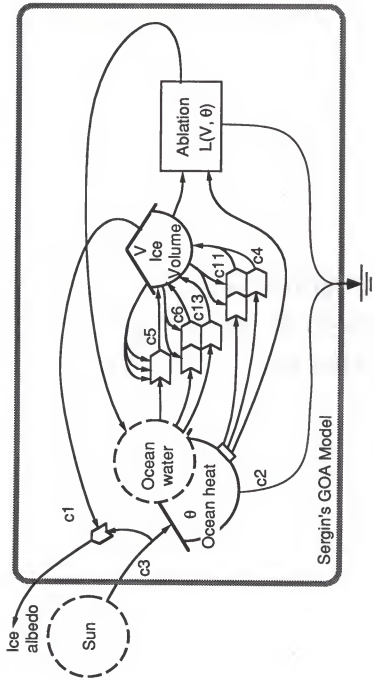
Figure 1-8. Energy circuit language translation of Sergin's (1980) simplest case model of the system of glaciers, oceans, and atmosphere, with author's equations given below. Dashed elements inferred for continuity and clarity.

$$d\theta = k1*[k3*S + k4*\theta + k5] \text{, which has the form:}$$

$$c3 + (-c1)*V + (-c2)*\theta$$

$$dV = [1 + ka*V]*[ke*\theta*V + k10*S*V + k11*V + kc*V*L + kd*L] \text{, which has the form:}$$

$$c4*\theta*V + c5*V3 + c6*V2 - c7*V2*L + c11*\theta*V + c12*V2 + c13*V + (-c14)*V*L$$

$$dL = (kf*V/[kg*V + Kh])*(k15*\theta + k16*S + k17) - ki*L \text{, which has the form:}$$

$$f(V)*[c8*\theta*L + c9*V*L + c10*L],$$

where:

c's are coefficients, constant over the simulation period
θ = average surface temperature in the northern hemisphere
V = volume of northern continental ice
L = ablation rate (loss rate) of northern continental ice
S = ice surface area, directly proportional to V
f(V) is a limiting factor curve for increasing V

composed of 3 accumulated storages representing two possible pulsing pairs: 1. ocean heat and ice volume, and 2. ice volume and ablation. Sergin's model and simulations did not make clear which pair was responsible for the oscillation, but the combination of linear, quadratic, and cubic pathways, as in the model, often produces pulsing oscillations.

Daisyworld, a model of thermal regulation: Watson and Lovelock (1983) developed an aggregated model of thermal regulation called Daisyworld. In their model, competitive species of plants with temperature-optimum growth rates stabilized surface temperature at the optimum by influencing planetary albedo. Their results suggested that simple systems with feedbacks and optimal environmental responses can adjust their environment towards the optimum.

Figure 1-9 gives an energy circuit language translation of the Daisyworld model, with the author's simulation equations included in the legend. The general systems model clearly shows three key aspects of the model: the competition for area between the daisy species, conservation of total area limiting total growth, and growth rate optimum based on local temperature. As illustrated in the diagram, the two species of daisies had exactly the same coefficients of growth and decay, except for the effect of local temperature. This temperature was an indirect function of the relative areas of the daisy species, by way of albedo. Overgrowth by either species would lead to deviation from the temperature optimum, creating a negative feedback to restore species balance and optimal conditions.

To analyze the thermal behavior of Daisyworld, Watson and Lovelock used analytical solutions in the case of steady state, but the model was amenable to simulation. For varied values of solar intensity, the authors found regulation of temperature near their arbitrarily set growth optimum of 22°C.
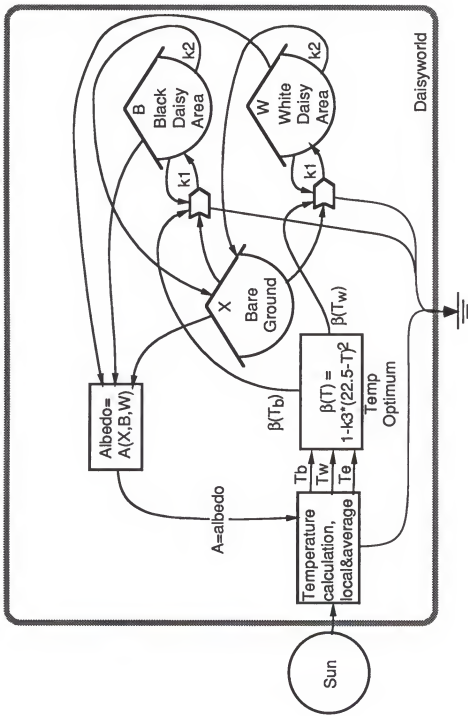
Figure 1-9. Energy circuit language translation of Daisyworld (Watson and Lovelock, 1983), a hypothetical world where only two species of plant grow, black daisies and white daisies, with equations below.

$dW = W*(X*β(T)-γ)$, which has the form $k1*X*W*β(T) -k2*W$

$dB = B*(X*β(T)-γ)$, which has the form $k1*X*B*β(T) -k2*B$

$X=TA-W-B$

$A = 0.5*X+0.25*B+0.75*W$

$β(T) = 1 -k3*(22.5-T)^2$

$Te = k4*(1-A)^{0.25}$

$Tw = Te -k4*(A-0.25)$

$Tb = Te +k4*(0.75-A)$

where:

Except for k1b and k1w, k's are constant coefficient values

X= bare ground

W= area covered by white daisies

B= area covered by black daisies

TA = total area, which is constant, i.e. X+W+B=constant.

$β(T)$ = growth rate of all daisies, a function of temperature

A= planetary albedo, an area-weighted average of the albedos of bare ground, black daisies, and white daisies.

Te = average surface temperature, a function of the heat balance between incoming solar radiation and outgoing infrared heat; this depends only on average albedo A.

Tw = local temperature of white daisy area, which is estimated as a linear function of albedo difference from the average.

Tw = local temperature of black daisy area, which is estimated as a linear function of albedo difference from the average.

They also found temperature regulation behavior when the model was modified to include a cloudiness function based on areas of daisy species.

Global climate models: Because of the everyday influence of weather on the human economic system, many climate simulation models have been developed to predict short range phenomena such as the path of storms, likelihood of tornadoes, and outbreaks of cold air in temperate zones. Although very little of this simulation has been done with overview models of the type used in this study, a brief review of the efforts is provided.

While weather forecasting models often concentrate on small areas of the Earth, climate models are truly global in scope. Their purpose is to simulate whole-earth climate conditions and changes resulting from perturbations such as increased carbon content in the atmosphere.

Budyko (1969) and Sellers (1969) independently developed one dimensional global climate models that relied on an energy balance approach. Although they accurately calculated many Earth parameters, these models proved very sensitive to small perturbations of incoming energy and led to further investigation of climate stability (Henderson-Sellers, 1987).

Radiative-convective climate models, in which convection is assumed to maintain a certain temperature decline with height in the atmosphere, were being developed at about the same time (See Manabe and Strickler, 1964; Manabe and Wetherald, 1967; and Hansen et al., 1981). These models had more robust temperature regulation.

Another class of climate models is the statistical-dynamical models, which focus on the interaction of traveling low pressure systems, such as cold fronts, with relatively fixed motions of trade winds and tropical Hadley cells (See Green, 1970; Potter et al., 1979; and MacCracken and Gann, 1988). These models divide the atmosphere into a few layers, and use averaged parameters

over large surface areas to study climate motions. Statistical dynamical models have helped study large scale atmospheric eddies and have roughly established some of their properties.

The most popular and commonly used class of climate model today is the general circulation model, which divides the atmosphere into a three dimensional grid of boxes on the scale of hundreds of miles on a side (See for example Hansen et al., 1983, Manabe and Wetherald, 1975). The behavior of each box is calculated with a number of equations based on physical laws that relate mass, energy, momentum, pressure, temperature, and humidity. Changes to any box are induced by flows of material and energy crossing the boundary from adjacent boxes.

General circulation models have been used to predict effects on climate of changes in, for example the speed of Earth's rotation, the amount of CO_2 in the atmosphere, and the rate of solar insolation. (See Hansen and Lacis, 1990; Washington and Meehl, 1989; Stouffer et al., 1989). Although there is considerable variation of results among the main models being used, they generally agree in direction of response of annually averaged parameters to perturbations. For example, each model responds to a doubling of atmospheric carbon dioxide with an increase in annually averaged surface temperature, but the increase in temperature varies among the models from about two to five degrees centigrade.

Global models of the economic systems

Marchetti's model of resource substitution: A vital issue in economics is resource depletion and substitution. Marchetti (1977) used a mathematically driven model of economic resource substitution to predict the type of fuel preferred by the global human economic system. His model made the

simplifying assumption that the growth of market share of a new energy source is proportional to the share of the market not penetrated by that energy source.

An energy circuit translation of Marchetti's model, which lists in the legend his original equations and their simplification for the energy diagram, is given in Figure 1-10. The diagram shows a simple autocatalytic growth of one storage fed by another, a very common configuration for general systems models. The model has no limits to energy sources and no storage depreciation.

Marchetti's model did not attempt to predict total fuel use, but only proportions of the total use allocated to each fuel. His plot of the simulations is a series of smooth, hump-shaped curves on a semilogarithmic plot, showing rising and then declining market share for wood, coal, and petroleum based fuels. Wood and coal, however, are presently being consumed at greater real rates than ever before, despite their lower market share.

Forrester's and Meadows' WORLD models: One of the most ambitious models designed to forecast resource depletion rate, population crest, and industrial and agricultural productivity was the WORLD model by Forrester (1971), which was subsequently modified and simulated by Meadows et al. (1972). These models aggregated Earth storages into those of resources, assets (capital), land, population, and pollution, and then developed complex controls on the input and output rates to the storages based on system storage levels. In this sense, the models were very similar to general systems models, in which flows (= rates) are normally proportional to a production function that depends on stored quantities in the system.

In order to compare the WORLD models with the energy systems models used in this study, the model of Meadows et al. (1972) was aggregated further in Figure 1-11, with some details omitted, such as the mechanisms of human
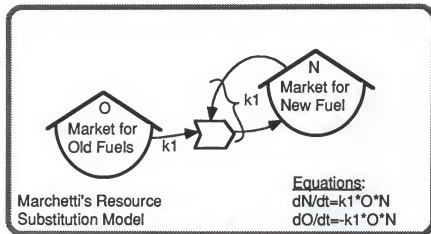
Marchetti's original equation: (1) $1/F * dF/dt = \alpha * (1-F)$
where F=market share, and α is a constant.
Rearranging: (2) $dF/dt = \alpha*F*(1-F)$
O = market for old fuels,
N=market for new fuels, total
market = N+O = M=constant.
Then   (3) $(1-F) = O/M$
                                      (4) $F = N/M$.
                                      (5) $dF/dt = d(N/M)/dt = 1/M * dN/dt$
Substituting (3,4,5) into (2):   (6) $1/M*dN/dt = \alpha*O*N*(1/M^2)$
or   (7) $dN/dt = (\alpha/M)*O*N$.
By conservation of total market   (8) $dO/dt = -(\alpha/M)*O*N$

Figure 1-10. Energy circuit language translation of Marchetti's (1977) resource substitution model, showing derivation of the kinetics from Marchetti's original equation.
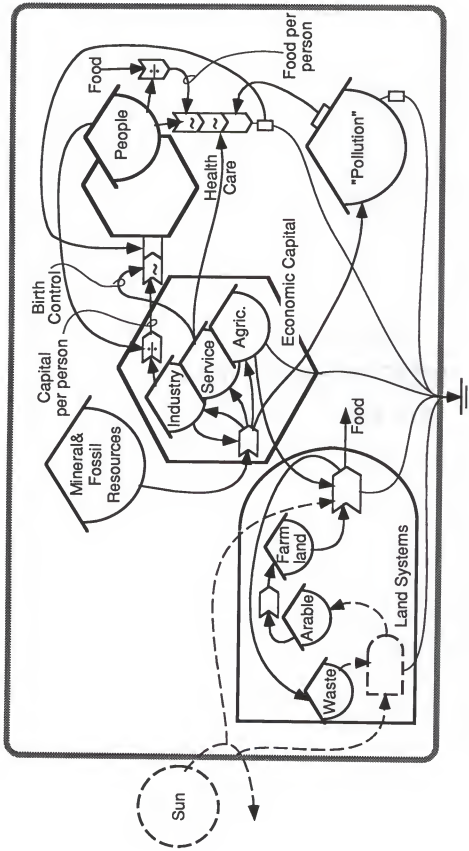
Figure 1-11. An energy circuit language translation aggregating the World model of Meadows et al (1972), with dashed elements inferred for clarity. Tilde symbol (~) in interactions indicating either a greater complexity or empirically determined relationship.

reproduction and aging. The form was simplified for understanding of the main processes and components. Dotted lines represent elements implied but not explicitly included in the WORLD models.

The simplified view of the WORLD model shows how ecological systems interact with capital to produce food. Industry (the consumer symbol in the middle of the diagram) is driven by nonrenewable energy and mineral resources. People are the rightmost (top of the hierarchy) consumer, who match the low transformity food items with high quality industrial output to build economic systems that feed back to draw maximum power. Pollution, produced by industry, is shown at bottom right, with pathways to natural systems and people's health.

The Forrester/Meadows WORLD models relied on large quantities of empirical data and educated assumptions, which were combined to define rates of inflow and outflow to the storages. For example, industrial output per capita was plotted against per capita resource use with just two points corresponding to the USA and world averages in 1970. Then a sigmoidal curve was fitted to these points based on the belief that more resources must go into agriculture when resources are limited, while more resources are used for structural maintenance when resources are plentiful. This sigmoidal curve was used to estimate industrial output at any particular time based on world resource use.

An interesting aspect of the WORLD models was their treatment of land and soil resources. Potentially arable land was converted to agriculture at a rate determined by development cost, agricultural capital level, land yield, and other variables. Arable land was then removed from agriculture in proportion to land wastage rates, determined by soil lifetimes. Once land was put into wastage there was no return to a productive state, and energy resources were

not used to help fertilize land and restore its productivity. The short time scale of simulations (200 years) may justify this approach.

A contrast between the WORLD models and the energy systems approach is the treatment of human fertility. The WORLD models used data on observed fertility versus GNP of various countries in 1970 to predict future global fertility. Because the world is interlinked and hierarchically organized, applying spatial correlations to temporal phenomenon may be inappropriate. A typical energy systems model might use industrial output as a multiplier to population production. Factors such as birth control and health care can be aggregated. The practice of aggregating complex sets of components may help avoid redundancy inherent in combining various empirical relationships.

The World models predicted growth in population and industry until the early middle 21st century, when decline of mineral and energy resources brought about leveling and decline in food, industry, and so population. Interestingly, their simulations suggested that degradation of fertile lands and rising pollution could limit industrial growth, even if nonrenewable resources were still plentiful.

Nordhaus' optimal emissions model: In order to recommend the appropriate level of government control on carbon dioxide emissions, Nordhaus (1994) developed a global model that contained aggregated representations of both economic and climate systems. Given the cost of reducing emissions and the damage incurred as a result of higher temperatures, his simulation model optimized the total level of industrial production and, therefore, predicted the best level of atmospheric carbon dioxide. He found that approximately 10% reductions in carbon dioxide would lead to the greatest industrial production, while limiting emissions to today's levels would cause large declines in production.

Figure 1-12 is an energy circuit language translation of Nordhaus' model, with the author's equations listed in the legend. The main model interaction is industrial production, driven by the implied (dashed) source of natural energies and materials. The production process is affected by T (temperature change), and μ (cleanup effort). Both of these tend to reduce industrial production. Cleanup effort, however, also decreases emissions, which in turn abates temperature change, and increases industrial production. For simplicity, the climate system was diagrammed here as a "black box", temperature determined by CO_2 levels and other greenhouse gases.

The energy circuit language diagram shows at a glance how the source μ, which stands for government cleanup effort, simultaneously affects both emissions (decrease) and clean-up costs (increase). Thus, the overall effect of changes in μ is a trade-off between less damage but more cost.

Nordhaus' original equations are given in the figure legend, along with their simplification to facilitate the energy language translation. Exponents 0.25 and 0.75 for the production function in Nordhaus model were intended to represent the declining marginal return on increasing capital and labor. This formulation may be necessary because of the way population and technology were determined outside simulation. In contrast, an energy systems model would include internal storages for population and technology, and would automatically simulate declining marginal returns, as one of the storages becomes limiting.

The climate system was composed of submodels for radiation balance and temperature change. A simple equation was used to describe the instantaneous radiation balance for the level of carbon dioxide. That radiation balance then drove the global heat model, which included temperature

μ Government

A Technology

O Other greenhouse gases

L People

Decarbonation σ

Natural Resources

$\Omega(\mu,T) = \dfrac{(1-k6^*\mu^{2.887})}{(1+k7^*T^2)}$

$L^{0.75}$

$K^{0.25}$

K Capital

k3

$Q = k1^*\Omega^*A^*K^{0.25}*L^{0.75}$

Production

k4*K

E

M CO2

$k5^*(M-590)$

Carbon Sink

$T = f(CO2)$

Temperature change

Legend facing page
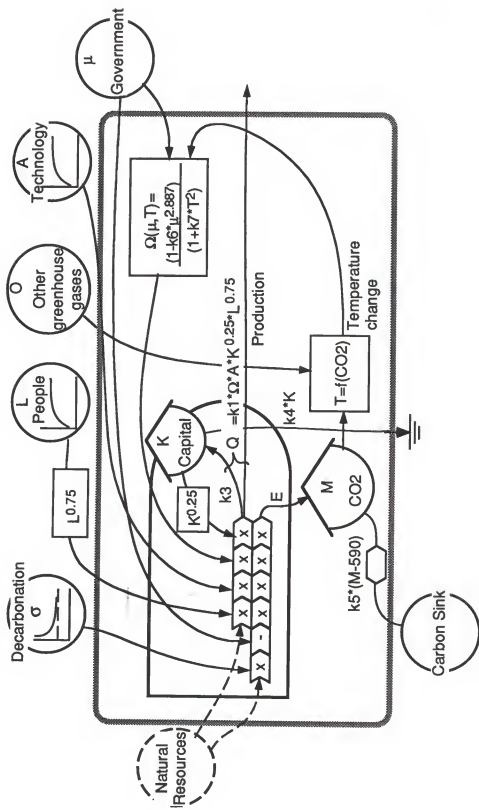
Figure 1-12. An energy circuit language translation of Nordhaus' (1994) model of economic production and carbon emissions, with dashed elements added for completeness. Author's equations given below.

Author's original equations	Which have the form of or imply
$Q = \Omega^* A^* K^{0.25} {}^* L^{0.75}$	$Q = k1^* \Omega^* A^* K^{0.25} {}^* L^{0.75}$
$Q = C + I$	$C = k2^* \Omega^* A^* K^{0.25} {}^* L^{0.75}$, and
	$I = k3^* \Omega^* A^* K^{0.25} {}^* L^{0.75}$
$K = (1-\delta_K)^* K_{(t-1)} + I_{(t-1)}$	$dK/dt = I - k4^* K$
$E = (1-\mu)^* \sigma^* Q$	$E = (1-\mu)^* \sigma^* \Omega^* A^* K^{0.25} {}^* L^{0.75}$
$M - 590 = \beta^* E_{(t-1)} + (1-\delta_M)^* (M_{(t-1)} - 590) + O$	$dM/dt = \beta^* E - k5^* (M-590)$
$F = 4.1^* [\log(M/590)/\log(2)] + O$	
$T = T_{(t-1)} + 1/R_1^* [F - \lambda^* T_{(t-1)} - R_2^* \tau_{12} [T_{(t-1)} - T^*_{(t-1)}]$	
$T^* = T^*_{(t-1)} + 1/R_2^* [R_2^* \tau_{12}^* T_{(t-1)} - T^*_{(t-1)}]$	
$D = Q^* \theta_1^* T^2$	
$TC = Q^* b_1^* \mu^{b2}$	
$\Omega = (1 - b_1^* \mu^{b2})/[1 + \theta_1^* T^2]$	$\Omega = (1 - k6^* \mu^{2.887})/(1 + k7^* T^2)$

where:
Q = production, K = capital, L = labor
I = investment, E = emissions of CO2
Subscript (t-1) means value of variable in previous time step
M = CO2 in air, β = fraction of emissions going into air
δ_K = fractional loss of capital, δ_M = fractional loss of CO2 excess
F = radiative forcing in watts, O = greenhouse gases other than CO2
T = average surface temperature, T* = deep ocean temperature
D = damage, production loss from climate, TC = cost of reducing emissions
Ω = combined damage and cost function.

accumulations by the deep and surface oceans, with appropriate heat capacities.

Nordhaus' model is a good example of the types of assumptions and equations employed in recent simulations, and it has the added advantage of being aggregated to a level that can be easily understood. Important explicit assumptions included future leveling of population and technology, linear depreciation on capital, and a quadratic dependence of damage (loss of production) on temperature. Unlimited resources, or infinite substitutability, was implicitly assumed.

Pulsing of urban structure on fossil fuel resources: Odum (1987) used a variation of a minimodel by Alexander (1978) to simulate production-consumption cycles calibrated for urban structure and fossil fuels. The diagram (Figure 1-13) shows the paired modules of slow linear resource production, and frenzied quadratic consumption, which use energy sources to cycle matter between a dispersed state and a highly concentrated, activated form (urban structure).

The model pulsed in an oscillatory fashion with a period of about one million years. The shape of the urban pulses closely resembled those projected by Hubbert (1972) for the fossil fuel era. Odum also calibrated the model for wood and soil biomass storages, which generated pulses on a much shorter time scale. He proposed the model was appropriate for such situations as the rise and fall of early Mayan culture.
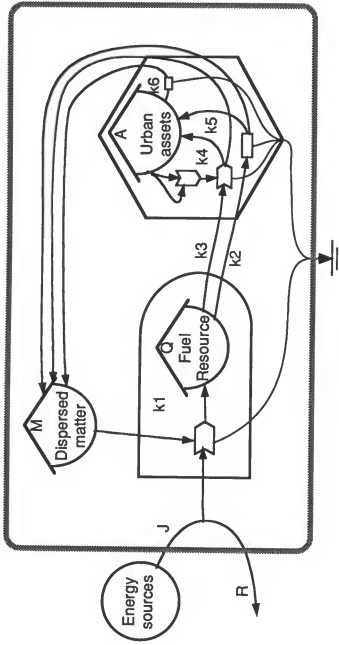
Figure 1-13. Production-consumption minimodel of fossil fuel and urbanization with quadratic pulsing mechanisms after Odum (1987). Author's equations shown below.

$R = J/(1 + k0 \cdot M)$

$dQ/dt = k1 \cdot R \cdot M - k2 \cdot Q - k3 \cdot Q \cdot A^2$

$dA/dt = k4 \cdot Q \cdot A2 + k5 \cdot Q - k6 \cdot A$

$M = K - k7 \cdot Q$

Where:
R = Unused energy sources
J = Energy inflow
K = Total material in cycle
A = Urban assets
Q = Fuel resources

METHODS OF MODELING AND SIMULATION

General Systems Modeling Philosophy

The philosophy of modeling used in this study was to start from the top down, which means starting from the general principles common to all systems as explained in Appendix D, and more fully elaborated on in Odum (1983), and somewhat in Von Bertalanffy (1968). For example, most systems in this study were modeled as consisting of one or more autocatalytic storages; i.e. storages that reinforce their own growth and actively acquire resources. General systems studies suggest this is the type of storage that exists and serves as a systems building block in the real world. This is also the type of storage that helps a system maximize power, which may be the direction in which all systems evolve (Lotka, 1925; Odum, 1983).

In general systems modeling, so called random variation is seen as noise from the next smaller scale, while stochastic or episodic events are seen as pulsing from the larger scale. All interactions, storages, and processes, therefore are determinate in the general systems model. System trends, overall behavior, and sensitivity to perturbations are the most important insights to be gained from the simulations, whose predictive power should be examined in light of possible, unknown inputs from processes on different scales.

The most important element of the general systems model is the diagram, which includes all information needed to specify system behavior, and shows all this information in a coherent framework. Common flaws like storages with

no outflow, absence of driving energy, or the violation of conservation laws easily can be seen and corrected. Also and more significantly, system configuration can be examined to make sure that such general principles as hierarchical relations, autocatalytic growth, producer-consumer pulse pairs, and appropriate feedbacks are included in the model layout.

Contrasting general systems modeling is the bottom-up approach, which is used in most scientific modeling today, and often starts from empirical equations relating variables such as humidity, solar insolation, and plant production. These equations are then assembled to outline the whole system behavior, and they are simulated exactly the same way as those generated from general systems models.

Brief Description of the Process

The methods in this study involve using Energy Circuit Language, a symbolic diagramming and simulation structure that is based on general systems principles (See Odum, 1983). This language and the concepts behind it are described more fully in the Introduction section titled "Background on General Systems Theory. Global processes are simulated with the following methodology as illustrated by the demonstration model Bensed1, as shown in Figures 2-1 through 2-4 and Tables 2-1 and 2-2.

First an <u>overview energy systems diagram</u> (Figure 1-1, Introduction) is developed for the system of concern to map out the overall structure and interactions among the parts. Refer to the Appendix D for conventions of energy systems diagramming.

Next an <u>aggregated diagram</u> (Figure 2-1) is drawn to concentrate attention on the main driving energies and interaction modules, and to facilitate writing difference equations, the discrete form of differential equations which are

used in computer simulation. Numerical values are then assigned to pathways, sources, and storages using literature sources, calculations, and assumptions. Thus whole system structure can be quantitatively examined as a unit.

A labeled diagram (Figure 2-2) is then generated from a copy of the aggregated diagram, in which sources and storages are labeled with variables to be used in the simulation program, and flows are labeled with their coefficients. In some cases the entire equation for each flow is written into the diagram for extra clarity.

Difference equations (in Figure 2-2) are then written to explicitly define the relationship of the mathematics to the energetics. The diagram uniquely specifies these equations, which are the discrete form of differential equations from calculus. The equations are printed below the labeled diagram so that the mathematical model and the diagrammed model can be conveniently compared and examined together.

A calibration table (Table 2-1) is made that lists values and units for sources, storages, and flows, documents all literature sources, calculations, and assumptions used in obtaining the values, and shows how flow coefficients are calculated from flow equations and values for storages, sources, and flows.

Then a computer program (Table 2-2) is written, incorporating the difference equations and calculated coefficients, that simulates the behavior of the system through time. The program is debugged by running it with calibration values, and testing that all flows match the calibration flows.

The program is tested for accuracy and validated (Figure 2-3) against real data where possible. The program and coefficients may be changed to develop a better fit to observed time series.

Finally, <u>model behavior</u> (Figure 2-4) is tested under varied conditions to elucidate whole-system behavior, study emergent properties, and sometimes to predict future behavior of the system.

<div align="center">

<u>Simple Example</u>

</div>

In order to illustrate the methodology of modeling and simulation, a very simple general systems model was developed based on the concept of a Benard Cell (See Benard, 1900). This Benard model (Figure 2-1) illustrates the phenomena of receptive and activated storages, energy sources crossing the system boundary, and material conservation in a recycling flow.

In a general Benard model, an energy source or sources interact with a dispersed, low quality storage of materials to create an activated storage of high quality and concentration that feeds back to capture more energy. This configuration serves especially well for demonstrating the methodology used in this study, because it is simple and straightforward. The other simulation models used herein are more detailed and complex.

<u>Overview Energy Systems Diagram</u>

Figure 1-1 (See introduction) is an overview diagram of the Earth's sedimentary cycle system. It includes five main compartments: hydrologic systems, the aggregated tectonic realms of marine, mountains, and cratons from Veizer, the human subsystem, and the main connecting pathways between these compartments. It also includes those compartment details necessary and important to the purpose of the model, which is to highlight the main interactions between systems of people and those of large scale Earth dynamics.
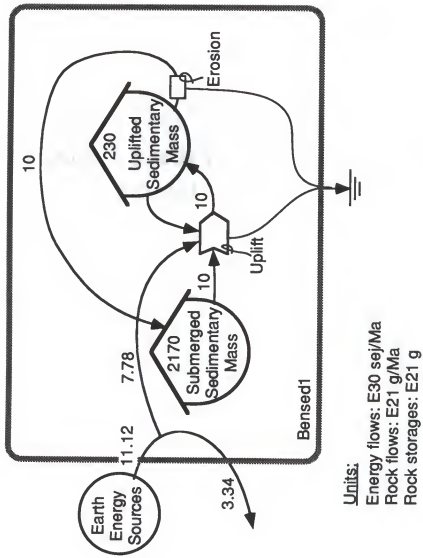
Figure 2-1. Example of simulation methods using earth's sedimentary cycle in extreme aggregate, modelled as a Benard Cell. Uplift and erosion as opposing yet linked processes in the overall cycle of material.

Units:
Energy flows: E30 sej/Ma
Rock flows: E21 g/Ma
Rock storages: E21 g

Aggregated Diagram

In Figure 2-1 , the elements of a Benard model are diagrammed very simply. The model is aggregated into two compartments, and is calibrated with data from the Earth sedimentary cycle. Here the Benard cell configuration is used to study Earth's sedimentary cycle in the broadest possible overview. All Earth energy sources have been lumped together. Likewise, sediments have been lumped into just two storages: those above sea level (uplifted) and those submerged below sea level. All processes using energy to create land storage have been aggregated into a single interaction, denoted by uplift, and the processes that return material to the dispersed, low quality storage have been classed together and labeled erosion.

Labeled Diagram

Figure 2-2, the labeled diagram for Bensed1, is a synthesis of much information concerning the overall state of the system, and conveys all the information needed to understand the simulation. This diagram shows Benard1, the same system as in Figure 2-1, except now the sources, storages and pathways are labeled with symbols used in simulating, and with calibration values used for calibration.

This diagram helps to quantitatively examine the relationships of all the components of the model. Units are specified, so that a quick glance can indicate how realistic the values are, and gives an idea of the relative magnitude of the flows, storages, and turnover times. This quantitative overview especially helps make sense out of more complex systems with many pathways.
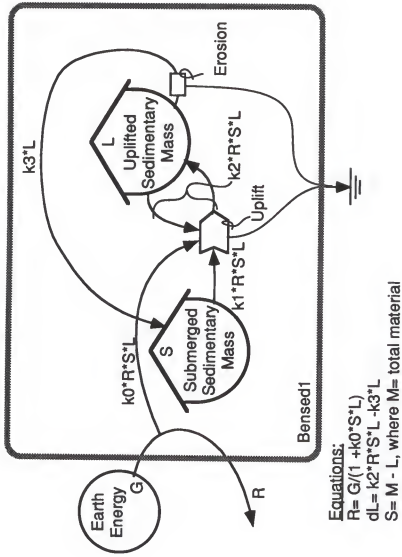
Figure 2-2. Aggregated sedimentary cycle model as in Figure 2-1, showing values of sources, flows and storages, labels for those items, and the simulation equations associated with the model.

Equations:
$R = G/(1 + k0*S*L)$
$dL = k2*R*S*L - k3*L$
$S = M - L$, where $M =$ total material

The diagram is then used to generate difference equations that fully describe the dynamic behavior of the model. These equations are written in below the diagram so that they can be directly compared to the model configuration. Thus all information needed to specify the model's dynamic behavior is contained in this diagram, Figure 2-2.

Difference Equations

At the bottom of the labeled diagram of Figure 2-2 , difference equations are written that describe the system's mathematical behavior. For example, the difference equation describing the rate of change of the storage L is: $dL = k2*R*S*L - k3*L$, where $k2*R*S*L$ is the inflow to the storage and $k3*L$ is the storage's outflow. In other words, the change in storage from one time interval to the next is the difference between inflow and outflow. In the equation $R = G/(1 + k0*S*L)$, limited-flow source mathematics are implemented, in which tapped flow is proportional to the amount not being used. The equation $S = M - L$ is a simple material conservation constraint, where the total material amount (M) in the system is fixed, as it practically is in the Earth system.

Calibration Table

Table 2-1, the calibration table for Bensed1, contains all information regarding information sources and model calibration, and as such is really a summary documentation of the development of the simulation program. Each source, storage, and flow is listed as a line item in the table. The information for each line includes a short description of the item, the symbol used in programming, and the calibration value with units. For pathways the flow equation (normally a multiplication of each component entering the interaction,

Table 2-1. Calibration values of sources, sources, and flows, and the calculated coefficients for Bensed1, the aggregated benard model of the sedimentary cycle, as diagrammed in Figure 2-2.

Item	Description	Symbol or Equation	Value	Units	Coeff.	Value
Sources						
1.	Earth energies	D=	11.12 E30	sej/Ma		
Storages						
2.	Sediments	S=	2170 E21	g		
3.	Uplifted sediments	L=	230 E21	g		
Flows						
4.	Unused energies	R=	3.34 E30	sej/Ma		
5.	Used energies	k0*R*S*L=	7.78 E30	sej/Ma	k0=	4.67E-06
6.	Uplift	k1*R*S*L=	10 E21	g/Ma	k1=	6.00E-06
7.	Land production	k2*R*S*L=	10 E21	g/Ma	k2=	6.00E-06
8.	Erosion	k3*L=	10 E21	g/Ma	k3=	4.35E-02

Notes to Table 2-1.
1. Taken as sum of solar equivalents of solar, deep heat and tidal energies (Odum, 1996)
2. Total sediments minus those uplifted on land.
   Total sediments=   2400 E21g   Dobrovolsky, 1994
   2400-230=   2170 E21g
3. Percent sed. material outcropping= 66% (Ronov, 1982). Land area= 150E6km^3 (Dobrovolsky, 1994). Mean land elevation= 875m (Ryabchikov, 1975). Then:
   Uplifted Seds= Outcrop%sed * Land area * mean elevation * density
   =66% * 150E6km^3 * 875m * 2.65kg/L * 1E6m^2/km^2 * 1000g/kg=
                           230 E21g
4. Total energy not used in earth system, taken as 30% after albedo.
   30% * 11.12=   3.34 E30sej/Ma
5. Used energies are those not lost to albedo in item 4.
   (1-30%) * 11.12=   7.78 E30sej/Ma
6. Uplift= continental denudation in steady state, use present day values obtained from Gregor, 1970   10 E21 g/Ma
7. Land production equal to uplift in steady state.
8. Erosion equal to land production in steady state.

unless indicated otherwise with a symbol inside the pointed bullet) and the calculated value of the pathway coefficient (the k values) are also shown.

For example, line item 6 in Table 2-1 would be read as follows: "Uplift equals J1, which equals the product of coefficient k1, unused energy R, submerged rocks S, and uplifted rocks L; the calibration value is 10E21 grams/million years. Therefore, the coefficient k1 must equal 6.00e-6. The coefficients are assumed to be valid for realistic storages values during simulation.

Documentation of literature sources, calculations and assumptions used in obtaining the numerical values in the model are contained in the table notes. The notes are numbered according to the line item they represent. Literature sources are fully specified in the Bibliography section of this dissertation.

<u>Computer Program</u>

Table 2-2 is a listing of the computer program for Bensed2, written in QuickBasic 4.5® computer language. It is very simple, and contains code to specify the source constants, the coefficients, and perform an iterative calculation for incremented values of time. It also has code to plot the results to the screen.

Typically, the program's syntax is verified by using a steady state initial condition, confirming that the system remains at steady state, and that the values obtained are those expected. If this works, realistic initial values are used, and model growth is examined.

If there are errors in program syntax, the model is debugged by checking each statement for syntax errors or logical errors. Debugging is often a time consuming process. Even a simple program like Bensed1 may have many small errors that need correction.

Table 2-2. Listing of the computer program for simulating Bensed1, the model in Figure 2-2.

```
10 ' ** PC Basic Simulation Program: Energy Circuit Model       **
20 ' ** Bensed1 Aggregated Benard Model of Sed. Cycle          **
30 CLS
40 SCREEN 9, 7: COLOR 7, 0
50 Xmax = 500: Ymax = 250   'Plot boundaries
60 Xoff = 25: Yoff = 25     'Plot offsets
70 LINE (Xoff, Yoff)-(Xoff + Xmax, Yoff + Ymax), 15, B
80 ' ** Next set the source constant                           **
90 G = 11.12
100 M = 2400
110 ' ** Next set the model coefficients                       **
120 k0 = 4.67E-06
130 k1 = 5.9988E-06
140 k2 = 5.9988E-06
150 k3 = .0435
160 ' ** Next set the iteration time step                      **
170 dt = .1' (million years)
180 ' ** Next set the plot scaling factors                     **
190 Sm = 2500
195 Lm = 500
200 tm = 200
210 ts = 0      'Starting year of simulation
220 ' ** Next set initial conditions                           **
230 S = 2390
240 L = 10
250 ' ** Start iterative loop here                             **
260 X = t / tm * Xmax
265 ' ** Plot statements follow                                **
270 PSET (X + Xoff, Yoff + Ymax - S / Sm * Ymax), 15
280 PSET (X + Xoff, Yoff + Ymax - L / Lm * Ymax), 15
285 ' ** Equations follow                                      **
290 R = G / (1 + k0 * S * L)
300 dL = k2 * R * S * L - k3 * L
305 ' ** Next update storages                                  **
310 L = L + dL * dt
320 S = M - L
330 t = t + dt
340 ' ** Repeat iteration if t < tm                            **
350 IF t < tm GOTO 250
360 END
```

Validation

After a model is debugged, real world data are compared to validate the model; to check its level of matching the real system under study. Figure 2-3 shows the simulation results for starting Bensed1 with initially very low values of uplifted sediments, possibly corresponding to a time on the early Earth when little uplifted sediments existed. The simulation showed uplifted sediments increased with a sigmoidal growth pattern, taking approximately 130 million years to reach steady state.

If the validity of the simulations are unsatisfactory, then the aggregated diagram is re-evaluated, with the simulation results in mind, to try to find a better configuration. This process can be cycled through many times in order to find the most appropriate model configuration for the scales and processes of interest. Bensed1 was a very simple model with little data to check against; however, it showed a response time on the order of a hundred million years, which may be appropriate for sedimentary uplift into mountain ranges (Veizer, 1988a). Extensive validation of Bensed1 was not done because of the simple nature of the model.

Model Behavior

When the model validity and correctness are satisfactory, test runs are made to check effects of different conditions on simulation results. This is the "what-if?" process of asking questions that are the basis for predictive management of any system. Here whole system performance and behavior is studied and emergent properties are sought.
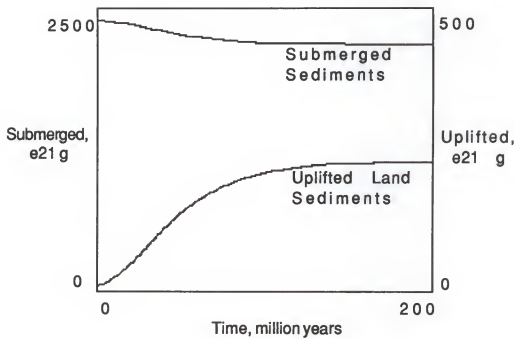
Figure 2-3. Simulation results of the model Bensed1, as shown in Figures 2-1 and 2-2, calibrated in Table 2-1, with program listed in Table 2-2. Most material initially was in the submerged sediment storage.

Figure 2-4 shows the results of a sensitivity study of the model Bensed1. The energy sources for the system were halved and doubled to gauge the effects of changing driving energies. As seen in the figure, the characteristic sigmoidal growth shape of the uplifted sediments was not altered. Greater driving energies not only led to higher levels of sediments stored on the continents, however, but also increased the speed with which steady state was attained. In this model, an increase in driving energies led to an even greater increase in the activated storage, with a linear response of activated storage to driving energy.
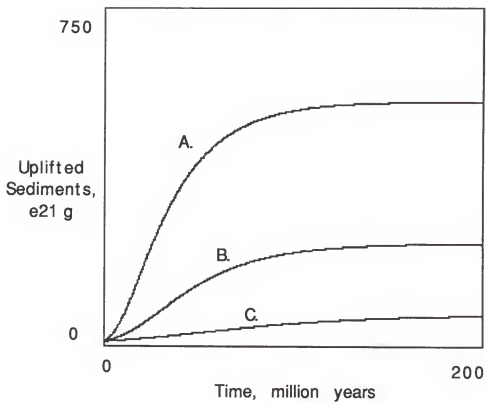
Figure 2-4. Sensitivity study of simulation results for Bensed1, the model in Figure 2-2, as calibrated in Table 2-1, with program listed in Table 2-2. A. Energy source doubled, causing faster growth to a higher stored amount. B. Base Case. C. Energy sources halved, causing slower growth to lower storage amount.

CHAPTER 3
MODELS OF THE SEDIMENTARY CYCLE

The narrowest definition of the sedimentary cycle includes only one-way movement of solid material from land to the ocean at the Earth's surface. In that sense, it is not a true cycle. In this study, the term sedimentary cycle encompasses the true circulation of all material in the Earth's crust and atmosphere, including solids, solutes, liquids, and gases. The sedimentary system contains nested loops of material transfers and the energy sources that drive them.

The hydrologic cycle subsystem includes storages of water in the ocean, on land, and in the atmosphere. These are linked by the flows of evaporation, rain, and runoff, with the overall cycles going from ocean to vapor to land, and back to the ocean via rivers. Embedded in the large cycle are the closed loop circulations of ocean to vapor and land water to vapor. The hydrologic cycle is a necessary subsystem of the sedimentary cycle, because water acts as a control for chemical reactions and physical transport of materials.

The surficial part of the solid material cycle is also sometimes referred to as the sedimentary cycle. It involves all processes that move or change solid material at the Earth's surface, including weathering, erosion, transport, deposition, lithification, and uplift. The solid sedimentary cycle is linked to the hydrologic cycle by the erosive and transport capacity of rivers, which contribute to uplift by lateral transport and loading. Cycles of water and material transfer on land, in the sea, and in the air are linked and interdependent, and all are driven by inflowing energies of sun, tides, and deep heat.

Production and Consumption of Sediments

Main Model

In order to better understand the organization and structure of the sedimentary cycle, the parts were hierarchically aggregated as suggested by the emergy per gram of important geological quantities, calculated in Table 1-1 of the Introduction. In Figure 3-1, ocean crust provides initial sediments that are consumed in mountain building. Emergent mountains reinforce their own growth and also contribute to cratons. Cratons, in turn, autocatalytically consume mountains in continent building, and slowly lose material that cycles back to sediments or returns to the mantle.

The system is divided into three main hierarchical levels: 1) ocean crust and sediments, 2) land sediments and mountain ranges, and 3) basement rock, or cratons. The definitions follow those of Veizer's (1988a) tectonic realms, as explained in the Introduction section "Emergy per Mass in the Sedimentary Cycle". These main storages are arranged from left to right in the diagram in order of increasing turnover time, total mass, and emergy per gram. Productive processes proceed from left to right, while controlling feedbacks and dispersing materials follow pathways from right to left.

The model in Figure 3-1 is a hypothesis of the important interactions, structures, and controlling feedbacks operating in Earth's sedimentary cycle. The system configuration is based on general systems principles and the calculated hierarchical position of the main self-organized storages. Possible mechanisms for four production influences are given in Table 3-1. The table shows four mechanisms for each of four pairs of processes and influences. For

88
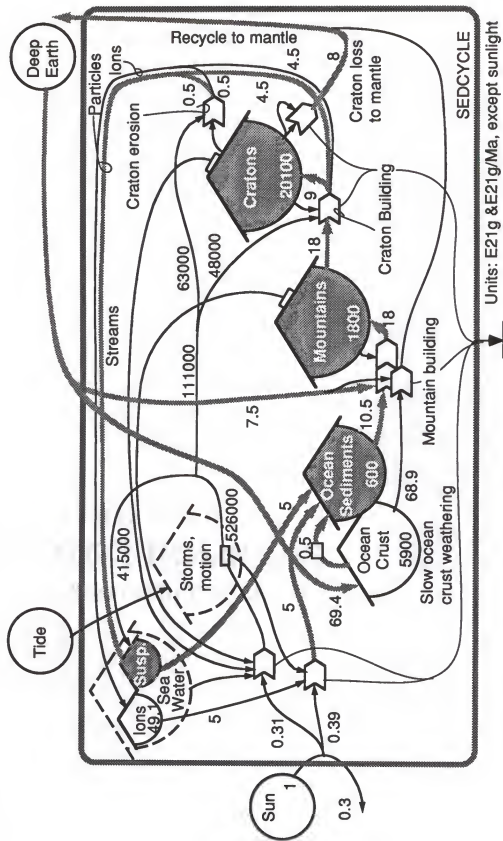
Figure 3-1. Hierarchical model of sediment production and consumption. Dashed elements with turnover time much different from the scale of interest. Ocean dashed denoting constant internal source, dashed storms signifying simple flow. Solar units standardized to one inflow.

Units: E21g &E21g/Ma, except sunlight

Table 3-1. List of possible mechanisms for four pairs of processes and influences in the sedimentary cycle model of Figure 3-1.

Item	Process	Influence	Mechanism
1	Mountain Building	Sediments	Provide material for collisional upthrust
2			Free Energy for volcanism
3			Lateral isostatic force on adjacent mountains
4			Form accretionary prisms
5	Mountain Building	Mountains	Isostatic uplift of low density material
6			Barrier to ocean plate movement force subduction
7			Cause atmospheric uplift, storms, erosion, further uplift
8			Force quick deep subduction, raise chemical potential
9	Craton Building	Mountains	Atmospheric uplift, storms, weathering, differentiation
10			Provide old mountain roots for deep craton layers
11			Breach sea level, weather faster, differentiation
12			Increase gravitational potential, pressure, metamorphism
13	Craton Building	Cratons	Provide altitude for mountains, weathering, differentiation
14			M-A-S-H process filter of magmatic material
15			Land area cause heat and humidity gradients, storms, weathering, differentiation
16			Reroute deep heat flow, intensify mantle convection

example, lines 1 through 4 give four ways that the sediment storage contributes to mountain building. The mechanisms shown are just a few of the many that may operate in the real world. Explicit inclusion of each and every mechanism would quickly lead to baffling complexity and high probability of model error.

Crustal material is shown recycling to the mantle in ocean crust subduction, which is coupled to mountain building, and directly from cratons. The model has this process proportional to the square of craton mass. The square function is often used with highest-level storages, to indicate a higher per unit loss of material at large storage amounts. Rea and Ruff (1996) estimated the rate of sediment subduction to be 2.5E21 g/Ma, and Reymer and Schubert (1986) calculated about 10% of subducted sediments actually returns to the mantle. Because 0.25 is very small compared to total sedimentary cycling of 10, this pathway was assumed to be zero.

Pathway values show the transfer of material in units of E21g/Ma. They were determined from literature sources and made consistent with the assumption of long-term average steady state for all storages. For example, a value of craton weathering of one (Dobrovolsky, 1994), and total craton turnover of 9 (Ronov and Yaroshevskiy, 1976, and Veizer, 1988a), were balanced by a calculated delamination loss of 8, all in units of E21g/million years. Future work can explore the effects of relaxing the steady state assumption for cratons.

Figure 3-2 is the same diagram of the hierarchically aggregated sedimentary cycle modified for simulation. Pathways are shown with their coefficient values, which appear in the differential equations at the bottom. The level of each storage is specified by one of the differential equations, and tapped flows appear as algebraic equations of the storages. Coefficients were
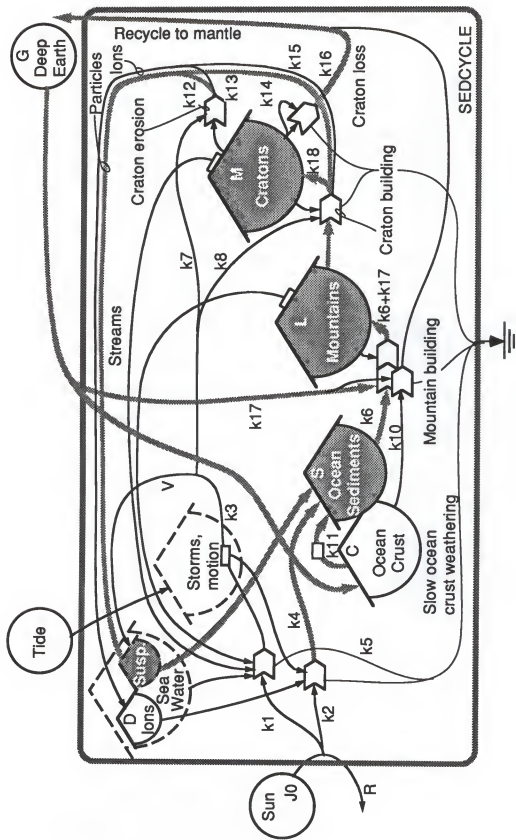
Figure 3-2. Aggregated hierarchical model of Earth's sedimentary cycle as in Figure 3-1, showing pathway coefficients. Model equations given below:

dD/dt= k12*M*V +k14*L*V -k4*R*D
dC/dt= k5*G -k10*C*G -k11*C
dS/dt= k11*C +k13*M*V +k15*L*V -k6*S*G*L
dL/dt= k6*S*G*L +k17*S*G*L -k14*L*V -k15*L*V
dM/dt= k18*L*V -k16*M² -k12*M*V -k13*M*V
R=J0 / (1 +k1*O*L*M +k2*D)
V= k3*O*L*M / (1+k7*M +k8*L*M)

calculated as shown in Appendix Table A-2, whose notes document all the assumptions, calculations, and literature sources used in obtaining the calibration condition of Figure 3-1.

Figure 3-3, part A., shows simulation results for the hierarchical sedimentary cycle model of Figure 3-1 , as calibrated in Appendix Table A-2, with computer program listed in Appendix Table B-1. Ocean crust quickly reached a steady value, followed by early growth of oceanic sediments. Then young mountains increased at the expense of oceanic sediments. They grew steadily and overshot their steady state value, and then triggered the growth of cratons, which then grew with a sigmoidal curve until the system reached steady state. Total material processing increased in steps as mountain ranges and later cratons developed and fed back to increase system performance.

In the simulation the total time required for craton growth was about 4 billion years and Earth system evolution took about ten billion years. This behavior contrasts both steady state assumptions in the model and most observational models of continental growth, which suggest rapid growth from about 4 to 2 billion years ago, followed by slower growth or steady state. This time frame may not be possible for a storage with turnover time as slow as 2.5 billion years, determined for continental roots by Veizer (1988a) from age studies of cratonic rocks. Therefore the model simulation suggests that either the actual turnover of cratons is faster than that used, or the real system has yet to achieve steady state.

In order to explore the effect of declining deep heat over time, the deep Earth source was started with a larger value that decreased exponentially during simulation. The formula for declining deep heat was that of McGovern and Schubert (1989), for radiogenic heat production. This formula for exponential decline is a strong oversimplification, because many factors
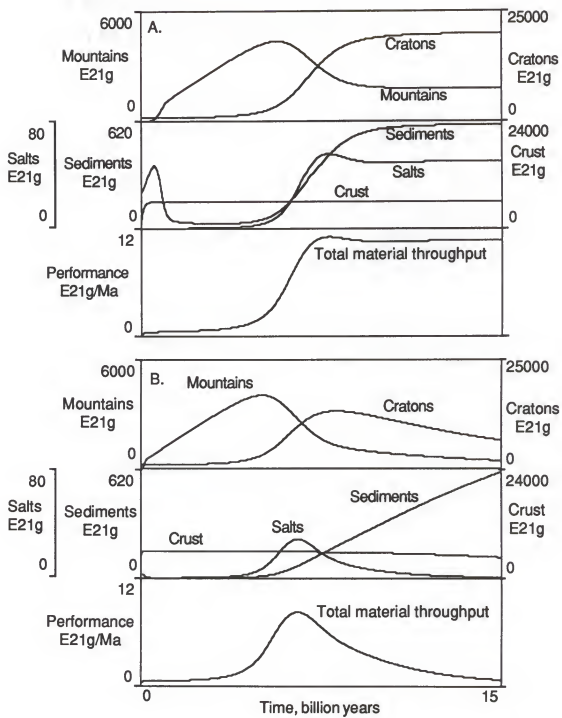
Figure 3-3. Simulation results for the model in Figure 3-1 and 3-2, as calibrated in Appendix Table A-2, computer program listed in Appendix Table B-1. A. Base case, and B. with exponentially declining contribution from deep earth as described in text.

influence overall Earth internal energy storage. These include declining radioactive heating; dwindling residual heat from the core; changing tidal and gravitational heat; increasing resistance to heat flow of growing continents; concentration of radioactive elements in continental crust; increased transfer of pressure in geosynclines; increased material cycling from growth of continents, enhanced free energy in surface sediments transferred to the deep Earth and mantle; and slowed mantle convection with cooling temperatures.

In Figure 3-3 part B, the scale for sediments was enlarged by a factor of ten, but the model behaved essentially the same as the base case for the first seven billion years. Then mountain building stopped processing sediments, which increased to over ten times the base case amount. Cratons, young mountains, and total material throughput subsequently declined as Earth's energy diminished. These results suggest that, if radiogenic heat is a major component of deep Earth energy, mountains and cratons may undergo significant reduction in size as surficial energy of sun, wind, and rain drives erosion faster than mountain building.

Model with Pulsing Pathways

To investigate pulsing characteristics of the hierarchical sedimentary cycle, the model of Figures 3-1 and 3-2 was modified, as shown in Figures 3-4 and 3-5, to include both quadratic and linear pathways between the storages (shown as dotted lines in the figure). Linear pathway depend only on the mass of the donor storage, while quadratic pathways are in proportion to the product of the donor storage and the square of the receiver storage. For example, the linear pathway from mountains to cratons is a linear function of mountain mass, and could represent slow, metamorphic conversion of mountain roots and sediments into cratonic rocks. The quadratic pathway is a product of the
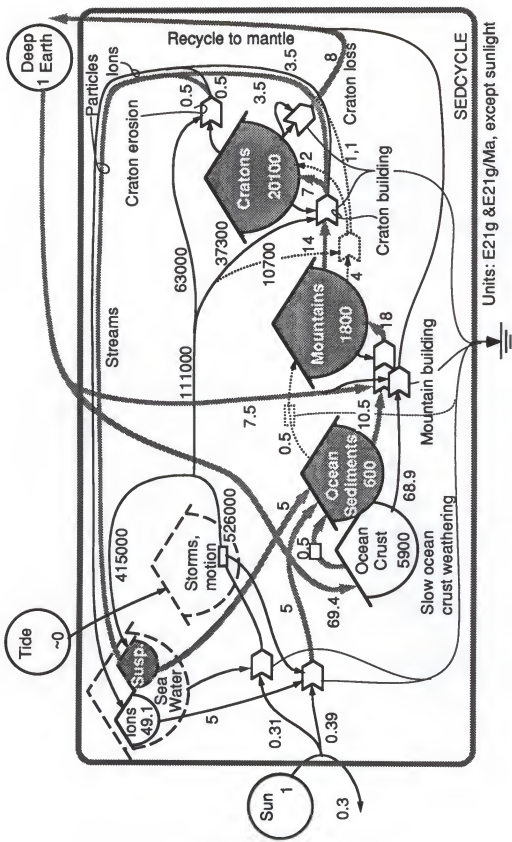
Figure 3-4. Hierarchical model of sediment production and consumption, showing calibration condition for the addition of pulsing pathways (shown by dotted lines). Units: E21g &E21g/Ma, except sunlight standardized to one inflowing unit.
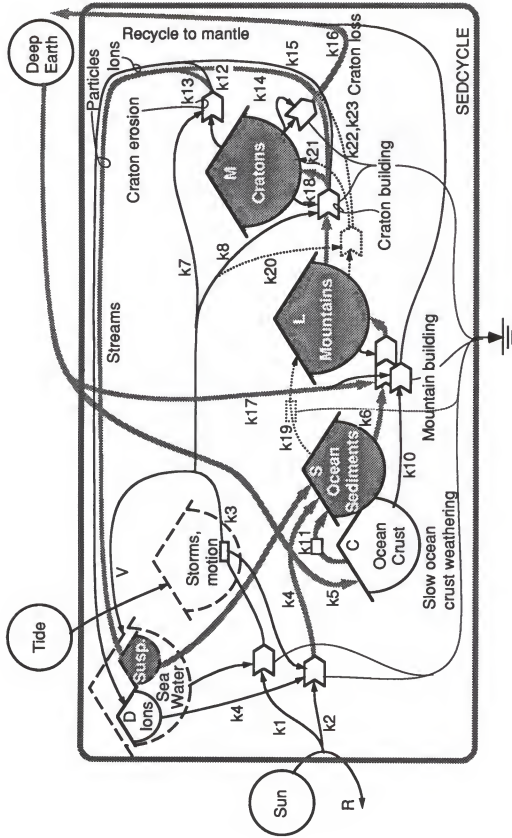
Figure 3-5. Hierarchical model of sediment production and consumption including pulsing pathways, showing pathway coefficients and storage symbols, which appear in the model differential equations below.

$dD/dt = k12*M*V + k14*L*M*V + k22*L*V - k4*R*D$

$dC/dt = k5*G - k10*C*G - k11*C$

$dS/dt = k11*C + k13*M*V + k15*L*V + k23*L*V - k6*S*G*L - k19*S$

$dL/dt = k6*S*G*L + k17*S*G*L + k19*S - k14*L*M*V - k15*L*M*V - k22*L*V - k23*L*V$

$dM/dt = k18*L*V + k21*L*V - k16*M2 - k12*M*V - k13*M*V$

$R = J0 / (1 + k1*O + k2*D)$

$V = k3*R*O / (1 + k7*M + k8*L*M + k20*L)$

mountain mass and the square of the craton mass, and may model the way craton mass can increase both geopotential of mountains and their exposure to atmospheric volatiles, increasing weathering and erosion in two separate ways. Figure 3-6 gives simulation results for the sedimentary cycle model including these pathway modifications. When calibrated as in Figure 3-4 and Appendix Table A-3, simulation results were as shown in A. Pulsing behavior occurred only after system storages built up to sufficient values, so that the quadratic pathway for mountain growth could take over. Subsequent overshoot reset storages to levels that could initiate more pulses, with a pulsing period of about 3 to 4 billion years. In part B., initial storages were equal to their calibration values, and the system reached its steady state oscillation in about four billion years. As in the non-pulsing sedimentary cycle model, overall system dynamics were slow for the pulsing model, with initial transients of about 5 billion years. But pulsing dynamics allowed the system to develop large storages very quickly. Mountains built up in only a few tens of million years, and cratons followed with about a billion year time lag. Perhaps this timing reflects the period of fast and massive continent building in the late Archean proposed by many authors (for example, Taylor and McLennan, 1981, 1985, 1996; O'Nions, 1981; Armstrong, 1981; Veizer, 1988a).

Long system transients to the initial conditions suggest the real Earth system could be still evolving. Moreover, the behavior of slow evolution to a dynamically oscillating steady state offers a broader context in which to view the familiar debate of uniformitarianism versus evolutionism for the whole Earth.

Craton turnover time of 2.5 billion years should be taken as a maximum value, because it is based on Veizer's ages of detrital zircons with Uranium/Thorium-Lead aging systematics. This aging system reflects elapsed time since extreme events of melting or strong metamorphism, and may be
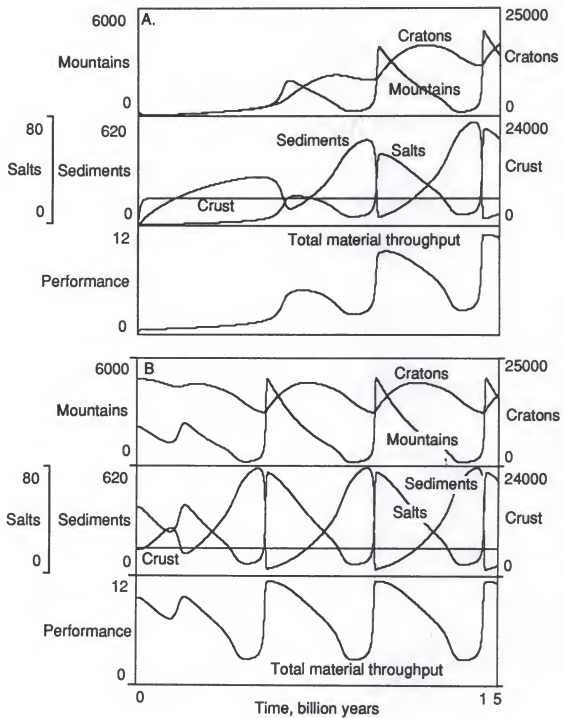
Figure 3-6. Simulation results for the hierarchical model of sediment production and consumption including pulsing pathways as in Figure 3-5. All units either E21g or E21g/Ma. A. Base case starting with low storage values. B. Initially high storages.

inappropriate for the system as defined in Figures 3-1, 3-2, 3-4 and 3-5, because cratons can lose material by simple erosion and regain that same material without melting or metamorphism. Shorter turnover time, or an increased rate of craton outflow in the model calibration, would speed system response, perhaps better reflecting present concepts of Earth evolution.

In Figure 3-7, the linear contribution to young mountains was adjusted to the limits of pulsing behavior. Part A. shows that the result of a ten percent increase was a dampening of oscillations. In part B, a 25 percent increase delayed the onset of pulsing to about 8 billion years. Further changes in this pathway shifted the system to a non-pulsing regime. The system pulsed over a somewhat narrow range of this parameter, reflecting typical model sensitivity to changes in many other variables (not shown).

To gauge the impact of human civilization on the overall sedimentary cycle, erosion and transport processes were accelerated in the model starting from a steady state condition (Figure 3-8). Estimates of human induced erosion range as high as 1.5 times the pre-industrial rate (see Gregor, 1970; Garrels and MacKenzie, 1971), but it is likely that most of this enhancement is due to depletion of soil, which can only be a short term phenomenon. Acceleration, therefore, was simulated for long-term gains in the erosion rate of 10, 25, and 50 percent, by adjusting the coefficients of chemical and particulate transfer to the sea, k12, k13, k14, and k15.

Figure 3-8, part A, shows the effect of surface weathering accelerated by 10%. Sediments initially increased as more were brought to the sea, but then decreased as mountain building used them up. The final result was larger cratons and more mountains, but less sediments, just the opposite of what might be expected, suggesting that more efficient use of surface energy could drive tectonic processes and influence overall Earth storages. Acceleration of
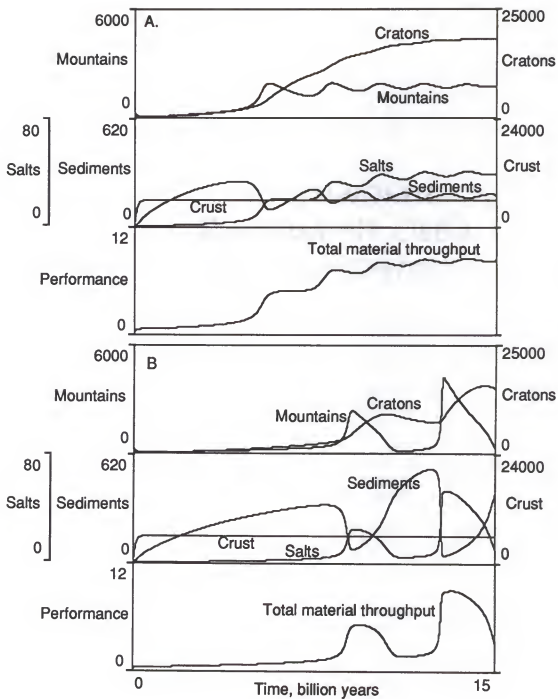
Figure 3-7. Effect of adjusting the linear contribution to young mountains, on the simulation of the hierarchical model of sediment production and consumption, with pulsing pathways added. A. Linear mountain building (pathway marked k19 on Figure SC6) increased 10%, and B. decreased 25%.
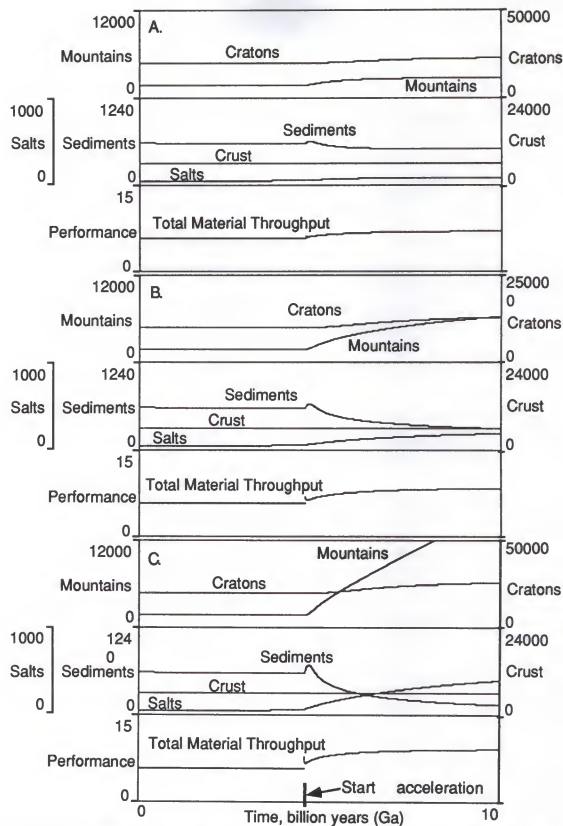
Figure 3-8. Response of the hierarchical model of sediment production and consumption to human induced acceleration of weathering and transport starting at 4.6 Ga. Acceleration of A. 10%, B. 25%, and C. 50%.

erosion by 25% (B.) and 50% (C.) further enhanced the mountain building process, leading to larger increases in mountain ranges and cratons. System performance, as measured by total sediment throughput, increased directly as the erosion rate.

Summary of Sediment Production and Consumption Model

The main features of the model were a division of the solid crustal sedimentary cycle into three storages of oceanic, mountainous, and cratonic material. These were arranged to highlight the hierarchical relationships among the components, and their interactions focused on the autocatalytic nature of mountain building and craton formation. The model simulated with a pattern similar to other continental growth models, but the timing of growth was somewhat longer in duration. The result suggested that Earth's transient response is long enough that evolution is still occurring even today. Alternatively, the half life of cratons, which measured their time to actual melting, may have been inappropriately long, because cratonic material can disperse to other reservoirs by weathering and incorporation into oceans and mountains, which doesn't involve melting.

In response to exponentially declining deep heat, the model behaved similarly to the base case of constant deep source, except that the continental size began a gradual downward trend after reaching a maximum. This occurred on similar time scale to the base case model. The major difference in this case of declining contribution, was that sediments increased linearly throughout the model simulation, to very large levels. This result suggests that the contribution of deep heat to the sedimentary cycle is not declining as fast as Earth's radiogenic heat production.

Inclusion of pulsing pathways in the model suggested a possible major internal period for Earth building events of around 3 billion years. This period remained constant for relatively large variations in calibration conditions, suggesting a robust pulsing regime. Evidence for similar pulsing in the real system should be explored.

<u>Hierarchical Configuration of Benard-Cell Blocks</u>

<u>Model Description</u>

An alternative configuration of the sedimentary cycle that emphasizes standard compartments at each scale is shown in Figure 3-9. The compartments were connected in series to stress the concept of transformity matching, in which storages of widely disparate quality must interact via an intermediate quality unit. Hence, a productive interaction may require components of similar concentration and quality. In increasing hierarchical order from left to right, the three compartments were atmosphere-ocean, sediment-mountains, and mountains-cratons, where vapor, mountains, and cratons represent hierarchical centers of increasing concentration and feedback work potential.

As explained in the methods section herein, a Benard cell is a chemical reaction in which a driving energy source energizes a certain portion of a disordered material pool in an autocatalytic fashion; i.e. the energized material feeds back to its own production process. Ocean water is an example of a disordered material pool, of which a small part is energized by a flow of solar energy. The energized vapor feeds back via many processes, including storms, to enhance its own production while using up solar energy. Thus the water cycle in aggregate overview exhibits the essential features of a Benard cell.
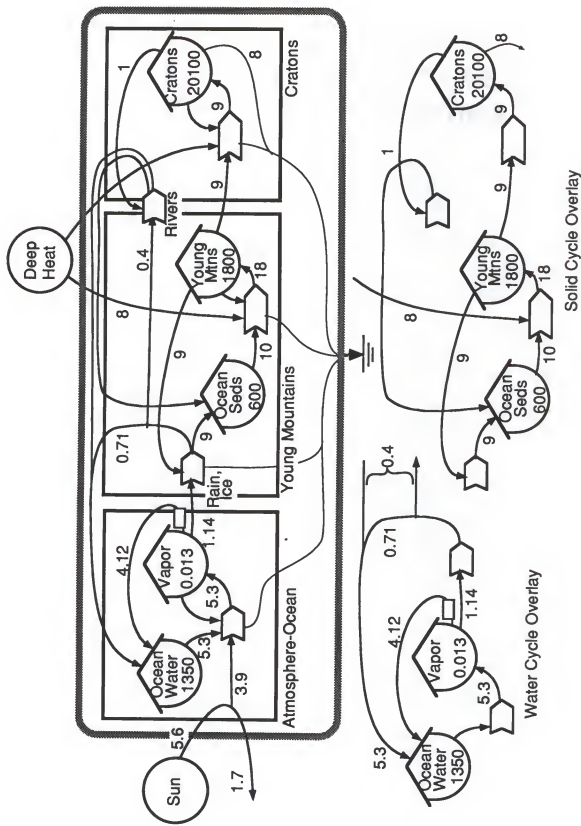
Figure 3-9. Diagram of the sedimentary cycle stressing the concepts of natural aggregation of systems into self-organized compartmental units, interacting according to the principle of transformity matching. Increasing concentration, territory of influence, and feedback work potential from left to right in hydrology, mountain, and craton compartments. Water and solid cycle overlays broken out to clearly show the cycling of those materials.

The mountain and craton building units similarly use energy and ordered storage to upgrade disordered, dispersed materials.

Figure 3-9 illustrates a hierarchical Benard-cell block model for the exogenic cycle. It is composed of three Benard cell blocks that are linked by transfers of material and energy. The left block contains the previously described ocean-vapor cell, the middle block contains a sediment-continent block, and the right block represents the continent-mountain Benard cell. The disordered storage for this last block is the same as the ordered storage for the second compartment. At bottom the material cycle overlays for water and solids are shown separately for clarity.

The middle Benard cell block represents mountain building processes, where sediments, a disordered pool of material, are refined into mountains by deep processes, and recycled via streamflow and glaciers. Mountains may enhance their own growth by many mechanisms. At the small scale, MASH (Melting-Assimilation-Storage-Homogenization) processes use pre-existing silicic material to filter out mafic components of upwelling magmas (Perfit, 1995). At a larger scale, low-density, silicic mountain rocks float high, compared to mafic, oceanic material, due to isostatic adjustment.

The right block in Figure 3-9 consists of the craton building cycle, where some of the mountains are recycled into sediments and some are upgraded into cratons. Cratons, the energized storage, are formed by interactions with deep energies and reinforce their own growth. Mechanisms for reinforcement include enhancement of mountain erosion rates by the catching of rainwater, leading to accumulation and concentration of large amounts of mountainous material on continental margins, and its subsequent burial, metamorphism, and incorporation into cratons. Figure 3-10 is a slightly modified version of Figure 3-9 in which, to speed simulations, the vapor storage was replaced by a simple

109
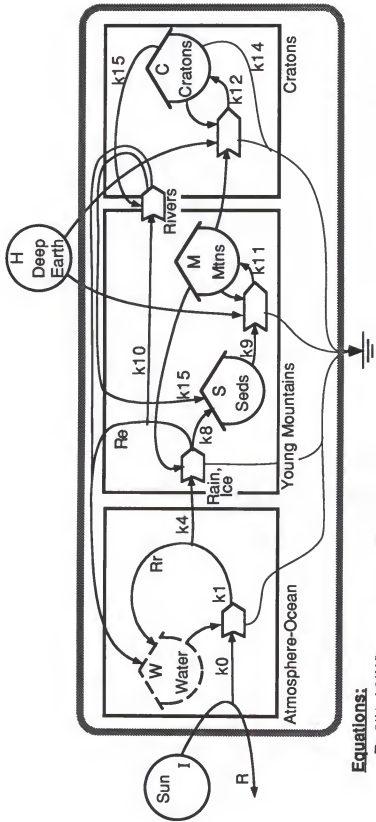
Equations:

R= I/(1+k0*W)

Rr= k1*W*R/(1 +k4*M)

Re= k4*Rr*M/(1+k10*C)

dM= k11*S*H*M -k12*M*H*C -k8*Rr*M

dC= k12*M*H*C -k14*C -k15*Re*C

dS=k8*Rr*M +k15*Re*C -k9*S*H*M

Figure 3-10. The diagram from Figure 3-9, modified with water vapor as a simple flow, showing simulation symbols for sources, storages, and flow coefficients. Simulation equations given at bottom. Water storage dashed to denote constant internal source.

flow. In the diagram the sources and storages were labeled with their appropriate variables, and flows were labeled with their pathway coefficients. The model calibration is shown in Appendix Table B-2, and the simulation program is listed in Appendix Table A-3.

Simulation Results

Simulation results for the hierarchical Benard Earth model, as shown in Figure 3-10, calibrated in Appendix Table A-3 and programmed in Appendix Table B-2, are given in Figure 3-11. In part A, the base case, intense mountain building occurs from about 1 to 2 billion years, where the zero time is taken as Earth formation. Thereafter, cratons grew quickly, peaking at around 2.5 billion years and overshooting their ultimate steady state value. This timing of intense mountain building and rapid continent formation is consistent with geochemical and isotopic evidence for the differentiation of continents and with the observed abundance of greenstone belts, thought to represent intense mountain building, in the early Archaean (cf. Veizer, 1988a, 1988b; Taylor and McLennan, 1981, 1985, 1996).

The model showed a marked tendency toward oscillation, even without the linear and quadratic pathways that normally induce pulsing behavior. Part B of the figure shows that the oscillations dampen with time, but continue to be noticeable to almost 10 billion years. The tendency for this system to overshoot, given the simplicity of the configuration and the realistic turnover times used for the storages, suggests that the issue of temporal decrease in continent mass should be investigated more thoroughly. This possibility has been largely discounted by many workers, partly because of the observed constancy of
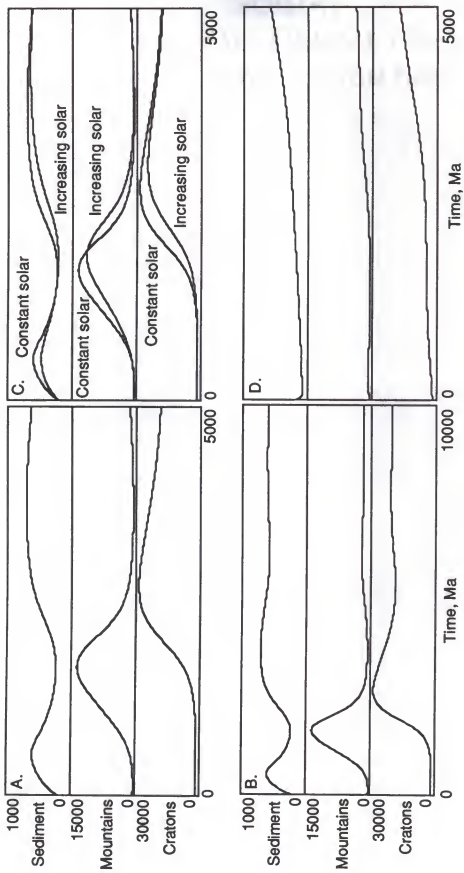
Figure 3-11. Simulation of the Benard Earth model as diagrammed in Figure 3-10, and as calibrated is Appendix Table A-3. Scales in units of E24g. A. Base Case, B. Time scale doubled, C. With increasing solar intensity, superimposed on base case, D. Exponentially declining deep earth contribution.

continental thickness and freeboard, and partly because isotopic patterns of lead, strontium, and neodymium have been shown to be consistent with steady state and growing continental size (cf. Armstrong, 1981; O'Nions and Hamilton, 1981; Taylor and McLennan, 1981, 1986, 1996; Reymer and Schubert, 1984; Veizer, 1988a, 1988b).

In Figure 3-11, part C, the effect on the model of changes in solar intensity was studied. Here, the sun's power output was increased linearly to 30% above its initial value at 5 billion years. In effect, this change represents less intense insolation on the early Earth. Although the final state of the system was indistinguishable from the base case, the growth of sediments, mountains, and cratons was enhanced by greater insolation. The effect of a low initial state and linear increase in insolation was a time delay of about 10% in the attainment of peaks and steady states.

In order to study the impact of exponentially decreasing internal Earth heat production, the deep Earth source contribution was decreased exponentially during model simulation according to the equation for declining radiogenic heat production of McGovern and Schubert (1989), which was $Q=Qoe^{-\lambda t}$, where Qo was set to 7.92 to make the current contribution one unit, and λ was 4.54E-4, with t measured in millions of years. Simulations showed extremely different behavior from the other cases. Greater early deep heat built mountains faster. This quickly used up the sediments, perhaps because their production depended on surface energies that were initially low, compared to the very high deep heat. Growth episodes in mountains and cratons never got started, and all storages showed increasing trends over all geologic time.

Although not shown, simulating on expanded time scales showed even more erratic behavior, and overgrowth of storages much past their steady state. This result suggests that a simple Earth contribution according to declining heat

production can cause very different system behavior over geologic time, as the source declines by about 7 times. A more realistic Earth source may include components that vary less with time, such as residual heat from the core and heat contributed by chemical and compression potentials of overturning materials from the surface.

Results Summary for the Hierarchical Block Model

As in the previous model, this one featured a division of material into hierarchical storages of oceanic, mountainous, and cratonic compartments. This model, however, used standard compartments at each scale of operation. This change eliminated the long lag time of the previous model, sedcycle, for the accumulation of mountains, and the model grew much more quickly. By three billion years, the simulation overshot its final steady state, but transient oscillations did not die out until about 8 billion years.

In Figure 3-11 part A, there was an initial, very large episode of mountain building, very reminiscent of scenarios for the emplacement of massive greenstone belts in the sedimentary record that don't form today. This took place from about 1 to 2.5 billion years into Earth's history. Then, craton development dominated the scene from 2 to 3 billion years, after which damped oscillations to a steady state were the main pattern. This behavior seems more realistic than the very slow response of the previous model, and it may indicate the model is a better representation of the real system.

For increasing solar input, system behavior was changed only by a slight lag. Adding an exponentially declining deep source completely changed the simulation results. This suggests that widely changing energy sources in this hierarchical Earth model, and possibly on the real Earth, would lead to a very different development history than that observed. An interesting aspect of this

model's behavior was the overshoot and subsequent decline not only of the mountains, but also of the cratons. They overshot their steady state value by about 25%, and then began a long slow decline. Finding evidence for this in the real system would be very intriguing.

Surficial and Deep Parts of the Sedimentary Cycle as Cogwheels in the Earth's Overturn Engine

Model Description

In the following text, the complex of reactions, mechanisms, and pathways that collectively convert hard rock into sediments and vice versa, will be referred to as transformation. The collection of processes driving Earth overturn will be referred to as the overturn engine.

In large scale overview, the rock transformation system consists of the reactions among mineral suites that are unstable in their present location, be it in the deep Earth or at the surface. In each place, free energy is used up as the reaction proceeds towards the stable products. Goldschmidt (1933), and later Rubey (1951), Siever (1974), and Li (1972) summarized the surface portion of the overall sedimentary cycle reaction as follows:

(1)   Igneous Rocks + Acid volatiles --> Sediments + Salts

Where igneous rocks were mostly of continental origin, and consisted of mostly aluminous framework silicates and ferromagnesian chain silicates, acid volatiles were carbon dioxide and hydrogen sulfide, sediments were mostly quartz sands, clays, and carbonates, and salts were ionic constituents of seawater. See Appendix D for a listing of the complete reaction proposed by Li (1972), and a calculation of its thermodynamic properties. If the Earth's sedimentary system is essentially cannibalistic (cf. Garrels & MacKenzie, 1971),

then the opposite reaction proceeds at depth, re-creating igneous rocks and acid volatiles that may later reach the surface yet again.

The fact that subduction zones are sites of concentrated energy release is shown by their associated uplift and volcanic activity. This energy may be in the form of chemical potentials and compression heating. In addition, the horizontal displacement of large quantities of sediments via erosion and river transport, causes uplift and subsidence in areas of erosion and deposition, respectively. This action deforms the crust, and can generate deep heat which is related to surface energies. Odum (1996), based on Sclater's (1981) overall Earth heat data, calculated that the total heat flow from the Earth was about twice that contributed by radiogenic and residual sources. He postulated that this heat deficit was accounted for by surface energy transfer to the deep Earth.

A preliminary calculation indicates that the overall mineral transformation reaction (Equation 1, previous page) is endothermic (see Appendix C), and so actually absorbs heat from its surroundings. Because the overall free energy is negative, however (Appendix Figure D-2), there is a net transfer of energy from the surface to depth, which can feed back to help drive rock formation and uplift.

Figure 3-12 shows a diagram of Cogwheel, a system of linked material cycles that together drive the Earth's overturn engine, and are responsible for the transformation of hard rock to sedimentary material on the Earth's surface. In this model, each material transformation is modeled as autocatalytic. For example, the more sediments that exist on land, the more water held in close contact with minerals, and thus the faster water mediated reactions may proceed. The autocatalytic mechanism in the deep reservoir may involve the heat contributed by free energy and crustal deformation as explained above.
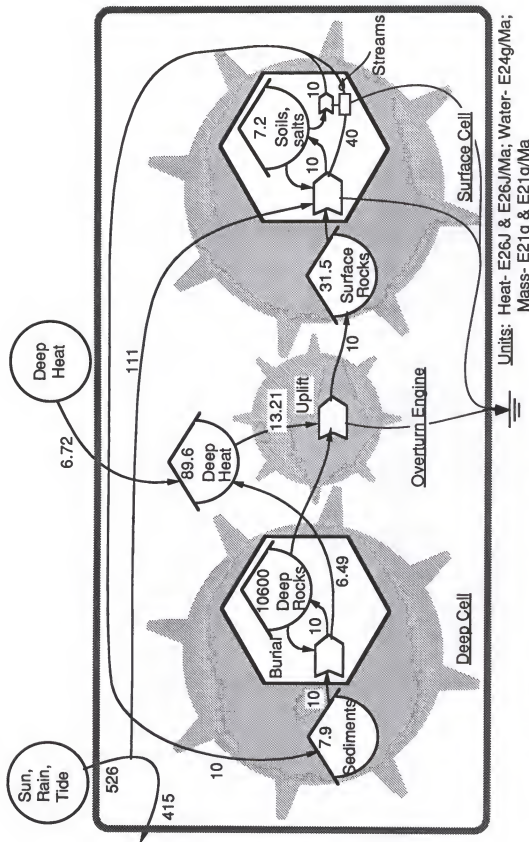
Figure 3-12. Earth cycles envisioned as two cells of material transformation, linked by the "cogwheel" of Earth's overturn engine. Cells driven independently by separate surface and deep heat sources, but each is necessary for the operation of the whole system.

Units: Heat- E26J & E26J/Ma; Water- E24g/Ma; Mass- E21g & E21g/Ma

In this model, the Earth's overturn engine is, therefore, driven by the deep heat contributed by all sources, including compression potentials of buried rocks, energy released by exothermic reactions, radioactive heat, and residual deep heat flowing up from the mantle. The overturn engine is the coupling mechanism for uplift and burial of material in the constant, but slow, process of Earth renewal. Each part of the system: the deep part and the surface part, here is symbolically viewed as a cogwheel, neither of which could operate the same system independently.

Simulations

Figure 3-13 gives the details of the numerical simulation of the model. It lists symbols for the pathway coefficients, storages, and sources, and gives the calibration values for flows, storages, and sources. These values were developed as listed in Appendix Table A-4, and the computer simulation program is listed in Appendix Table B-3.

Simulation results for the base case of model Cogwheel are given in Figure 3-14 part A. In order to observe the transient response of the model, initial values for storages were set at 25% of their calibration value, except for deep rocks, which was set to 100%. Soils grew quickly to their steady state in a few million years. Undersea sediments grew only after soils were available to provide sedimentary material, and the remaining storages grew to steady state in a few tens of millions of years. In parts B and C of Figure 3-14, the deep Earth heat source, Hr, was changed by 50%, and simulations were made starting with the steady state condition. For less Earth heat in B., less uplift reduced the storage of surface rock, suggesting a decrease in continent size. The storage of soil remained approximately constant, while undersea sediments and total heat storage both decreased by about 50%, the same
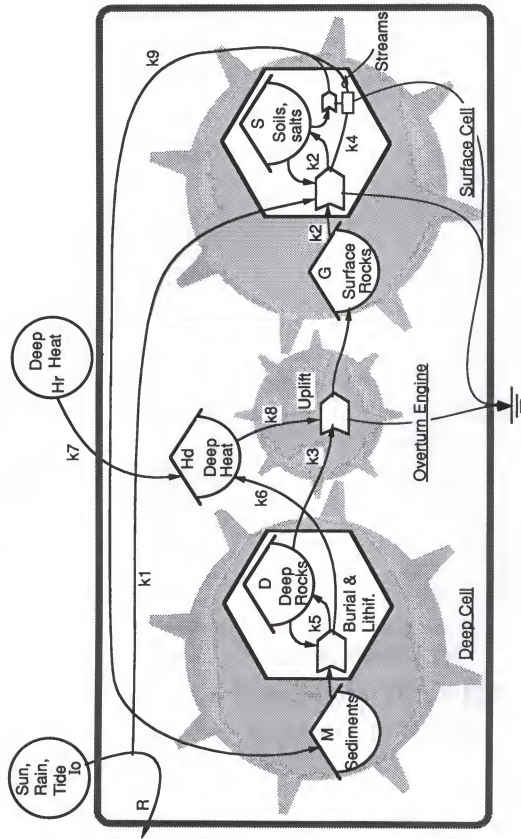
Figure 3-13. Cogwheel model of sedimentary cycle, as in previous figure: storages and sources labeled with symbols, pathways with coefficients, and equations given below.

Equations:

$R = Io/(1+k1*G*S)$

$dM = k4*R*G*S - k5*M*D$

$dD = k5*M*D - k3*D*H$

$dH = k6*M*D - k8*D*H + k7*Hr$

$dG = k3*D*H - k2*R*G*S$

$dS = k2*R*G*S - k9*R*G*S*S$
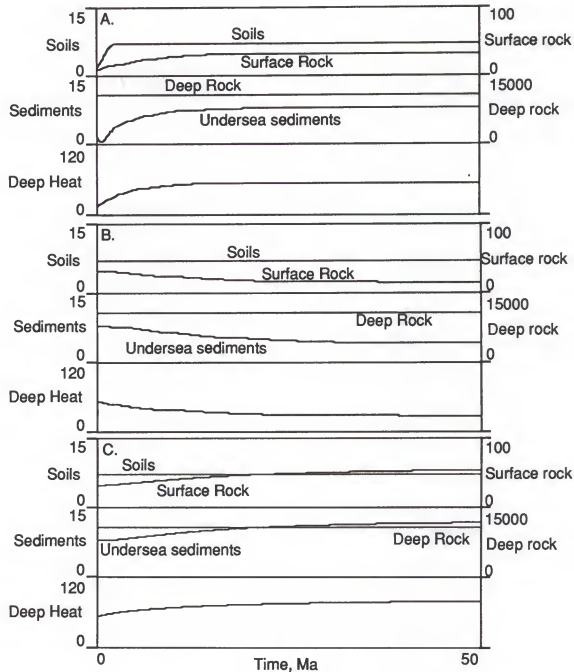
Figure 3-14. Simulation results for the cogwheel model in Figure3-13, as calibrated in Appendix Table A-4, with program listed in Table B-3. A. Base case: initial storages 25%; B. Deep source Hr decreased 50%; C. Deep source Hr increased 50%.

amount as the decrease in the heat source. This led to a decrease in surficial contribution to deep heat, the pathway marked k6 on Figure 3-13, so that it approximately matched the deep source contribution (pathway k7) to Earth heat.

In Figure 3-15, the surface energy source was changed by plus and minus 50% to study its effects on model behavior. In A., a 50% decrease in surface energy again had no effect on soil storage, probably because surface energy equally influenced productive and destructive pathways. However, the total surface rocks increased by about 50%, probably because they were being eroded more slowly by the lower-energy surface processes. An initial decrease in sediments was later counteracted as larger reserves of surface rock caused faster erosion. There was only negligible change in the total sedimentary processing (pathway marked k2, or k9, in Figure 3-13). As shown in part B of Figure 3-15, a 50% increase in surface energies drew down surface rocks, and led to a transitory, ten percent rise and in sea sediments (Storage M in Figure 3-13). Eventually, the storage of sediments returned to its steady state value, and the share of energy provided by the surficial pathway (k6) matched that of the deep pathway (k7) just as in the simulations of Figure 3-14. This result suggests that model storages will build up in such a way as to create matching energies for the two heat production pathways, and that the surficially provided heat will track the amount contributed by the deep source. However, the only way to increase total material flow in the system was to increase the deep source.

Results Summary for the Cogwheels Model

In this model, weathering and transport of materials contributed to the store of deep Earth heat through the dissipation of compression and chemical
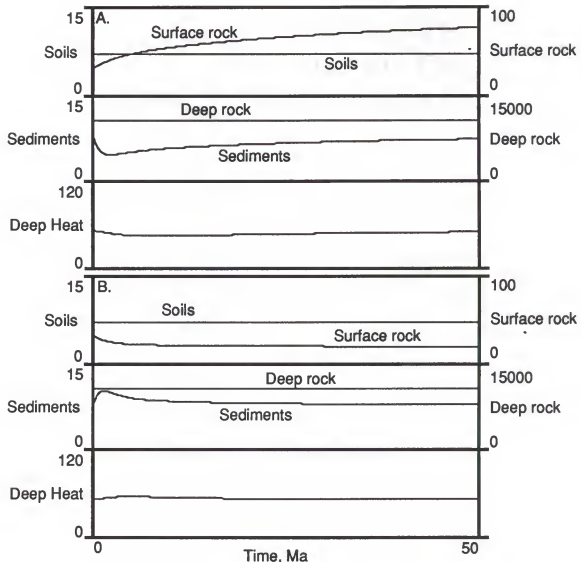
Figure 3-15. Simulation results for the cogwheel model in Figure 3-13, as calibrated in Appendix Table A-4, with program listed in Table B-3. A. Surface energy source I0 decreased 50%; C. Surface energy source I0 increased 50%.

potentials deep within the Earth. This linked the overall overturn of Earth material, a sort of convection of the crust, to the deep energy of radiogenic and residual heat, and to solar energy that drives the hydrologic, atmospheric, and weathering processes.

Simulations showed that changes in residual and radiogenic heat, significantly influenced the overall rate of Earth overturn, while changes in surficial energy, only produced transient changes in the overall rate. These transient changes only lasted until the storages adjusted to steady state, at which time the overturn rate showed no change from the base case.

This model should be considered very preliminary and speculative, compared to the previous models that had more foundation on geological knowledge and hierarchical theory. It points out, however, that the very large storage of deep crustal rocks may have a large role in buffering the crust from changes in external energies.

Short-Term Dynamics of Fueled Industry and the Sedimentary Cycle

Man's consumptive activity has widespread impacts on both rates and processes of erosion and transport (cf. Stallard, 1988; Dobrovolsky, 1994; Schlesinger, 1992; Garrels et al., 1975). These influences range from the easily discernible worldwide increase in soil erosion due to agricultural practices, to less noticeable impacts such as decreased overall biomass, and on to known changes that have an unknown impact on weathering cycles such as changes in carbon dioxide concentration.

In order to gain insight into the important interactions between people and the sedimentary cycle on short time scales, the aggregated overview diagram was developed as shown earlier in the Introduction (Figure 1-3). As

explained in the earlier section, available energies of sun, tide, and deep heat drive the Earth's biological, climatological, oceanic, and geological systems. Industrial systems consume Earth system storages and release concentrated wastes, thus linking people's activities with all aspects of the Earth system.

To simulate key aspects of human interactions with the sedimentary cycle, an industrial model (Figures 4-40 and 4-41) from Chapter 4 was connected to a short-term model of the subsystem of plants, soil, and water (Figure 3-16). The resultant overall diagram is given in Figure 3-17. This model was aggregated to work properly on short time scales of approximately 1000 years or less, because no allowance was made for changes in uplift rates, total continental area, climate, or percent organic matter of soil. Those parameters could vary significantly on longer time scales, but were assumed here to be constant.

The model in Figure 3-17 further aggregates soil (from Figure 3-16) into a single material storage, in essence assuming that the proportion of organic matter will remain constant. In the diagram, soil absorbs water according to its mass. Erosion of particulate matter is proportional to a negative exponential of live plant biomass. Weathering is controlled by acid production during soil oxidation, and the effect of changing temperature is neglected. Atmospheric material transfers are simple flows rather than storages. Along with fossil fuels, agricultural yield drives the production of economic assets.

The figure shows calibration values for sources, storages, and flows, mostly calculated from actual data as documented in Appendix Table A-5. Where data were unavailable, some of the values were developed by matching model simulations to historical trends in fossil fuel use, to arrive at best estimates. Calculations and assumptions were documented in the notes to the table.
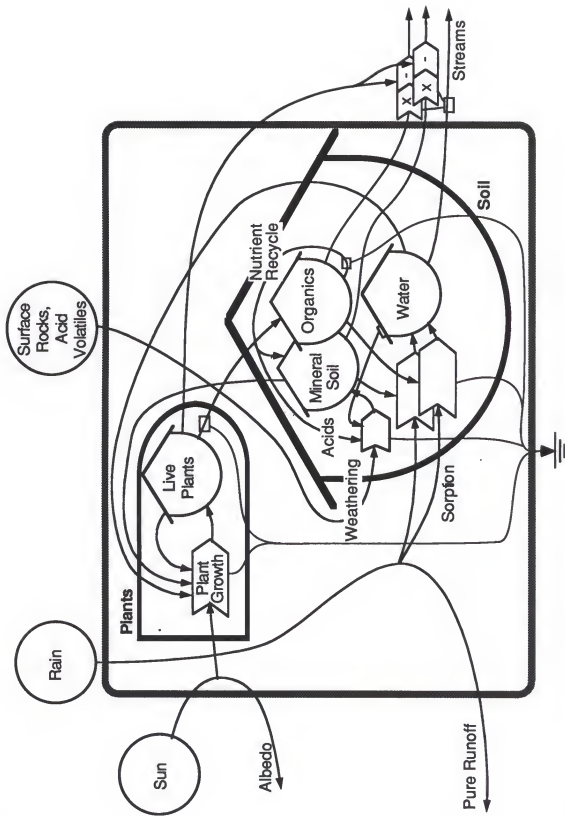
Figure 3-16. Aggregated overview of the subsystem of plants, soil, and water on human time scale.
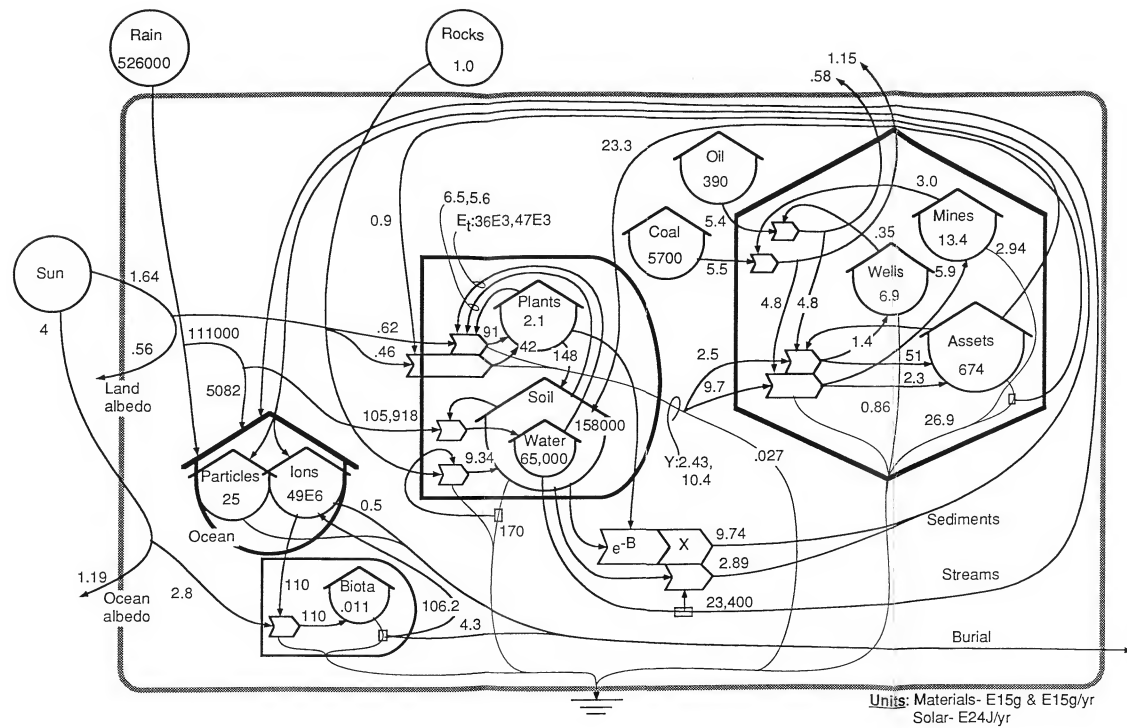
Figure 3-17. Diagram of the simulation model for the short term dynamics of the fossil fuel economy and the sedimentary cycle. Numbers shown for sources, storages, and flows for calibration condition, model year 1990 as estimated in Appendix Table A-5.

In Figure 3-18, the overall diagram is labeled with simulation symbols. Each flow is labeled with its appropriate coefficient, while storages and sources are labeled with their corresponding computer program variables. The figure legend includes the difference equations used to simulate system behavior. See Appendix Table B-4 for a listing of the computer simulation program.

Figure 3-19 shows simulation results of the model diagrammed in Figures 3-17 and 3-18, calibrated in Appendix Table A-5, with program listed in Appendix Table B-4. The simulation generated reasonable values for all storages and flows in the year 1990. For example, oil consumption from the simulation was ~5E15 g/yr, which matched real data for that year (Energy Information Administration, 1992). Additionally, particulate erosion in the simulation was 9.75 E15g/yr, while estimates of that parameter in the real global system range from 13.5 (Schlesinger, 1992) to 20.5 (Dobrovolsky, 1994). The decline of land vegetation from the pre-industrial level was about 20% in the simulation, while Dobrovolsky (1994) estimated about 25% for the real world. The gross features of the sedimentary cycle, therefore, may be reasonably well depicted by the model.

Interestingly, the total soil mass did not significantly change during the simulation, suggesting that the soil, because of its large mass and long turnover time, may provide a significant buffering effect against human perturbation of the ecological system. Or perhaps the aggregated representation of the soil is insufficient to capture the very high quality being lost to farming practices.

Erosion peaked at just under 30E15g/yr around the middle of the 21st century, while weathering rates declined minimally, mostly because of a drop in soil water. Total biomass recovered to its pre-industrial level near year 2200. Based on the simulation, this model suggested that, although the effects of

Figure 3-18. Diagram of the simulation model for the short term sedimentary cycle in Figure 3-17, except showing sources and storages labeled with programming symbols, and flows with pathway coefficients. Difference equations as follows:

$$dMs/dt = S*W*e^{k14*B} - k21*Ms$$

$$dMd/dt = k20*W*S - k5*R2*Md + k7*Bo - k22*Md$$

$$dB/dt = k9*R1*B*W*S + k10*R1*B*W*S*E - k11*B$$

$$dBo/dt = k6*Md*R2 - k7*Bo - k8*Bo$$

$$dS/dt = k11*B + k12*S*R + k17*E - k13*R1*B*W*S - k26*R1*B*W*S*E$$
$$\quad - S*W*e^{k14*B} - k23*S - k20*W*S$$

$$dW/dt = k4*R3*S - k18*R1*B*S*W* - k19*R1*B*W*S*E - k27*W$$

$$dC/dt = -c20*C*Ec$$

$$dO/dt = -c21*O*Eo$$

$$dEo/dt = c14*Ro*Ry*E - c16*O*Eo - c15*Eo$$

$$dEc/dt = c17*Rc*Ry*E + c11*Rc*Ry*E - c12*E$$

$$dE/dt = c10*Ro*Ry*E + c11*Rc*Ry*E - c12*E$$

$$R1 = Sl/(1 + k1*B*W*S + k2*B*W*S*E)$$

$$R2 = So/(1 + k3*Md)$$

$$R3 = Rl/((1 + k4*S)$$

$$Y = k24*R1*B*W*S + k25*R1*B*W*S*E$$

$$Ry = Y/(1 + c8*Ro*E + c9*Rc*E)$$

$$Ro = c21*O*Eo/(1 + c23*Ry*E)$$

$$Rc = c20*C*Eo/(1 + c22*Ry*E)$$
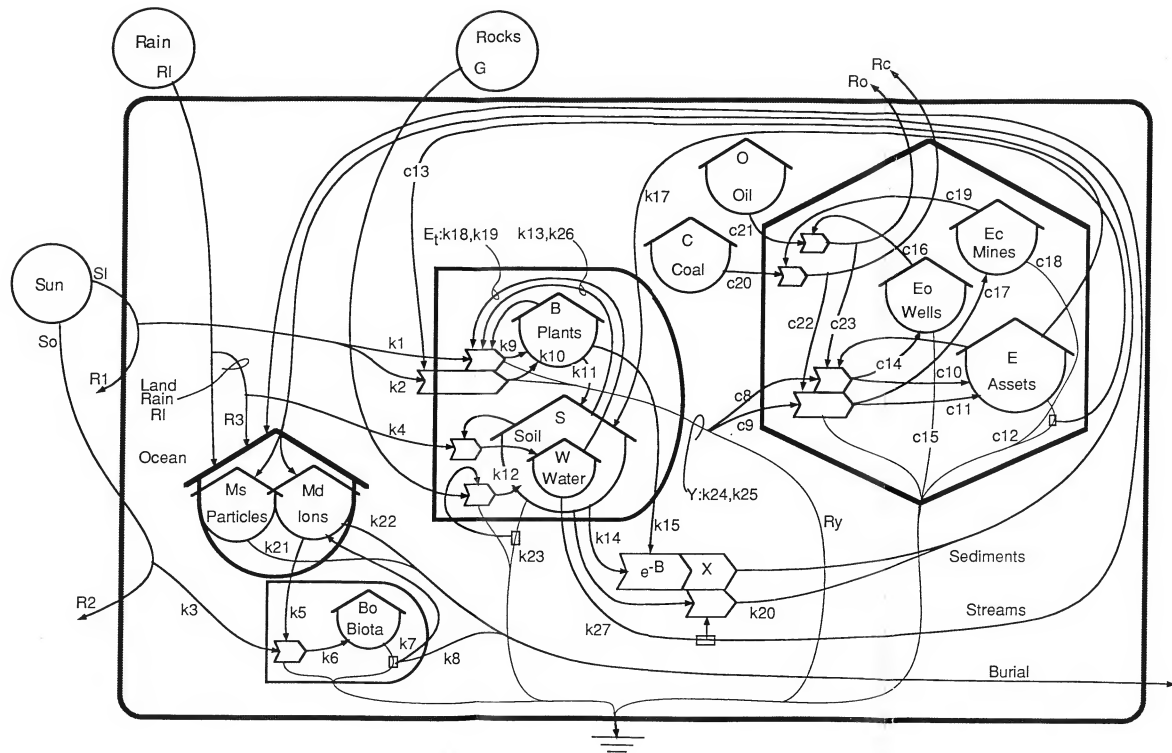
(Legend Facing Page)
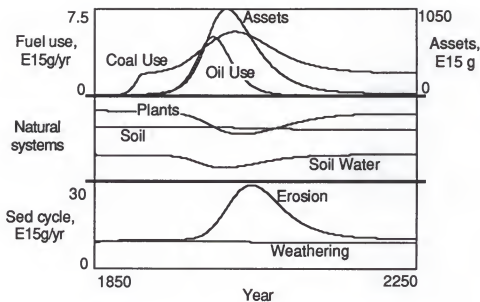
Figure 3-19. Simulation results for the model diagrammed in Figure 3-17, as calibrated in Appendix Table A-5. Additional scale information: Soil- 0 to 200,000E15 g; Soil water- 0 to 100,000E15 g; Plants- 0 to 3000E15 g.

industrial society on overall erosion rates and biomass levels are significant and will expand in the immediate future, the long-term effects may be minor.

CHAPTER 4
CONCEPTS AND COMPONENTS IN WHOLE-EARTH SYSTEMS

Global scale models must incorporate some level of grouping, or aggregation; the optimum level should emphasize the important mechanisms and energies determining behavior at the scale of interest, while retaining predictive power in the face of reasonable changes in forcing functions and internal storages. To find the appropriate aggregation of components, models of subsystems and components may be developed to reveal significant structures, compare effects of parallel pathways, and show where partially redundant mechanisms can be lumped together. Additionally, subsystem models are useful for emphasizing certain areas of inquiry, focusing on particular questions, and examining the relationship of the component to the larger system.

Much scientific effort has been spent to develop detailed models of Earth subsystems such as oceans and atmosphere (See for example Deardorff, 1978; Dickinson, 1984; Eagleson, 1982; Gordon and Stern, 1982; Henderson-Sellers, 1987; Manabe and Bryan, 1985; Mintz, 1984; Ramanathan, 1981; and Sellers et al., 1986). These models are then to be coupled with other similar subsystems, and it is hoped that the resulting "super models" will have the ability to simulate real global processes such as carbon dioxide increase and average temperature change. Beyond understanding, the ultimate goal of these models is to predict accurately changes in environmental parameters that will occur as a result of anthropogenic or other causes. Then, management

strategies can be developed to minimize harmful effects and enhance positive changes.

The drawbacks of the approach outlined above are bewildering model complexity and loss of information between various subsystems. Many of the subsystems models are so complex that no one individual can comprehend the models' inner workings, and it takes a team of highly trained specialists to debug, analyze, and interpret results. Personnel turnover, and small changes in software and hardware can seriously affect these simulations. Few have confidence in the results.

In connecting separate subsystem modules, the appropriate, significant feedbacks can be included, but it is very difficult to visualize them and make sure they are correctly implemented. A sense of overall system structure and driving energies may be lacking.

In this study, subsystem models are developed independently of whole-system models, and for a different purpose. Here models dealing with subsystems of hydrology, thermal properties, and economics are developed to focus attention on particular areas and address particular questions. These subsystem models may also help determine which storages and pathways can be lumped, and which driving energies are important, when developing models at the larger scale. This in turn helps determine the appropriate levels of aggregation and the relationships to be included in integrated, holistic models.

Generic Models of the Hydrologic Cycle for a Regional Landscape

In order to understand the important relationships and mechanisms in human interactions with a regional hydrologic cycle, some simple models that emphasized surface energy, vapor, rain, surface water, and management were simulated on time scales of days to years. The main features of the models

were import and export of both vapor and heat from outside the defined system boundaries, solar heating, autocatalytic vapor consumption by storms to produce rain, and management options of drainage, dams, and pumping.

Heat from solar energy directly and indirectly drives the hydrologic cycle on global and regional scales. Heat evapotranspires water, moving it to the atmosphere as vapor, developing the potential energy that drives cloud formation and rain storms. Because solar energy drives both evaporation and condensation (rain), the effect of changed solar energy inputs on the regional hydrologic system could be quite complex.

A realistic, yet aggregated, hydrologic model can help understand the interactions of rain, cloud formation, and evapotranspiration, and the effects from human modifications of the landscape, such as drainage, dams, and agriculture. Figure 4-1 is a detailed model of a local area's hydrologic system, in which the land and atmosphere self-organize with autocatalytic reinforcement to maximize overall function. In the model, storm production from heat and evapotranspiration gives rise to rain, surface water, and so groundwater and streams. It served as a starting point for developing simulation models for assessing human influence on tropical and subtropical regional hydrology.

Hydro1.1

In order to focus attention on water flows and their variation, an aggregated model was developed as shown in Figure 4-2. The figure is a diagram of Hydro1.1, a simplified hydrologic cycle for a regional landscape. The model included three water storages: vapor in the air, colloidal water in clouds, and liquid water on the surface. Water vapor interacted with heat to form clouds via rising vapor in updrafts. Cloud formation was an autocatalytic
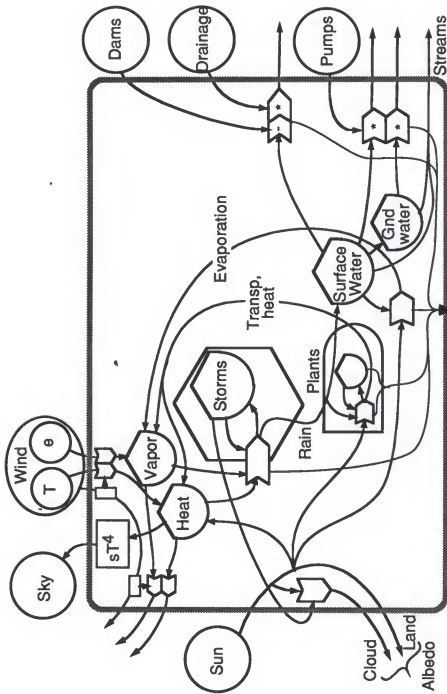
Figure 4-1. Detailed model of a generic convective hydrologic cycle for a local area, where winds bring in heat and vapor, some of which goes into storms and rain, thereby feeding ground and surface water storages. Driving heat energy and overview cloud feedbacks shown at left. Human water control by dams, drainage, and pumping shown at right.
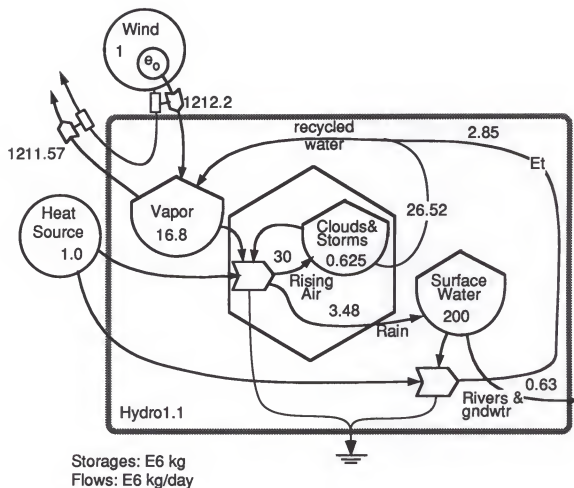
Figure 4-2. Diagram of Hydro1.1, an aggregated model of the generic convective hydrologic cycle for a local landscape. Inflowing heat and solar heat lumped and solar heat lumped and treated as a constant force source. Numbers for storages and flows based on a typical 1 km2 area in Florida, as calculated in Appendix Table A-6.

process, because of such well known feedbacks as increased precipitation nuclei, and release of latent heat leading to further uplift of air parcels.

Precipitation was a function of storm activity, while recycling of cloud water to vapor was linear. The real world develops storms that transfer water to the surface in fits and starts; i.e. as pulsed events, but no attempt was made here to add pathways that would simulate pulsed oscillation. A steady state model may be adequate for assessing average behavior, characteristics and responses to manmade change. Direct condensation (dew) is comparatively small (Miller, 1977), and was aggregated with precipitation.

The values for sources, storages, and flows in Figure 4-2 were for a hypothetical, one square kilometer area of land in Florida, as shown in Appendix Table A-6. These calibration values are appropriate for systems with humid inflowing winds and very direct sunlight such as the summer Everglades and the Amazon rainforest. By matching these values to the conditions for a region, this model can simulate the hydrologic coupling of land and atmospheric convection wherever both evapotranspiration and rainfall are large.

In Figure 4-3, Hydro1.1 is shown labeled with storage and source variables, and flow coefficients. Coefficients were calculated in the calibration table, Appendix Table A-7, and documentation on assumptions, calculations, etc. is provided in Appendix Table A-6.

Simulation results for Hydro1.1, the model in Figure 4-3, with the computer program listed in Appendix Table B-5, are given in Figure 4-4 part A. The simulation was started with low initial storages in order to examine system dynamics. While vapor adjusted very rapidly, clouds and surface water reached steady state much later, both in approximately 500 days. Because clouds' turnover time was only 30 minutes, their growth may have been tracking that of
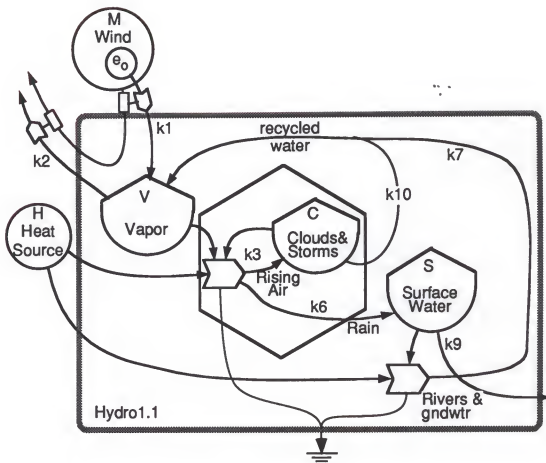
Equations:
dV/dt=k1*M+k7*H*S+k10*C-k2*V-k3*H*C
dC/dt=k3*H*C-k6*S-k10*S
dS/dt=k6*C-k7*H*S-k9*S

Figure 4-3. Diagram of Hydro 1.1, an aggregated model for the generic hydrologic cycle in a local area as in Figure 4-2, labeled with symbols for flows, storages, and sources.

139
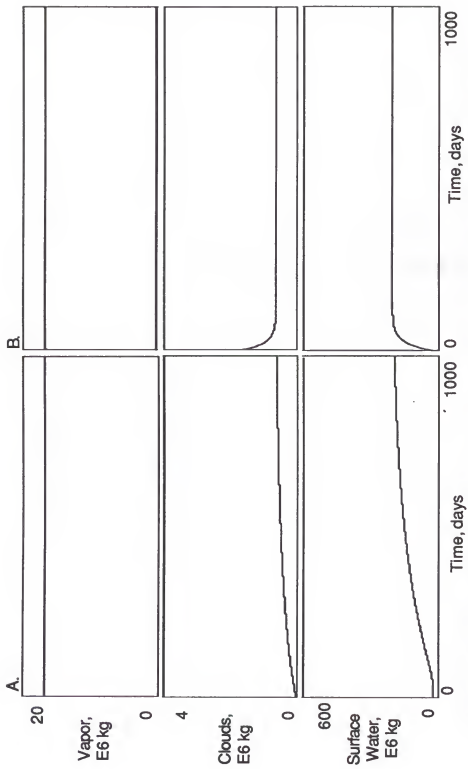
Figure 4-4. Simulation results for Hydro 1.1 (A.), the model in Figure 4-3, as calibrated in Appendix Table A-7; and (B.) for Hydro 2.1, the model in Figure 4-6, as calibrated in Appendix Table A-8. Initial storage values one eighth steady state. Hydro 1.1 shown adjusting more slowly; clouds in Hydro 2.1 showing initial overshoot.

surface water. Thus the model behavior showed a strong link between surface water stored on the land and cloud amount.

The sensitivity of Hydro1.1 to incoming moisture and to land drainage was studied as shown in Figure 4-5. Moisture inflow was adjusted by changing the source constant e_o, while drainage changes were simulated by varying k9, the coefficient for surface water drainage. The model proved to be very sensitive to changes in incoming moisture, because a mere one percent change in that flow resulted in more than a tenfold increase in the amounts of both clouds and surface water. Because real-world air masses vary in moisture content by much more than this amount while precipitation does not, the result was not consistent with real system function.

As shown in Figure 4-5, part II, Hydro1.1 was much less sensitive to the drainage parameter, as a doubling of the drainage coefficient approximately halved the amounts of both clouds and surface water. These results suggested a strong, linear relationship between landscape dewatering and rain amount, but the conclusions were thrown in doubt by the model's unrealistic response to changes in incoming vapor.

Hydro2.1

In order to make Hydro1.1 more realistic, it was modified to include conservation of solar energy. The modified model, Hydro2.1, is shown in Figure 4-6. Notice that, as opposed to the constant force source used in Hydro 1.1, the sun was represented as a flow limited source, so that no more than the a set amount can enter the system. Solar energy in the model was divided between latent heat of evaporation and sensible heat of temperature increase. Solar energy could also be lost to cloud reflection. As in the previous model,

141
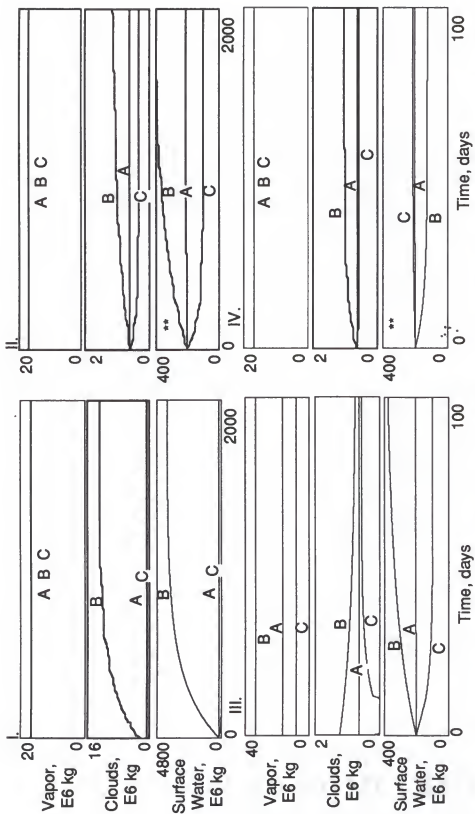
Figure 4-5. Sensitivity studies for Hydro 1.1 (I and II) and Hydro 2.1 (III and IV), the models in Figure 4-3 and 4-7 and calibrated in Figures A-7 and A-8, respectively. I. Response of Hydro1.1 to one percent change in moisture inflow. II. Response of Hydro1.1 to halving and doubling drainage. III. Response of Hydro 2.1 to halving and doubling moisture inflow. IV. Response of Hydro2.1 to order of magnitude drainage changes. A. Standard Run. B. Parameter increased. C. Parameter decreased. ** Opposite response between the models, with Hydro1.1 and Hydro2.1 showing decreased and increased cloudiness, respectively, due to increased drainage.
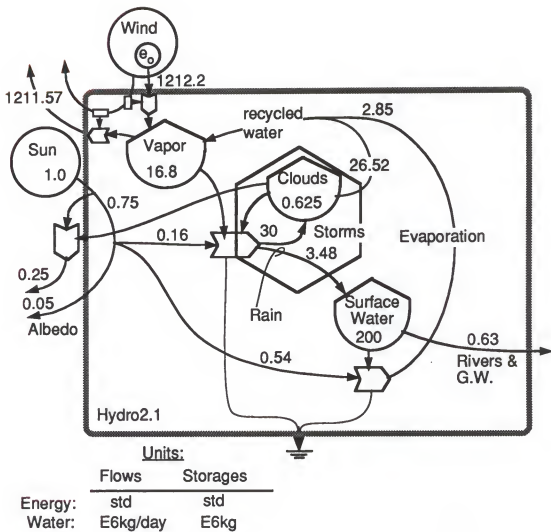
Figure 4-6. Diagram for model Hydro2.1, an aggregated model of a generic convective hydrologic cycle for a regional area, showing substitution of solar energy between latent and sensible heating, and the role of clouds reflecting sunlight. Values based on a one square kilometer area in Florida, as calculated in Appendix Table A-6.

Hydro1.1, the values shown in Figure 4-6 were calculated for a hypothetical, one square kilometer area of land in Florida.

The labeled diagram for Hydro2.1, which includes symbols for flows coefficients, storages, and sources, is shown in Figure 4-7. From the diagram, difference equations to describe system dynamic behavior were written in the figure legend. From those equations and the values given in Figure 4-6, coefficients were calculated as shown in the calibration table (Appendix Table A-8). Documentation on assumptions, calculations, etc., is provided in Appendix Table A-6.

Simulation results for Hydro2.1, the model in Figure 4-7, are given in Figure 4-4 part B. As in Hydro1.1, small initial storages were used to examine system dynamics. Vapor again reached its steady state value very quickly. Clouds increased rapidly and overshot their steady state value, and both clouds and surface water reached steady state in about 10 days. Also similar to Hydro1.1, clouds and surface water seemed linked because of their similar adjustment times, but here they adjusted much more rapidly.

The sensitivity of Hydro2.1 to incoming moisture and to land drainage was studied as shown in Figure 4-5 parts III and IV. The model was much less sensitive than Hydro1.1 to changes in incoming moisture; both vapor and clouds changed by less than a factor of two when incoming moisture was adjusted by a factor of ten. The model was also much less sensitive than Hydro1.1 to the drainage parameter, but it showed an interesting reversal of effect from Hydro1.1, as increased drainage led to more rain, opposite to the effect in the previous model.

Figure 4-8 shows a graph of rainfall versus total amount of surface water, as produced by simulations of Hydro1.1 and Hydro2.1. This graph includes four lines, two from Hydro1.1 (Figures 4-2 and 4-3) and two from Hydro2.1 (Figures
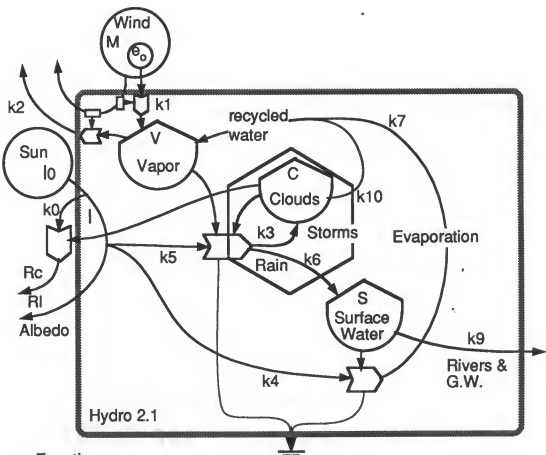
Equations:
RI= I/(1 +k4*S +k5*V*C)
I= I0/(1 +k0*C)
dV/dt= k1*M*e_o +k7*RI*S +k10*C
        -k2*M*V -k3*RI*V*C
dC/dt= k3*RI*V*C -k6*C -k10*C
dS/dt= k6*RI*V*C -k7*RI*S -k9*S

Figure 4-7. Diagram for model Hydro 2.1, an aggregated model of a generic convective hydrologic cycle for a regional area, as in Figure 4-4, and also showing programming symbols for flow coefficients, storages, and sources, with difference equations at bottom.
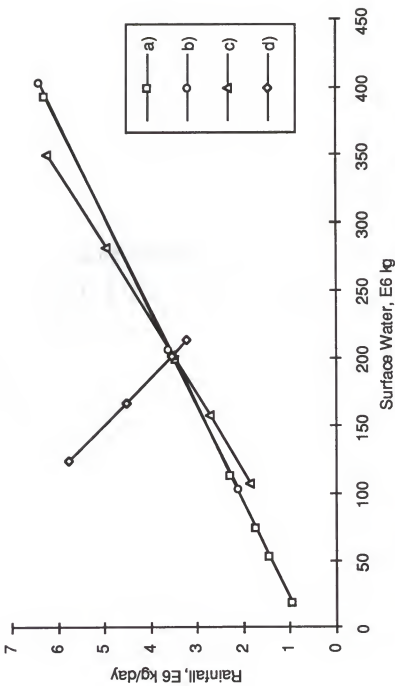
Figure 4-8. Various relationships between amount of surface water and amount of rainfall, as calculated in the simulations of Hydro 1.1 and Hydro 2.1, the models in Figures 4-2 and 4-4, respectively. a) Adjustment of incoming moisture in Hydro 1.1. b) Adjustment of drainage coefficient k9 in Hydro 1.1. c) Adjustment of incoming moisture M in Hydro 2.1. d) Adjustment of drainage coefficient k9 in Hydro 2.1

4-6 and 4-7). For each model, the co-variation of rainfall and surface water was examined by independently varying two parameters: incoming moisture and drainage coefficient. When the amount of incoming moisture was varied, both models showed a linear, positive relationship between amount of surface water and rainfall. However, the models showed significantly different behavior due to changes in drainage. Hydro2.1 predicted that landscape drainage would lead to increased rainfall, thus buffering the loss of surface water. Because of the much more realistic results of the sensitivity analysis of Hydro 2.1, it probably better reflects the workings of the real system.

The key to understanding this simulation result is that this particular hydrology system was driven by a great abundance of moisture coming in with the air mass via winds. This moisture import was much greater than the moisture recycled from surface water. Therefore, changes in surface water caused only negligible changes in atmospheric vapor. Drainage caused a shift in solar energy allocation from evaporation to temperature heating, which led to more thermals, more clouds, and thus more rain.

Results Summary for the Hydro Models

Both Hydro1.1 and Hydro2.1 modeled local convective hydrologic systems driven by sunlight and inflowing vapor. Hydro2.1, however, used a limited flow source to represent solar input. It was, therefore, able to show the substitution effect, where solar energy can either raise temperature or evaporate water. Once it does one of those things, it is no longer available to do the other.

This change made a large difference in model simulations. It produced much more realistic responses to changes in inflowing moisture content, and introduced a significant buffering effect to the production of local convective

rainfall. Hydro2.1 seemed, therefore, to be a much better representation of real hydrologic processes, and it suggested a significant buffering mechanism to human dewatering of the landscape, or human introduction of water retention structures. It also suggested that significant dewatering of the landscape could lead to flooding problems, because rainfall would change very little, yet faster drainage would fill downstream rivers and ponds more quickly. These results apply especially to tropical and subtropical systems with abundance of both sunlight and moisture, producing convective storm activity with much water on the land surface.

Using Isotope Behavior to Estimate Hydrologic Parameters

By including separate tanks and pathways for isotopes in overview hydrologic models, the fractionation implied by the model can be calculated if the behavioral differences among the isotopes are known. Model-predicted isotope ratios may then be checked against those measured for the real system, so that model realism may be evaluated. If pathways in the system are well defined, and certain rates or quantities are in doubt, those rates or quantities may be adjusted so that simulations yield values of isotopic ratios close to those in the real system, thus providing estimates of the flows or quantities that were in doubt. Including isotopes can provide realistic constraints for the model.

For example, the cloud formation rate and cloud evaporation rate may be estimated by using a model that includes different isotopes in water. Fortunately, the isotopic composition of water is relatively easy to measure. In addition, Hydro 2.1 is easily adapted to model fractionation behavior by including extra storage tanks and pathways for the isotope of interest.

Figure 4-9 is a diagram of Dfrac 2.1, the generic hydrologic cycle for a regional landscape, identical to that in Figure 4-6, except it includes separate

148

Units
Water flows: E6kg/day
Water storages: E6kg
Energy flows: standardized to one unit per day total influx.
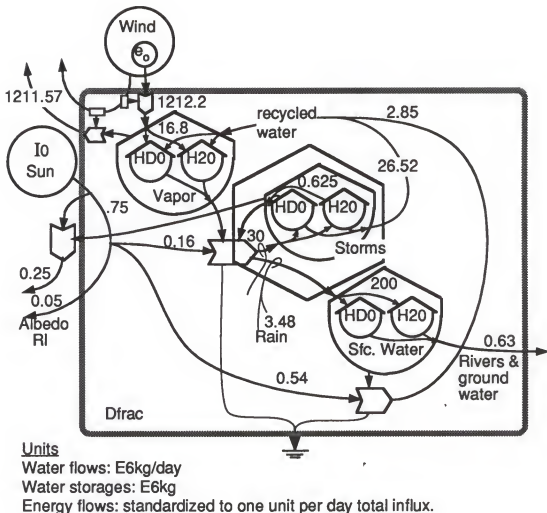
Figure 4-9. Diagram for model Dfrac, an aggregated model of a generic convectional hydrologic system for a regional area as in Figure 4-6, used to study the effects of isotopic fractionation due to evaporation and condensation processes. See text and Appendix Table A-9, item 19 for explanation of flow values.

tanks for heavy water (HDO) and light water (H_2O). Figure 4-10, the labeled diagram, gives programming symbols for sources, storages, flow coefficients, and the equations used for simulation. Isotopes of oxygen could be used just as easily, but would show less fractionation because of their lower fractionation factor.

By mass, deuterium is a very small component of water, so the storages and flows given in Figure 4-9 were practically equivalent to those in Figure 4-6. Therefore, coefficients k1H through k10H in Figure 4-9 were identical to coefficients k1 through k10 in Figure 4-6 (the values are calculated in Appendix Table B-6). Coefficients k1D through k10D were equal to k1H through k10H, except for evaporation and condensation steps where small mass differences are fractionated. Thus coefficients k3D, k7D, and k10D were changed by a factor of alpha as explained in Appendix Table A-6, item 19. Alpha was taken as a constant for the model (temperature changes were neglected) with a value of 1.074 as given in Faure (1986).

The parameter ∂D (del D) is the most widely accepted way to convey deuterium isotopic ratios, and it is defined as $\partial D = 1000*(R-Rstd)/Rstd$, where R is the actual atomic ratio of deuterium to hydrogen in the sample, and Rstd is a known standard ratio. For convenience the 1000 multiplier scales the number to a range with fewer zeroes. Model ratios in mass units are converted to atomic ratios using the molecular weights of H_2O and D_2O, and a factor of two must be included because there are two hydrogens in a water molecule, but only one deuterium in a HDO molecule.

Figure 4-11 shows a simulation of the isotopic hydrology model Dfrac 2.1, the model in Figure 4-10, calibrated as explained above. Each deuterium-water tank began with zero storage, and deuterium was added to the system only by the incoming vapor. This initial condition caused initial ∂D
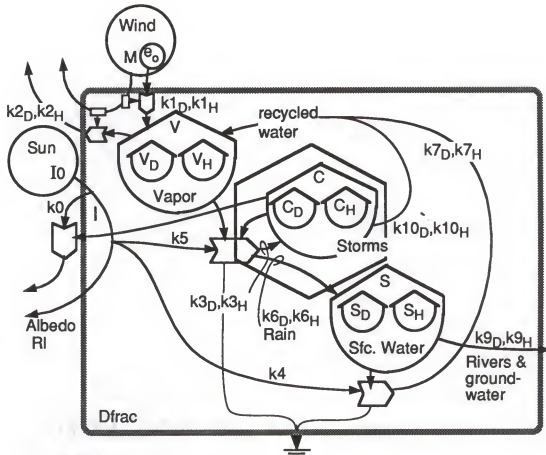
Equations:

$I = I0 / (1 + k0*C)$

$RI = I/(1 + k4*S + k5*V*C)$

$dV_H/dt = k1_H*M*e_o - k2_H*V_H - k3_H*V_H*RI*(C_D+C_H) + k7_H*S_H*RI + k10_H*C_H$

$dC_H/dt = k3_H*V_H*RI*(C_D+C_H) - k6_H*C_H*V_H*RI - k10_H*C_H$

$dS_H/dt = k6_H*C_H*V_H*RI - k7_H*S_H*RI - k9_H*S_H$

$dV_D/dt = k1_D*M*e_o - k2_D*V_D - k3_D*V_D*RI*(C_D+C_H) + k7_D*S_D*RI + k10_D*C_D$

$dC_D/dt = k3_D*V_D*RI*(C_D+C_H) - k6_D*C_D*V_D*RI - k10_D*C_D$

$dS_D/dt = k6_D*C_D*V_D*RI - k7_D*S_D*RI - k9_D*S_D$

$k_D=k_H$, except for evaporation and condensation steps:
$k3_D=k3_H*a$, $k7_D=k7_H/a$, $k10_D=k10_H/a$, where a=fractionation factor.

Figure 4-10. Labeled diagram for model Dfrac, the model in Figure 4-9, showing symbols used for system components, and giving equations used in simulations. Coefficients used in equations are labeled in the diagram. Subscripts D and H indicating Deuterium and Hydrogen, respectively, for the various storages and pathways.
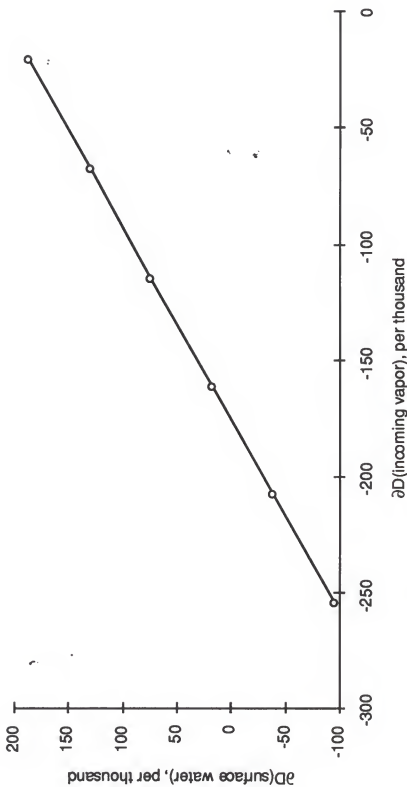
Figure 4-12. Effect of varying the isotopic composition of the incoming vapor, on the steady state isotopic composition of the surface water, as predicted by simulation of the model in Figure 4-10, assuming precipitation, evapotranspiration, surface water outflow, vapor inflow, and cloud amount are known. $\partial D = 1000^*(R/Rstd)$, where R is the ratio of deuterium atoms to hydrogen atoms, and Rstd is a known ratio. A constant value of 1.074 was used for Alpha (Faure, 1986)

values to be large and negative for each of the three water storages. The isotopic ratios of clouds and vapor adjusted quickly, reaching steady state in a fraction of a day. The slower turnover of surface water (317 days vs. 20 and 30 minutes for clouds and vapor) was reflected by its much slower approach to isotopic steady state in about 400 days.

The deuterium content of the three storages decreased in the order: Surface Water > Clouds > Vapor. This is the sequence observed in nature. However, observed values of deuterium in Florida's land surface waters are around -5 ‰ (calculated based on oxygen isotope data from Gremillion, 1994, using relationship from Craig, 1961), much lower than model predictions of around +125 ‰. This difference may be due to the real system having isotopically lighter inflowing vapor (model assumed vapor in equilibrium with Standard Mean Ocean Water), and/or the assumed cloud formation rate of 30E6 kg/day may have been errant. Real world values for ∂D of vapor and clouds are poorly known.

In order to evaluate model sensitivity to variations in the isotopic composition of the incoming vapor, Figure 4-12 was developed from simulation results. The figure indicates a linear relationship between the ∂D of the incoming vapor and the steady state ∂D of the surface water. That relationship suggests that the ∂D of the incoming vapor in Florida would be -190 ‰ in order to give the observed surface water ∂D of -5 ‰. Comparing this to vapor in equilibrium with Standard Mean Ocean Water (SMOW), at around -68 ‰, suggests water vapor influx to Florida has already been depleted in deuterium by about 122 ‰. The first step in refining this model would be to measure the isotopic content of the actual vapor inflow. These data seem to be lacking in the literature. A finer adjustment could be to calculate the fractionation factor, alpha, for the average temperature at which water condenses in clouds.
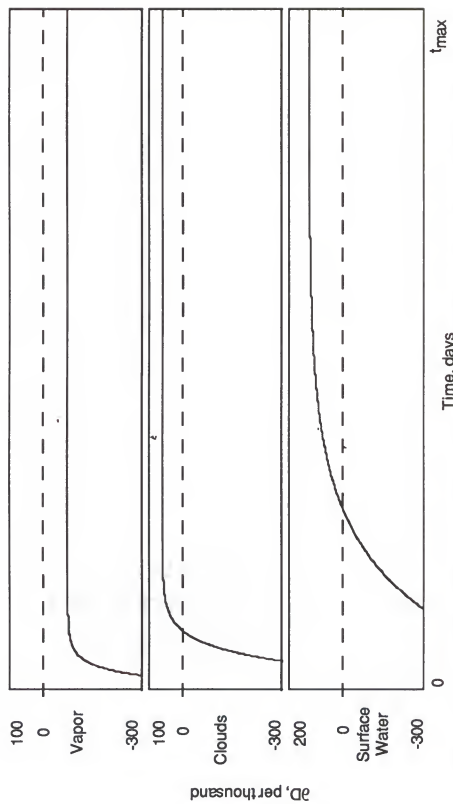
Figure 4-11. Simulation results of the model in Figure 4-10, calibrated as described in the text. The horizontal dashed lines represent zero for ∂D, the formula for which is ∂D=1000*(R/Rstd), where R is the ratio of deuterium atoms to hydrogen atoms, and std represents a standard, known value. The value for t_{max} was 1 day for vapor and clouds, and 500 days for surface water.

Important, but poorly known, parameters in the model include the rates of cloud formation and cloud evaporation. A mass balance shows that in steady state, cloud formation = cloud evaporation + precipitation. Thus the rate of cloud formation constrains that of evaporation and vice versa. A lower limit to cloud formation is the precipitation rate (about 3.5E6 kg/day in this model), because at least as much water has to go into clouds as comes out in rain. Re-evaporation of clouds leaves them isotopically heavier, so higher rates of cloud formation lead to isotopically heavier(higher ∂D) clouds, and hence also heavier precipitation.

In order to evaluate the sensitivity of the model to variations in the rate of cloud formation, a graph was plotted in Figure 4-13, which shows how isotopic content of surface water varies with cloud formation rate. As expected, fast-forming clouds were heavier, because of greater cloud evaporation. The range of ∂D(surface water) due to this effect, however, was only about 70 ‰ for all realistic values of cloud formation rate. So this parameter could only partially account for the large difference between observed and predicted values of isotopic composition. It is possible that both isotopically light inflowing vapor and low rates of cloud formation play roles in decreasing the amount of deuterium in Florida's surface waters. Alternatively, model assumptions may be incorrect. For example, alpha, the fractionation factor, is temperature dependent, but here was assumed constant. In addition, it is possible that most evaporation from Florida's land surface occurs by transpiration, and this process may cause little fractionation compared to simple evaporation (Yakir and Wang, 1996).
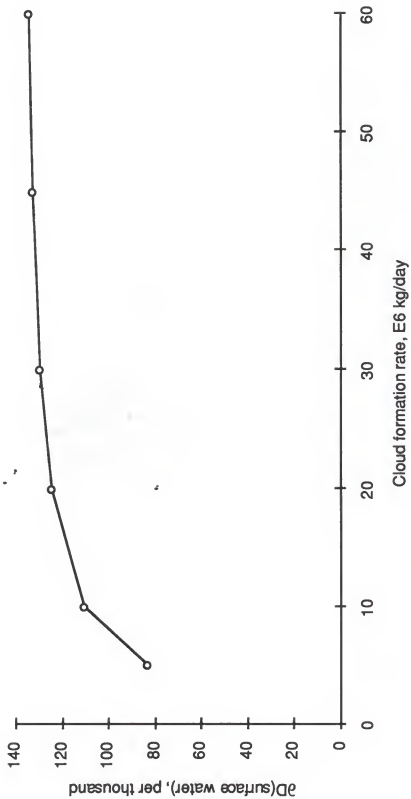
Figure 4-13. Effect of varying cloud formation rate on the steady state isotopic composition of surface water, as predicted by simulation of the model in Figure 4-10, assuming that precipitation, evaporation, and vapor inflow are known. $\partial D = 1000^*(R/Rstd)$, where R is the ratio of deuterium atoms to hydrogen atoms, and Rstd is a known ratio.

Temperature Regulation by the Hydrologic Cycle

The geological record indicates that the Earth's surface temperature has varied within definite limits over the Earth's life span, supporting liquid water and for its entire life and biological activity probably for the last 4 billion years. In contrast, astronomical models suggest that solar intensity may have varied by as much as 30% over the 5 billion years of Earth history (Schneider and Londer, 1984). These facts have spurred attempts to understand mechanisms for Earth temperature regulation in the face of rising solar output (cf. Sagan and Mullen, 1972, Owen et al., 1979, and Walker et al., 1981)

In order to gain insight into the possible role of the hydrologic cycle in regulating Earth's surface temperature, simple general systems models were developed to overview the system. These models may suggest the amount of surface temperature buffering provided by existing system dynamics, without invoking non-uniformitarian mechanisms other than varied solar input.

To clarify the basic nature of the Earth's system of heat and hydrology, a simple conceptual diagram was drawn that lays out the main aspects of energy and water processing on Earth (Figure 4-14). Major pathways for energy entrance, exit, and use are shown alongside the processes of water cycling in the system. In the figure, thin arrows stand for energy flows, thick arrows for water flows, and tank symbols for aggregated storages of water and heat. Layer thicknesses of the aggregated storages are given.

In order to understand and appreciate the complex configuration of the Earth's hydrologic temperature regulation system, the conceptual drawing in Figure 4-14 was redrawn in energy circuit language format as shown in Figure 4-15. This diagram focuses attention on the interactions and feedbacks among
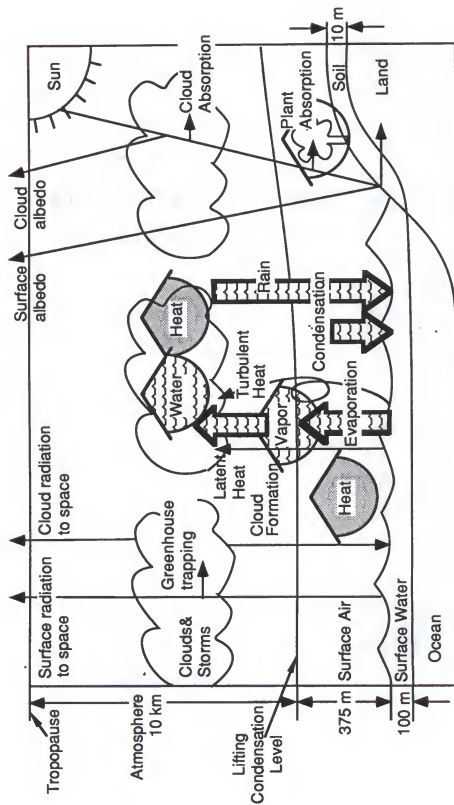
Figure 4-14. Main modelled interactions of the hydrologic cycle's buffering of earth temperature variation due to changes in solar intensity. Wide arrows represent flows of water, thin arrows represent energy and heat transfers, dotted tanks show stored heat, and tanks with wavy-lined fill are for water. Measurements represent layer thicknesses used to calculate heat capacities.
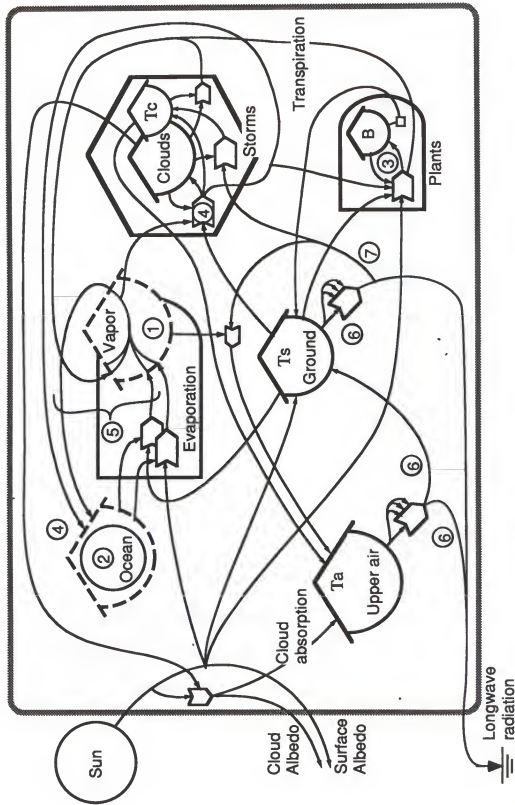
Figure 4-15. A diagram of Earth's temperature regulation system in the face of varying solar output, modelling the buffering of surface temperature by cloud reflection and by transfer of latent heat away from the surface, both effects increasing energy pathways not controlled by temperature. Circled notes as follows:

① Dashed storage representing turnover time too small or too large to affect this simulation: for fast flows a flow union is used to generate a running average

② Substitution of a constant force source for slow storages. Sea availability held constant (constant internal source).

③ Uptake of latent heat with evaporation and transpiration.

④ Release of latent heat with condensation (in clouds or at surface).

⑤ Slow exchange calibrated as a balance.

⑥ Radiation pathways important during the timescale of the model. Upper air radiating both out to space and back to ground.

⑦ Greenhouse effect of both clouds and vapor in absorbing longwave radiation.

the various elements of the hydrologic cycle and the Earth heat dissipation system. It shows the main processes of evaporation and precipitation as a coupled system of production and consumption. The producer/consumer pair of evaporation and storms then provides the water needed for plant growth, which feeds back to absorb solar energy and also enhances vapor production by transpiration.

Four major points emphasized in Figure 4-15 are energy pathway substitution, feedbacks to albedo, autocatalytic storms with turbulence, and "greenhouse" energy trapping. Sunlight is shown to be absorbed by three main pathways, each increasing at the expense of the others. For example, if plants expand and absorb more sunlight, less is available to go into surface heating. Also, increases in latent heating due to evaporation can occur only by grabbing some of the available energy.

Albedo feedbacks of the model's temperature regulation system are present in the clouds and the land plants. Clouds have a two-sided effect: they both absorb heat into the system and reflect it away according to their mass (i.e., cloud surface area was assumed to vary linearly with mass). In this general systems model, the overall effect of clouds , which is often debated because of their dual action in absorbing and reflecting, can be examined by computer simulation of the non-linear differential equations. In the same way the overall effect of plants on the system may be studied. They are shown absorbing sunlight in proportion to their overall size, which affects the total amount of sunlight not absorbed (albedo).

Storm generation is an autocatalytic function, growing on the inputs of heat and vapor. Thus cloud amount, turbulent heat loss, precipitation, and latent heat transfer, which all are functions of storm activity, are non-linear

functions of the system state. Changes in any one of them can alter the others in unforeseen ways.

Energy is trapped as heat in the surface system by the "greenhouse" action of both clouds and vapor. Because vapor and clouds vary together as part of the production/consumption pair, their net greenhouse effect can be best examined by simulating the system over time. According to Kiehl and Trenberth (1997) water vapor is a much more important greenhouse gas than carbon dioxide. Variations in the hydrologic system, therefore, may have an amplifying or buffering effect on climate changes due to increased carbon-dioxide concentrations. This model focuses on climate and temperature changes due to changed solar intensity. It may help understand the relative roles of the various greenhouse gases in climate change.

Energy Division Among Pathways

In order to draw attention to the different pathways by which solar energy enters and exits the system, and how those pathways can change in relative importance, the overview system of hydrologic temperature regulation was aggregated as shown in Figure 4-16. In the model titled Tempreg1, incoming solar radiation may be reflected by clouds or surface, or it may be absorbed. Once absorbed at the surface, solar derived energy can leave through many pathways, including latent heating as vapor, turbulent heat release through convection, or radiation due to the temperature. Because radiation is directly dependent on temperature, relative increases in the other pathways of heat release can buffer surface temperature changes. Increases in the hydrologic cycle may, therefore, lessen the amount of temperature rise necessary to obtain a heat balance, if solar intensity increases.
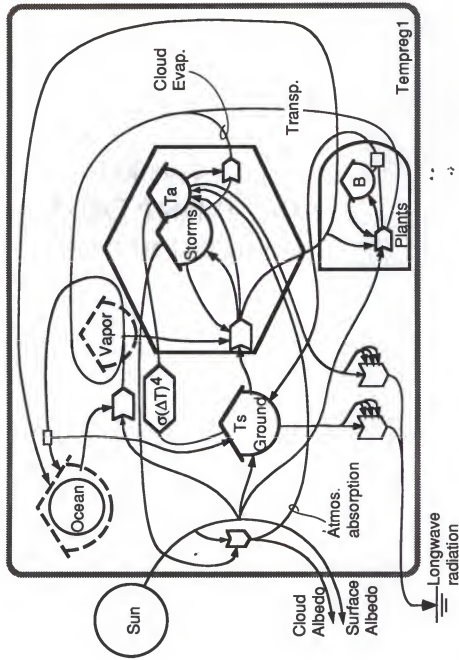
Figure 4-16. Tempreg1, a model of earth's hydrologic temperature regulation aggregated to emphasize the different pathways of solar energy through the system, including substitution between latent and sensible heating, reflection of short-wave radiation by storms, and biotic heat relocation by transpiration. Values for pathways in the real earth system given in the overlay diagrams for the heat and water cycles in Figure 4-17.

Tempreg1 includes the linked processes of cloud formation and land vegetation production. Both of these processes influence the distribution of solar energy among system pathways, clouds by reflecting and absorbing, and vegetation by transpiring (latent release) and by changing surface albedo. All of the above mentioned processes are connected in the model, which represents a complex network of feedbacks and interactions.

In order to focus attention on the individual cycles of heat and water, isolated overlays of those cycles were developed as shown in Figure 4-17, and numerical values for the whole-earth system were included with units given in the figure. The heat cycle overlay of (A.) shows the various pathways taken by solar energy in its journey through the Earth system. It is of note that as more energy goes into latent heating of evaporation, less energy goes into sensible heating that raises the temperature of the surface. Latent heat released in the upper atmosphere increases the temperature there. This increased atmospheric temperature limits the radiated heat release from the surface, which is proportional to the fourth power of the difference in temperatures. So a complex feedback loop including latent heating to surface temperature is operating.

The water overlay (Figure 4-17 part B.) shows the pathways taken by water in its various forms as it moves from ocean to atmosphere to land to plants, back to atmosphere, and finally back to the ocean via streams (groundwater aggregated here), oceanic rain, or condensation. Vapor was represented as a simple flow, which is tapped by storm activity producing storms and rain. Vapor not caught by storms returns to the surface as condensation. Whereas 2690E15g/day of vapor is condensed into clouds, only 1400E15g/day is precipitated. The remaining 1290 units are re-evaporated. Also, of 300E15g/day of land precipitation, two thirds is recycled to the
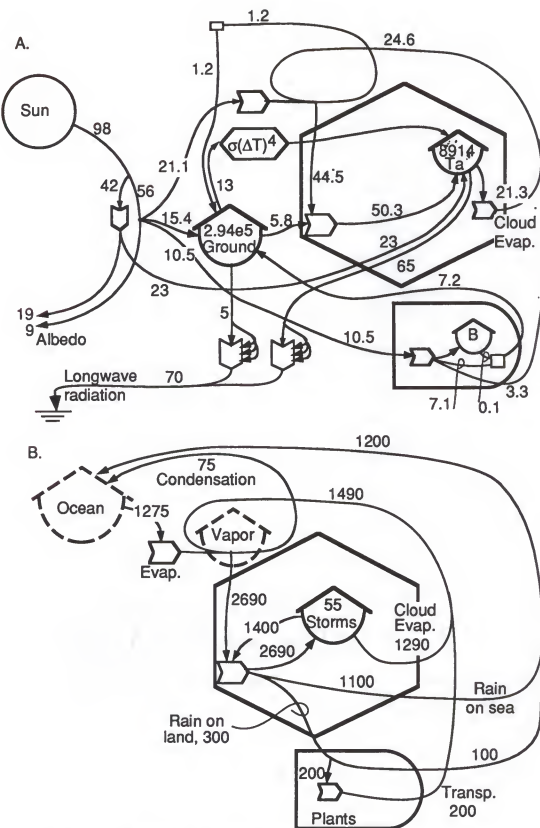
Figure 4-17. Cycle overlays for the temperature regulation diagram of Figure 4-16. A. Heat cycle overlay, units standardized to 100 units inflowing per day. B. Water cycle overlay, units of E15g/day.

atmosphere by evapotranspiration, and only one third reaches the ocean in streams.

Figure 4-18 gives the diagram for Tempreg1 showing the information necessary to simulate the system dynamics. In the figure, sources, storages, and flow coefficients are labeled with their variable symbols used in the computer program (listing provided in Appendix Table B-8), and the difference equations implied by the diagram are listed on the facing page. The model was calibrated as shown in Appendix Table A-9.

Simulation output for Tempreg1 is shown in Figure 4-19, with the model calibrated as in Appendix Table A-9, and computer program listed in Appendix Table B-8. In part A, initial storages of ground heat and storms were approximately a sixth of their steady state, calibration value. The system adjusted with a quick initial gain in storm amount, which led to an early favoring of atmospheric heat gain over surface heat gain, due to the high albedo and absorption of the larger cloud mass. Eventually, surface temperature surpassed atmospheric temperature, after which a renewed increase in atmospheric temperature took place. This was made possible by lowered cloudiness, which enabled more insolation to reach the surface, leading to heating and re-radiation.

In Figure 4-19 part B., model response to changes in insolation was examined. Here a 30% change of solar intensity was introduced, and the resulting cloud cover and temperature changes were tracked. Surface temperature varied by about 6% due to the changed solar intensity, corresponding to about 305°K and 271°K, or about 17°C temperature changes from the base case of 288°K. This compares to a hypothetical fourth power radiation law change of about 19°C, implying the total temperature buffering effect of this system is small. In this case, enhanced plant growth caused a
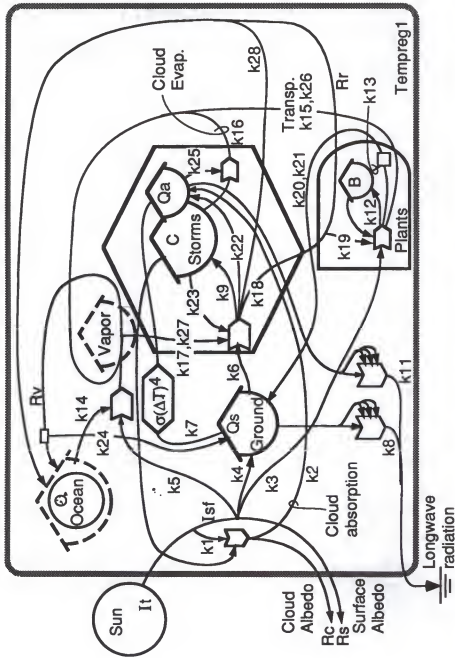
Figure 4-18. Tempreg1, the hydrologic temperature regulation model from Figure 4-16, labeled with symbols for sources, storages, and flow coefficients. For equations see facing page. Fa and Fp are conversion factors to compute temperature from the amount of heat stored.

Equations for model Temoreg1:

$Isf = It / (1 + k1*C)$

$Rs = Isf / (1 + k3*B*Rr + k4 + k5*O)$

$Rr = J18 / (1 + k19*Rs*B)$

$Rv = (k14*Rs*O + k15*Rs*Rr*B + k16*C) / (1 + k17*Ts*C)$

$Rc = k1*Isf*C - k2*Isf*C$

$dQs = k4*Rs + k20*Rs*Rr*B + k21*B + k24*Rv - k6*Ts*Rv*C - k7*(Ts-Ta)^4 - k8*Ts^4$

$dQa = k2*Isf*C + k7*(Ts-Ta)^4 - k22*Ts*Rv*C - k11*Ta^4 - k25*C*Ta$

$dC = k8*Ts*Rv*C - k16*C - k23*Ts*Rv*C$

$dB = k12*Rs*Rr*B - k13*B$

$Ts = Qs*Fs$

$Ta = Qa*Fa$
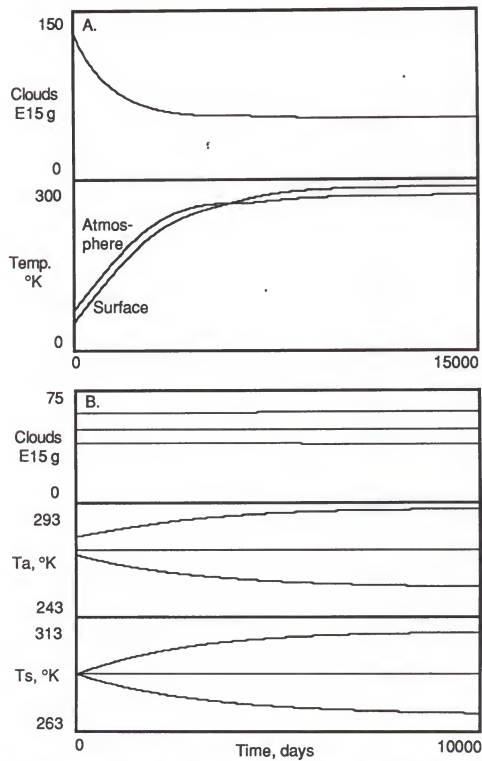
Figure 4-19. Simulation of Tempreg1, the model in Figure 4-18, as calibrated in Appendix Table A-9. A. System dynamics starting with initially low values of stored heat. B. Sensitivity analysis to varying intensity of solar output, up and down 30 percent from present values, with absolute surface temperature varying about 6 percent.

slight decrease in albedo, soaking up more heat at the surface. This positive feedback partially offset the greater surface heat loss due to more storm activity. The buffering capacity of this system was related to increased heat transport away from the surface by storms.

Production of Vapor and Consumption by Storms

Figure 4-20 is a diagram of Tempreg2, a configuration which emphasizes the production/consumption aspect of water vapor in the Earth's hydrologic temperature regulation system. On the left, ocean water with little available energy, and dispersed radiant energy of sunlight interact to produce vapor and surface heat, which both feed the autocatalytic consumption module of storms, which pump heat away from the surface as both latent and turbulent energy.

The model includes an explicit storage for atmospheric vapor, production of which is an exponential function of surface temperature in accordance with the Clausius-Clapeyron relation. Additional feedbacks include the action of both vapor and clouds in trapping outgoing longwave radiation via the greenhouse effect. This model does not explicitly include the biota. Rather, their effect on evaporation and albedo is aggregated with the other units.

In Tempreg2, vapor is produced by an interaction between surface water and surface heat, as an exponential of the surface heat, which is related to temperature by aggregate heat capacity. An autocatalytic module of clouds and storms consumes the vapor, returning much of it to the surface as rain, but transferring large quantities of energy to the atmosphere in the forms of latent and turbulent heat. This action is the Earth's general circulation in aggregate. Storms feedback to the inflowing energy by reflecting some and absorbing some, both according to their amount in a linear relationship. Vapor also acts to
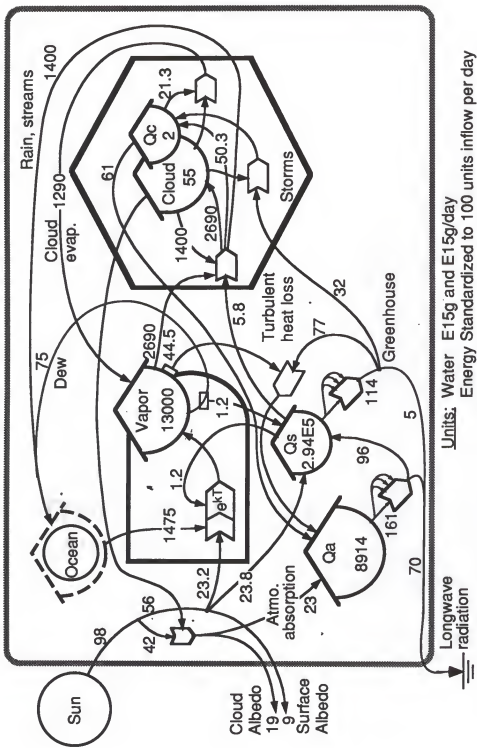
Figure 4-20. A model of hydrologic temperature regulation aggregated to emphasize the relationships among surface temperature, humidity, storm activity, and greenhouse radiation trapping. Showing calibration values estimated for real earth system: values less than 1000 representing energy flows and others water flows, except for dew which is a water flow.

Units: Water E15g and E15g/day
Energy Standardized to 100 units inflow per day

trap outgoing radiation by greenhouse absorption. Thus the model explicitly defines a proposed configuration of the cloud-vapor-temperature system.

In Figure 4-20, numerical values are labeled on each source, storage, and flow, according to the notes to the calibration table (Appendix Table A-10). Care was taken to ensure that energy and water balanced for the model as a whole and for the individual storages.

Figure 4-21 shows the model Tempreg2 readied for simulation, including symbols for pathway coefficients, storages, and sources used in the computer program (listed in Appendix Table B-9). Difference equations specified by the model configuration are given on the facing page to the figure.

Simulation results for Tempreg2, the model in Figure 4-20, as calibrated in Appendix Table B-9, are shown in Figure 4-22. In A., the initial storages were a quarter of their calibration value. After a period of transient adjustment, clouds and vapor both went to zero, where they stayed until the surface heating system built up sufficient heat to start the hydrologic cycle. A divergence in surface and upper air temperatures early in the simulation seemed to provide impetus to the establishment of the hydrologic cycle, which over time brought about a lower temperature difference. The model's response to much changed initial conditions showed its overall stability, and suggested a role for the hydrologic cycle in helping stabilize Earth's surface system. The model demonstrated a temperature buffering effect similar to, but greater than, the earlier model Tempreg1.

In Figure 4-22 part B., input solar power was varied by plus/minus thirty percent, and the sensitivity of temperature and water parameters was examined. A smooth transition to this abrupt change in solar power was observed for all variables. The temperatures and hydrologic parameters all tracked the solar input, increasing if solar power was raised. The largest
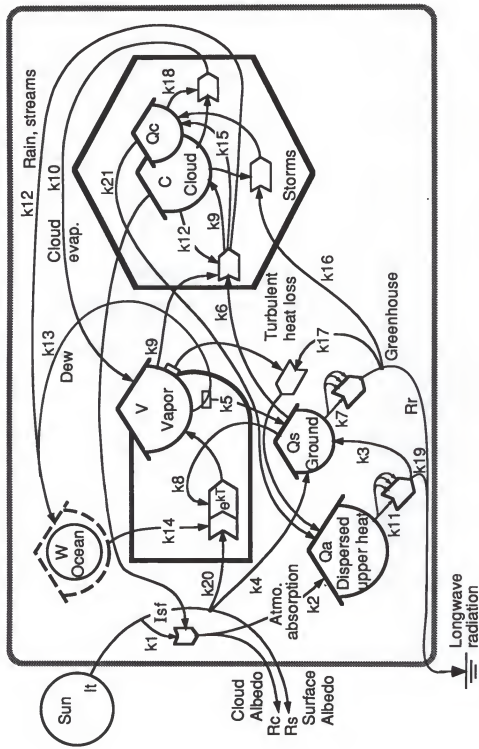
Figure 4-21. Tempreg2, the hydrologic temperature regulation model from Figure 4-20, labeled with symbols for sources, storages, and flow coefficients. For equations see facing page.

Equations:

Rs= Isf/(1 +k20*W*e^{K*}Ts)

Rr= J7/(1 + k17*V +k16*C)

dV= k14* W*Rs*e^{K*}Ts +k10*C*Qc - k9*Ts*V*C

dC=k9*Ts*V*C -k10*C*Qc -k12*Ts*V*C

DQc= k15*Ts*V*C +k16*Rr*C -k18*C*Qc -k21*Qc

dQs= k4*Rs +k3*Ta^4 +k5*V -k6*Ts*V*C -k7*Ts^4 -k8*W*Rs*e^{K*}Ts

dQa= k2*Isf*C -k11*Ta^4 +k17*Rr*V +k21*Qc

Ts=Qs/Cs

Ta=Qa/Ca; where Ca,s= aggregated heat capacity (See Appendix Table AT2)
K determined Appendix Table AT2, item 20.
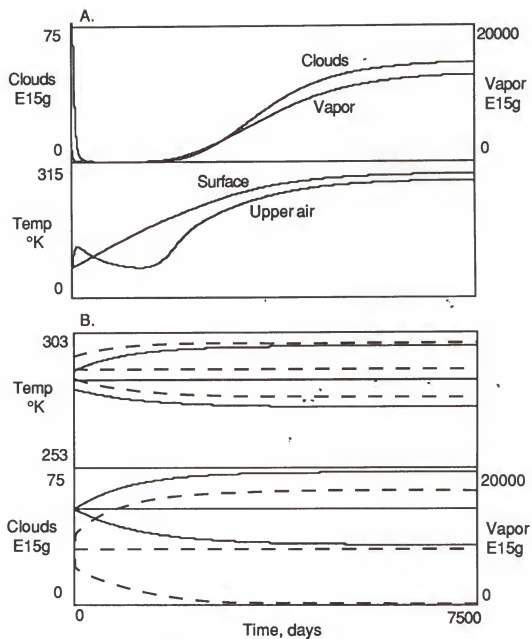
Figure 4-22. Simulation results of Tempreg2, the model in Figure 4-21, as calibrated in Appendix Table A-9. A. Model dynamics with initial storages one quarter of their calibration value B. Study of sensitivity to varying incoming solar radiation intensity by 30 percent up and down: dashed lines showing surface temperature and vapor, and solid lines showing upper air temperature and cloud amount.

percentage change was in atmospheric vapor, which almost doubled in the case of greater solar power. Percentage changes in surface and upper air temperatures were much smaller, around 4.5 percent, corresponding to a temperature change of about 13 °C. For comparison, the fourth power relationship of temperature to radiation would give a surface temperature variation of 6.7 percent, or about 19°C. In other words, the model system Tempreg2 provided about 40% of additional buffering to the Earth's surface temperature, compared with the case of radiant heat changes only. This was enough to maintain average surface temperature above freezing in the case of 30% less solar power.

Results Summary for Temperature Regulation Models

Table 4-1 summarizes the main results for the simulations of Tempreg1 and Tempreg2, the aggregated Earth temperature regulation models. The models are compared to each other and to a one dimensional, radiational surface heat balance model. The one dimensional model is summarized by the equation (see Ramanathan et al., 1989), $S_O/4*(1-\alpha) = \sigma T^4$, where α= albedo, S_O= solar constant, s= a constant, and T= Earth temperature. In words the equation says that absorbed heat equals that emitted.

The first line of Table 4-1 shows the predicted surface temperatures for an Earth with 30% greater solar power input. The heat balance equation, although it gives an unrealistically low surface temperature, does closely predict the mean radiating temperature of the average Earth, and, therefore, may be a good standard for comparison. It shows a difference in temperature of approximately 21°C, while Tempreg1 predicted an 18.2° rise, and Tempreg2 an increase of 13.4°C.

Table 4-1. A comparison of key results for three models of Earth temperature regulation, the simple heat balance equation, model Tempreg1, and model Tempreg2. Headings "Base" and "30%" refer to two scenarios: present conditions and with a 30% increase in solar power.

Parameter	Heat Balance Base	Heat Balance 30%	Tempreg1 Base	Tempreg1 30%	Tempreg2 Base	Tempreg2 30%
Temperatures						
Surface Temp, °C	-22	-1	15	33.2	15	28.4
Atmos Temp, °C	--	--	0	17.8	0	21.7
Overall Energy Balance						
Total energy loss	100	130	100	130	100	130
% stratos albedo	--	--	2	2	2	2
% cloud albedo	--	--	19	20.4	19	21.5
%surface albedo	30	30	9	8.2	9	5.1
% cloud radiation	--	--	65	64.4	65	67.9
% surface radiation	70	70	5	4.9	5	3.47
Surface Energy Balance						
Total heat loss	70	91	48.2	59.2	48.2	59.1
% Turbulent	--	--	12.3	12	12.3	17.7
% Latent	--	--	49.4	50.1	49.4	70.6
% Radiant	100	100	38.3	37.9	38.3	10.9

Notes
1. Energy units are standardized so that 100 represents the present total of incoming energy.
2. -- represents the fact that the model makes no prediction.
3. Heat and energy values shown refer to net exchanges, i.e. radiation is the longwave emitted minus that received; latent heat release is that due to evaporation minus that due to surface condensation.

The overall energy balance portion of Table 4-1 compares the albedo changes and changes in radiation from surface and clouds for the three cases. Cloud albedo, which can act as a whole-earth cooler, increased from the heat balance model to Tempreg1 to Tempreg2. However, surface albedo percentage declined in that order, tending to counteract the temperature buffering provided by cloud albedo in Tempreg1 and Tempreg2.

The surface energy balance section of the table provides information about changes in methods of surface heat loss in the various cases. The energy balance equation makes no prediction in this regard, while Tempreg1 showed little change from base case to the 30% case. However, Tempreg2 predicted significant changes in relative importance of heat loss mechanisms. Turbulent and latent heat both climbed in importance, while radiant loss declined to less than a third of its base case value. This marked decrease in the relative magnitude of radiant heat loss, which is a power law of temperature, provided temperature buffering against raised insolation.

Figures 4-23 and 4-24 graphically display these changes in Earth energy balance. Both Tempreg1 and Tempreg2 are represented by the left-hand bar in the figures, because each model is calibrated with present conditions. The middle bar represents Tempreg1 with solar power increased 30%, while the right hand bar gives the data for solar power increase in Tempreg2. Figure 4-23 gives the overall energy balance. Of note is that in Tempreg2, clouds were more important both in radiational losses and in albedo losses, and surface processes of albedo and radiation became less significant.

Figure 4-24 shows the changes in surface heat loss mechanisms, highlighting the large redistribution of heat loss from radiant heat to latent and turbulent. The result suggests that hydrologic interactions may significantly buffer Earth's surface temperatures, and that the overall effect of increased
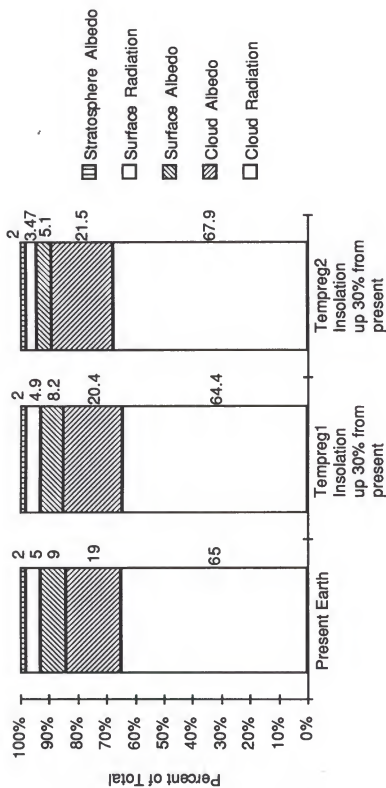
Figure 4-23. Percentage of total earth energy loss due to albedo and longwave radiation.
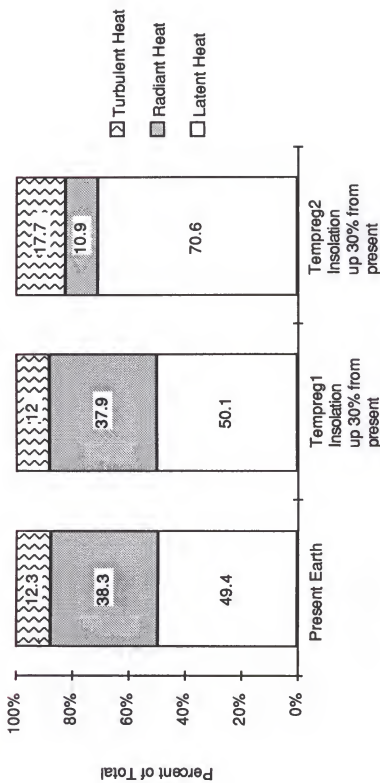
Figure 4-24. Percentage of surface heat loss due to latent, radiant, and turbulent loss mechanisms.

cloudiness is a reduction of surface temperature. Thus, inorganic systems of energy and materials may play a role in the regulation of Earth surface conditions, similar to the role that has been hypothesized (Lovelock, 1972) for the organic, biological systems of energy and materials. This hydrologic buffering action can add significant short-term regulation to the long-term temperature regulation proposed for weathering and CO2 feedbacks by Kerrick and Caldeira (1996).

Similar to the many separate temperature regulation mechanisms of the human body (Holling, 1995), it would seem that the Earth also has several overlapping systems that can regulate temperature on various time scales and to varying degrees. Rather than looking at these various explanations as mutually exclusive, perhaps they should be viewed as partially redundant components, which may complement each other to achieve the optimum control of temperature for total system function.

Global Systems of Human Industry and Fossil Fuels

Uses of nonrenewable fossil fuels and minerals are the basis for present industrial development of the whole Earth. In order to better understand the nature of the human industrial system and its relationship to ecological and geological resources, historical trends of fuel use were examined (Figures 4-25 through 4-29) and aggregated models were developed (Figures 4-30, 4-31, 4-33, 4-37, 4-40, and 4-41). Because records of fuel consumption are readily available, fuel use trends helped suggest appropriate model configurations, and were used to validate model simulations.

The Coal System

Coal was the first fossil fuel to be widely used for global industrial growth. Marchetti (1980) described coal's rise to prominence and later replacement as a global industrial fuel. Figure 4-25 gives the history of consumption levels of coal during the period 1860 to 1940. This period was chosen to screen out influence from the oil economy, which started after about 1940 (See subsequent paragraphs on oil economy.) The data for coal use was compiled from Clark, 1991; Energy Information Administration, 1995; Smil, 1987; and Davis, 1990; United Nations reports, various years; Cassedy and Grossman, 1990; and Fulkerson et al., 1990.

The pattern revealed for coal consumption was a sigmoidal growth curve, one which appears in many systems of various types (See Odum, 1987). It is usually associated with growth of systems until a limiting factor is reached, after which growth levels off. Because the coal resource was not significantly depleted at this time (over 99% remaining), the limit on this growth curve was not the availability of coal itself.

Figure 4-26 expands on the time frame of Figure 4-25, to include the years from 1940 to the present that were highly influenced by the oil system. After 1945, coal use again started to increase, in a much more linear fashion than the initial growth in consumption over the years 1880 to 1915. This graph suggests that the large increases in industrial assets due to the oil economy were feeding back in particular locations and circumstances to tap the lower quality coal resource, matching two distinct energy resources to mutually catalyze the use of both. This is quite similar to an earlier episode where the coal system fed back to catalyze use of wood (for structure and energy) in
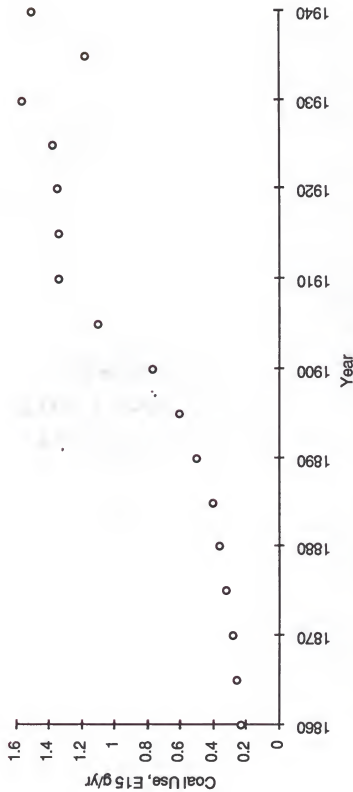
Figure 4-25. World coal use for the period 1860-1940, showing sigmoidal growth curve over the period 1880 to 1920, corresponding to coal's primary role in fueling world economic activity. Long plateau in coal use from ca. 1915 to 1945 suggesting a limiting factor in global economic development. Small depletion of the coal resource at this time (see Figure 4-29) suggesting that coal availability was not the limiting factor.
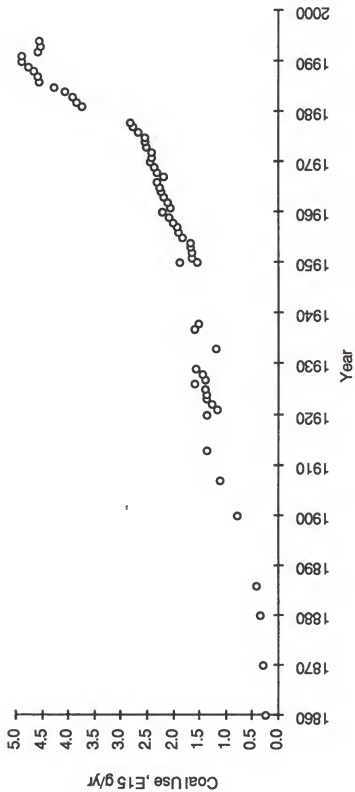
Figure 4-26. World Coal Use for the period 1860-1995, with an approximately linear growth curve for the period from 1945 through the present, corresponding to the time of oil as the primary economic fuel. Data assembled from Clark, 1990; Energy Information Administration, 1995; Smil, 1987; and Davis, 1991; United Nations reports, various years; Cassedy, 1990; and Fulkerson, 1990.

certain locations and circumstances, promoting deforestation in the industrialized countries.

The Oil System

Figure 4-27 offers insight into the changes occurring in the global industrial system after 1945 that could have contributed to the renewed growth of coal consumption. Oil-based growth of global civilization began at about that time, as shown by the growth curve of world oil consumption in the figure (Oil and gas data compiled from Fulkerson et al., 1990; Masters et al., 1990, Meadows et al., 1992; Cassedy and Grossman, 1990, World Resources Institute, 1991; Energy Information Administration, 1995; and United Nations reports, various years). Here again, a very distinguishable sigmoidal growth curve presents itself, with peak growth occurring near 1970, quickly followed by much slower growth and a leveling in the 1980's and 1990's. Hall et al. (1986) showed that energy return on investment, which is a measure of a resource's potential to expand industrial production (similar to net emergy in Odum, 1996) declined sharply after the oil embargo in 1972.

This trend suggests that a limit was being reached on the possible world growth of oil-based industry, just as the earlier sigmoidal shaped coal consumption curve suggested a limit on that system. However, at the time of slowed growth of the oil use, there was a significant (20% to 25% gone) depletion of the initial oil resource (See Figure 4-29). This fact suggests that declining net emergy (due to decreased availability of oil) may have played some part in the slowed use of that resource.

Figure 4-28 gives the growth curve for consumption of the suite of petroleum-based fuels, including crude oil, natural gas liquids, and natural gas. It is not very different from the curve for oil itself, suggesting that oil and gas are
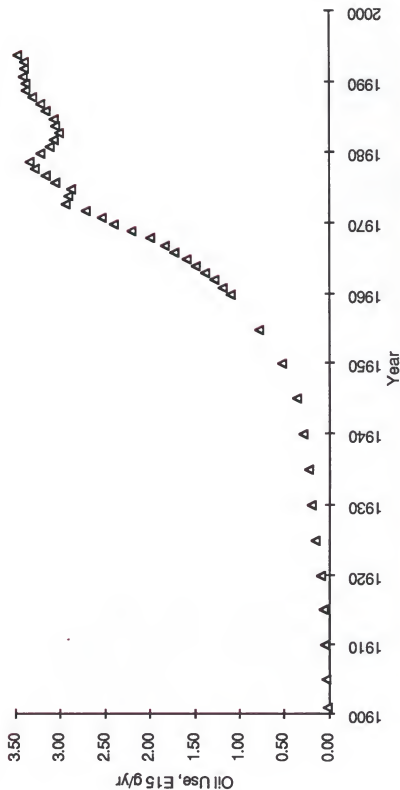
Figure 4-27. World Oil Use for the period 1900 to 1995, showing overall sigmoidal shape which suggests dynamics similar those of coal. Use level stabilizing much higher than coal, especially compared to the total estimated resource. Data assembled from Fulkerson, 1990; Masters, 1990, Meadows, 1992; Cassedy, 1990; World Resources Institute, 1991'; Energy Information Administration, 1995; and United Nations reports, various years.

186
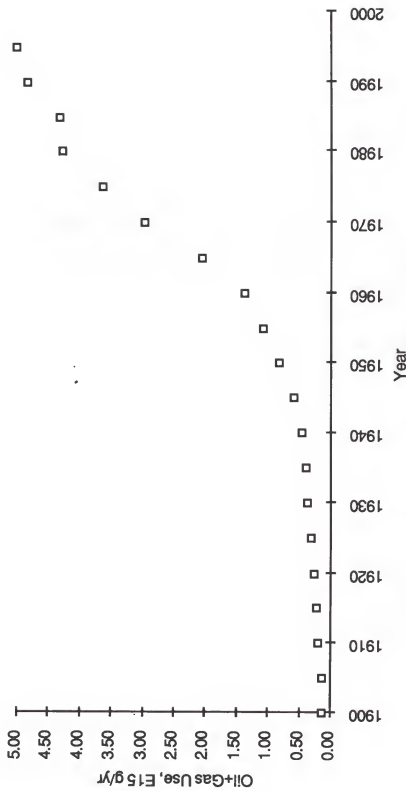
Figure 4-28. World use of petroleum products (crude oil and natural gas), over the period 1900 to 1995, showing little difference between overall petroleum curve and that for for oil alone, suggesting aggregation of oil and gas for simulations. Data assembled from Fulkerson, 1990; Masters, 1990, Meadows, 1992; Cassedy, 1990; World Resources Institute, 1991; Energy Information Administration, 1995; and United Nations reports, various years.

part of the same phenomenon, and, therefore, may be aggregated for the purposes of modeling and simulation.

<u>Coal and Oil Together</u>

Figure 4-29 gives the depletion curves for the total initial whole-earth resources of oil, natural gas, and coal, and that for the combined oil and gas. This graph is given on a percentage basis, and shows that the consumption levels of petroleum based fuels have been much greater, in comparison to the total resources, than the consumption levels of coal.

Comparing Figures 4-25 and 4-28, the leveling in coal use occurred around year 1910, while the growth of oil use did not start until about 1940. Also, by comparing Figures 4-26 and 4-27, it is evident that the growth of oil use did not cause decline in coal use. Rather, coal use increased all during the boom years of oil from 1940 to 1980. These facts suggest that the "coal plateau" from 1910 to 1940 was not due resource switching. Rather, coal's quality was too low, limiting its potential to further build industrial assets. Perhaps increased in coal use late in the 20th century was facilitated by global industrial expansion from oil use.

<u>Models Inferred from the Data</u>

The data discussed above on consumption of fuels suggest a model of the global industrial system that allows growth based on fossil fuel use, but also is limited by other factors. A very simplified, conceptual diagram of a model that meets these requirements is shown in Figure 4-30. In this model, the producer symbol on the left incorporates all ecosystem production, including agricultural systems and natural systems. The agricultural system is dependent on feedback from the human industrial system (fertilizer, clearing, planting, etc.),
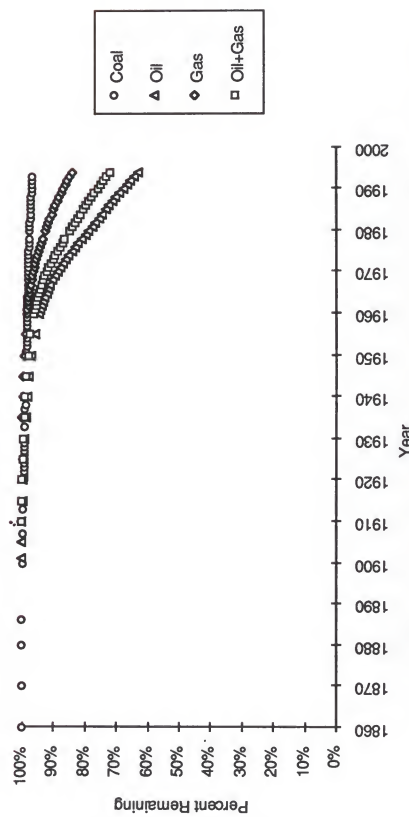
Figure 4-29. Depletion curves for coal and for petroleum resources, for years 1860 to 1995 showing coal depletion of less than 0.5 percent during coal growth, but oil depleted of about 40 percent during its growth. Consumption data assembled from Clark, 1990; Energy Information Administration, 1995; and UN, various years. Initial resource data assembled from Fulkerson, 1990; Masters et al, 1990; Meadows et al, 1992; World Resources Institure, 1991; Cassedy, 1990; and Pachauri, 1985.
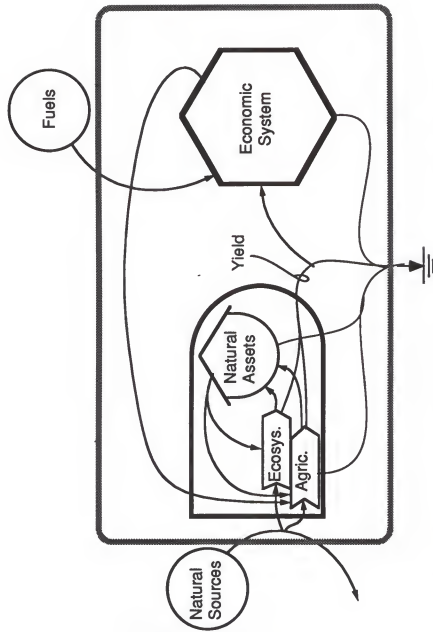
Figure 4-30. An aggregated model of the human economic system's relationship to natural resources, with both ecosystems and agricultural systems producing a harvestable yield, but agriculture giving more yield, and less natural assets. Fuels acting as a supplement to the economic system, drawing additional natural sources into agriculture.

and it competes for natural sources with the non-managed, natural ecosystems. Both of these production processes contribute a yield and build natural assets, such as soils, trees, and any other structure that helps utilize available energy. Agriculture, however, is a higher yield system, where yield is defined as production which is harvestable by people.

Thus, in this simplified model, the human industrial system grows by increasing the "harvestable yield", and fuels supplement that process by driving industrial growth, which feeds back to divert natural resources into high yield agriculture. This higher yield has a price, because it diverts some resources from the natural assets (soil, for one) that are required for all production systems, both natural and agricultural.

Figure 4-31 is an expanded diagram of the consumer system on the right in Figure 4-30. It contains two storages in the industrial system: fuel exploitation structure and general assets. It also contains two autocatalytic loops. The loop for growth of general assets is a simple one; feeding back to its own production process. The feedback for exploitation structure is more circuitous, as more exploitation structure (mines and wells) taps more fuels, which feed into the general industrial process, which develops more exploitation structure. Both of these growth modes rely on the yield of production systems as a basic input to the process; if they are using all of the yield, they will grow no more. However, these processes also grow more industrial assets, which feed back to increase yield, constituting another self-reinforcing growth mechanism.

Simulation of Fossil Economy Models

Simple coal model

Figure 4-32 shows a modified version of Figure 4-31, changed slightly by eliminating the feedback pathway from industrial assets to yield. Values for all
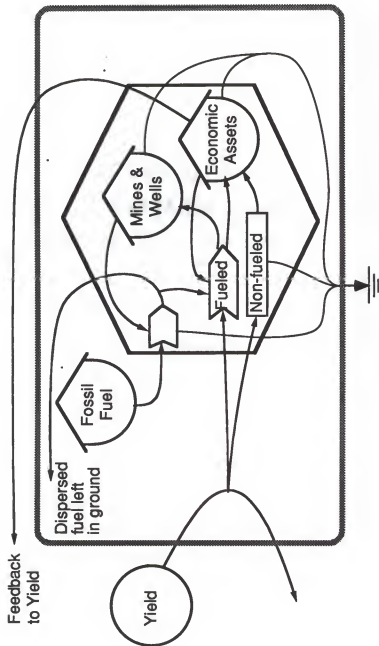
Figure 4-31. Aggregated conceptual diagram of the way human economies use fossil fuel to match natural systems with industrial agriculture, showing more details of the consumer module from Figure 4-31. Details of the industrial feedback to yield not shown, but see Figure 4-40 for a possible configuration.
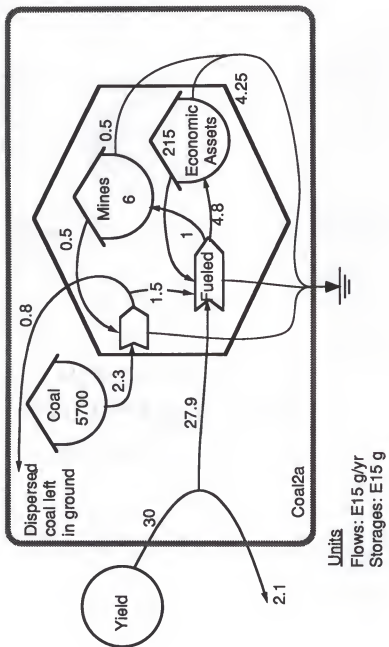
Figure 4-32. Coal2a, the generic fueled-economy model from Figure 4-31 adapted to simulate the coal-based industrial economic system in aggregate overview. Calibration values represent the height of the coal economy around the mid 1920's.

Units
Flows: E15 g/yr
Storages: E15 g

flows and pathways are shown, as developed in Appendix Table A-11. Because yield was modeled as a constant flow source, industrial assets fed back to increase the proportion of yield tapped, not the total yield. In the real system, industrial assets amplify agricultural yield in many ways. For simplicity, the linear pathway from yield to assets, which represented simple non-fuel agricultural practices, was eliminated. Figure 4-33 gives the same model, including variables for sources, storages, and pathway coefficients, and the differential equations used for simulating.

Simulation results for Coal2a, the model in Figure 4-33 (calibrated in Appendix Table A-11, program in Appendix Table B-10), are shown in Figures 4-34 through 4-36. Figure 4-34 part A shows the results for standard initial conditions and coefficient values, over a 200 year time span, beginning in the year 1800. The sigmoidal shaped growth curve of coal consumption is reflected very well by the simulation, and the time span of the growth is very close to historical data. General assets, E, increase at a much slower rate than the fuel consumption, reflecting their longer turnover time. R2, the amount of unused coal, remains at around 30 percent, which may be interpreted as the amount of coal which remains in the mines. The unused yield from nature, R, decreases as the system grows with the fuel subsidy.

Longer term behavior of the model is shown in Figure 4-34 part B, with a 2000 year time span. Over a 1500 year time span, coal supports a relatively stable industry, which then decreases quickly as coal reaches a certain level of availability that cannot support ongoing exploitation. Interestingly, the annual amount of coal left in the ground and rendered unavailable, denoted in the graph as the unused portion of coal, steadily decreases as does coal availability. In other words, efficiency of exploitation by simple systems may be automatically increased as resource becomes more limiting.
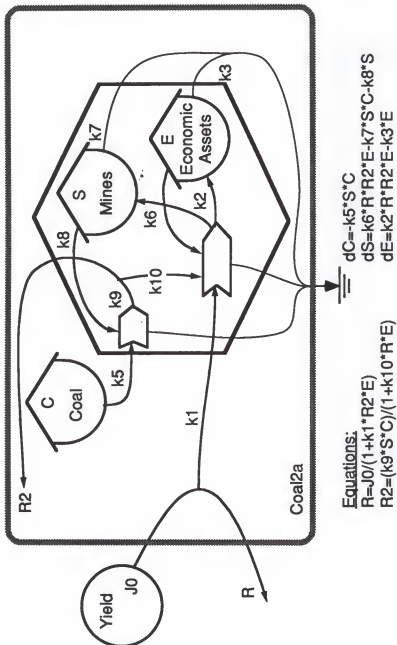
Figure 4-33. Coal2a, the model from Figure 4-32, showing programming symbols for sources, storages, and pathway coefficients, and listing the difference equations used for simulating.

Equations:

$$R = J0/(1+k1*R2*E)$$

$$R2 = (k9*S*C)/(1+k10*R*E)$$

$$dC = -k5*S*C$$

$$dS = k6*R*R2*E - k7*S*C - k8*S$$

$$dE = k2*R*R2*E - k3*E$$
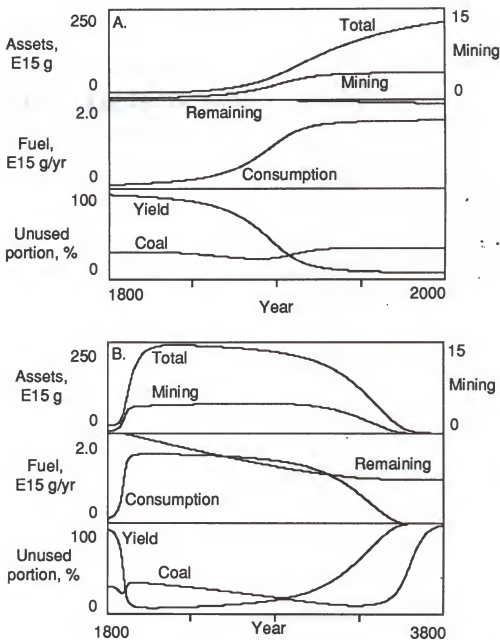
Figure 4-34. Simulation results for Coal2a, the model in Figure 4-33, as calibrated in appendix Table A-11. A. Simulation up to the present showing a quickly attained peak and a following plateau in fuel use, and a more slowly attained peak in total assets. B. Long term behavior showing long plateau in levels of fuel use and asset storage. Fuel resource not completely used up, and efficiency of coal use (inversely related to unused coal) showing self-adjustment over the period.

Figure 4-35 shows some sensitivity analyses of the model to changed initial conditions and coefficients. A doubling of the initial fuel resource changes only the rate of attainment of the temporary steady state, and does not affect the plateaus in storages and rates. A halving of initial fuel resource never allows the model to get going, and the small initial storages decrease to zero.

Changes in J0, the yield from natural systems, cause different effects. An increase of this parameter leads to a similar increase in model storages and rates, suggesting that J0 is a limiting factor in the model. This means that the coal system may have been more limited by food and natural resources besides the coal itself.

Part C shows the effect of changing coefficient k1, which determines the amount of yield that must be tapped to support a given level of industrial activity. Decreasing this coefficient means more yield is left over for the same level of activity, so that more can be supported with the leftover yield.

Figure 4-36 shows the results on the simulations of changing the turnover times of the storages, and of changing coefficient k10, which determines the level of fuel use required to support global industry. Increasing the turnover time of either storage will speed up the attainment of the steady state. The turnover time of exploitation structure produced a larger effect than that of general industrial assets. Halving the coefficient k10, which in effect halved the fuel levels required to support the same industry, also had interesting effects on the simulations. Predictably, the fuel consumption levels at steady state declined by about half. Overall industrial structure did not show any gains in steady state level, however, and the amount of unused fuel increased by about a factor of two.
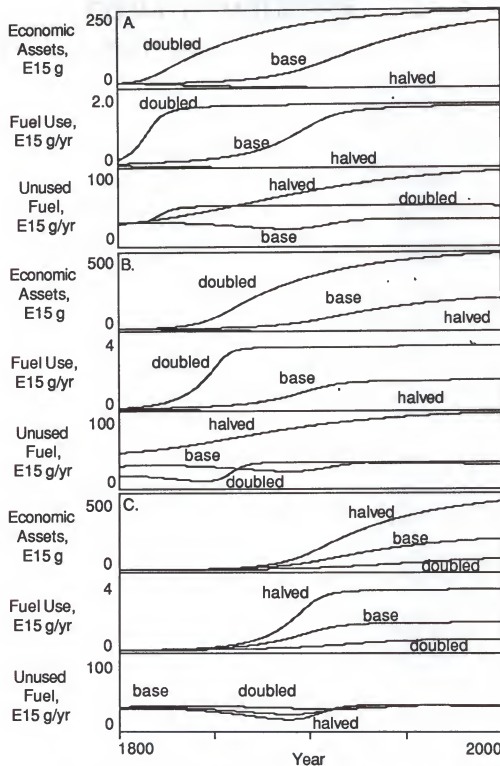
Figure 4-35. Sensitivity analyses for Coal2a, the model in Figure 4-33, as calibrated in appendix Table A-11. A) halved and doubled initial fuel resource. B) halved and doubled flow source J0. C) halved and doubled coefficient k1.
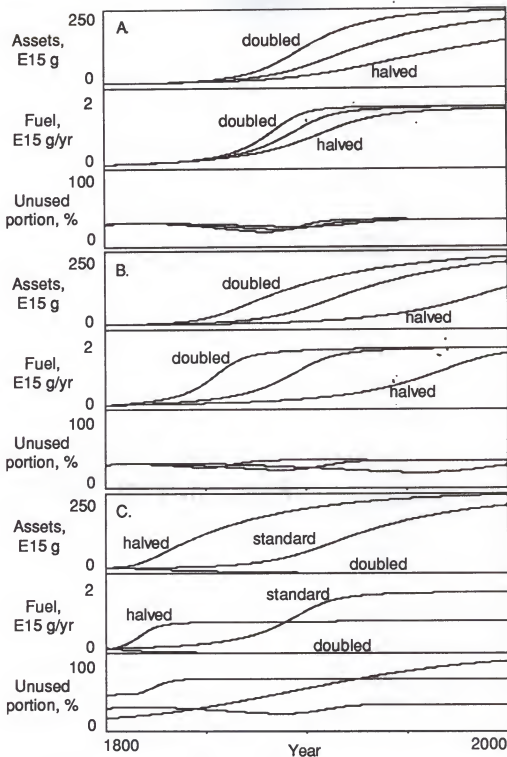
Figure 4-36. Sensitivity studies of model Coal2a, as diagrammed in Figure 4-33 and calibrated in Appendix Table A-11. A) Turnover time of economic assets changed by halving and doubling k6, k7, and k8. B) Turnover time of coal mines similarly varied. C) Coefficient k10, which determines the amount of fuel required to build assets, varied.

Simple oil model

The model Oiluse3, diagrammed in Figure 4-37, was designed to show the quantitative dynamics of petroleum use in the same framework as the coal use models. This model has the same configuration as the coal use model, but was calibrated with data developed for the present consumption, initial amount, and depletion of the petroleum resource. Values for flows and storages were developed in Appendix Table A-12, which also computes the coefficients for the model. J0, the yield from natural systems, was adjusted upward to reflect the greater feedback effect of the oil system on the management of natural systems. It is modeled as a constant flow, however, which is probably not the case for the real world, in which agricultural yields have increased with increasing support from fossil fuels.

Figure 4-38 shows the variables used for sources, storages, and pathway coefficients, and their places in the differential equations. Appendix Table B-11 lists the computer program used to simulate the simple oil model.

Figure 4-39 gives the short term and long term simulation results for Oiluse3, the model in Figure 4-37 (calibrated in Appendix Table A-12, program in Appendix Table B-11). It reproduces fairly accurately the major dynamics in historical data for petroleum consumption and depletion, as given in Figures 4-27, 4-28, and 4-29. The long term simulation of Figure 4-39 part B suggests that the major limitation on petroleum consumption is not an external limiting factor, as in the coal case, but the availability of petroleum itself. The model suggests that petroleum-based industry is a relatively short-lived phenomenon, especially compared to the coal system, which simulated plateaus in fuel consumption and storage of assets. The coal economy lasted longer because its performance was limited by renewable and coal's inability to convert more
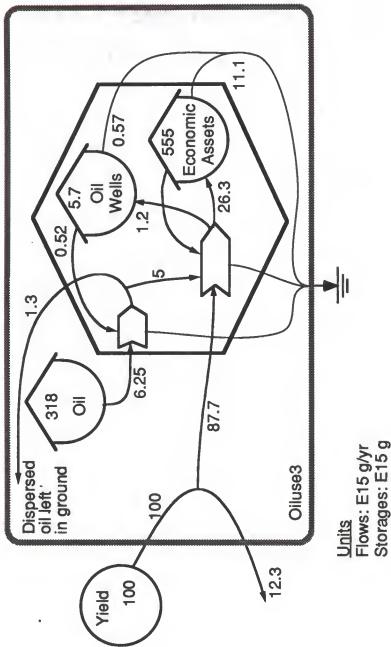
Figure 4-37. Oiluse3, adapted from the generic fuel-driven economy model in Figure 4-31 to simulate dynamics of the oil driven economic system. Numbers give calibration values, which approximately represent the present day state of the system.

Equations

$R = J0/(1 + k1 \cdot R2 \cdot E)$

$R2 = (k8 \cdot S \cdot O)/(1 + k9 \cdot R \cdot E)$

$dC = -k7 \cdot S \cdot C$

$dS = k4 \cdot R \cdot R2 \cdot E - k5 \cdot S - k6 \cdot S \cdot C$

$dE = k2 \cdot R \cdot R2 \cdot E - k3 \cdot E$
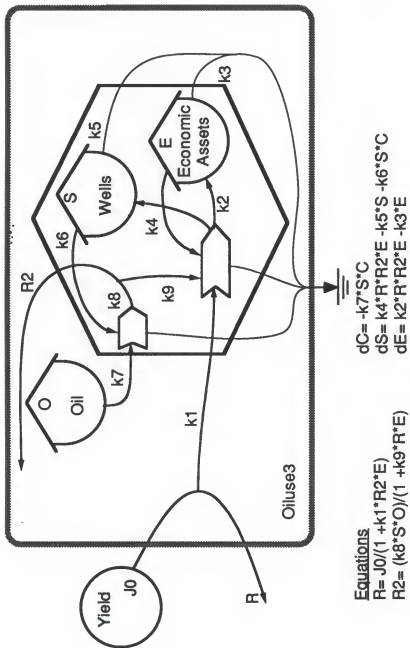
Figure 4-38. Oiluse3, an adaptation of the generic fuel-driven economy model in Figure 4-31, showing simulation details including symbols for sources, storages and flow coefficients, and difference equations describing the model.
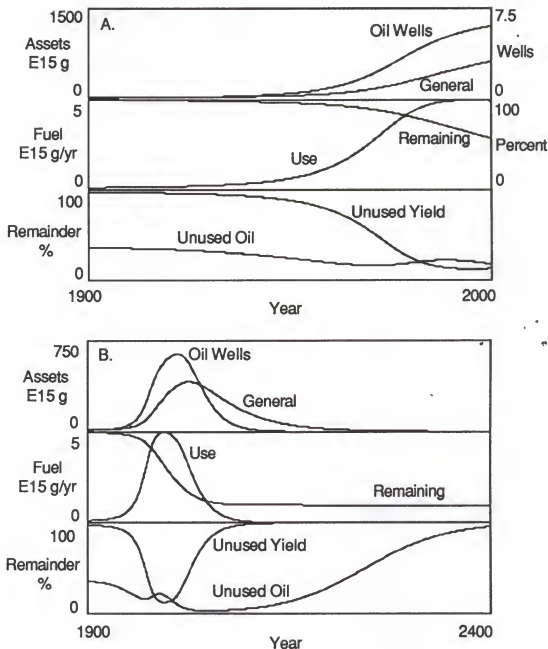
Figure 4-39. Short term (A.) and long term (B.) simulations of model
Oiluse3, as diagrammed in Figure 4-38 and calibrated in Appendix Table
A-12. Trends in fuel use and remaining amount matching historical data
fairly closely (Compare Figures 4-27 and 4-29). Present rate of crude oil
consumption, approximately 1.5% per year, decreasing quickly in B.

natural systems to high-yield agricultural systems. The model indicates a practical depletion of petroleum resources by about the year 2050, at which time the availability will have decreased to the point that it is no longer beneficial to pump petroleum. Note that at that time, there remains in place about one quarter of the initial resources.

Synthesis of the Fueled Civilization Models

A model which combines the coal and oil driven industrial systems, (Figures 4-33 and 4-37) with the interactive model for industrial and natural systems, is shown in Figure 4-40. This diagram is an aggregated synthesis of the major ideas developed for the overall fuel-civilization-nature interactions in this section of the study. The producer on the left consists of natural and managed ecosystems, each of which produces a certain level of harvestable yield and a certain level of maintenance of natural assets. On the right is the consumer civilization system, which pumps in natural yields in proportion to its own size. This process is facilitated by the use of fuels, which do everything from running tractors to refrigerating foods to paving roads. Additionally and importantly, industrial assets feed back to the natural systems by encouraging managed systems at the expense of unmanaged systems.

In Figure 4-40, values are shown for the calibration state of the storages and flows. These values were developed in Appendix Table A-13, which lists the literature sources, calculations and assumptions used to derive the values.

Figure 4-41 gives a diagram of Coaloil, the model from Figure 4-40, slightly modified by eliminating the nonfuel pathway from yield to industrial assets. This pathway may be negligible during times of high fuel consumption, and the purpose of this model is to simulate those times. The diagram shows variables for sources, storages, and pathway coefficients, and the difference
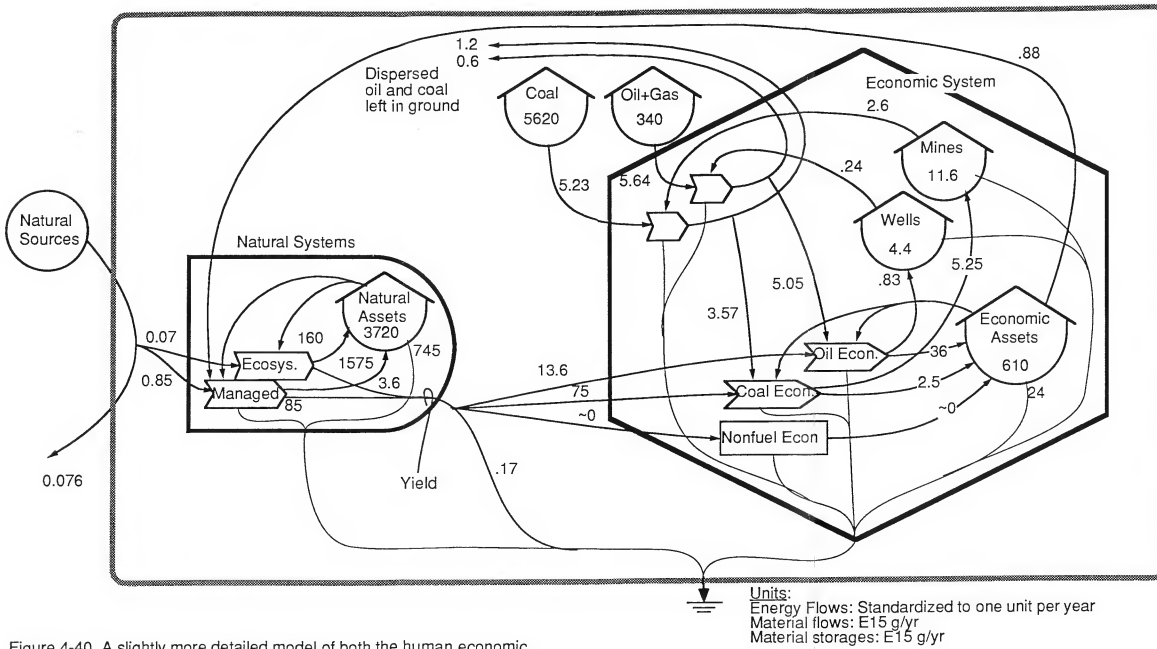
Figure 4-40. A slightly more detailed model of both the human economic system and its relationship to natural resources. Model incorporating concepts developed in Figures 4-30, 4-31, 4-33 and 4-37, with a competition between natural systems and agriculture, which produces more yield but less assets, and is supported by the economy.

Units:
Energy Flows: Standardized to one unit per year
Material flows: E15 g/yr
Material storages: E15 g/yr
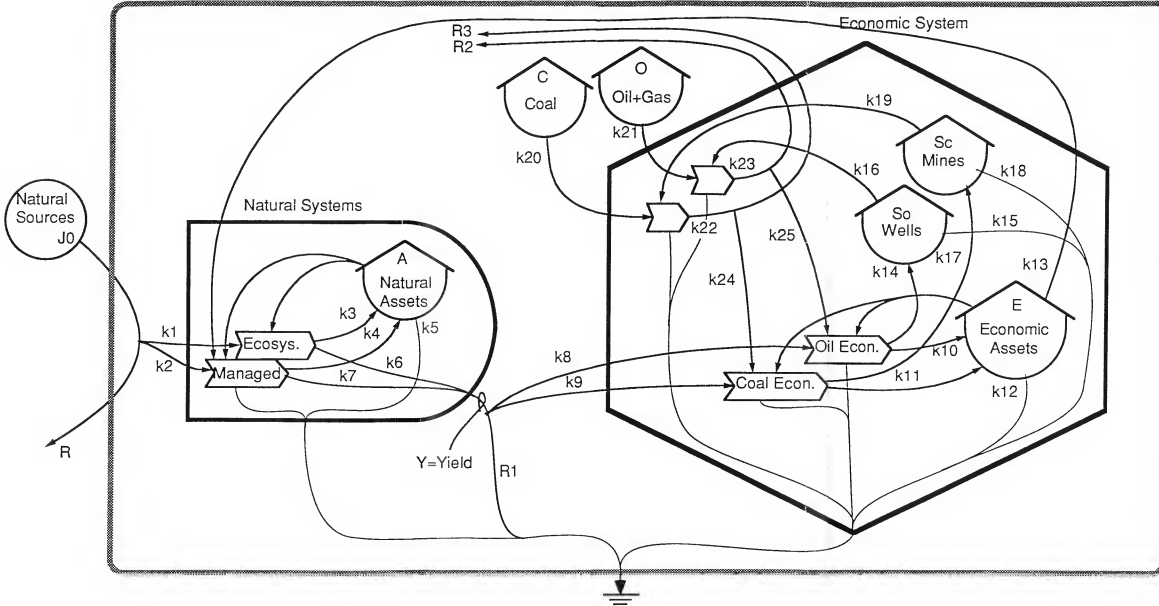
Figure 4-41. The detailed model of global economics and fuels from Figure 4-40, slightly modified for simulation purposes, and labeled with variables for sources, storages, and flow coefficients. Difference equations shown at bottom.

Equations:

$R = J0/(1+k1^*A+k2^*A^*E)$

$R1 = Y/(1+k8^*R2^*E+k9^*R3^*E)$

$R2 = (k23^*O^*So)/(1+k25^*R1^*E)$

$R3 = (k25^*C^*Sc)/(1+k24^*R1^*E)$

$dA = k3^*R^*A+k4^*R^*A^*E-k5^*A$

$dC = -k20^*C^*Sc$

$dO = -k21^*O^*So$

$dSc = k17^*R1^*R3^*E-k18^*Sc-k19^*C^*Sc$

$dSo = k14^*R1^*R2^*E-k15^*So-k16^*C^*So$

$dE = k10^*R1^*R2^*E+k11^*R1^*R3^*E-k12^*E$
$\quad -k13^*R^*A^*E$

equations for simulating. Short-term and long-term simulations of Coaloil, the model of Figure 4-41 (calibrated in Appendix Table A-13, program in Appendix Table B-12), are shown in Figure 4-42. Recent trends in fossil fuel use were matched reasonably well by the simulation, as seen by comparing part A with the previous Figures 4-25 through 4-29. The coal plateau of the early 1900's, coal's subsequent linear growth; and oil-use's extremely fast exponential growth and subsequent leveling were all duplicated by the simulation. Also importantly, values for industrial structure and depletion of natural assets were obtained that matched those from the literature (Dobrovolsky, 1994 and Appendix Table A-13).

Part B. of Figure 4-42 gives the long term simulation of the same model. The simulation predicted petroleum consumption to fall off quite rapidly following a peak in the 1990's, and also predicted a peak in global industrial assets by about the year 2015, followed by a decline over the ensuing 50 years to near pre-petroleum levels. This result is supported by a recent oil industry report (Campbell, 1997) that predicts a maximum in global oil and gas production near the year 2010.
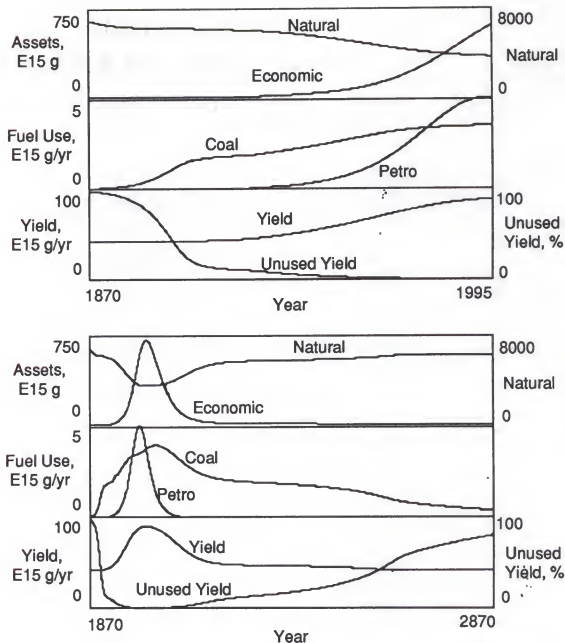
Figure 4-42. Simulation of Coaloil, the model in Figure 4-41, as calibrated in Appendix Table A-13. A. Short term simulation matching key patterns in fuel use of both coal and oil, especially the coal plateau, the oil consumption growth pattern and depletion pattern, and the increase of coal use as oil consumption grows. B. Long term simulation of the same model, for 1000 year time scale, predicting economic assets to peak at around year 2050.

CHAPTER 5
PULSING

Pulsing behavior is common to systems of all kinds, and geological examples include earthquakes, volcanoes, continent building, and hotspot activity, to name but a few. In order to understand the essence of the store and pulse phenomena in aggregate overview, simple models with many characteristics of pulsing were simulated. Systems that pulse have mechanisms that first produce storages of energy in a slow building mode, and then autocatalytically consume the stored energy in frenzied activity, resetting the system to its initial state.

In this chapter, models of pulsing systems will be developed starting from the simplest configurations and proceeding to the more complex. The resulting simulations will be examined to determine if they can reproduce patterns seen in real pulsing systems, such as robustness of pulsing over widely varied conditions, episodic events, and noisy pulse transfer from the smaller scale. Then, possible reasons for pulsing will be explored in light of the Maximum Power Principle (Lotka, 1925; Odum, 1987). Finally, a very simple pulsing model of the sedimentary cycle will be developed and the simulation results will be compared to geological records.

Two Module Pulsing Model

One of the simplest models that exhibits pulsing behavior is Pulse 2.0, in Figure 5-1. It has two autocatalytic units in series, the first driving the second

209

Units
Storage: Joules
Flow: Joules/day

Equations
R= J0/(1 +k0*A)
dA/dt= k1*R0*A -k2*A -k3*A*B -k6*A
dB/dt= k4*A*B -k5*B +k6*A
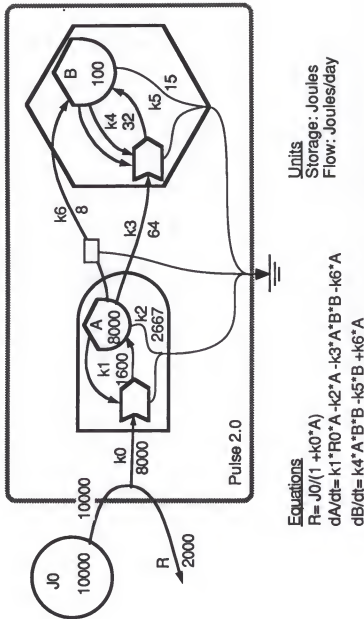
Figure 5-1. Diagram of Pulse 2.0, a very simple pulsing system, with no material cycles and no active feedbacks. Values and labels given for sources, storages, and pathways, and difference equations specified at bottom.

with a linear flow and further coupled to the second unit by a quadratic autocatalytic pathway. Storing in the left unit (producer) is followed by sharp pulsing consumption and growth by the right unit (consumer). A close geological analog for this model is the volcano, where the producer module stores molten rock in a magma reservoir, which is periodically consumed in a frenzied pulse of volcanism. The storage in the consumer module may represent explosive structure, the "plumbing" of the volcano, most of which only exists during the actual eruption.

Unit A has a large, dispersed storage with fast turnover, while B has a smaller, more concentrated, slower storage. In this simple model material cycles and active feedbacks, which are ubiquitous in the real world, are not included.

Figure 5-1 shows that Pulse2.0 was calibrated in a dynamic condition, as opposed to steady state. Storage A is declining, because its total inflows (1600), are less than its total outflows (2723). On the other hand, B is growing, because its inflows outnumber its outflow by 40 to 8. Calibration of pulsing models in dynamic state is convenient because the model always oscillates.

The simple differential equations that describe the model are given beneath it in the figure; Appendix Table A-14 shows the calibration procedure, using values from the diagram. Appendix Table B-13 lists the simulation program.

Figure 5-2, the simulation of Pulse 2.0, shows how the model oscillated with pulsing at a frequency of about one cycle per 150 years. Unit A showed growth to noticeable plateaus, while B entered frenzied consumption phases that resembled spikes in the time graph.

In Figure 5-3, Pulse 2.0 was simulated with varying efficiency of energy transfer to the producer A. For the volcano example, this could translate to
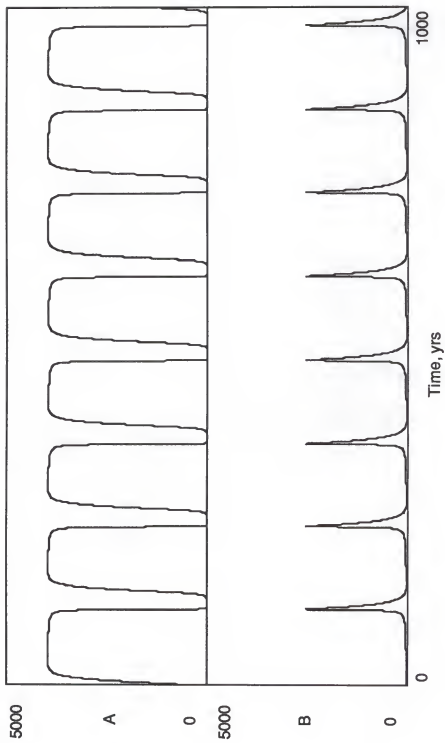
Figure 5-2. Simulation results for Pulse 2.0, the model in Figure 5-1, with coefficients as calibrated in Appendix Table A-14.

a) n=19%

b) n=19.2%

c) n=19.4%

d) n=20%

Time, yrs

Time, yrs
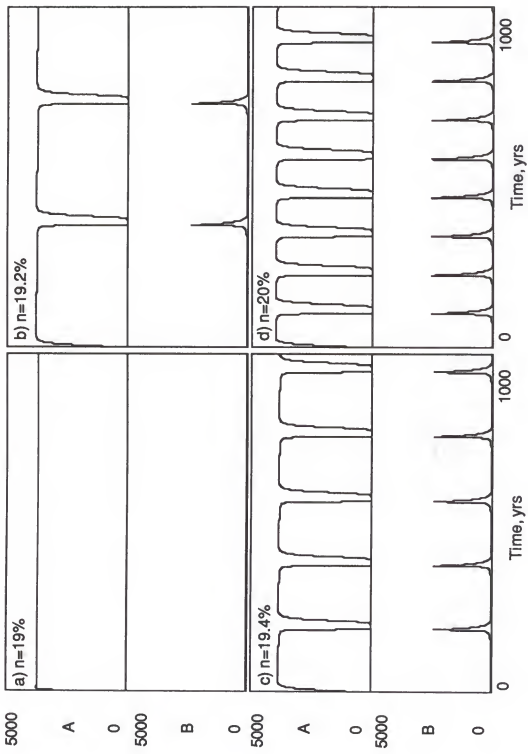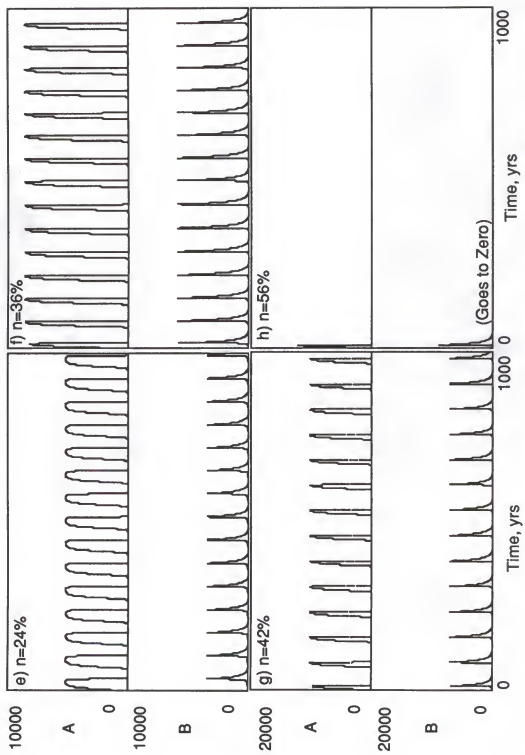
Figure 5-3. Sensitivity study for Pulse 2.0, the model in Figure 5-1, for varied levels of efficiency n of energy transfer to the producer A. Pulsing occurred over a broad range of efficiency, but pulse frequency and percent "downtime" varied.

varying the percentage of upwelling heat stored in the magma chamber. The model pulsed for efficiency values from 19.2% to almost 56%, and showed especially sensitive behavior right around 20%, where broad plateaus in A occurred for a narrow range of efficiency. Efficiencies outside this range destabilized the model, causing one or both of the storages to go to zero.

In Figure 5-4, the efficiency of energy transfer to the consumer was varied to gauge its effects on system dynamics. In the volcano analogy, this variation could represent the percentage of energy of the magma pool used to make eruptive structure. At and below 44% efficiency, the consumer dwindled to zero. Slightly higher efficiency induced a damped oscillation to steady state, non-zero values, and further increased efficiency changed the period and magnitude of pulses. The pulsing behavior continued up to 100% transfer efficiency, the thermodynamic limit.

This short example, the simulation of model Pulse 2.0, served to illustrate the complexity and variability of pulsing patterns that can be generated by extremely simple systems. The model also showed that the range of efficiencies which generate pulsing behavior was quite large, so that if the system configuration is conducive to pulsing, the pathway coefficients (the guts of the system) are not especially sensitive.

Coefficients for decay and autocatalytic pumping, however, were restricted to very limited ranges, to generate pulsing behavior. Perhaps a selection mechanism for those coefficients is at work in evolving systems that pulse.

Three Module Pulsing Model

To extend the results from Pulse 2.0 to more general cases, additions and changes to that simplest case were explored. If pulsing is general in real,
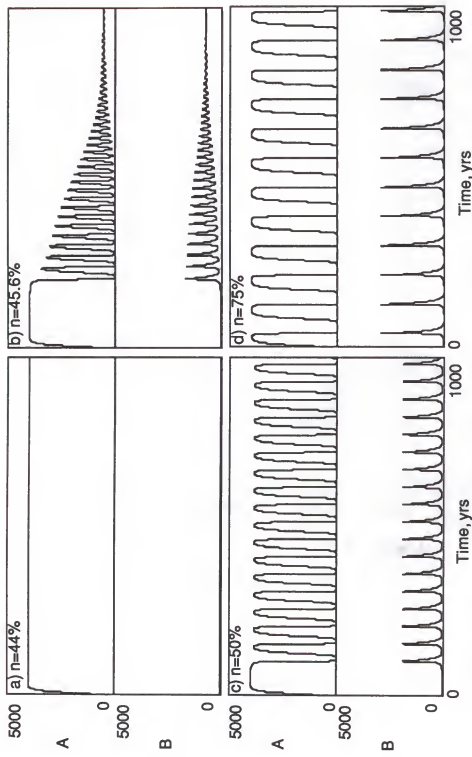
Figure 5-4. Sensitivity study for Pulse 2.0, the model in Figure 5-1, for varied levels of efficiency n of energy transfer to the consumer B. Pulsing occurred over a broad range of efficiency, and damped oscillations occur at efficiency of approximately 45%.

complex systems, then more complex models should also show pulsed oscillatory behavior. These extended models can indicate conditions required for and whole system effects of the store and pulse phenomena.

Pulse 3.01, the model in Figure 5-5, adds the additional consumer unit C to Pulse 2.0 (Figure 5-1). Like unit B, C is fed by both linear and quadratic autocatalytic pathways, from a single unit. There is also a linear pathway from A to C. To extend the volcano analogy to this model, the left producer now represents a lower quality unit that produces concentrated heat, possibly a hydrothermal surface system that channels heat along groundwater routes. Then, the magma chamber is the middle unit, or first consumer, which stores the heat irregular pulses, and the right unit is the volcanic eruptive structure as before.

The calibration condition for this model is identical to that for pulse 2.0, except for the new pathways. Again, storages (including C) are calibrated dynamically, not in steady state. Appendix Table A-15 shows the calibration values for sources, flows, and storages, and the calculated model coefficients k1 through k11. The Basic language simulation program for the Pulse 3.01 is given in Appendix Table B-14.

Simulation of Pulse 3.01 produced a rich variety of oscillatory pulsing behavior, as shown in Figures 5-6 and 5-7. The figures show studies of sensitivity to varied transfer efficiencies to the units A and C in Figures 5-6 and 5-7, respectively. The calibration condition as per Appendix Table A-16 is simulated in both Figure 5-6 b), for efficiency n=40%, and in Figure 5-7 c), for efficiency n=50%.

In Figure 5-6 the pulsing period of A and B were controlled by the pulsing of the next higher level C. In each of the four cases, A and B pulsed at their own natural frequency (which varies with efficiency), until C reached its critical
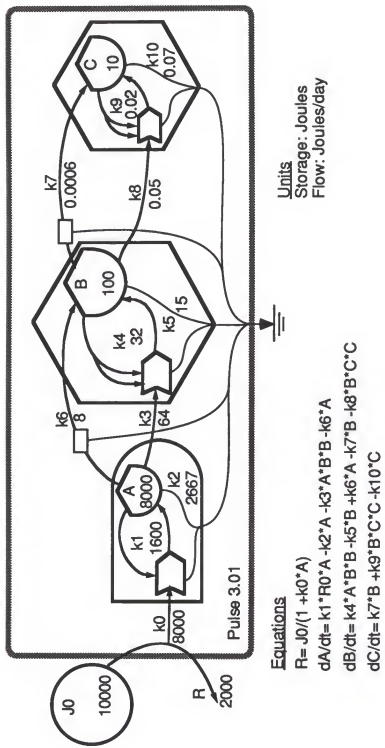
Figure 5-5. Configuration of a simple three module pulsing system, Pulse 3.01, showing calibration values for sources, flows, and storages, and the pathway coefficients.

Units
Storage: Joules
Flow: Joules/day

Equations

$R = J0/(1 + k0*A)$

$dA/dt = k1*R0*A - k2*A - k3*A*B*B - k6*A$

$dB/dt = k4*A*B*B - k5*B + k6*A - k7*B - k8*B*C*C$

$dC/dt = k7*B + k9*B*C*C - k10*C$
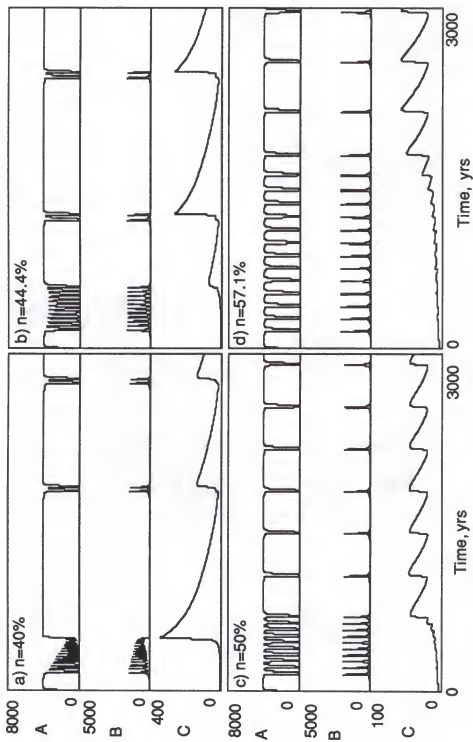
Figure 5-6. Sensitivity study for Pulse 3.01, the model in Figure 5-5, as calibrated in Appendix Table A-15. Efficiency n of energy transfer to the producer A was varied by adjusting coefficient k1.

a) n=50%   b) n=40%   c) n=33%   d) n=13.3%

Time, yrs

A   B   C

8000   5000   100   400   0   3000
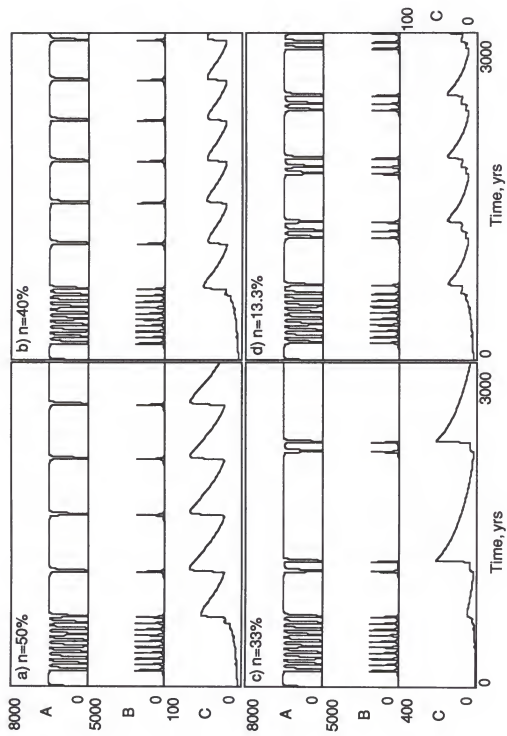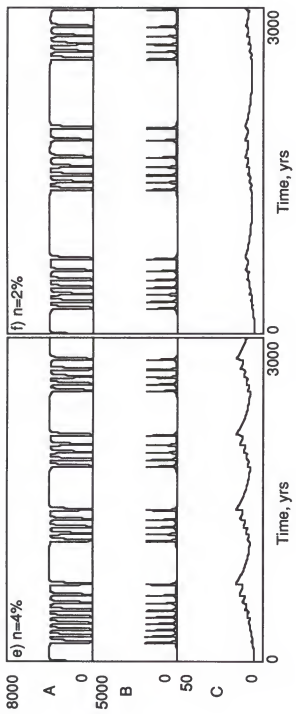
Figure 5-7. Sensitivity study for Pulse 3.01, the model in Figure 5-5, with varied efficiency n of energy transfer to the high order consumer C. Efficiency was varied by adjusting coefficient k8.

pulsing value. After that, C prevented A and B were from pulsing by regulating B. Only after C decayed sufficiently could B once again grow and pulse. At that time, however, C was ready to pulse almost immediately, because of its slow turnover time and slow decline in size.

Component C controlled the pulsing period of A and B in many of the simulations. However, if pulsing is a general phenomenon at all scales, then each scale may be expected to pulse at its own frequency, rather than being controlled by the higher scale. Figure 5-7 is a study of the model's sensitivity to varied efficiency of energy transfer to the unit C. System behavior was closer to the cross-scale pulsing paradigm, in which pulsing occurs at each scale, and each scale sees smaller scale pulsing as noise and larger scale pulsing as disasters. A and B pulsed at their own period during some time intervals, while they were controlled by C during other intervals. At very low efficiencies (n=2% and n=4%) system behavior was remarkably episodic; B pulsed at seemingly chaotic intervals, while C oscillated with somewhat more consistent frequency.

Model Pulse 3.0 is the same as Pulse 3.01 (Figure 5-5), except that the linear pathway between A and C was deleted. The simulations of both models were very similar. Pulse 3.0 was calibrated identically to Pulse 3.01, as in Appendix Table A-16. This model simulated highly episodic behavior, as shown in Figure 5-8. Component C's controlling influence on the pulsing behavior of A and B is again very apparent. Changes observed in pulsing patterns, which reflected a switching on and off of a controlling influence (component C), indicated that the store and pulse phenomena is very dependent on pairs of units which pulse together. In Pulse 3.01 and Pulse 3.0, the unit pairs that exhibited pulsing behavior changed during model runs. At certain times, A and B were the pulsing pair. At other times, it was B and C that pulsed together. The lack of coexisting, different pulsing frequencies was
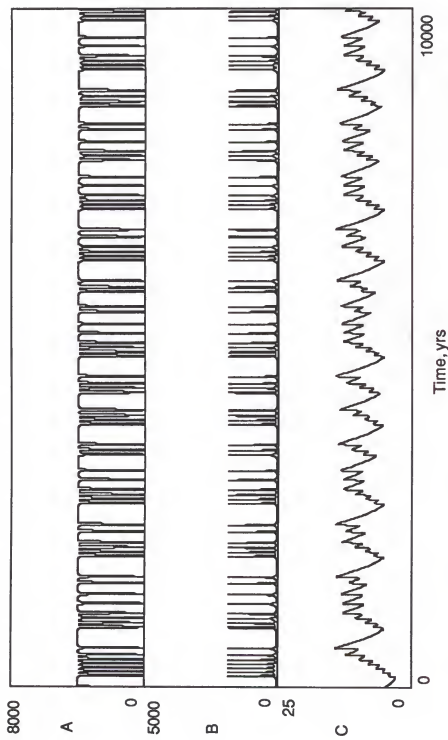
Figure 5-8. Simulation of Pulse 3.01, similar to the model in Figure 5-5, except the linear pathway from producer A to high order consumer C was removed. The lack of noticeable repetition of pattern was remarkably similar to episodic behavior.

significant. These results strengthen the link between coupled units and the store-pulse phenomenon.

Three Module Model with a Slow Storage

Pulsed oscillatory behavior in nature sometimes depends on the slow buildup of a storage which is unavailable to normally occurring consumption mechanisms. In this case, a rarer, more intense consumption unit can develop, initiating pulsing in a separate period. Examples in nature include wood buildup in forests that can be consumed by fire, but not insects; and stress energy storage in transform faults that can be consumed by violent earthquakes, but not by low energy slip or simple deformation.

The model Pulse 3.1, shown in Figure 5-9, is very similar to the previously described Pulse 3.01 (Figure 5-5), except that a slow storage M has been included. M is fed by producer A, and contributes to higher order consumer C. Mid level consumer B is cut out of the loop, so to speak, by A's development of a high quality storage, which is unavailable to B. In this model, both first level consumer B and slow storage M are necessary to the existence and growth of second level consumer C.

Pulse 3.1, the model in Figure 5-9, is calibrated in Appendix Table A-16, and Appendix Table B-15 lists the computer code for the simulation program. Pulse 3.1 generates pulsing at two distinct frequencies, as shown in Figure 5-12(b).

Figures 5-10 to 5-12 show simulation results for Pulse 3.1, the model in Figure 5-9. Each figure shows a sensitivity analysis for changed values of efficiency of energy transfer to each of the three modules.

In Figure 5-10, unit A's efficiency was varied by changing the coefficient $k1$. For the standard run, with the coefficients as in Appendix Table A-16, the

224

Pulse 3.1

Equations

R= J0/(1 +k0*A)

dA/dt= k1*R0*A -k2*A -k3*A*B*B -k6*A

dB/dt= k4*A*B*B -k5*B +k6*A -k7*B -k8*B*C*C

dC/dt= k7*B +k9*B*C*C -k10*C

Units
Storage: Joules
Flow: Joules/day
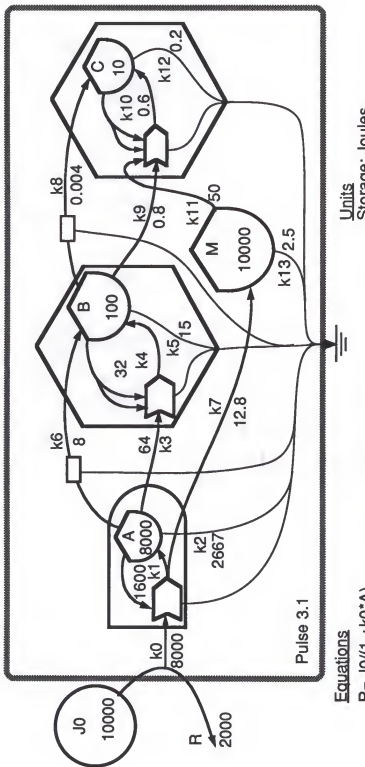
Figure 5-9. System diagram of Pulse 3.1, a simple three module pulsing configuration,
with a slow storage M unavailable to mid-level consumer B. Calibration values are
shown for the sources, flows, and storages, and the pathway coefficients are labeled.
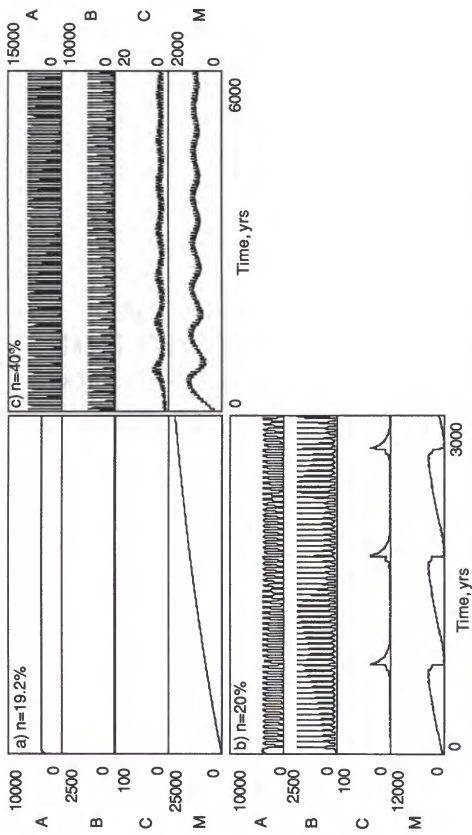
Figure 5-10. Sensitivity study for Pulse 3.1, the model in Figure 5-9, as calibrated in Appendix Table A-16. Efficiency n of energy transfer to the producer A was varied by adjusting coefficient k1.

efficiency was 20%, and two distinct pulsing frequencies existed. A slight decrease in this efficiency cut off pulsing by not allowing the first order consumer B to reach its critical pulsing level, where the autocatalytic pathway would take over.

Increases in unit A's transfer efficiency led to small increases in the pulsing frequency, but also to a dampening of the oscillations of the second order consumer C. This may have been due to the higher amplitude of oscillation for A and B, which caused short term changes in the C, effecting a high frequency on/off switching of its autocatalytic pulsing mechanism.

Figure 5-11 shows a sensitivity study for Pulse 3.1, in which the efficiency of energy transfer to unit B was varied from 46% through the calibration value of 50%, and up to the thermodynamic limit of 100%. Here, a small decrease in the efficiency induced oscillation damping, while higher efficiency spread out the pulses of the entire system. Because the first order consumer B grew more and faster from producer A, and A was drawn down lower, the pulsing period was lengthened.

Figure 5-12 shows a sensitivity study for Pulse 3.1, when the efficiency of energy transfer to the second order consumer C is varied from 25% through 175%. This efficiency may exceed 100% due to additional energy inputs from slow storage M (efficiency n is defined as J10/J9, the flow into third order consumer C divided by the flow out of second order consumer B). The model output was very robust to changes in this efficiency, but did show cessation of pulsing at very low values, and dampened oscillations at very high values. At the low efficiency levels, unit C never reached its critical pulsing level, while high efficiencies enabled C to maintain enough storage to hold M low and suppress pulsing.
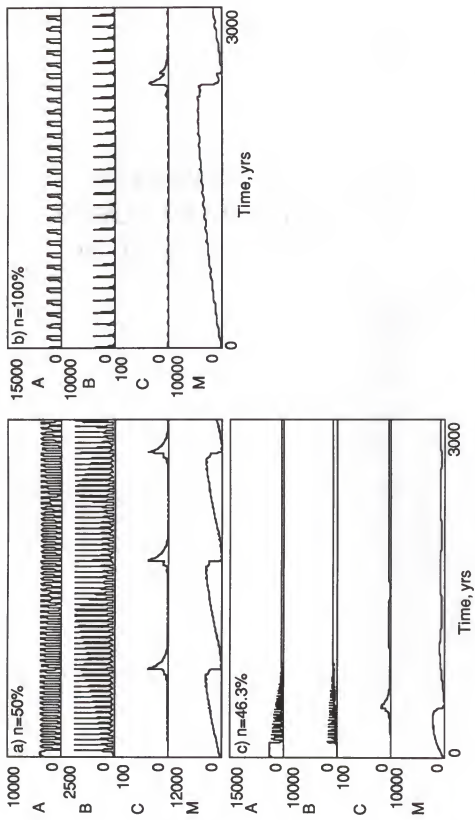
Figure 5-11. Sensitivity study for Pulse 3.1, the model in Figure 5-9, as calibrated in Appendix Table A-16. Efficiency n of energy transfer to the consumer B was varied by adjusting coefficient k4.
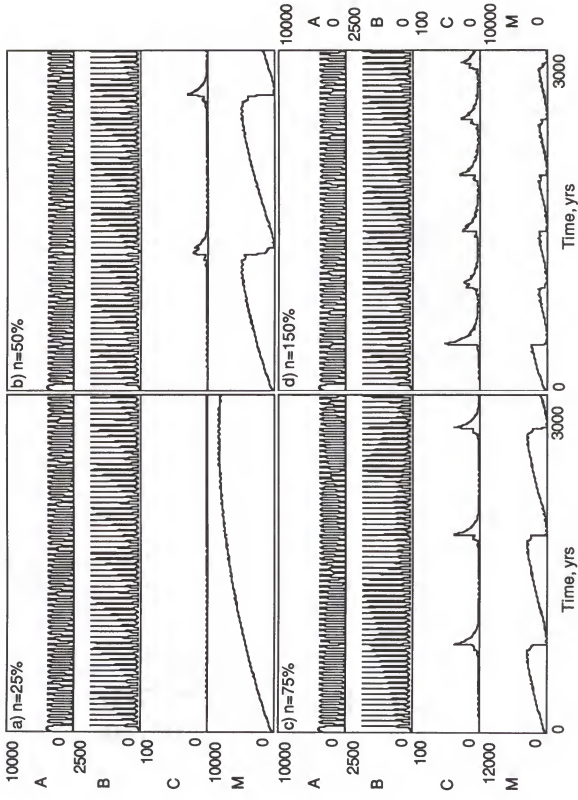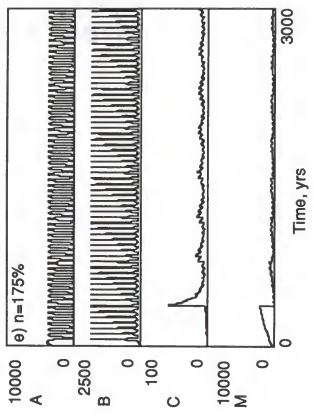
Figure 5-12. Sensitivity study for Pulse 3.1, the model in Figure 5-9, as calibrated in Appendix Table A-16. Efficiency n of energy transfer to the high order consumer C was varied by adjusting coefficient k10.

The "random" positions of A and B during the time of C's pulse had a significant effect on the size and shape of C's pulsing waveform. In this system, small scale events influenced some aspects of larger scale parameters, but not the overall period or general behavior or the whole system.

In general, systems that include a slow storage, which is unavailable to a certain consumption unit, can produce pulsing behavior at several scales, no matter the number of scales modeled. Pulsed oscillations can be initiated by higher order, rarer consumption units that require larger energy storages to start, but then grow in frenzied consumption modes.

Pulse 3.1's simulation results also reinforced the notion that coupled units encourage, and may even be required for, oscillatory pulsing behavior. In that model, units A and B pulsed together, while the slow storage M and consumer unit C formed the second pulse pair.

Four Module Pulsing Model

Pulse 4.0 is a further extension of Pulse 2.0 and Pulse 3.01. It was calibrated similarly to Pulse 2.0 and Pulse 3.0, except that the third module C was adjusted to match the new, fourth unit D, so that each pair functioned as a producer/consumer couple. This model represents systems that include long chains of energy transformation, such as ecosystems with many trophic levels, or perhaps whole-earth sediment cycling from ocean ridges to sediments to mountains to continents. Pulse 4.0, shown in Figure 5-13, was calibrated in Appendix Table A-17, and the computer code is shown in Appendix Table B-16. Its simulation results are given in Figure 5-14.

The simulation patterns shown in Figure 5-14 indicate some important features of pulsing models. For instance, two pairs of storages act as the basic pulse units, with A and B tightly coupled in their pulse, and C and D also pulsing

231
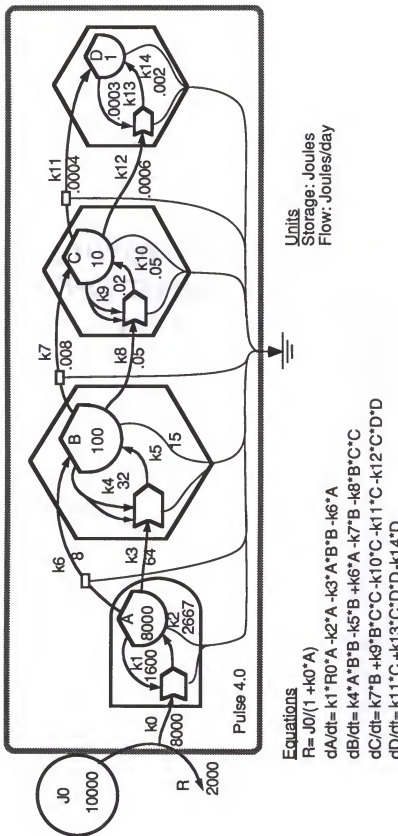
Figure 5-13. System diagram of Pulse 4.0, a simple four module pulsing configuration. Calibration values are shown for the sources, flows, and storages, and the pathway coefficients are labeled.

Units
Storage: Joules
Flow: Joules/day

Equations

$R = J0/(1 + k0*A)$

$dA/dt = k1*R0*A - k2*A - k3*A*B - k6*A$

$dB/dt = k4*A*B - k5*B + k6*A - k7*B - k8*B*C*C$

$dC/dt = k7*B + k9*B*C*C - k10*C - k11*C - k12*C*D$

$dD/dt = k11*C + k13*C*D - k14*D$
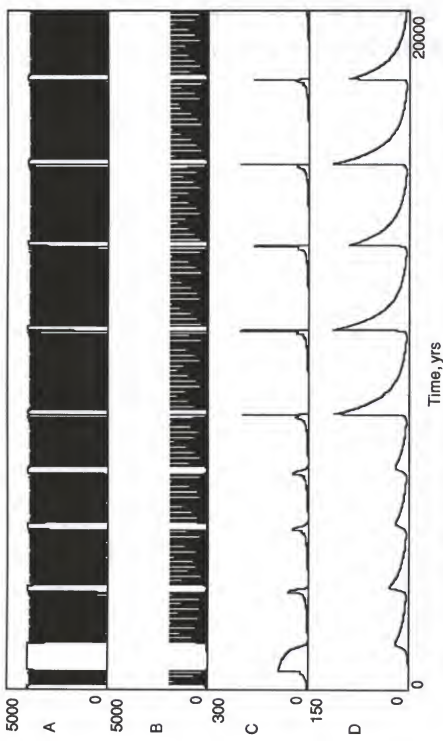
Figure 5-14. Simulation output for Pulse 4.0, the model in Figure 5-13, as calibrated in Appendix Table A-17. Some interesting features are the "noisy" variation of producer A and low level consumer B, regulation of low level pulsing by the high level pulsing, and changing pulse magnitudes on the higher level.

as a couple. This pattern suggests the idea that pulsing in nature is more apt to arise from tightly coupled production/consumption cycles which require at least two storages to properly model.

In this case, two frequency regimes were noticeable, corresponding to the A-B pair and the C-D pair. The A-B pair pulsed at a frequency on the order of 200 years while the C-D pair pulse frequency was close to 2000 years. The order of magnitude difference in pulse-pair frequency seemed necessary to limit interference, and allowed the low frequency pair to proceed independently of the high frequency pair. Figure 5-14 shows that some interference did occur during times when C was large. In this case pulsing at the higher scale actually facilitated small scale pulsing of the A-B pair, by regulating the average size of C. Larger values of C prohibited pulsing of the A-B pair by holding down B values.

The simulations of Pulse 4.0 also established the general possibility of multi-level pulsing on different frequencies, even without an intermediate slow storage as in Pulse 3.1. Many system configurations can lead to oscillatory pulsing on different scales. Also interesting in the simulation results of Figure 5-14 were the episodic behavior in both spacing and magnitude of the pulses. This type of irregular, aperiodic pattern was termed "chaos" by Scott (1991).

Pulsing and Power Maximization: a Simple Case

The observed generality of pulsing requires explanation. If systems evolve to maximize the flow of power (cf. Lotka, 1922, Odum and Pinkerton, 1955) or empower (cf. Odum, 1983, 1996), then perhaps pulsing somehow allows systems to pump energy at higher rates. In order to examine this hypothesis, Alexander (1978) developed a simple two storage, energy driven model of material activation and recycle, very similar to that in Figure 5-15 part

A.
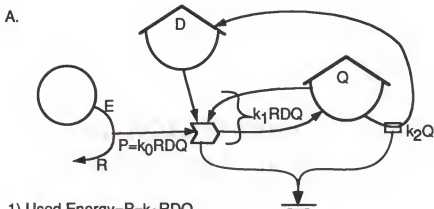
1) Used Energy=$P=k_0RDQ$

2) $R=E/(1+k_0DQ)$

3) $T = Q+D$ (total material = T)

Then substituting for 2) and 3) into 1):

$P=k0(E/1+k_0TQ-k_0Q^2)(T-Q)Q=(k_0EQT-k_0EQ^2)/(1+k_0TQ-k0Q^2)$,

which has the graphical form in B):

B.

$$P= \frac{k_0EQT - k_0EQ^2}{1 + k_0TQ - k0Q^2}$$

Q, % of T
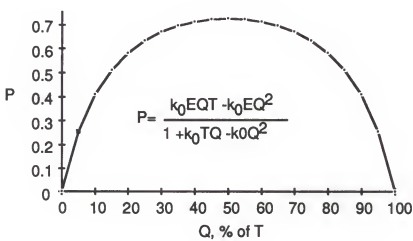
Figure 5-15. A. Simplified model of energy capture and material recycle to study effects of pulsing on system power flow, with summary equations. B. Graph of power as a function of storage Q: Total power flow can be increased by pulsing if pre-pulse value of Q is greater than 50% of total material.

A, except with no limit on the energy source. He simulated pulsing in the model by dumping the activated storage into the dispersed storage at arbitrary time intervals. By integrating power over time, he found that pulsing increased long-term average power flow in some cases.

In order to evaluate the possible power maximization of pulsing behavior on systems with limited power sources, the model in Figure 5-15, part A was constructed. This model is a very simple autocatalytic configuration of material activation and recycle to dispersed storage, which may be one of the simplest representations of real systems. Because of material conservation inside the system, the nonlinear equations can be simplified and solved for power draw as a function of the activated storage, as shown in the bottom of Figure 5-15 part A. When this somewhat complex function is graphed, a parabolic curve is obtained with maximum power flow when Q equals 50% of the total material storage. This result indicates that the effect of pulsing on the system depends on the pre-pulse value of Q. If it is greater than 50% of total material, then dumping some of Q can result in greater power flow. If the pre-pulse value of Q is less than 50% of total material, however, any decrease in Q will decrease power flow. In fact, any influence that makes this simple system operate closer to 50% storage in Q helps maximize power.

This simple example illustrates that if systems with recycling material, have a production function that depends on two different storages of material, an optimum in the activated storage can exist for maximum power. Real systems with more complex configurations may have power maxima at many different values of the activated storage (as a percent of total), but pulsing in general may be consistent with power maximization from limited sources.

To test the accuracy of the graph in part B of Figure 5-15, the simplified expression for power, $P = (k_0 * E * Q * T - K_0 * E * Q2) / (1 + k_0 * T * Q - k_0 * Q2)$, was

differentiated with respect to Q, with the result as follows: $dP/dQ = (k_0*E*T -2*k_0*E*Q) / (1 +2*k_0*T*Q -2*k_0*Q^2 +k_0^2*T^2*Q^2 -2*k_0^2*T*Q^3 +k_0^2*Q^4$. When the numerator was set to zero, the expression yielded $Q=T/2$, which indicates a local minimum or maximum, agreeing with the graph that the maximum power draw is when Q is 50% of the total material T.

In order to test this concept of power maximization, the model was prepared for simulation as shown in Figure 5-16. In the figure, pathways are labeled with flow values and flow coefficients, while storages and sources are labeled with their calibration value and programming symbol. The model was calibrated as shown in Appendix Table A-18; the first case was for a steady state condition in which Q was 50% of T, and the second calibration was for a steady state where $Q=0.75$ T. The pulse events in this system transfer material from Q to D, but the amount transferred and the interval between pulses are unspecified. These parameters, therefore, may be manipulated to test model response.

Simulation results for the model, program listed in Appendix Table B-17, are shown in Figures 5-17 and 5-18. In Figure 5-17, the model was run as in the first calibration case, with the steady state value of Q equal to 50% of T. The three graphs show behavior as pulsing interval is lengthened, so that the system spends an increasing proportion of time at its steady state. The total power draw increased from A to C, because the optimum condition was more closely approximated.

The simulations of Figure 5-18 used the second calibration condition, in which Q's steady state value was 75% of T. Proceeding from graph A to C, the pulse interval and transfer amount were changed to make the system operate closer to the optimum power range, in which Q is 50% of total material. Total power draw $\sum P$ increased in each case, indicating that the system draws most
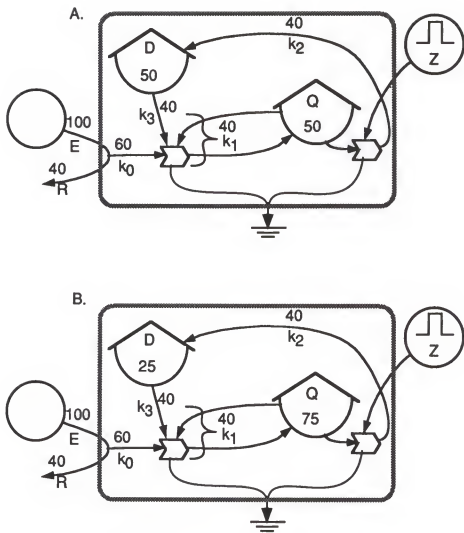
Figure 5-16. Diagram of the limited flow source pulsing model, to to test the optimal power draw response. Calibration values shown for the two steady state conditions: A. 50% and B. 75% of the total material stored in Q.
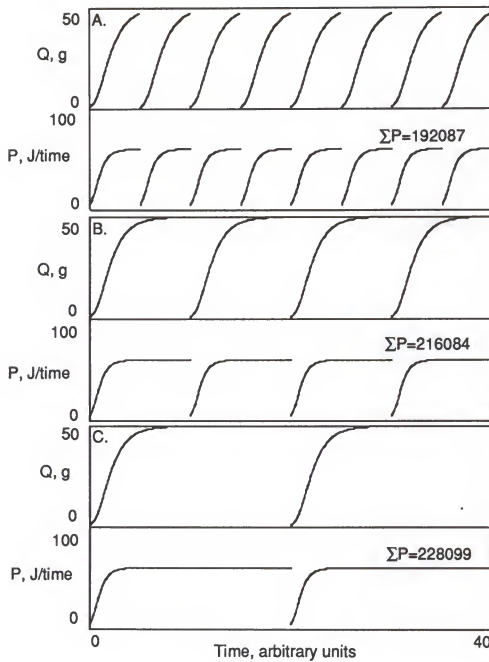
Figure 5-17. Simulation of the model in Figure 5-16, as calibrated in Appendix Table A-18 Case 1; computer program as listed in Appendix Table BD1. Pulsing intervals in arbitrary units: A. 5; B. 10; C: 20. ΣP denoting total integrated power draw.
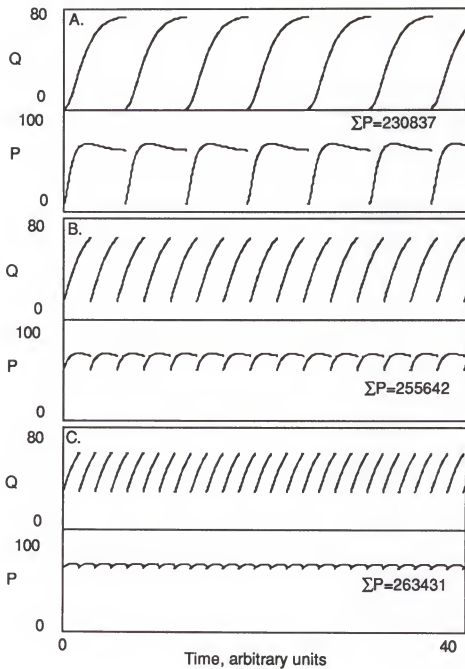
Figure 5-18. Simulation of the model in Figure D2, as calibrated in Appendix Table AD1 Case 2; computer program as listed in Appendix Table B-17, except with coefficients adjusted. Series of graphs A. to C. showing increasing total power draw (ΣP) as pulsing confines Q values closer to the optimum of 50% total material.

power when the appropriate amounts of raw material D and ordered product Q, are available. In real systems with more complex production functions, the percentage of material in the ordered storage need not be 50%. Rather, the individual system configuration will specify the optimum material allocation, and if the system has a tendency to go past that point, pulsing mechanisms may improve system performance.

A Model of Sedimentary Cycle Pulsing

The sedimentary cycle exhibits oscillations and pulsing on many scales of time (see for example Rea and Ruff, 1996; Lerman and Meybeck, 1988). In order to gain insight into the properties of the sedimentary cycle over long time periods, a highly aggregated model with pulsing properties was developed (Figure 5-19, part A.). The model has storages of land and mountains connected by two separate pathways: the slow linear path and the quadratically reinforced path. The slow linear pathway, perhaps representing ocean-continent convergence, is simply proportional to the amount of land existing, and is not reinforced by the existence of mountains. The quadratically reinforced pathway may reflect the deep mountain roots' concentration of the subduction zone to a smaller area, enhancing mountain building. Also, this quadratic pathway can reflect the way mountains shed enormous amounts of material to the continental margins, depressing them and uplifting adjacent areas. Each module represents an aggregate of many mechanisms. The two modules then function as the store-pulse pair mentioned in the pulsing section of the discussion herein.

The model was calibrated with realistic values for storages and flows for the modern day cycle as shown in Appendix Table A-19. Simulation results (computer program listed in Appendix Table B-18) are given Figure 5-19 part B,

A. Diagram of a simple sedimentary cycle model with pulsing properties, showing calibration values, with differential equations at bottom.
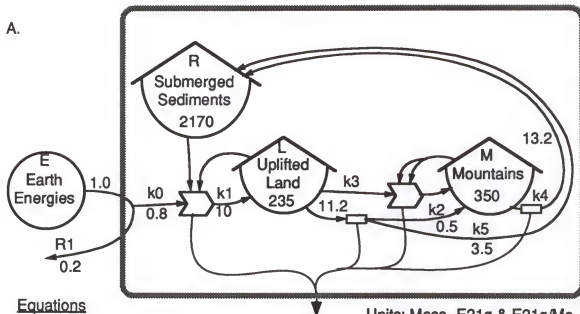
Equations

$dM/dt = k2*L + k3*L*M^2 - k4*M$

$dL/dt = k1*R1*R*L - k2*L - k3*L*M^2 - k5*L$

$R = TM - L - M$

$R1 = E/(1 + k0*R*L)$

Units: Mass- E21g & E21g/Ma
Energy- standard
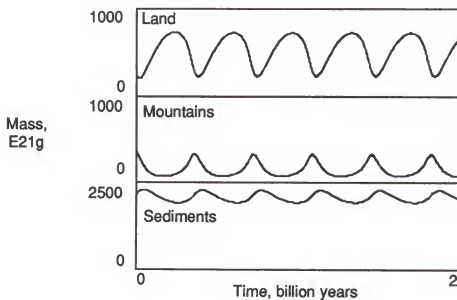
Figure 5-19. A. Diagram of a simple sedimentary cycle model with pulsing properties, showing calibration values, with differential equations at bottom. B. Simulation of the model in A, as calibrated in Appendix Table B-18, showing pulsing of land, mountains, and total sediments over geologic time.

which shows how the system pulses with a period of about 0.4 billion years. Land builds mass slowly in the beginning of the cycle, drawing from the overall supply of sediments. Then the frenzied consumption of land by mountains generates a sharp pulse of activity, recycling material into the dispersed, submerged sediments. The overall behavior is quite similar to that envisioned in Wilson cycles of ocean basin oscillation. The specific mechanisms that may cause the real system to function this way are open to speculation.

The robustness of model behavior was tested by varying each of the coefficients, the energy source, and the total material, and observing the percent change that would eliminate pulsing in the simulation. In most of the tests, 25% change up or down was the limit of pulsing robustness. The real system with pathways of many orders (i.e., many pathways that depend on the receiver storage to a different power law) may show more robust pulsing because of the special properties of higher order pathways that come into play only during periods of growth and decline. These pathways may also act during external perturbations such as asteroid impacts or mantle disturbances.

CHAPTER 6
DISCUSSION

Driving Energies and Material Cycles

There is an ongoing discussion in the Earth Sciences concerning the relative importance of surficial versus deep process, and external versus internal energy sources in shaping the Earth's evolution and form. The cogwheels model of the sedimentary cycle (Figure 3-12) aggregated Earth processes into deep and surficial compartments, where the overall Goldschmidt-simplification reaction proceeds in opposite directions. In model simulations, the overall rate of the sedimentary cycle ultimately depended on internal sources. Changes in external sources simply changed the amount of stored material in the various reservoirs.

The general situation of cycling materials was investigated by Lotka (1925), who suggested that material tends to bottleneck, or accumulate, behind the limiting process. Self regulation of the material flows is accomplished by increasing the storages at the bottlenecks, so that their donor-controlled outflows catch up with the overall system rates. In the cogwheels model, varied surface energies changed the amount of material stored in erodable land. More surface energy eroded land more quickly; less surface energy eroded less quickly. Varied deep energies, however, resulted in changes in the overall rate of sedimentary processing, along with changes in material storage amounts. Thus deep energies may have greater influence on the Earth system, but surface energies modulate the manifestation of those energies in the form of

243

created storages; i.e., the continental area and thickness, and mean elevation above sea level.

In comparing turnover times of Earth system storages, Veizer (1988a) similarly concluded that populations of slowly cycling solid Earth components are more important than fast cycling populations of biota, soils, etc. These simulations indicate the reason for and expression of that importance.

Homeostasis

Many workers (cf. Berner et al., 1983; Butcher et al., 1992; Dobrovolsky, 1994; Holland, 1981; Sagan and Mullen, 1972) have posited the homeostasis of the Earth climate and chemical conditions over much of Earth history. Mostly because of the persistence of life forms, they reasoned that life sustaining temperatures, atmospheres, liquid oceans, and to some extent land and shallow water, must have existed at least since life began some 3.5 billion years ago. This fact has puzzled scientists who recognized the probability of large changes in solar output and Earth heat production over that time span.

Climate and Hydrology

In this study two models of the hydrologic cycle have demonstrated simple homeostatic behavior of aggregated models of climate, rainfall, and temperature. In Hydro 2.1 (Figure 4-2), a very strong homeostatic process involved the switching of solar energy from latent to sensible heating. Processes which decreased rainfall of surface water led to more sensible heating of the surface, and the resultant convectional activity counteracted the initial decrease. This strong regulation mechanism was linked to the very large vapor storages compared to the amount actually precipitated; convective overturn was the probable limiting factor to precipitation in the model.

The model Tempreg2 in Figures 4-20 and 4-21also showed homeostatic properties involved in the hydrologic cycle. In that model exponential vapor production with heat, drove autocatalytic storms, which increased albedo because of reflective clouds. This formed a natural negative feedback that buffered surface temperature when solar output changed. Compared to the radiation only model (Few, 1992) this system buffered surface temperature by 40%. The model response was sufficient to, by itself, account for the regulation of surface temperature to the life sustaining range, in response to a 30% change in solar output postulated by astronomical models (Sagan and Mullen, 1972; Schneider and Londer, 1984). This behavior provides a uniformitarian mechanism for temperature regulation, which may supplement that from the lucky coincidence of changing CO_2 concentrations (Walker et al., 1981).

<u>Atmospheric CO_2</u>

A feedback mechanism proposed for CO_2 regulation is increased weathering due to hotter, wetter more acidic conditions (See Berner and Caldeira, 1997; Walker et al, 1981), which draws down atmospheric carbon dioxide levels. The cogwheels model in Figure 3-12 herein suggests that long-term weathering rate must match long-term Earth uplift rate if continental size is close to steady state. Sustained increases in weathering would eventually decrease the land mass subject to weathering, which would lead to a new, smaller stable size for the world's land mass. Then the amount of exposed weatherable rock would limit the rate of weathering so that it again would equal the Earth uplift rate. The overall effect would be a transfer of carbon from the atmosphere to the reservoir or deep rock and a decrease in total weatherable rock on land.

In general, any process that transfers carbon to deep Earth storage can change the amount of CO_2 in the atmosphere. Compared to the storage of carbon in the atmosphere, the reduced carbon content of the lithosphere is about five orders of magnitude greater and is comparable to the storage of carbonate carbon in the lithosphere. Therefore, both carbonate and reduced carbon in the lithosphere could easily buffer the atmospheric content by any process that enhances the carbon transfer to the lithosphere. Because the lithosphere reservoirs of carbon are so large, they would experience negligible change in storage, and therefore only negligible change in rate of recycle to the atmosphere.

If the major buffering mechanism for atmospheric carbon were the transfer of organic carbon to the lithosphere via increased burial, then the feedback process could easily be primary production of the biota. This rate depends on temperature, moisture, and atmospheric CO_2 just as the weathering rate does, but it has the added benefit of not drawing down additional major Earth reservoirs such as the weatherable rocks. Perhaps the biotic regulation mechanism can function over longer time scales without the side affect of changing the size of land masses.

It seems likely that both carbonate and organic carbon lithospheric reservoirs function as major buffers of atmospheric CO_2. An aggregated model such as Cogwheels, that also includes carbon transfers, could be helpful in understanding the important principles in regulation of atmospheric carbon dioxide.

Timing of Earth Development

Veizer (1988a) suggested appropriate aggregation of the sedimentary cycle into the major domains of oceans, mountains, and cratons. When his

turnover times were included in models, simulations gave system transient times in excess of 10 billion years. The steady state of Earth's system has been debated much in the literature (cf. Taylor and McLennan, 1981, 1996; Armstrong, 1981; Moorbath and Windley, 1981; Veizer, 1988a) and general consensus has been that the system has recently achieved or is approaching steady state. The simulation of model sedcycle (Figures 3-1 and 3-2) suggested that the building of young mountains could take on the order of 5 billion years before the onset of large scale craton formation, which could take another few billion years (See Figure 3-3). Thus the model indicated the possibility that the real Earth system could still be in a transient state of growth.

Addition of higher order pathways to the sedcycle model produced pulsing behavior, but with the same slow several billion year buildup of mountains necessary to trigger massive craton formation. If this model organization is valid, then whole Earth transient behavior is likely to endure longer than the present Earth age. These results support the view that the Earth system is continuing its evolution and development, and probably has not yet reached steady state.

In contrast to the results of the sedcycle model, the hierarchical Benard block model of Earth process (Figures 3-9 and 3-10) produced faster growth of the storages to high values in only about three billion years. However, significant oscillations continued about to 5 billion years, as mountain belts and cratons overshot their steady state values. Thus initial overshoot and later decline of Earth system storages was predicted by the Benard block hierarchical model. This possibility has received little support from other researchers, but may be worth re-examining.

Pulsing, Episodes, and Multiple Scales

Paradigms about system evolution to steady state may be giving way to the pulsing view, where most systems are subject to oscillations in storages over time scales which are long relative to their growth period (See Beyers and Odum, 1993; Odum, 1996). Many geological pulses, however, have irregular periods, which have thus been termed "episodes" to account for their seemingly unpredictable timing and magnitude. One goal of this study was to examine simple models' pulse characteristics for the possible exhibition of episodic behavior. In addition, the basic characteristics of systems that pulse, the how's, why's, and when's of pulsing, should be better understood, if we are to gauge the usefulness of aggregated models, and their possible improvements.

Toward those ends, a series of increasingly complex pulse models were examined, beginning with Pulse 2.0 (model in Figure 5-1, results in Figures 5-2 to 5-4), a basic producer-consumer configuration with a frenzied, quadratic consumption pathway. Simulations demonstrated that a simple deterministic model can pulse over broad variations in parameters, with consistent periods and frequencies during individual runs.

The next pulse model (Pulse3.01, Figure 5-5) added another consumption unit to study the more complex interactions with two possible pulse pairs. Simulation showed (Figures 5-6 to 5-8) interesting variations in pulse period during individual model runs, but all were associated with startup transients that gave way to regular repeating periodic patterns. However, as shown in Figure 5-7 part D, the quasi-steady state could involve a number of distinct pulsing periods which could appear episodic when viewed on a shorter time span.

The next step in pulsing complexity study was taken with the model Pulse3.1 in Figure 5-9, with simulations given in Figures 5-10 to 5-12. In this model an intermediate slow building storage was added that linked the first and third modules, effectively providing two separate pathways for pulsing at the highest level. This configuration produced pulsing behavior on two completely unrelated frequencies, one determined by the timing of A and B, the producer and first consumer; the second frequency determined by timing of C and M, the end consumer and slow storage. The pulsing patterns produced, with consistent period and amplitude, produced pulsing on two distinct scales, the smaller scale looking remarkably like noise compared to the larger.

Pulse 4.0 was the most complex pulsing model studied (Figure 5-13, simulated in Figure 5-14). It consisted of the basic production-consumption model, with the addition of two extra consumer units in series. Thus three possible pulse pairs operated together (A-B, B-C, and C-D in Figure 5-13), providing the opportunity for many different patterns to emerge in a single simulation. As shown in the simulation of Figure 5-14, in which A-B and C-D were the key pulse pairs, a range of pulse magnitudes and periods occurred, especially obvious for the C-D pair. The independent pulse frequencies for the two pairs set up a random condition at the initiation of D's pulses, which influenced its magnitude and the time necessary for the next pulse to happen. Thus, pulsing behavior at small scales contributed to the seeming episodicity of larger scale pulses, that were actually following deterministic laws of the aggregated simulation model. Perhaps real systems exhibiting seemingly unpredictable, episodic behavior, may be modeled with multi-scale pulsing configurations to better predict timing and magnitudes of the next pulse, earthquake, or eruption.

Glacial Multiscale Oscillations

Mudelsee and Schulz (1997) used a glacial model from Saltzman and Verbitsky (1993) to simulate ice mass during the Mid-Pleistocene Climate Transition. With a two-storage model, they switched the system to pulsing mode by increasing ice accumulation rate to match historical data. This change initiated glacial calving events in the model due to increased bedrock depression. Their model was driven by oscillating orbital forcing functions, and closely reproduced ice volumes calculated from oxygen isotope records.

Figure 3 from Mudelsee and Schulz (1997) showed a pulsing behavior very similar to that shown by the model Pulse 3.1 herein (Figure 5-9). Figure 5-12 part b shows the slow buildup around smaller scale oscillations of stored material M, followed by rapid pulsed consumption by consumer module C, after which the system was reset to the slow buildup mode. This type of model may help understand the overall characteristics of glacial dynamics. In modeling glacial pulsed oscillations, the key element is the consumer of glaciers, assumed by Mudelsee and Schulz (1997) to be bedrock-depression-induced calving of the Barents/Kara ice sheet.

Other possible consumption mechanisms include an unspecified high order glacial ablation function (Sergin, 1979) and changes in oceanic thermohaline circulation (Broecker and Denton, 1990). Whatever the mechanism, systems theory suggests it should be large and easily observed because of the scale of structure needed to feedback and rapidly consume the energy of the accumulated ice. Therefore, finding this ice-consumption unit may involve looking for evidence of large accumulation of some material storage during the time of large scale glacial retreat.

Assessment of Methods

Simulating the behavior of systems of very large scale is sometimes assumed to require supercomputers which run spatially explicit models. These models should capture the complex interactions and feedbacks among various elements of widely varying size, time characteristics, and effect. A large goal of this study was to examine the suitability of aggregated, general systems modeling for large, complex systems. Special attention was paid to the sedimentary cycle, which was defined to include the complete cycle of material from hard rock to sediments, and returning to hard rock. Including the Earth's entire crust, the hydrosphere, and much of the atmosphere, this system is truly large in scale and contains many complex interactions.

The main sedimentary cycle model in this study (Figure 3-2) aggregated the entire solid crust cycle into three main storages: oceanic material, mountains, and cratons. Then, using systems concepts of autocatalysis and hierarchy, and using known geological processes such as weathering and erosion, the system diagram explicitly showed the proposed structure of the sedimentary system. After calibrating with values obtained from literature sources, calculations, and assumptions, model simulations showed patterns very similar to other proposed patterns of crustal formation and differentiation.

In Figure 3-3 part A, there was an early episode of building mountains, which then supported growth of stable cratons, and the whole process took around ten billion years to stabilize. This is longer than the 3 to 6 billion years of transient conditions envisioned for the Earth crust system by other workers (cf. Armstrong, 1981; Reymer and Schubert, 1986; Veizer, 1988a; Taylor and McLennan, 1996), but the pattern of sigmoidal growth was the same. Those workers, however, all implicitly lumped the continents into one storage. The

combined mass of the two continental material storages in this model, mountains and cratons, approached steady state by about 7.5 billion years, much closer to other estimates. This study indicates that aggregated models can reproduce the gross features of very large, complex systems. Therefore, these models may help address questions about the overall influence of particular changes, such as, in this case, increased insolation, increased erosion due to human activity, and decreasing production of radiogenic heat.

Summary

Geological study, like many fields today, has become partitioned into multiple sub-fields which use individual sets of terms, concepts, and frameworks for understanding. The splintering of scientific thought into rarer and smaller specialties has hindered the synthesis of information into useful forms that enhance overall understanding. The results here suggest the utility of using aggregated models of very large scale systems, if general systems principles are attended and incorporated in the system configuration.

A numbered list follows summarizing the major points of this study:

1. Models of the sedimentary cycle and related processes were developed in energy systems language to overview the main features of the Earth.

2. Overviews were represented according to the natural energy transformation hierarchy, arranged on paper from left to right.

3. Position of geological components in the energy hierarchy was estimated by calculating emergy per unit mass. (Emergy is the available energy of one kind required directly and indirectly to make a product). Higher values are at higher levels of natural work.

4. Based on previous work by Veizer (1988a), the major divisions of the sedimentary cycle were identified as rocks of marine settings, mountains, and continental platforms (cratons).

5. Solar emergies of the major divisions of the cycle were calculated as 0.94, 1.8, and 10E9 solar emjoules per gram (sej/g), respectively, for marine rocks, mountains, and cratons (See Table 1-3).

6. By simulating models that were organized hierarchically, the duration of sedimentary evolution was estimated to be between 5 and 10 billion years, suggesting that the Earth's surface system is still evolving, but nearing steady state.

7. Simulations of hierarchically organized models of the sedimentary cycle approximated trends derived from isotopic and paleontological evidence.

8. Pulsing configurations in these models suggested a major period of oscillation of 3.5 billion years, following an initial transient period of about 5 billion years.

9. When deep energies were represented with an exponentially declining source, very different model behavior was produced, suggesting that the loss of radiogenic deep Earth energy may be partially offset by the slower decay of residual heat and by increases in transfer of surface energy.

10. A model, which emphasized similar structures at each scale, built main Earth storages in less than 3 billion years, but experiences oscillatory transients for another few billion years. Because no special pulsing pathways were included, the model suggested an innate oscillatory tendency for the large-scale Earth system.

11. Incorporating concepts of Goldschmidt's overview reaction (Goldschmidt, 1933) of the sedimentary cycle, and the transport of surface energy to the deep Earth (Odum, 1996), the cogwheel model of sedimentary

processing suggested that the ultimate driver for the rate of material flow through the sedimentary cycle, is deep heat. Surface energies caused only transient changes in the flow rate.

12. A model of short-term interactions of the fossil fuel driven economy and the sedimentary cycle indicated that peak petroleum use would occur near year 2000, followed by a decline to very low levels in the next century. In the early 21st century, continental denudation was predicted to achieve a maximum of 4 times the pre-industrial rate, and global biomass was predicted to fall to a minimum of 60% of the pre-industrial state.

13. A model of convective precipitation displayed strong buffering of surface water storage on land, related to the distribution of solar energy between latent and sensible heating. Simulations showed a 20% increase in drainage rate caused more sensible heating and storms, and surface water on land changed by only 2%.

14. A global model of hydrologic and heat interactions suggested that hydrology alone could account for a 40% buffering of surface temperature if solar input changed by 30%.

15. Models of fossil fuels and economics suggested that petroleum use would peak by year 2000, and decline to zero over the next century.

16. Coal's historical record suggested it cannot drive today's economy, and simulations agreed.

17. The causes and effects of pulsing were explored using generic models, which produced concurrent, multi-scale oscillations, and episodic patterns.

18. A model of pulsed recycle suggested pulsing can maximize power by optimizing loading in production functions.

19. A model of pulsed mountain building, which emphasized the connection between uplifted and submerged sediments, and the autocatalytic action of mountains, produced oscillations with a period of a few hundred thousand years, similar to timing of Wilson cycles of ocean basin closure.

20. Models of human economies were aided by excellent time series trends in fuel use, which suggested appropriate, known configurations that typically give rise to similar trends. There were two key historical patterns matched by the models: 1. the cooperative behavior of coal and oil systems, where increasing oil use actually stimulated coal mining and use, rather than replacing it as in many models of energy resource competition; and 2. The limited growth pattern of coal use <u>before</u> coal itself was limiting and <u>before</u> any significant growth in oil use. Model adaptation to match those trends gave extra weight to future predictions of coal and oil use, and general economic activity.

21. In hydrologic models, heat and water budgets were combined with energy and material constraints, to form holistic pictures of systems, and to analyze their self regulation capacity. Simulations helped establish the importance of limited energy sources and of competing pathways of energy consumption in regulating precipitation and temperature.

22. In the sedimentary cycle, the major components and all relevant relationships between them were explicitly defined using hierarchical theory. The models so defined were simulated and produced behavior that supported this hierarchical view of the cycle.

Conclusion

In this study, the general systems concepts of energy hierarchy, autocatalysis, self-organization, and scale-similarity were used to model very large scale systems of sedimentary cycling, hydrology, and civilization. By

using a top-down approach, where common configurations and hierarchical considerations determined the main connections, a bias for particular mechanisms was avoided. This approach enabled a logical simplification of the very complex systems of the Earth. Units were organized hierarchically according to their emergy per unit mass.

According to general systems mechanisms of pulsing, cycles of land formation may exist with a period of 3 to 4 billion years. Simulations of the sedimentary cycle indicated the transient time for growth of continents, without pulsing, may be greater than the present age of the Earth. They suggested that long-term changes in rate of material turnover could occur because of changes in deep-Earth energy, but not because of changes in solar energy, which acts at a low position in the energy hierarchy.

Aggregated models of the Earth's hydrologic systems explained the way self organization regulates surface temperature and water storage on the land.

Models that included assets of civilization showed decline with the near-term depletion of oil and gas resources. Substitution of coal did not support the current level of economic activity. When linked to a simplified model of erosion and plant production, simulations predicted a peak in global erosion of three times the pre-industrial rate at year 2025, with a simultaneous minimum in worldwide biomass of about 60% the pre-industrial level.

The results show new ways to overview the Earth quantitatively based on energy and general scientific principles. They lay the groundwork for future efforts to predict and manage the Earth's large-scale systems, for a better cooperation between man and nature.

APPENDIX A
TABLES FOR DOCUMENTATION AND CALIBRATION OF THE MODELS

This appendix contains tables with the details used in calibrating simulation models, including values, calculations, assumptions, and literature sources. The format of the tables lists each source, storage, and flow in the model as a line item, and each line item has entries for a general description, a brief symbol used for that variable, and the value and units for the variable in the calibration case. For flow variables, the flow equation and the value of the calculated flow coefficient are also shown.

The variables used in the calibrations were also used in the energy circuit language diagrams of the text, and in the computer programs listed in Appendix B. Calibration symbols correspond to diagram labels for sources and storages, and flow symbols ("J"s) correspond to the like-numbered flow coefficients ("k"s) in the labeled diagrams.

For most of the models, all documentation of sources, calculations, and assumptions is given in notes to the table, where note number corresponds to the item number from the table. Some of the documentation is, however, given in separate tables, if it was inconvenient to assemble all the information into one table. In these cases, the calibration table headings indicate which tables give the appropriate documentation. For example, Appendix Tables A-7 and A-8 show the calibration of the generic hydrology models of Figure 4-2 and 4-6. To avoid repetitive information, the documentation of assumptions, calculations, and sources for both those tables is given in Appendix Table A-9.

Appendix Table A-1. Calculations, literature sources, and assumptions for Table 1-1.

1	Ocean water		
	Ocean Volume=	1.35E+09 km^3	Schlesinger, 1992
	1.35E9 km^3 * 1E15 cm^3/km^3 * 1g/cm^3 =		1.35E+24 g
	Production (streamflow)=		Schlesinger, 1992
		40000 km^3/yr	Schlesinger, 1992
	40,000km^3/yr * 1E15 cm^3/km^3 *1g/cm^3=		4.00E+19 g/yr
	Turnover time = 1.35E9 km / 4E4 km^3/yr =		33750 yr
2	Ocean ions		
	Ocean salinity=	35 g/kg	Berner and Berner, 1987
	Salt mass = ocean mass * salinity = 1.35E24g * 35g/kg * 0.001kg/g =		
			4.73E+22 g
	Inflow=	4.50E+15 g/yr	Dobrovolsky, 1994
	Turnover time=4.73E22g /4.5E15g/yr =		1.05E+07 yr
3	Suspended sediments		
	Stream load =	2.05E+16 g/yr	Dobrovolsky, 1994
	To calculate stored amount, need average settling distance and velocity.		
	Estimate velocity from Stokes Law: v =[1/18*(rs-rf)*g*d^2]/u		
	rs=particle density=	2.65 g/cm^3	Boggs, 1987
	rf=fluid density=	1.03 g/cm^3	Fetter, 1988
	g=gravity constant=	9.8 m/s^2	
	d=avg particle diam.	3.90E-03 mm	Boggs, 1987
	u=viscosity=	1.31E-02 poise	Fetter, 1988
	Then v=[1/18*(2.65-1.025)*9.8*(.0039e-3)^2]/0.013077=		
		1.03E-05 m/s, or	324 m/yr
	Estimate settling distance by weighted average of shelf and abyssal sedimentation.		
	Fraction on shelf=	0.80	Schlesinger, 1992
	Abyssal fraction=	0.20	Schlesinger, 1992
	Avg shelf depth=	100 m	Neumann & Pierson, 1966
	Avg abyss. depth=	3500 m	Neumann & Pierson, 1966
	Avg settle distance = 0.8*100 + 0.2*3500 =		780 m
	Turnover time=distance/velocity =780 m/324m/yr =		
			2.41 yr
	Storage=Inflow*turnover time (st. state)=	4.94E+16	
4	Oceanic Sediments		
	Defined as all sedimentary material in the oceans.		
	Sub-cont'l sediment	600 E21 g	Ronov&Yaroshevskiy, 1976
	Total inflows	10 E15g/yr	Longterm average
	Turnover time=storage/inflow=	6.00E+07 yr	
	Emergy/mass= Earth emergy/prod rate=	9.44E+08 sej/g	

Notes for Appendix Table AT1--continued

5   Continental Sediments

Defined as the total mass of sedimentary material on continents.

Storage=	1850 E21g	Ronov&Yaroshevskiy, 1976
Turnover time=	2.50E+08 yr	Veizer, 1988a
Production=Mass/turnover time=		7.4 E15 g/yr
Emergy/mass=Earth emergy/prod rate=	1.28E+09 sej/g	

6   Cratons

Defined as the total mass of metamorphic and igneous rock in continental blocks.

Mass=	20.1 E24 g	Ronov&Yaroshevskiy, 1976
Half Life=	1.73E+09 yr	Veizer, 1988
Turnover time=half life/0.693=	2.50E+09 yr	
Production=mass/turnover time=	0.81 E15 g/yr	

To estimate transformity, hypsometric curve shows that the land may support the mountains.

Emergy/mass=Earth emergy/prod rate=   1.17E+10 sej/g

7   Vapor

Atmospheric vapor=   0.013 E21 g   Berner&Berner, 1987

Production is set equal to total throughflow; i.e., evaporation + transpiration + cloud evaporation + Rain evaporation.

    1050000 E15 g/yr   Berner&Berner, 1987

Emergy/mass=Earth emergy/prod rate=

=9.44E24sej/jr / 1050000E15g/yr=   8.99E+03 sej/g

8   Clouds

A measure of clouds and storms is the amount of liquid water in clouds.

Cloud water=   0.11 kg/m^2   Greenwald, 1995

Summing:0.11kg/m^2 * 510E6km^2 * 1E6m^2/km^2=

    5.61E+16 g

Cloud turnover time   30 min   Wallace&Hobbs, 1987

Production rate=quantity/turnover time=5.61E16g/30min=

    982872 E15 g/yr

Approximating: 1000000 E15 g/yr

Emergy/mass=Earth emergy/prod rate=

=9.44E24sej/yr / 1000000E15g/yr=   9440 sej/g

9   Rainstorms

Storms are hierarchical cloud centers that are necessary to create rain and snow.

Storage= 10% of cloud storage (assumption)

Storms=   5.61E+15 g

Total water going into rainstorms is that rained out, which is rain reaching the ground plus that evaporated on the way down.

Notes for Appendix Table AT1--continued

	Rain to ground=	500000 E15 g/yr	
	That evaporated=	250000 E15 g/yr	Assumption
	Total=	750000 E15 g/yr	
	Emergy/mass=Earth emergy/prod rate=		12587 sej/g
10	Plant production		
	This is average plant dry matter.		
	Production=	172 E15	Dobrovolsky, 1994
	Mass=	2500 E15 g	Dobrovolsky, 1994
	Turnover time = mass/production =	14.5 yr	
	Emergy/mass=Earth emergy/prod rate=	5.49E+07	
11	Soil		
	Defined as the top meter of land		
	Soil mass=	0.16 E21 g	Schlesinger, 1992
	Soil formation=	11.55 E15 g/yr	=sediment production
	Turnover time=mass/formation=	13853 yr	
	Emergy/mass=Earth emergy/prod rate=	8.17E+08 sej/g	
12	Acid volatiles		

Carbon dioxide will be used here because it is the most important acid source for continent weathering.

	CO_2 concentration=	325 ppm	Wallace and Hobbs, 1977
	Atmosphere mass=	5.14 E21 g	Wallace and E21 g
	Total CO_2=concentration*mass=		1.67E-03

Volatiles used=sediments yielded-rocks weathered

	Sediment load=	11.55 E15 g/yr	Li, 1972
	Rocks weathered=	10.5 E15 g/yr	Gregor, 1970

In steady state, acid production equals that used:

$$1.05 \text{ E15 g/yr}$$

Emergy/mass=Earth emergy/prod rate= 8.99E+09 sej/g

Table A-2. Calibration values for sources, storages, and flows in the overall sedimentary cycle model of Figure 3-1.

Item	Description	Symb.	Value	Units	Equation	Coeff. Value
Sources						
1.	Sun	J0	1	std		
2.	Deep earth	G	1	std		
Storages						
3.	Sea water	O	1322	E21g		
4.	Ions	D	49.1	E21g		
5.	Ocean Crust	C	5900	E21g		
6.	Undersea sediments	S	600	E21g		
7.	Uplifted sediments	L	1800	E21g		
8.	Cratons	M	20100	E21g		
Remainders						
9.	Albedo	R	0.3	std		
10.	Rain on sea	V	415000	E21g		
Flows						
11.	Hydrologic heat	J1	0.31	std	k1ROLM	2.16E-11
12.	Other insolation	J2	0.39	std	k2RD	2.65E-02
13.	Total rain	J3	526000	E21g/Ma	k3ROLM	3.67E-05
14.	Precipitation	J4	5	E21g/Ma	k4RD	3.39E-01
15.	Ocean crust prod'n	J5	69.4	E21g/Ma	k5G	6.94E+01
16.	Mountain building	J6	18	E21g/Ma	k6SGL	1.67E-05
17.	Rain to cratons	J7	63270	E21g/Ma	k7VM	7.58E-06
18.	Rain to mountains	J8	47730	E21g/Ma	k8VLM	3.18E-09
19.	Enhanced mtn build	J9	-	E21g/Ma	k9SGLM	-
20.	Ocean crust loss	J10	69.4	E21g/Ma	k10CG	1.18E-02
21.	Oc'n crust weather	J11	0.5	E21g/Ma	k11C	8.47E-05
22.	Craton ion loss	J12	0.5	E21g/Ma	k12VM	5.99E-11
23.	Craton particle loss	J13	0.5	E21g/Ma	k13VM	5.99E-11
24.	Sediment ion loss	J14	4.5	E21g/Ma	k14VLM	3.00E-13
25.	Sed. particle loss	J15	4.5	E21g/Ma	k15VLM	3.00E-13
26.	Craton to mantle	J16	8	E21g/Ma	k16M^2	1.98E-08
27.	Deep earth to mtns	J17	7.5	E21g/Ma	k17SGL	6.94E-06
28.	Craton production	J18	9	E21g/Ma	k18VLM	5.99E-13

Notes to Table A-2
1. Total insolation standardized to one inflowing unit.
2. Deep earth source standardized to one unit.
3. Water in the sea= 1322 E21g Schlesinger, 1992
4. Total sea ions= 49.1 E21g Berner&Berner, 1987
5. Ocean crust mass= 5900 E21g Ronov&Yaroshevskiy, 1976

6. Undersea sediments are those not on continental blocks.
600 E21g Ronov&Yaroshevskiy, 1976
7. Uplifted sediments are those on continental blocks.
1800 E21g Ronov&Yaroshevskiy, 1976
8. Cratons are the total mass of continental basement rocks.
20100 E21g
Ronov&Yaroshevskiy, 1976
9. Total earth average albedo
0.3 std Kiehl and Trenberth, 1997
10. Rain on sea 415000 E21g/Ma Berner&Berner, 1987
11. Hydrologic heat is the latent heat of evaporation and that to turbulence of storms.
Latent heat 24%+turbulent heat 7%. Kiehl&Trenberth, 1997
Total = 0.31
12. Other insolation is that leftover after subtracting hydrologic heat.
1-0.3 -0.31= 0.39
13. Earth Rain= 526000 E21g/Ma Berner&Berner, 1987
14. Chemical precipitation is equal to ionic input in steady state.
5 E21g/Ma Gregor, 1970
15. Ocean crust production is the creation of ocean crust from mantle.
Crust half life= 58 Ma Veizer, 1988a
So turnover time= 84 Ma Half Life/0.693
Amount (item 5)/turnover time = production= 70.49 E21g/Ma
16. Balancing total erosion (items 22-25) and mantle reabsorption (item 27) 18 E21g/Ma
Rain to cratons in proportion to percent outcrop area 10%.
17. Land Rain= 111000 E21g/Ma Berner&Berner, 1987
assuming 57% of that= 63270 E21g/Ma
18. Rain to sedimentary areas is the remaining rain=
47730 E21g/Ma
19. Enhanced mtn building is a flow that may be used for future upgrading of the model.
20. Subduction of ocean crust balances the production (item 15)
70.49
21. Ocean crust weathering is the slow weathering of basaltic ocean

<u>Notes to Table A-2--continued</u>

      crust under the sea.   0.5 E21g/Ma Assumption

22. Longterm average, half of erosion ions and half particles. Also total
      erosion is about 10.5.   Gregor, 1970
      90% of erosion rom sedimentary rocks.   Dobrovolsky, 1994
      So total craton erosion is 10% of 10.5, or about 1
      Half is ions: 0.5 E21g/Ma

23. Half is particles: 0.5 E21g/Ma

24. Rest of erosion is from sedimentary young mountains: 9E21g/Ma
      Half is ions: 4.5 E21g/Ma

25. Half is particles: 4.5 E21g/Ma

26. Craton half life=   1733 Ma   Veizer, 1988a
      Turnover time=   2500 Ma   Half Life/0.693
      Turnover=Mass (item 8) / turnover time=
                                 8.04 E21g/Ma

27. Mantle contribution to mountains and ocean crust sedimentation
      (item 21) balancing craton loss to mantle (item 26).
                                 7.54 E21g/Ma

28. Craton production balancing loss (item 26) and erosion (items 22
      and 23)   9.04

Appendix Table A-3. Calibration values for sources, storages, and flows in the overall sedimentary cycle model of Figure 3-4.

Item	Description	Symb.	Value	Units	Equation	Coeff. Value
Sources						
1.	Sun	J0	1	std		
2.	Deep earth	G	1	std		
Storages						
3.	Sea water	O	1322	E21g		
4.	Ions	D	49.1	E21g		
5.	Ocean Crust	C	5900	E21g		
6.	Undersea sediments	S	600	E21g		
7.	Uplifted sediments	L	1800	E21g		
8.	Cratons	M	20100	E21g		
Remainders						
9.	Albedo	R	0.3	std		
10.	Rain on sea	V	415000	E21g		
Flows						
11.	Hydrologic heat	J1	0.31	std	k1ROLM	2.16E-11
12.	Other insolation	J2	0.39	std	k2RD	2.65E-02
13.	Total rain	J3	526000	E21g/Ma	k3ROLM	3.67E-05
14.	Precipitation	J4	5	E21g/Ma	k4RD	3.39E-01
15.	Ocean crust prod'n	J5	69.4	E21g/Ma	k5G	6.94E+01
16.	Mountain building	J6	18	E21g/Ma	k6SGL	1.67E-05
17.	Rain to cratons	J7	63270	E21g/Ma	k7VM	7.58E-06
18.	Rain to mountains	J8	47730	E21g/Ma	k8VLM	3.18E-09
19.	Linear craton feed	J9	0	E21g/Ma	k9L	0.00E+00
20.	Ocean crust loss	J10	69.4	E21g/Ma	k10CG	1.18E-02
21.	Oc'n crust weather	J11	0.5	E21g/Ma	k11C	8.47E-05
22.	Craton ion loss	J12	0.5	E21g/Ma	k12VM	5.99E-11
23.	Craton particle loss	J13	0.5	E21g/Ma	k13VM	5.99E-11
24.	Sediment ion loss	J14	4.5	E21g/Ma	k14VLM	3.00E-13
25.	Sed. particle loss	J15	4.5	E21g/Ma	k15VLM	3.00E-13
26.	Craton to mantle	J16	8	E21g/Ma	k16M^2	1.98E-08
27.	Deep earth to mtns	J17	7.5	E21g/Ma	k17SGL	6.94E-06
28.	Craton production	J18	9	E21g/Ma	k18VLM	5.99E-13

Notes to Appendix Table A-3

1. Total insolation standardized to one inflowing unit.
2. Deep earth source standardized to one unit.
3. Water in the sea= 1322 E21g Schlesinger, 1992
4. Total sea ions= 49.1 E21g Berner&Berner, 1987
5. Ocean crust mass= 5900 E21g Ronov&Yaroshevskiy, 1976

6. Undersea sediments are those not on continental blocks.
   600 E21g Ronov&Yaroshevskiy, 1976
7. Uplifted sediments are those on continental blocks.
   1800 E21g Ronov&Yaroshevskiy, 1976
8. Cratons are the total mass of continental basement rocks.
   20100 E21g
   Ronov&Yaroshevskiy, 1976
9. Total earth average albedo
   0.3 std Kiehl and Trenberth, 1997
10. Rain on sea 415000 E21g/Ma Berner&Berner, 1987
11. Hydrologic heat is the latent heat of evaporation and that to turbulence of storms.
    Latent heat 24%+turbulent heat 7%. Kiehl&Trenberth, 1997
    Total = 0.31
12. Other insolation is that leftover after subtracting hydrologic heat.
    1-0.3 -0.31= 0.39
13. Earth Rain= 526000 E21g/Ma Berner&Berner, 1987
14. Chemical precipitation is equal to ionic input in steady state.
    5 E21g/Ma Gregor, 1970
15. Ocean crust production is the creation of ocean crust from mantle.
    Crust half life= 58 Ma Veizer, 1988a
    So turnover time= 84 Ma Half Life/0.693
    Amount (item 5)/turnover time = production= 70.49 E21g/Ma
16. Balancing total erosion (items 22-25) and mantle reabsorption (item 27) 18 E21g/Ma
    Rain to cratons in proportion to percent outcrop area 10%.
17. Land Rain= 111000 E21g/Ma Berner&Berner, 1987
    assuming 57% of that= 63270 E21g/Ma
18. Rain to sedimentary areas is the remaining rain=
    47730 E21g/Ma
19. Linear feed to cratons possibly equivalent to straight metamorphism.
    Assumed 1/3 of total. 3 E21g/Ma
20. Subduction of ocean crust balances the production (item 15)
    70.49 E21g/Ma
21. Ocean crust weathering is the slow weathering of basaltic ocean

Notes to Appendix Table A-3--continued

      crust under the sea.   0.5 E21g/Ma   Assumption

22.   Longterm average, half of erosion ions and half particles. Also total
      erosion is about 10.5.   Gregor, 1970
      90% of erosion rom sedimentary rocks.   Dobrovolsky, 1994
      So total craton erosion is 10% of 10.5, or about 1
      Half is ions: 0.5 E21g/Ma

23.   Half is particles: 0.5 E21g/Ma

24.   Rest of erosion is from sedimentary young mountains: 9E21g/Ma
      Half is ions: 4.5 E21g/Ma

25.   Half is particles: 4.5 E21g/Ma

26.   Craton half life=   1733 Ma   Veizer, 1988a
      Turnover time=   2500 Ma   Half Life/0.693
      Turnover=Mass (item 8) / turnover time=
                      8.04 E21g/Ma

27.   Mantle contribution to mountains and ocean crust sedimentation
      (item 21) balancing craton loss to mantle (item 26).
                      7.54 E21g/Ma

28.   Craton production balancing loss (item 26) and erosion (items 22
      and 23)   6.04

Appendix Table A-4. Calibration values of sources, storages, and flows for Benard2, the model in Figure 3-9, with the calculated coefficients.

Item	Description	Symbol or Equation	Value Units	Coeff.	Value
Sources					
1.	Sun	I	5.6 E24 J/yr		
2.	Deep Heat	H	1 standard		
Storages					
3.	Ocean Water	W	1350 E20 g		
4.	Sea Sediments	S	600 E21 g		
5.	Mountains	M	1800 E21 g		
6.	Cratons	C	20100 E21 g		
Remainders					
7.	Unused sunlight	R	1.7 E24 J/yr		
8.	Rain on ocean	Rr	4.12 E20 g/yr		
9.	Evapotranspiration	Re	0.71 E20 g/yr		
Flows					
10.	Used sun	$J0=k0RW=$	3.9 E24 J/yr	k0=	1.70E-03
11.	Total rainfall	$J1=k1RW=$	5.3 E20 g/yr	k1=	2.31E-03
12.	Rain on land	$J4=k4RrM=$	1.14 E20 g/yr	k4=	1.54E-04
13.	Mountain erosion	$J8=k8RrM=$	9 E21g/Ma	k8=	1.21E-03
14.	Sedim transform.	$J9=k9SHM=$	10 E21g/Ma	k9=	9.26E-06
15.	Runoff	$J10=k10ReC=$	0.4 E20 g/yr	k10=	2.80E-05
16.	Mtn building	$J11=k11SHM=$	18 E21g/Ma	k11=	1.67E-05
17.	Craton building	$J12=k12MHC=$	9 E21g/Ma	k12=	7.46E-07
18.	Craton loss	$J14=k14M=$	8 E21g/Ma	k14=	4.44E-03
19.	Craton recycle	$J15=k15ReC=$	1 E21g/Ma	k15=	7.01E-05

Notes to Appendix Table A-4.
1. Incident sunlight on earth=5.6E24 J/yr (Berner&Berner, 1987)
2. Standardized to 1
3. Water in ocean=1350E21 g (Berner&Berner, 1987)
4. Undersea sediments=600E21 g (Dobrovolsky, 1994)
5. Mass in young mtns=1800E21 g (Dobrovolsky, 1994)
6. Craton mass=20100E21g (Dobrovolsky, 1994)
7. Albedo=30% (Berner&Berner, 1987)
   0.3*5.6E24J/yr=1.7E24 J/yr
8. Ocean rain=4.12E20 g/yr (Dobrovolsky, 1994)
9. World evapotranspiration =0.71E20g/yr (Schlesinger, 1992)
10. Used sun = total-albedo=5.6-1.7=3.9E24 gJ/yr
11. Total rainfall=total evaporation=5.3E20 g/yr (Dobrovolsky, 1994)

Notes to Appendix Table A-4--continued

12. Land rain=1.14E20 g/yr (Dobrovolsky, 1994)
13. 90% of total erosion from young mountains (Dobrovolsky, 1994)
    Total land erosion=10E15 g/yr (Gregor, 1973)
    Mountain erosion = 90%*10= 9E15g/yr
14. Sediment transformation=10E15 g/yr(assume steady state)
15. Land runoff= 0.4E20g/yr (Dobrovolsky, 1994)
16. Mtn building balancing craton loss and mtn erosion in steady state
    Item 18 + item 13 = 18E15g/yr
17. Craton building =loss to mantle (item 18) + recycle (item 19)
                    =9E21g/Ma
18. Craton half life =1733 Ma (Veizer, 1988a)
    Turnover time= half life/0.693 = 2500Ma
    Turnover = mass (item 6)/turnover time= 8.04E21 g/Ma
    Craton loss= total turnover to mantle = 8.04E21g/Ma
19. Craton recycle =erosion of cratons, 10% of sed cycle (item13.)

Appendix Table A-5. Calibration values of and documentation for sources, storages, and flows in Cogwheel, the model in Figure 3-12, with the calculated coefficients.

Item	Description	Symbol or Equation	Value Units	Coeff. Value
Sources				
1.	Surface energies	Io	526 E24g/Ma	
2.	Resid&radio heat	Hr	6.72 E26J/Ma	
Storages				
3.	Sea sediments	M	7.9 E21g	
4.	Deep rocks	D	10600 E21g	
5.	Surface rocks	G	31.5 E21g	
6.	Soils	S	7.2 E21g	
7.	Deep heat	H	53.2 E26J	
Remainders				
8.	Albedo	R	415 E26J/Ma	
Flows				
9.	Rain on Land	J1=k1RGS=	111 E24g/Ma	k1= 1.18E-03
10.	Weathering	J2=k2RGS=	10 E21g/Ma	k2= 1.06E-04
11.	Uplift	J3=k3DH=	10 E21g/Ma	k3= 1.77E-05
12.	Streams	J4=k4RGS=	44 E21g/Ma	k4= 4.67E-04
13.	Lithification	J5=k5MD=	10 E21g/Ma	k5= 1.19E-04
14.	Heat inflow	J6=k6MD=	6.49 E26J/Ma	k6= 7.75E-05
15.	Resid&radio heat	J7=k7Hr=	6.72 E26J/Ma	k7= 1.00E+00
16.	Earth heat flow	J8=k8DH=	13.21 E26J/Ma	k8= 2.34E-05
17.	Soil Erosion	J9=k9RGSS=	10 E21g/Ma	k9= 1.48E-05

Notes for Appendix Table A-5.

1. Surface energies are all the energies that participate in transformation of hard surface rocks into sediments. The hydrologic cycle is used to represent total surface energies.
   Total Precipitation= 526 E18g/yr Dobrovolsky, 1994
2. Residual and radio heat is the heat contributed by residual deep heat in the mantle and core flowing up through the crust and the radioactive heat production.
   6.72 E20J/yr See item 15
3. Deep sediments: altered surface rocks susceptible to burial, defined as the loose sediment cover in the sea. Assume top 20m for shelves and top 5m for non-shelf as unlithified.
   Shelf area=78E6km^2, other sea area=283E6km^2 Ryabchikov, 1975
   20m*78E6km^2 +5m*283E6km^2 *0.85porosity *2650kg/m^3 *1e3g/kg
   *1E6m^2/km^2= 7.8 E21g
4. Deep rocks: take the sedimentary shell and the granite layer of the

Notes for Appendix Table A-5--continued

    continents, as given by Dobrovolsky, 1994   10600 E21g

5.   Surface rocks: defined as mostly unaltered rocks in top 100m.
    From item 6, loose sed cover layer is ~20m, so 80m layer is rock.
    80m*150E6km^2*0.99porosity*2650kg/m^3*1e3g/kg*1E6m^2/km^2=
                                  31.5 E21g

6.   Soils: Defined as loose sedimentary cover on land which supports life
    and feeds back to enhance weathering via acid concentration.
    Dobrovolsky (1994) gave aproximate sedimentary cover values on land:
    Steep slopes:10-20cm; Plains:10's of meters; Tectonic depressions:
    100's of meters. Assume relatively small areal extent of slopes and
    depressions cancels. Then average land cover is 20m loose sediments.
    20m*160E6km^2*0.85porosity*2650kg/m^3*1E3g/kg*1E6m^2/km^2=
                                    7.2 E21g

7.   Deep heat defined as heat in Earth's crust.
    Avg heat capacity=   0.3 cal/g°C McBirney, 1993
    Avg Crust Temp   400 °C   McBirney, 1993
    Crust Mass   10600 E24g Dobrovolsky, 1994
    10600E21g*400C*0.3cal/gC*4.186J/g=   53.2 E26J

8.   The unused surface energy may be taken as the earth's albedo, which
    is 30%. 0.3*56100E26 J/Ma=   16800 E26J/Ma

9.   Rain on land=   111000 E15g/yr Dobrovolsky, 1994

10.   Weathering is the total conversion rate of hard rock and acid volatile to
    sediments. In steady state it is equal to continental denudation.
    Gregor, 1970, gives a rate of about   10 E15g/yr

11.   Uplift: in a steady state system, this must replace the losses to
    weathering, and therefore equals weathering.   10 E15g/yr

12.   Streamflow=   44000 E15g/yr Dobrovolsky, 1994

13.   Sediment burial is the physical transport of sediments to depth. In
    steady state, it must equal weathering   10 E15g/yr

14.   Lithification is the transformation of weathered sedimentary material
    back to hard rock, be it sedimentary, metamorphic, or igneous. In
    steady state, it must equal the burial rate.   10 E15g/yr

15.   Heat passed downward as chemical and compression potentials
    Calculated as difference of heat outflow and internal generated heat.
    Total earth heat flow=   13.21 E26J/Ma Sclater, 1980
    Residual and radiogenic heat=   6.72 E26J/Ma Sclater, 1980
    The net transferred down is then   6.49 E26J/Ma

16.   Radiogenic and residual heat: 6.72 E20 J/yr Sclater, 1980
    Total earth heat flow toward surface=   13.21 E26J/Ma Sclater, 1980

17.   Soil erosion=yearly soil transport to the oceans, equal to weathering in
    steady state (see item 12.)   · 10 E15g/yr

Appendix Table A-6. Calibration values of sources, storages, and flows for the model in Figure 3-18, with the calculated coefficients.

Item	Description	Symbol or Equation	Value	Units	Coeff.	Value
Sources		Sym.				
1.	Sun on oceans	So	4	E24J/yr		
2.	Sun on land	Sl	1.64	E24J/yr		
3.	Rain	R	526000	E15g/yr		
4.	Rocks	G	1	unit		
Storages						
5.	Ocean solutes	Md	4.91E+07	E15g		
6.	Suspend'd mass	Ms	25.0	E15g		
7.	Marine Life	Bo	3.4	E15g		
8.	Soil	S	158,000	E15g		
9.	Soil water	W	38,000	E15g		
10.	Land Plants	B	2020	E15g		
11.	Coal	C	5700	E15g		
12.	Oil+Gas	O	390	E15g		
13.	Econ. structure	E	674	E15g		
14.	Coal mines	Ec	13.4	E15g		
15.	Oil wells	Eo	6.9	E15g		
Remainders						
16.	Land albedo	R1	0.56	E24J/yr		
17.	Ocean albedo	R2	1.19	E24J/yr		
18.	Uncaught rain	R3	5082	E15g/yr		
19.	Unused yield	R4	0.027	E15g/yr		
20.	Unused coal	R5	1.15	E15g/yr		
21.	Unused Oil+gas	R6	0.58	E15g/yr		
Flows						
22.	Sun to ecosys.	J1=k1*R1*S*W*B	0.61	E24J/yr	k1=	8.98E-14
23.	Sun to agric.	J2=k2*R1*S*W*B*E	0.60	E24J/yr	k2=	1.31E-16
24.	Sun to mar. life	J3=k3*R2*Md	2.8	E24J/yr	k3=	4.78E-08
25.	Rain into soil	J4=k4*R3*S	105918	E15g/yr	k4=	1.32E-04
26.	Ocean uptake	J5=k5*R2*Md	110	E15g/yr	k5=	1.88E-06
27.	Oc'n production	J6=k6*R2*Md	110	E15g/yr	k6=	1.88E-06
28.	Ocean recycle	J7=k7*Bo	106.20	E15g/yr	k7=	3.12E+01
29.	Biota to seds.	J8=k8*Bo	4.28	E15g/yr	k8=	1.26E+00
30.	Ecosys. prod.	J9=k9*R1*S*W*B	91	E15g/yr	k9=	1.34E-11
31.	Agric. prod.	J10=k10*R1SWBE	32.5	E15g/yr	k10=	7.10E-15
32.	Plant death	J11=k11*B	172	E15g/yr	k11=	
33.	Weathering	J12=k12*G*S	9.34	E15g/yr	k12=	5.91E-05

Appendix Table A-6--continued

Item	Description	Symbol or Equation	Value	Units	Coeff.	Value
34.	Uptake	J13=k13*R1*W*S*B	6.46	E15g/yr	k13=	9.51E-13
35.	Particle erosion	J14=k14SWe(k15B)	9.74	E15g/yr	k14=	3.95E-07
36.	Erosion stopping	J15=k15*0	N/A	N/A	k15=	2.72E-03
37.	Dissolved waste	J16=k16*E	unkn.	E15g/yr	k16=	0
38.	Particle waste	J17=k17*E	24.40	E15g/yr	k17=	3.62E-02
39.	Water uptake	J18=k18*R1*W*S*B	36000	E15g/yr	k18=	5.30E-09
40.	Water uptake	J19=k19*R1WSBE	46802	E15g/yr	k19=	1.02E-11
41.	Diss. erosion	J20=k20*S*W	2.82	E15g/yr	k20=	4.70E-10
42.	Settling	J21=k21*Ms	8.66	E15g/yr	k21=	3.46E-01
43.	Precipitation	J22=k22*Md	0.5	E15g/yr	k22=	1.02E-08
44.	Soil oxidation	J23=K23*S	139	E15g/yr	k23=	8.80E-04
45.	Ecosys. yield	J24=k24*R1*S*W*B	2.430	E15g/yr	k24=	3.58E-13
46.	Agric. yield	J25=k25*R1SWBE	10.350	E15g/yr	k25=	2.26E-15
47.	Agric. uptake	J26=k26*R1SWBE	5.55	E15g/yr	k26=	1.21E-15
48.	Yield to oil econ	I8=c8*R4*R5*E	2.61	E15g/yr	c8=	1.25E-01
49.	Yield to coal	I9=c9*R4*R6*E	10.45	E15g/yr	c9=	9.90E-01
50.	Oil econ. build	I10=c10*R4*R5*E	1.43	E15g/yr	c10=	6.83E-02
51.	Coal econ. build	I11=c11*R4*R6*E	2.27	E15g/yr	c11=	2.15E-01
52.	Asset decay	I12=c12*E	26.9	E15g/yr	c12=	3.99E-02
53.	Management	I13=c13*R1SWBE	0.88	E15g/yr	c13=	1.92E-16
54.	Well building	I14=c14*R4*R5*E	1.43	E15g/yr	c14=	6.83E-02
55.	Well decay	I15=c15*Eo	0.86	E15g/yr	c15=	1.25E-01
56.	Well use	I16=c16*O*Eo	0.35	E15g/yr	c16=	1.30E-04
57.	Mine building	I17=c17*R4*R6*E	6.16	E15g/yr	c17=	5.84E-01
58.	Mine decay	I18=c18*Ec	2.94	E15g/yr	c18=	2.19E-01
59.	Mine use	I19=c19*Ec*C	3.04	E15g/yr	c19=	3.98E-05
60.	Coal flow	I20=c20*C*Ec	5.53	E15g/yr	c20=	7.24E-05
61.	Oil+gas flow	I21=c21*O*Eo	5.36	E15g/yr	c21=	1.99E-03
62.	Used coal	I22=c22*R4*R6*E	4.8	E15g/yr	c22=	4.55E-01
63.	Used Oil+gas	I23=c23*R4*R5*E	4.8	E15g/yr	c23=	2.29E-01
64.	Streamflow	J27=k27*W	23406	E15g/yr	k27=	6.16E-01

<u>Notes for Appendix Table A-6</u>
Sources
General: To obtains the values given in Figure S20, first the natural system
was calibrated alone from its pre-industrial values as given herein, then the
industrial sector was added as calibrated in Appendix Table AS3 for the
model in Figure S16. Finally, coefficients were adjusted slightly so
simulations matched historical data. Therefore, there are some differences
between the values given in Figure S20 and in this table.

1. Sun on land
2. Sun on oceans

Solar Constant=	0.5 cal/cm^2-min	Berner & Berner, 1987
Converting units:	1.10E+16 J/km^2-yr	
Land Area=	149 E6 km^3	Butcher et al, 1992.
Ocean Area=	361 E6 km^4	Butcher et al, 1992.
Sun on land= solar constant*land area=		**1.64** E24J/yr
Sun on ocean= solar constant* ocean area=		**3.97** E24J/yr
Albedo=	0.3	Berner&Berner, 1987
Sun reflected from land=sun on land * albedo=		0.49 E24J/yr
Sun absorbed on land=sun on land-sun reflectec		1.15 E24J/yr
Sun reflected from sea=sun on sea*albedo		1.19 E24J/yr
J01=S01*(1-albedo) = 2.78E24 J/yr		2.78 E24J/yr

Note: Alternative setup is to assume that the energy available to the
biota is that striking the surface, then solar const is 55% of above, and
albedo is 7.3% (Data from Berner and Berner, 1987, Fig. 2.4)
Average Solar Const = 0.55*1.1e16= 6.05e15 J/km^2-yr

S0=6.05E15*149E6=9.01e23 J/yr	0.90 E24J/yr
S01=6.05E15*361e6 = 2.18E24 J/yr	2.18 E24J/yr
R0=9.01E23*0.073 = 6.58E22 J/yr	0.07 E24J/yr
J0=9.01E23*(1-0.073) = 8.35E23 J/yr	0.84 E24J/yr
R01=2.18E24*.073 = 1.59E23 J/yr	0.16 E24J/yr
J01=2.18E24*(1-0.073) = 2.02E24 J/yr	2.02 E24J/yr

Reference: Lee, K.H., Atlas of Earth's Radiation budget, NAS 1.61:1263

3. Rain

Total earth rain=	496000 E15 g/yr	Schlesinger
	526000 E15 g/yr	Dobrovolsky
	496000 E15 g/yr	Berner&Berner
Use Dobrovolsky:	**526000** E15 g/yr	

4. Rocks
   Modelled as a constant force source: taken as a standard unit of one.
   The rate of delivery into the soil is calculated in the flows section.

   1 unit

Notes for Appendix Table A-6--continued
Storages
5. Dissolved ocean chemicals
Appendix Table AS7--continued
This is the total amount of dissolved and suspended
material contained in the world's oceans.
Dissolved Load = Average salinity * Ocean Mass

Salinity(g/kg)	35 g/kg	Berner&Berner, 1987
Ocean volume =	1.37E+09 km^3	Berner&Berner, 1987
Density of seawater=	1.025 g/cm^3	Fetter, 1988
TDS = Total Dissolved Solids = Salinity*Volume*Density=		
		4.91E+07 E15g

6. Suspended ocean chemicals
Settling velocity may be estimated from Stokes Law V=1/18(rs-rf)gd^2/u

rs=	2.65 g/cm^3	(Density of Particles)
rf=	1.025 g/cm^4	(Density of Water)
g=	9.8 m/s^2	(gravity)
d=0.0039 mm	0.0039 mm	Boggs, 1985
u=	0.013077 poise	Fetter, 1988

V=1/18(rs-rf)gd^2/u

1/18*(2.65-1.025)g/cm^3*9.8m/s^2/0.013077g/cm-s=		
Average settling velocity=		1.029E-05 m/s
or		324 m/yr

In steady state, Total Suspended Solids (TSS) is Input rate* settling
distance / velocity.

Input Rate =	2.05E+16 g/yr	Dobrovolsky
Settling distance weighted average of shelf and deep sedimentation		
Frac. settling on shelf	0.8	Schlesinger
Frac. settling in deeps	0.2	Schlesinger
Average shelf depth	100 m	Neumann&Pierson
Avg abyssal depth	3500 m	Neumann&Pierson
Avg settle distance=		390 m
TSS = Input rate*settle distance/velocity=		**24.66** E15g

7. Ocean biota

Ocean Biomass:	1.76 E9t C	Colinvaux, 1986
	3.4 E9 t dry wt	Dobrovolsky, 1994
Ocean Plant Mass (dry wt)=		3.95 E15g
or		**3.4** E15g

8. Soil
Mineral soil is the loose aggregate of silts, clays and sands, and
all the inorganic ionic species that make up the land cover.
It does not include bedrock, boulders, or unweathered rocks.

Notes for Appendix Table A-6--continued

	World avg soil depth=	1 m	Dobrovolsky, 1994
A.	Land Surface Area=	135 E6 km^2	Dobrovolsky, 1994

(Excluding glaciated and submerged area)
Soil volume= thickness * surface area=
1m * 150e6 km^2 * 1e15 cm^3/km^3*1km/1000m=

$$1.35E+20 \text{ cm}^3$$

	Average soil density=	2.65 g/cm^3	Dobrovolsky, 1994
	Average soil porosity=	50%	Dobrovolsky, 1994
	mass=volume*porosity*density=		178875 E15g
B.	Avg Soil Phos. cont.=	0.8 mgP/g soil	Schlesinger, 1992
	Earth total soil Phos.	128 e15 g	

Soil mass=(total P)/(P content)=
128e15gP / 0.8mgP / g soil * 1000mg/g=   **160000** E15g

	Global organic soil=	3.2 E12 t	Dobrovolsky, 1994
	3.2e12t * 1E6 g/t=		**3200** E15g
9.	Soil water	0.065 E6 km^3	Berner & Berner, 1987
		0.067 E6 km^4	Colinvaux, 1986
	65e3km^3*1e15 cm^3/km^3*1g/cm^3=		**65000** E15g

10. Land Plants

A.	Land biomass=	8.27 E11t C	Colinvaux, 1986
		5.6 E11t C	Schlesinger, 1992
	Dry Biomass % carbon	0.45	Dobrovolsky, 1994
	Biomass percent dry=	0.4	Dobrovolsky, 1994
	Upr bnd=8.27E11t*1E6 g/t / 0.45		1838 E15g
	Lwr bnd=5.6E11t*1E6 g/t / 0.45		1400 E15g
B.	Pre-industrial Biomass=	2.5 E12 t	Dobrovolsky, 1994
	present biomass=	1.88 E12 t	Dobrovolsky, 1994
	In dry weight,1.88e12 t * 1e6 g/t=		**2500** E15g

11. Coal- total present day resources of coal; i.e that amount of coal
geologically and economically thought to be recoverable.

	Coal Resources=	5380 E9 t	Cassedy, 1990
	converting:		**5380** E15g

12. Oil+Gas- resources defined as in item 11

	Oil resources=	1464 E9 bbl	Masters etal, 1990
	Gas resources=	9245 E12 ft^4	Masters etal, 1990
	Conversion Factors:	140 E3 g/bbl oil	Culp, 1979
		20 g/ft^3 gas	Culp, 1979
	Oil:		205 E15g
	Gas:		185 E15g
	Total oil+gas=		**390** E15g

Notes for Appendix Table A-6--continued

13. Economic structure- using total mining products produced per year,
    assuming a growth rate of dX/dt per year, and a turnover time of 50
    years, the total structure X may be calculated using dX/dt=gX=G-X/TT,
    where dX/dt= rate of change of the total structure, or growth rate.

    g=   percent growth rate = 1.63% (adapted from Miller, 1995)
    G=   Amount added per year (see below for mining results)
    TT=   turnover time of structure, used to calculate losses per year
    Then X= G/(g+1/TT)

World 1990 Data

    Total material production worldwide was the sum of major metals plus
    stone, sand, gravel, clays, salt, phosphate, lime, gypsum, soda, and
    potash.

Structure component	Production 1990	Data source
Metal	0.6	Bureau of Mines, 1991
Other	21.16	Bureau of Mines, 1991
Sawnwood	0.379	FAO, 1995
Panelwood	0.18	FAO, 1995
Paper etc.	0.24	FAO, 1995
Total Wood	0.799	
Plastics	0.051	Emery, 1986
Plant fiber	0.01	FAO, 1995

    Summing rock, wood, plastic, and fiber: 22.62 E15g/yr
    Then E= G/(g+1/TT) = 21.8e15 g/(0.0163+1/50)
                                      E=   **623** E15g

    Notes:
    1) If structural growth rate is flat (zero) then X=1090 e15 g
    2) If structural growth rate is 2.5% then X=484 e15 g
    3) Percent Ore abundances from Mason, 1951

14. Coal extraction structure
    Simulation of Figure S16 suggested appropriate value.
                                                  11.6 E15g

15. Oil extraction structure
    Simulation of Figure S16 suggested appropriate value.
                                                  4.35 E15g

Remainders

16. Land albedo
    See item 1&2 above   **0.49** E24J/yr

17. Ocean albedo
    See item 1&2 above   **1.19** E24J/yr

18. Uncaught land rain

Notes for Appendix Table A-6--continued

See item 17. below   **5000** E15g

19. Unused yield suggested by simulating Figure S16, and scaled for total yield.   **0.027** E15g

20. Unused coal- this is the resource left in the ground. It is no provides an available energy resource. Simulation of Figure S16 suggested the value: **1.2** E15g

21. Unused Oil+gas- this is the resource left in the ground. It is no provides an available energy resource. Simulation of Figure S16 suggested the value: **0.6** E15g

Flows

22. Sun to ecosystems- this is the amount of sunlight falling on the relatively unmanaged systems (ecosystems). The fossil fuel economy model (see Figure S16) suggests that approximately 7 or 8 percent of lands are presently lightly managed, while the rest are heavily managed with forestry, crops, grazing, etc.

                    i.e.   7.5 Percent

Percentages of land use: (United Nations, 1994)

Category	Percent of land
Crops	11
Pasture	26
Woodland	31
Other	32

If a third of the woodlands are lightly managed, and a tenth of the "other" category is lightly managed, then the percentage of land in the lightly managed regime is:

                  31/3+32/10=   13.53 Percent

A lower limit is then 7.5%*1.64e24 J/yr=   0.09

and an upper limit is   **0.16**

23. Sun to agriculture

This is the sun falling on heavily managed systems.

Sun on land - sun to ecosystems=   **1.02** E24 J/yr

24. Sun to marine biota- this is the total sunlight absorbed by the ocean biota. Ideally, this would be gross primary production divided by efficiency of sunlight use.

Ocean Net primary production=   24.9 E9 t C/yr

24.9E9 tC/yr*1E6 g/t*2.22 g dry/gC*10g wet/g dry=

                                 552.78 E15g/yr

Assume Ocean respiration= 0.33XNet production=

                                 182.42 E15g/yr

Gross primary production= net primary production + respiration

Notes for Appendix Table A-6--continued

735.20 E15 g/yr

On average a gram of biomass contains about 4 calories of heat, and the efficiency of open sea photosynthesis is 0.09%. Then:

735.2E15 g/yr*4 cal/g*4.186 J/cal / 0.09%= **0.014** E24 J/yr

25. Rain into soil

Caught rain = total rain - uncaught water

Uncaught water never is caught or tightly held by soil, in its journey from land to sea. Glacial water is of this sort. Probably a small percentage of other land precipitation, maybe 5%, never is incorporated into the soil.

Rain on land=	111000 E15 g/yr	Dobrovolsky, 1994
Glacial flow to ocean =	3000 E15 g/yr	Dobrovolsky, 1994
Other land precip.=	40000 E15 g/yr	Schlesinger, 1992
5% * 40,000=	2000 E15 g/yr	
Total = 3000+2000=	5000 E15 g/yr	

Total precipitation-uncaught water= 111,000 - 5,000 =

106000 E15 g/yr

26. Ocean biota uptake- use the total production of ocean plants.

Ocean production=	24.90 E9 tC	Colinvaux, 1986
Frac. carbon of dry wt=	0.45	Colinvaux, 1986
Ocean production=	110 E15 g dry	
From Colinvaux, carbon weight/Fcarbon=		55.33 E15 g/yr
From Dobrovolsky,		**110** E15 g/yr

27. Ocean biota production This is equal to the total production of the oceans, and equals uptake because there is no gaseous source of matter as in land photosynthesis. **110** E15 g/yr

28. Ocean biota recycle

Equals production - sedimentation **108.66** E15 g/yr

29. Biological sedimentation

Org flux to sea floor=	0.2 E15 gC/yr	Butcher, 1992
Frac Carbonate=Fc	0.2	Broecker & Peng, 1982
Frac Organic =Fo	0.8	Broecker & Peng, 1982
Frac C in Org.=Fco	0.45	(Dry Frac.*Carbon Frac.)
Frac C in CaCO3=Fcc	0.12	(Atomic Wt Fraction)

0.2e15 gC/yr * (Fc / Fcc + Fo / Fco) = **0.69** E15 g/yr

Alternate method: add up CaCO3 and org carbon fluxes, and call this biological sedimentation.

CaCO3 carbon sed=	0.15 E15 gC/yr	Kempe, 1973
Organic carbon sed=	0.04 E15 gC/yr	Kempe, 1973

Using carbon fractions as above, 0.15/0.12+0.04/0.45=

1.34 E15 g/yr

<u>Notes for Appendix Table A-6--continued</u>

30. Ecosys production- total production of mostly undisturbed ecosystems
    Land production=   130 E15 g/yr   Dobrovolsky, 1994
    Fossil fuel economy model suggested value the following value:
    25.2 E15 g/yr

31. Agric. production
    Fossil fuel economy model suggested value   **90.8** E15 g/yr

32. Plant death- use the conversion rate of live material to dead.
    130 E15 g   Dobrovolosky
    130 E15 g/yr

33. Rock weathering- use average uplift rate for land surface=
    2.4 cm/ka   Garrels, et al, 1975
    Uplift rate*land area*density= total mass uplift rate
    2.4cm/ka*149E6km^2*2.65g/cm^3*1E10 cm^2/km^2* 1 k1 1000 yr=
    9.48 E15 g/yr

Special note to items 34 and 35
Coefficients k14 and k15 were calculated using a five times increase in
particulate erosion due to industrial activities. (Garrels&Mackenzie,
1972) Also, a 10 percent decrease in total soil and soil water was
assumed. Then 2 equations in 2 unknowns were solved:
Eq. 1) k14*1.1*1.1*S*W*exp(k15*2500)=4
Eq. 2) k14*S*W*exp(k15*1880)=20
Solving, the values for k14 and k15 as given above were obtained.

34. Soil to ecosystems- if plants' uptake is in proportion to their elemental
    composition then: N,S,P,Ca,K are the main uptake elements=
    1.21% of dry   Dobrovolsky, 1994
    1.21% dry wt * 130E15g/yr dry wt=
    1.57 E15g/yr
    P is taken up and exists in plants primarily in the PO4 ion. Therefore
    actual mass of material taken up for P is P+Oxygen.
    P % of dry Org. matter   0.0013
    P wt% of PO4   32%
    Increment for oxygen in PO4 =.13%*323E15 gC*(1-32%)=
    0.38 e15g/yr
    Then total uptake=1.76+0.29=   1.95 E15 g/yr
    Alternatively, Dobrovolsky gives the total major element uptake by plants:
    Uptake=   9 e15 g/yr   Dobrovolsky
    9.00 E15 g/yr
    This is then the total uptake. The fraction in agriculture is its percentage
    of total production, from items 22,23,37,38.
    That to agriculture =   7.20 E15 g/yr
    That to ecosystems=   **1.80** E15 g/yr

Notes for Appendix Table A-6--continued

35. Particulate erosion

Suspended Load=		13.5 E15 g/yr	Schlesinger, 1992
		20.5 E15 g/yr	Dobrovolsky, 1994
Using Dobrovolsky,			**20.5** E15 g/yr

36. Plants' soil grip- in proportion to the plant live biomass, no flow
37. Dissolved waste- the dissolved portion of the industrial waste load.
38. Particulate waste- the particulate portion of the industrial waste load.
    i.) Mine waste

Worldwide 1990 Mining Data (Bureau of Mines, 1991)

Metal or nonmet	Production 1990 E15 g	% Ore abundance	Total Mined Material E15 g
Pig Iron	0.552	5	11.04
Aluminum	0.0181	30	0.06
Copper	0.00892	1	0.89
Mangan.	0.0086	35	0.02
Zinc	0.0073	4	0.18
Chrom.	0.003784	30	0.01
Lead	0.00335	4	0.08
Nickel	0.000949	1.5	0.06
Tin	0.000216	1	0.02
SubTotal	0.603219		12.38
Stone	11	95	11.58
Sand,Grvl	9	75	12.00
Clays	0.5	75	0.67
Salt	0.19	90	0.21
Phosphate	0.17	50	0.34
Lime	0.14	50	0.28
Gypsum	0.1	50	0.20
Soda	0.032	50	0.06
Potash	0.028	50	0.06
SubTotal	21.16		25.40
	Production		Earth moved
Totals	21.76		37.78

Mine waste=Earth moved-production=   16.01 E15g

ii.) Municipal, industrial, agricultural, energy, and construction solid waste for Selected countries (Canada, U.S., Britain, France, and Germany) was extrapolated for world production by a factor of three, derived from world and selected country aerial emission data: Selected country solid waste:

Notes for Appendix Table A-6--continued

               2164.4 E6 t   United Nations, 1993
    2164.4E6 t*3 t total/ t selected*1e6 g/t=
                 6.49 E15 g
    Then total solid waste= mine waste + municipal   **22.51** E15 g

39. Water uptake by ecosystems
    Total transpiration (Note 31)   71000 E15 g/yr
    Land percent in agric.(note 40)   7.5 percent
    Assuming transpiration rates are the same for ecosystems and
    agricultural systems: Eco transp=71000*0.075=   **5325** E15 g

40. Water uptake by agriculture
    Equals total transpiration-ecosys transpiration   **65675** E15 g

41. Dissolved erosion
    Dissolved Load=   3.7 E15 g/yr   Berner and Berner, 1987
                    3.93 E15 g/yr   Schlesinger, 1992
                    4.9 E15 g/yr   Dobrovolsky, 1994
    Salt spray return=   0.5 E15 g/yr   Dobrovolsky, 1995
    Net salts to oceans=   4.4 E15 g/yr
        Using Dobrovolsky   **4.4** E15 g/yr

42. Suspension settling
    From 6. above, average settling distance is about 390 m and average
    particle velocity is 324 m/yr. So average settling time is approximately
    1.2 years, and system is approximately steady state, so settling=~
    erosion   **20.5** E15g/yr

43. Chemical precipitation- all the loss of dissolved material to the
    sediments that is not biologically mediated. Includes evaporites, clay
    exchange, hydrothermal exchange, etc. May be negligible at present.
                                 0 E15g/yr

44. Soil oxidation- number of moles of CO2 released per year
    Carbon released=   60 E15 g/yr   Schlesinger
    Moles carbon = mass/atomic wt=   5 E15 mol
    Moles CH2O=moles carbon=   5 E15 mol
    Mass H2O=moles*atomic wt=   150 E15g/yr
    Note: may need to add in moles to balance HCO3- ions in streams.
    Alternate: residence time of soil approach
    Soil mean res. time=   25 yr   Schlesinger
    Oxidation=org. soil mass/res. time=   128 E15g/yr
    Including organic erosion   1.42 E15 g/yr
    Oxidation=turnover-erosion=   **126.58** E15g/yr

45. Ecosystem yield
    Fossil fuel economy model suggestedvalue   **0.57** E15g/yr

46. Agriculture yield

Notes for Appendix Table A-6--continued

Fossil fuel economy model suggestedvalue	**13.4** E15g/yr	
47. Soil uptake by agriculture		
See item #32 above.	**7.20** E15g/yr	
Note: The fossil fuel economy model (Figure S16)		
suggested values for items 48 through 63 below.		
48. Yield to oil econ	**13.6** E15 g/yr	
49. Yield to coal econ	**75** E15 g/yr	
50. Oil econ. build	**36** E15 g/yr	
51. Coal econ. build	**2.5** E15 g/yr	
52. Economic asset decay		
Approximately 25 year turnover time	**24** E15 g/yr	
53. Ecosystem manage	**0.88** E15 g/yr	
54. Well building	**0.83** E15 g/yr	
55. Well decay	**0.54** E15 g/yr	
56. Well use	**0.24** E15 g/yr	
57. Mine building	**5.25** E15 g/yr	
58. Mine decay	**2.5** E15 g/yr	
59. Mine use	**2.6** E15 g/yr	
60. Coal flow: that made unavailable but not burned	**5.23** E15 g/yr	
61. Oil+gas flow: that made unavailable but not burned		
	5.64 E15 g/yr	
62. Coal consumption: that actualy burned	**4.5** E15 g/yr	
63. Oil+gas consumption: that actually burned	**5.05** E15 g/yr	
64. Streamflow= **40000** E15g/yr	Schlesinger, 1992	

Appendix Table A-7. Calibration values for sources, storages, and flows for Hydro 1.1, the model in Figure 4-3, and the calculated coefficients.

Item Description	Symbol/Equation	Value	Units	Coeff.	Value
Sources					
1. Air Mass	M	1	Std		
2. Sunlight	I0	1	Std		
Storages				**Turn. time**	
3. Water Vapor	V	16.8	E6 kg	20 min	
4. Clouds, Storms	C	0.625	E6 kg	30 min	
5. Surface Water	S	200	E6 kg	317 days	
Flows					
6. Sun to ground	I=I0/(1+k0*C)	0.75	Std		
7. Cloud albedo	Rc=k0*I*C	0.25	Std	k0=	0.53
8. Land albedo	RI=I/(1+k4S+k5VC)	0.05	Std		
9. Vapor inflow	J1=k1*M	1212.2	E6 kg/day	k1=	1212.20
10. Vapor outflow	J2=k2*V	1211.57	E6 kg/day	k2=	72.12
11. Cloud Formation	J3=k3*V*RI*C	30	E6 kg/day	k3=	57.14
12. Sun to evap.	J4=k4*RI*S	0.54	Std/day	k4=	0.05
13. Sensible heat	J5=k5*RI*V*C	0.16	Std/day	k5=	0.31
14. Rain	J6=k6*C*V*RI	3.48	E6 kg/day	k6=	6.63
15. Evapotransp.	J7=k7*RI*S	2.85	E6 kg/day	k7=	0.29
16. Drainage	J9=k9*S	0.63	E6 kg/day	k9=	0.0032
17. Cloud evap.	J10=k10*C	26.52	E6 kg/day	k10=	42.43

Notes. See Appendix Table A-9 for documentation of values used.

Appendix Table A-8. Calibration values for sources, storages, and flows for
Hydro 2.1, the model in Figure 4-7, and the calculated coefficients.

Item	Description	Symbol or Equation	Value	Units	Coeff.	Value
Sources						
1	Wind	M	1	Std		
2	Sunlight	I0	1	Std		
3	Vapor pressure	eo	1	Std		
Storages						
4	Vapor	V	16.8	e6 kg		
5	Storms	C	0.625	e6 kg		
6	Surf. Wtr	S	200	e6 kg		
Flows						
7	Sun past clds	I=I0/(1+k0*C)	0.8	Std		
8	Cloud albedo	Rc=k0*I*C	0.25	Std	k0=	0.50
9	Land albedo	RI=I/(1+k4S+k5VC)	0.05	Std		
10	Vapor in	J1=k1*M*eo	1212.2	e6 kg/day	k1=	1212.20
11	Vapor out	J2=k2*M*V	1211.57	e6 kg/day	k2=	72.12
12	Storm formn.	J3=k3*RI*V*C	30	e6 kg/day	k3=	57.14
13	Latent heat	J4=k4*RI*S	0.5367		k4=	0.05
14	Convection	J5=k5*RI*V*C	0.1633		k5=	0.31
15	Rain	J6=k6*RI*V*C	3.48	e6 kg/day	k6=	6.63
16	Evaporation	J7=k7*RI*S	2.85	e6 kg/day	k7=	0.29
17	Streams	J9=k9*S	0.63	e6 kg/day	k9=	3.15E-03
18	Cloud evap.	J10=k10*C	26.52	e6 kg/day	k10=	42.43

Notes. See Appendix Table A-9 for documentation of values used.

Appendix Table A-9. Documentation of calculations and assumptions for the development and calibration of models Hydro 1.1 and Hydro 2.1, as shown in Figures 4-3 and 4-7.

Number of note corresponds to the item numbers in Appendix Table A-8, up to note number 18. Higher numbered notes are general.

Initial assumption: Look at a 1 km^2 area of land in Florida.

1. Wind source standardized to one unit.   1 Unit
2. Sunlight source standardized to one unit.   1 Unit
3. Vapor pressurestandardized to one unit.   1 Unit
4. V=Total weight of water vapor (below the lifting condensation level)

Tavg = 80F=	26.67 C	(Assumed)
RH = relative humidity =	80%	(Assumed)
Ws=saturation mixing ratio=	23 g/kg	(Calculated)
W=actual mixing ratio=RH*Ws=	18.4 g/kg	
Td=Dewpoint=	23 C	(Calculated)
LCL=Lifting Condensation Level	0.75 km	(Calculated)
Pressure at LCL=	925 mbar	(Calculated)
Volume=space below LCL =	0.75 km^3	(Calculated)
Rhod=density of dry air =	1.22 kg/m^3	(Calculated)
V=Volume*Rhod*W=	1.68E+07 kg	(Calculated)

5. C=Total weight of water in clouds

Suppose that clouds occupy, on average 20% of the space above the LCL and below about 2 km. Then:

Top of cloud zone=	2 km	(Assumed)
Thickness of cloud zone =	1.25 km	(Calculated)
Volume percentage cloud area=	20%	(Assumed)
Avg water density =	0.5 g/m^3	(Calculated)
Volume of cloud zone=	1.25 km^3	(Calculated)
C = Volume*density=	6.25E+05 kg	(Calculated)

6. S=Total weight of surface water, defined as pooled water and pore water in top 1 meter of soil.

Average Soil Porosity =	30%	(Assumed)
Saturation percentage =	33%	(Assumed)
Depth of Surface Interaction =	1 m	(Assumed)
Soil Volume=	1000000 m^3	(Calculated)
Density of Water =	1000 kg/m^3	(constant)
Pore Water=Poros.*Sat%*Vol*Dens.=	9.90E+07 kg	(Calculated)

Assume 10% coverage of surface water at a depth of 1 meter.

Pooled Surface Water Coverage =	10%	(Assumed)
Average depth =	1 m	(Assumed)
Volume =	100000 m^3	(Calculated)

Appendix Table A-9--continued

Density =		1000 kg/m^3	(constant)
Pooled Water = Vol * Density =		1.00E+08 kg	(Calculated)
S = pooled wtr + pore wtr =		1.99E+08 kg	(Calculated)

7. Sun past clouds is the solar radiation actually reaching the surface, calculated as the total minus the cloud albedo.

$$1-0.25= \quad 0.75 \quad \text{(Calculated)}$$

8. Rc = cloud albedo, the fraction of incoming solar reflected by clouds

Rc= 25% (Wallace, 1977)

9. Rl=land albedo, the fraction of incoming solar reflected by land

Rl= 5% (Wallace, 1977)

10. J1 = Vapor inflow rate, total weight of vapor entering the area with winds.

Thickness of vapor wedge = LCL =	0.75 km	(Calculated)
Average Wind Speed = vw =	3 km/hr	(Assumed)
Density of dry air = RHOd =	1.22 kg/m^3	(Wallace, 1977)
moisture content = W =	18.4 g/kg	(Calculated)
J1=LCL*vw*area*RHOd*W*conv. =	1.21E+09 kg/day	(Calculated)

11. J2 = total vapor outflow with wind.
For steady state, inflows must balance outflows for entire model.

J2=J1-J9 = 1.21E+09 kg/day (Calculated)

12. J3 = Cloud formation Rate = total weight of vapor that enters cloud form per day Turnover time of clouds is very short, on order of minutes

Turnover time of clouds (assumed) =	30 min	(Wallace, 1977)
=	0.020833 days	
J3=Cloud mass/turnover time =	3.00E+07 kg/day	(Calculated)

13. J4 = solar energy that goes into evapotranspiring water
Fl = fraction of energy used by the climate system for latent heating

Fl = 23/30 =	77%	(Wallace, 1977)
J4 = Fl * (I0-(Rl+Rc)*I0)	0.54 unit	(Calculated)

14. J5 = solar energy that goes into sensible heat transfer
Fs = fraction of energy used by the climate system for sensible heating

Fs = 7/30 =	23%	(Wallace, 1977)
J5 = Fs * (I0-(Rl+Rc)*I0)	0.16 units	(Calculated)

15. J6= Precipitation = total weight of rain falling on the area in one day.

Pr = Rain rate=	50 in/yr	(Viessman et al, 1989)
P=Pr*area*conv. factor	3.48E+06 kg/day	(Calculated)

Appendix Table AH5.--continued

16. J7= Evapotranspiration = total transfer of surface water to vapor phase.

Er= pan evaporation rate =	50 in/yr	(Viessman et al, 1989)
Tr=transpiration rate =	40 inch/yr	(Assumed)
E=Evaporation=Er*area*covr%*conv	1.27E+08 kg/yr	(Calculated)
T=Transp. = Tr*area*(1-covr%)*conv	9.14E+08 kg/yr	(Calculated)

Appendix Table A-9--continued

$$Et = E + T = \quad 1.04E{+}09 \text{ kg/yr} \quad \text{(Calculated)}$$
$$= \quad 2.85E{+}06 \text{ kg/day} \quad \text{(Calculated)}$$

17. $J9$ = Outflow = total weight of water leaving by overland or underground means.

Outflow=Precipitation-Evapotranspirat 6.26E+05 kg/day   (Calculated)

18. $J10$ = Cloud Evaporation=cloud formation-precipitation=

$J10 = J3 - P$ 2.65E+07 kg/day   (Calculated)

19. ALPHA = the fractionation factor for deuterium in water and vapor at 25C.

ALPHA=   1.074   (Faure, 1986)

Appendix Table AH5.--continued

20. $delDv$ = a measure of deuterium content of water.

R = ratio of D_2O molecules to H_2O molecules.

R (Lake Michigan water) =   0.000148   (Faure, 1986)

Rs= R(sea water near Florida)=   0.00015   (Assumed)

Rv=R(incoming vapor) =Rs/ALPHA=   0.00014 mol/mol

$delDv$=1000*(Rv-Rs)/Rs=   -68.9013   (Calculated)

21. $J1d$ = Amount of D_2O entering the system as water vapor in wind

WR=weight ratio of D_2O to H_2O in a sample.

WRv=R*[M(D2O)/M(H2O)] , where M = molecular weight.

WRv=Rv*20/18=   0.000155 kg/kg   (Calculated)

$J1d$ = total weight of D_2O vapor incoming with winds.

$J1d$=J1*WRv =   1.88E+05 kg/day   (Calculated)

22. Evaluation of the difference between the coefficients for D_2O and H_2O

There are a number of equations to work with:

1. $V = D + H$ (Initial mass balance)
2. $Vo = Do + Ho$ (Final mass balance)
3. $V = Vo{*}e^{\wedge}(-kv{*}t)$ (Linear outflow)
4. $D = Do{*}e^{\wedge}(-kd{*}t)$ (Linear outflow)
5. $H = Ho{*}e^{\wedge}(-kh{*}t)$ (Linear outflow)
6. $D/H = Do/Ho{*}f^{\wedge}(ALPHA-1)$ (Rayleigh fractionation)
7. $f = V/Vo$ (Definition of f)

Where: V=total atoms at time of interest
Vo=total initial atoms
D=total Deuterium atoms
Do=total initial deuterium atoms
H=total hydrogen atoms
Ho=total initial hydrogen atoms
ALPHA=fractionation factor
kv=coefficient of vapor outflow pathway
kd=coefficient of D outflow pathway
kh=coefficient of H outflow pathway

Appendix Table A-9--continued
                    f=fraction of vapor remaining
   Combining equations 3 and 7 ; 4 and 5 ; and 6 and 7 above we have:
   8. f=V/Vo=exp(-kv*t)
   9. D/H=Do/Ho*(e^(-kv*t))^(ALPHA-1)
   I. kd-kh=kv(ALPHA-1)
   Now if Ah is the fraction of hydrogen atoms we have
   II. kv=kh*Ah+kd*(1-Ah)
   Combining I. and II. gives III. kh=kv*(2-ALPHA+Ah*(ALPHA-1))
   And since 1 > Ah > 0.99 in all practical cases, we can approximate:
                    kh=kv (all cases)
                    kd=kv*ALPHA (condensation)
                    kd=kv/ALPHA (evaporation)
Appendix Table AH5.--continued
   Additionally we need to know the effect of two H's per H2O, and only one D
   per DHO.
        (1)   ALPHA=Rv/Rl, where
                    ALPHA = fractionation factor, equilibrium condition
                    R=ratio of deuterium to hydrogen atoms
                    Rv = R in vapor
                    Rl = R in liquid
   Because there are 2 H atoms in an H2O and only one D in a DHO,
        (2)   (D/H)atoms = 1/2* (DHO/H2O)molecules
   Substituting (2) into (1) gives
                    ALPHA= (1/2*(DHO/H2O)v) / (1/2*(DHO/H2O)l)
                    The 1/2 factor cancels from top and bottom so that
                    ALPHA=Rmolecules,vapor/Rmolecules,liquid
                    ...and molecules can be treated the same as atoms.
   When converting from mass ratio to atomic ratio, the factor 1/2 must be
   used along with the molecular weight conversion.

Appendix Table A-10. Calibration values of sources, storages, and flows for Tempreg1, the model in Figure 4-18, with the calculated coefficients.

Item	Description	Symbol/Eqn.	Value	Units	Coeff.	Value
Sources						
1.	Sun	$Io=$	100	Units/day		
2.	Ocean	$O=$	1	Std units		
Remainders						
3.	Sun thru ozone	$I=$	98	Units/day		
4.	Sun past atmos.	$Is=$	56	Units/day		
5.	Surf. albedo	$Rs=$	9	Units/day		
6.	Condensed vapor	$Rv=$	75	E15g/day		
7.	Streams	$Rr=$	100	E15g/day		
Storages						
8.	Surface temp.	$Ts=$	288	°K		
9.	Upr. atmos temp.	$Ta=$	273	°K		
10.	Storms, clouds	$C=$	55	E15g/day		
11.	Biomass	$B=$	2500	E15g/day		
Flows						
12.	Sun to clouds	$J1=k1IsC=$	42	Units/day	$k1=$	1.36E-02
13.	Cloud absorb	$J2=k2IsC=$	23	Units/day	$k2=$	7.47E-03
14.	Sun to plants	$J3=k3RsRrB=$	10.5	Units/day	$k3=$	4.67E-06
15.	Sun to heat surf.	$J4=k4Rs=$	15.4	Units/day	$k4=$	1.71
16.	Sun->ocean evap	$J5=k5RsO=$	21.1	Units/day	$k5=$	2.35
17.	Surf. heat to storms	$J6=k6TsRvC=$	5.8	Units/day	$k6=$	4.89E-06
18.	Grnd->cloud rad.	$J7=k7(Ts-Ta)^4=$	13	Units/day	$k7=$	2.57E-04
19.	Grnd->space rad	$J8=k8Ts^4=$	5	Units/day	$k8=$	7.27E-10
20.	Cloud formation	$J9=k9TsRvC=$	2690	E15g/day	$k9=$	2.26E-03
21.	Cloud loss	$J10=k10C=$	1290	E15g/day	$k10=$	23.45
22.	Cloud rad to space	$J11=k11Ta^4=$	65	Units/day	$k11=$	1.17E-08
23.	Live production	$J12=k12RsRrB=$	0.94	E15g/day	$k12=$	4.19E-07
24.	Biomass loss	$J13=k13B=$	0.94	E15g/day	$k13=$	3.77E-04
25.	Ocean evaporation	$J14=k14RsO=$	1275	E15g/day	$k14=$	1.42E+02
26.	Evapotranspiration	$J15=k15RsRrB=$	200	E15g/day	$k15=$	8.89E-05
27.	Cloud evaporation	$J16=k16CTa=$	1290	E15g/day	$k16=$	8.59E-02
28.	Cloud formation	$J17=k17TsRvC=$	2690	E15g/day	$k17=$	2.26E-03
29.	Rain on land	$J18=k18TsVC=$	300	E15g/day	$k18=$	2.53E-04
30.	Water to plants	$J19=k19RsRrB=$	200	E15g/day	$k19=$	8.89E-05
31.	Plant work heat	$J20=k20RsRrB=$	0.1	Units/day	$k20=$	4.44E-08
32.	Plant heating	$J21=k21B=$	7.1	Units/day	$k21=$	2.83E-03
33.	Storm heating	$J22=k22TsRvC=$	50.4	Units/day	$k22=$	4.25E-05
34.	Total precip.	$J23=k23TsRvC=$	1400	E15g/day	$k23=$	1.18E-03
35.	Lat heat cond'n.	$J24=k24Rv=$	1.2	Units/day	$k24=$	1.66E-02

Appendix Table A-10--continued

Item	Description	Symbol/Eqn.	Value	Units	Coeff.	Value
36.	Lat. ht. cld evap.	J25=k25J16=	21.4	Units/day	k25=	1.43E-03
37.	Lat ht. transp.	J26=k26TsRvB=	3.3	Units/day	k26=	1.47E-06
38.	Lat. ht. rainstorms	J27=k27TsRvC=	44.6	Units/day	k27=	3.76E-05
39.	Rain on sea	J28=k28TsRvC=	1100	Units/day	k28=	9.26E-04

Notes to Appendix Table A-10

1. Sun standardized to 100 units
      100 units
2. Assume constant ocean surface area, then standardize to 1 unit
      1 unit
3. Sun penetrating ozone is the sun getting into the troposphere.
      98 units   Schneider&Londer, 1984
4. Sun past clouds is the solar energy not absorbed or reflected in clouds.
      56 units   Schneider&Londer, 1984
5. Surface albedo is the amount of solar energy reflected at the surface.
      9 units   Schneider&Londer, 1984
6. Condensed vapor is that settling out as surface condensation.
Average mid latitude condensation:
      0.15 mm/day Miller, 1977
0.15 mm/day / 1e6 mm/km * 510E6 km^2 * 1E15g/km^3=
      76.5 e15 g/day
      Rounding: 75 E15g/day
7. Stream flow=   0.04 e6 km^3/d Berner&Berner, 1987
0.037E6km^3/yr * 1E15g/km^3 / 365d/yr=   101.37 e15g/day
      Rounding: 100 E15g/day
8. Surface temperature=   288 °K   Wallace and Hobbs, 1977
To find the equivalence of heat units and temperature units, the heat content of the surface storage was calculated as follows:

Surface heat is taken as the sum of the heat contained in the surface layers of water (100m), air (375 m), and soil (10m).

Layer thickness t as follows

	Water:	100 m	mixing depth
	Air:	375 m	half LCL: see app. tbl H5
	Soil:	10 m	assumption

Specific heat c as follows

	Water:	4218 J/kg-K	Wallace&Hobbs, 1977
	Air:	1004 J/kg-K	Wallace&Hobbs, 1977
	Soil:	2000 J/kg-K	Assumption

Density p as follows

	Water	1000 kg/m^3	Wallace&Hobbs, 1977
	Air:	1.25 kg/m^3	Wallace&Hobbs, 1977
	Soil	2000 kg/m^3	Assumption

Surface temp. T   288 °K   Avg. earth surface

Surface area a as follows:

	Water	3.50E+08 km^2	Dobrovolsky, 1994
	Air	5.10E+08 km^2	Dobrovolsky, 1994
	Soil	1.60E+08 km^2	Dobrovolsky, 1994

Heat content=c*T*p*t*a

H2O- 4218J/kg°K*288°K*1000kg/m^3*100m*360E6km^2*1E6m^2/km^2=

	Water	4.25E+25 J
	Air	6.91E+22 J
	Soil	1.84E+24 J

Then these must be converted to standard units as used in
Schneider&Londer. Their 100 units corresponds to 342 W/m^2.

100 units=342 W/m^2*510E6 m^2=   1.51E+22 J/day

A storage unit is then 1.51e20 J. Divide joule values by this number to
convert to standard units. Conversion factor= 1.51E+20

	Water		282,135 units
	Air		459 units
	Soil		12,231 units
		Total	294,825 units

9. Upper air temperature=

          273 °K Wallace and Hobbs, 1977

The equivalence between temperature and heat was determined by
finding the upper air heat content as follows:

Upper atmosphere heat is that above the lifting condensation level (LCL),
as outlined in Appendix Table AH5.

Atmosphere mass=	5.14E+18 kg	Wallace&Hobbs, 1977
Mass below 375m= density*area*thickness=		
	2.39E+17 kg	From item 8
Above 375 m= Total mass-that below 375 m=		
	M= 4.90E+18 kg	
Atmos. Temp=Ta=	273 °K	Wallace&Hobbs, 1977
Heat content=c*Ta*M=	1.34E+24 J	
Converting to units (See item 8):	8,914 units	

Notes to Appendix Table A-10--continued

10. Storms and clouds is a storage proportional to the total mass of water in clouds.

Cloud liquid water= 0.11 kg/m^2 Greenwald, 1995
0.11kg/m^2 * 1000g/kg * 1E6 m^2/km^2 * 510E6 km^2 =
56.1 E15g
Rounding: 55 E15g

11. Biomass is the total dry weight of living matter, which is approximately that of the land plant mass
2500 E15g Dobrovolsky, 1994

12. Sun to clouds is that solar energy absorbed and/or reflected by clouds
42 units Schneider&Londer, 1984

13. Sun absorbed by clouds
23 units Schneider&Londer, 1984

14. Sun to plants is that absorbed by plants, approximated here by that absorbed at the land surface, which is total incident sun minus that reflected.

Surface insolation= 198 W/m^2 Kiehl and Trenberth, 1997
Globe % land= 0.294 Dobrovolsky, 1994
Land surf. albedo= 12.20% Kyle and Vasanth, 1986
198J/s m^2 * (1-0.122) * 86400s/d * 360km^2 * 1E6m^2/km^2 =
5.41E+21 J/day
Converting (See item 8) 10.55 units/d
Rounding: 10.5 units/d

15. This is the remaining energy, after heat to plants and heat to evaporation is subtracted from that striking the surface. (item 4 - item 5 item 14- item 16)
15.4 units/d

16. Sun to ocean evaporation is that solar energy used to evaporate ocean water at the surface.

Surface evaporation= 1275 E15g/d See Item 25
Heat of vaporization= 2500 J/g Wallace and Hobbs, 1977
Latent heat= 21.1 units/d

17. Turbulent heat loss is the heat transferred up away from the surface by convection and storm winds

Turbulent heat loss= 5 units Schneider&Londer, 1984
However, the value used was selected in order to balance heat flows to the surface storage. Equals J4+J5+J20+J21+(latent heat of Rv)-J7-J8=
5.8 units/d

18. Ground to cloud radiation is the net radiation from ground to clouds.
13 units Schneider&Londer, 1984

19. Ground to space rad.= 5 units Schneider&Londer, 1984

20. Cloud formation is all the water that goes into clouds per day.

Notes to Appendix Table A-10--continued

Cloud turnover time=	30 minutes	Wallace and Hobbs, 1977
Water in clouds=	56.1 E15g	Item 10
production=storage/turnover time=		2692.8 E15g/d
Rounding:		2690 E15g/d

21. Cloud evaporation= formation - precipitation (item 20 - item 34)
    1290 E15g/d

22. Cloud radiation to space=
    65 units Schneider&Londer, 1984

23. This is the total photosynthesis of the biosphere or gross primary production
    Net production (dry wt.)=   172 E15g/yr Dobrovolsky, 1994
    Gross production= 2* Net Production   Assumption
    172e15gdw/yr * 2 / 365 d/yr=   0.94 E15g/d

24. Biomass loss is equal to community respiration, and is equal to gross
    production in steady state   0.94 E15g/d

25. Ocean evaporation=   4.23E+05 km^3/yr Berner&Berner, 1987
                           4.56E+05 km^3/yr Dobrovolsky, 1994
    (4.23e5 km^3/yr)*(1e9m^3/km^3)*(1000kg/m^3)/(365d/yr)*(1000g/kg)=
             1159 e15 g/ or approximating: 1200 e15g/d
    These estimates often aggregate dew estimated in item 6 to be 75E15g/d
    Adding this in, 1200+75=   1275 E15g/d

26. Evapotranspiration=   7.30E+04 km^3/yr Berner&Berner, 1987
    (7.3e4 km^3/yr)*(1E9m^3/km^3)*(1000kg/m^3)/(365d/yr)*(1000g/kg)=
                                               200 E15g/d
    Latent heat of transpiration is heat of vaporization (See item 16) times the
    transpiration rate = 200E15g/d * 2500J/g= 5.00E+20 J/d
    Converting to units (See item 8):   3.3 units/d

27. Cloud evaporation is the same as cloud loss, item 21.

28. Cloud formation=   2690 E15g/d See item 20

29. Rain on land=   1.10E+05 km^3/yr Berner&Berner, 1987
    (7.3e4 km^3/yr)*(1e9m^3/km^3)*(1000kg/m^3)/(365d/yr)*(1000g/kg)=
                                               301 e15 g/d
    Rounding: 300 E15g/d

30. Water to plants is approximately equal to evapotranspiration
                                               200 E15g/d

31. Plant work heat is the total community respiration. From item 24 above
    Community resp'n.=   0.94 E15g/d Item 24
    0.94E15g/d * 4kcal/g * 4186J/kcal=   1.58E+19 J/d
    Converting to standard units (see item 8) 0.1047 units/d
    Rounding: 0.1 units/d

32. Plant heating is the total shortwave heat absorbed by plants, which is
    land insolation minus respiration minus latent heat of transpiration.

Notes to Appendix Table A-10--continued

    Item 14 - item 31 = 10.5 - 0.1 =   7.1 units/d

33. Storm heating atmosphere is the total transfer of latent and turbulent heat to the atmosphere from the surface due to storm formation.
    Item 17 + Item 38 =   50.4 units/d

34. Total precipitation is that falling on oceans plus that falling on land. Equals total evaporation-condensation
    =1275+200-75   See items 6,25,26
          1400 E15g/d

35. Latent heat of condensation is heat of vaporization (See item 16) times the condensation rate (from item 6) = 75E15g/d * 2500J/g=
      1.88E+20 J/d
    Converting to units (see item 8):   1.2 units/d

36. Equals heat of vaporization (from item 16) times the cloud evaporation rate (from item 27) 1290E15g/d * 2500J/g=   3.23E+21 J/d
    Converting to units (see item 8):   21.4 units/d

37. Equals heat of vaporization (from item 16) times the transpiration rate (from item 26) 200E15g/d * 2500J/g=   5E+20 J/d
    Converting to units (see item 8):   3.3 units/d

38. Equals heat of vaporization (from item 16) times the cloud formation rate (from item 26) 2690E15g/d * 2500J/g=   6.73E+21 J/d
    Converting to units (see item 8):   44.6 units/d

39. Total precipitation - rain on land=   1100 E15g/d

Appendix Table A-11. Calibration values of sources, storages, and flows for Tempreg2, the model in Figure 4-18, with the calculated coefficients.

Item	Description	Symbol/Equ'n.	Value	Units	Coeff.	Value
Sources						
1.	Sun	$I_o=$	100	Unit/day		
2.	Surface Water	$W=$	1	Std		
Remainders						
3.	Sun thru ozone	$I_t=$	98	Unit/day		
4.	Sun past clouds	$I_{sf}=$	56	Unit/day		
5.	Surf. albedo	$R_s=$	9	Unit/day		
6.	Cloud reflection	$R_c=$	19	Unit/day		
7.	Surface rad to sky	$R_r=$	5	Unit/day		
Storages						
8.	Surface temp.	$T_s=$	288	°K		
9.	Upr. atmos temp.	$T_a=$	273	°K		
10.	Storms, clouds	$C=$	55	E15g		
11.	Vapor	$V=$	13000	E15g		
12.	Storm heat	$Q_c=$	2	Units		
Flows						
13.	Sun to clouds	$J1=k1 I_{sf} C$	42	Unit/day	$k1=$	1.36E-02
14.	Cloud absorb	$J2=k2 I_{sf} C$	23	Unit/day	$k2=$	7.47E-03
15.	Cloud to grnd rad	$J3=k3 T_a^4$	96	Unit/day	$k3=$	1.73E-08
16.	Surf. heat absorb	$J4=k4 R_s$	23.7	Unit/day	$k4=$	2.64
17.	Latent ht of cond.	$J5=k5V$	1.2	Unit/day	$k5=$	9.23E-05
18.	Turbulent heat	$J6=k6 T_s V C$	5.7	Unit/day	$k6=$	2.78E-08
19.	Surface radiation	$J7=k7 T_s^4$	114	Unit/day	$k7=$	1.66E-08
20.	Surf. ht to evap.	$J8=k8 W R_{se}(K T_s)$	1.2	Unit/day	$k8=$	4.65E-10
21.	Cloud formation	$J9=k9 T_s V C$	2690	E15g/day	$k9=$	1.31E-05
22.	Cloud evap.	$J10=k10 C Q_c$	1290	E15g/day	$k10=$	11.73
23.	Atmos. heat rad.	$J11=k11 T_a^4$	161	Unit/day	$k11=$	2.90E-08
24.	Rain	$J12=k12 T_s V C$	1400	E15g/day	$k12=$	6.80E-06
25.	Condensation	$J13=k13V$	75	E15g/day	$k13=$	5.77E-03
26.	Evaporation	$J14=k14 W R_{se}(K T_s)$	1475	E15g/day	$k14=$	5.72E-07
27.	Heat into storms	$J15=k15 T_s V C$	50.4	Unit/day	$k15=$	2.45E-07
28.	Cloud grnhouse	$J16=k16 R_r C$	32	Unit/day	$k16=$	0.116
29.	Vapor grnhouse	$J17=k17 R_r V$	77	Unit/day	$k17=$	1.18E-03
30.	Lat. ht cloud evap	$J18=k18 C Q_c$	21.4	Unit/day	$k18=$	0.19
31.	Upper air rad sky	$J19=k19 T_a^4$	65	Unit/day	$k19=$	1.17E-08
32.	Sun to evap.	$J20=k20 W R_{se}(K T_s)$	23.3	Unit/day	$k20=$	9.02E-09
33.	Storm heat disprs.	$J21=k21 {\cdot} Q_c$	61	Unit/day	$k21=$	30.5

Notes to Appendix Table A-11.
1. Sun standardized to 100 Units per day inflow   100 Units/d

Notes to Appendix Table A-11--continued

2. Assume constant ocean surface area, then standardize to 1 unit
                                                                    1 Units/d
3. Sun penetrating ozone is the sun getting into the troposphere.
                        98 Units/d   Schneider&Londer, 1984
4. Sun past clouds is the solar energy not absorbed or reflected in clouds.
                        56 Units/d   Schneider&Londer, 1984
5. Surface albedo is the amount of solar energy reflected at the surface.
                        9 Units/d   Schneider&Londer, 1984
6. Cloud reflection is the total sun to clouds minus that absorbed.
                        19 Units/d   Schneider&Londer, 1984
7. Surface radiation to sky is the surface radiation that gets past the
    greenhouse gases.   5 Units/d Schneider&Londer, 1984
8. Surface temperature=   288 °K   Wallace and Hobbs, 1977
    To find the equivalence of heat units and temperature units, the heat
    content of the surface storage was calculated as follows:

    Surface heat is taken as the sum of the heat contained in the surface
    layers of water (100m), air (375 m), and soil (10m).

    Layer thickness t as follows
                    Water: 100 m   mixing depth
                    Air: 375 m   half LCL: see app. tbl H5
                    Soil   10 m   assumption
    Specific heat c as follows
                    Water: 4218 J/kg-K Wallace&Hobbs, 1977
                    Air: 1004 J/kg-K Wallace&Hobbs, 1977
                    Soil   2000 J/kg-K Assumption

    Density p as follows
                    Water   1000 kg/m^3 Wallace&Hobbs, 1977
                    Air: 1.25 kg/m^3 Wallace&Hobbs, 1977
                    Soil   2000 kg/m^3 Assumption
    Surface temp. T   288 °K   Avg. earth surface
    Surface area a as follows:
                    Water   3.50E+08 km^2   Dobrovolsky, 1994
                    Air   5.10E+08 km^2   Dobrovolsky, 1994

                    Soil   1.60E+08 km^2   Dobrovolsky, 1994
    Heat content=c*T*p*t*a
    H2O- 4218J/kg°K*288°K*1000kg/m^3*100m*360E6km^2*1E6m^2/km^2=
                        Water   4.25E+25 J

Notes to Appendix Table A-11--continued

	Air	6.91E+22 J
	Soil	1.84E+24 J

Then these must be converted to standard units as used in Schneider&Londer. Their 100 units corresponds to 342 W/m^2.

100 units=342 W/m^2*510E6 m^2=   1.51E+22 J/day

A storage unit is then 1.51e20 J. Divide joule values by this number to convert to standard units. Conversion factor=   1.51E+20

	Water	282,135 units
	Air	459 units
	Soil	12,231 units
	Total	294,825 units

9. Upper air temperature=   273 °K   Wallace and Hobbs, 1977

The equivalence between temperature and heat was determined by finding the upper air heat content as follows:

Upper atmosphere heat is that above the lifting condensation level (LCL), as outlined in Appendix Table AH5.

Atmosphere mass=   5.14E+18 kg   Wallace&Hobbs, 1977

Mass below 375m= density*area*thickness=

                2.3906E+17 kg   From item 8

Above 375 m= Total mass-that below 375 m=

                M=   4.90E+18 kg

Atmos. Temp=Ta=   273 °K   Wallace&Hobbs, 1977

Heat content=c*Ta*M=   1.34E+24 J

Converting to units (See item 8):   8,914 Units

10. Storms and clouds is a storage proportional to the total mass of water in clouds.

Cloud liquid water=   0.11 kg/m^2 Greenwald, 1995

0.11kg/m^2 * 1000g/kg * 1E6 m^2/km^2 * 510E6 m^2 =

                56.1 E15g

                Rounding: 55 E15g

11. Vapor is the total water vapor in the atmosphere on average.

                13000 km^3   Berner&Berner, 1987

1.3E4km^3*1000kg/m^3*1E9 m^3/km^3*1000g/kg=

                13000 E15g

12. Storm heat is the high grade heat entrained into storms transformable into winds, updrafts etc. It may be estimated from storm turnover time and the total inflow.

Notes to Appendix Table A-11--continued

Storm turnover time=		30 min	Wallace&Hobbs, 1977
Total heat inflow rate=		82.3 Units/d	Items 27 and 28
30min * 82.3Units/d / 1440min/d =			1.71 Units
	Rounding:		2 Units

13. Sun to clouds is that solar energy absorbed and/or reflected by clouds
42 Units/d Schneider&Londer, 1984

14. Sun absorbed by clouds   23 Units/d Schneider&Londer, 1984

15. Cloud to ground radiation is the radiant energy emitted downward by
clouds.   96 Units/d Schneider&Londer, 1984

16. This is the sensible heat absorption is the sun's energy absorbed at the
earth's surface. Calibrated as total heat absorbed at surface minus that
going directly to latent heat of evaporation (Item 32).
Total heat absorbed=   47 Units/d Schneider&Londer, 1984
          Difference=   23.7 Units/d

17. Latent heat of condensation is that heat released at the earth's surface to
to simple condensation of moisture.
Condensation (Item 25)*Heat of vaporization (2500J/g)=   J
                    1.88E+20 J/d
          Converting and rounding: 1.2 Units/d

18. Turbulent heat loss is the heat transferred up away from the surface by
convection and storm winds
Turbulent heat loss=   5 units   Schneider&Londer, 1984
However, the value used was selected in order to balance heat flows to
the surface storage. Equals items (15,16,17) minus items (20,21)=
                    5.7 units/d

19. Surface radiation is the total energy emitted by the earth's surface in
radiant form.   114 Units/d Schneider&Londer, 1984

20. Calibrated as a balance between evaporation and dew, equal to item 17.
                    1.2 Units/d
To fully specify constants for the exponential equation, two corresponding
pairs of values must be known for temperature and vapor production.
In addition to the calibration condition, the rate of change of vapor
production was assumed to equal the rate of change of equilibrium vapor
pressure according to the First Latent Heat Equation.
$de/dT = L/[T*(Av-Al)]$, where: e= vapor pressure; T=temperature;

L=latent heat of fusion=	2.50E+06 J/kg	Wallace&Hobbs, 1977
Al=spec. volume wtr=	0.001 m^3/kg	Wallace&Hobbs, 1977
Av=spec volume vapor=	78.1 m^3/kg	Wallace&Hobbs, 1977
Then de/dT=2.5	111.1 Pa/°K	calculated

Notes to Appendix Table A-11--continued

    Sat. vapor pressure=   1700 Pa   Wallace&Hobbs, 1977
    So change in saturation vapor pressure per degree is   7%
    and this is also the assumed change in vapor production per degree.
    Equation for vapor production: $J8=k8*W*Rs*exp(KTs)$
    manipulating the above equation gives: $K=-\ln(1-\text{percent growth})$
        Equals   6.76E-02
    Now the other coefficients can be found by the normal method.

21. Cloud formation is all the water that goes into clouds per day.
    Cloud turnover time=   30 min   Wallace and Hobbs, 1977
    Water in clouds=   55 E15g   Item 10
    production=storage/turnover time=   2692.8 E15g/d
        Rounding: 2690 E15g/d

22. Cloud evaporation= formation - precipitation (item 20 - item 24)
         1290 E15g/d

23. Atmospheric radiation is the total heat radiated by the atmosphere.
        161 Units/d   Schneider&Londer, 1984

24. Total precipitation is that falling on oceans plus that falling on land.
    Equals total evaporation-condensation   See items 25 and 26
         1400 E15g/d

25. Condensed vapor is that settling out as surface condensation.
    Average mid latitude condensation:
         0.15 mm/d   Miller, 1977
    0.15 mm/day / 1e6 mm/km * 510E6 km^2 * 1E15g/km^3=
         76.5 e15 g/day
        Rounding: 75 E15g/day

26. i. Ocean evaporation=   4.23E+05 km^3/yr   Berner&Berner, 1987
         4.56E+05 km^3/yr   Dobrovolsky, 1994
    (4.23e5 km^3/yr)*(1e9m^3/km^3)*(1000g/m^3)/(365d/yr)*(1000g/kg)=
        1159 e15 g/ or approximating: 1200 e15g/yr
    These estimates often aggregate dew estimated in item 25 to be 75E15g/d
    Adding this in, 1200+75=   1275 E15g/d
    ii. Evapotranspiration=   7.30E+04 km^3/yr Berner&Berner, 1987
    (7.3e4 km^3/yr)*(1E9m^3/km^3)*(1000kg/m^3)/(365d/yr)*(1000g/kg)=
        200 E15g/d
    Then total evaporation = 1275 + 200 =   1475 E15g/d

27. Heat into storms is the total latent and sensible heat transported to upper
    air by storm activity, equal to latent (item 32 plus turbulent heat (item 18).
    Latent heat =cloud formation (item 21) * heat of vaporization (2500J/g)=
        6.73E+21 J/d
        or: 44.6 Units/d
    Plus turbulent heat (item 18)   5.7 Units/d

Notes to Appendix Table A-11--continued

Summing:		50.4 Units/d

28. Vapor greenhouse trapping is the absorption of longwave radiation by
    water vapor, here assumed to be all non-cloud absorption.

Avg. total absorption=	109 units	Schneider&Londer, 1984
Clear sky absorption=	265 W/m^2	Kiehl&Trenberth, 1997
Total energy input=	342 W/m^2	Kiehl&Trenberth, 1997

Standard Units defined as percent of total: 342/265*100=

		77 Units/d

29. Cloud absorption is the average total minus clear sky

		31.51 Units/d
Rounding:		32

30. Latent heat of cloud evaporation is that heat absorbed from the
    atmosphere due to cloud evaporation.

Cloud evaporation (item 22) * (2500J/g)=	3.23E+21 J
or:	21.4 Units/d

31. Cloud radiation to sky is the upward emitted radiant heat by clouds.

	65 Units/d	Schneider&Londer, 1984

32. Total latent heat of evaporation is the energy absorbed by evaporated
    water. Equals evaporation amount (item 26) * heat of vapor. (2500 J/g)

= 3.6875E+21 J/d, or		24.5 Units/d

    The portion directly contributed by insolation is the difference between
    total latent heat and the surface heat contribution (item 20)

		23.3 Units/d

33. Storm heat dispersal is the non-radiative dispersal of concentrated heat of
    storms mostly by physical tranport of winds etc.
    By balancing the inflows and outflows we get dispersal is turbulent and
    latent heat additions (item 27) plus greenhouse catching of clouds (item
    28) minus latent heat removal (item 30)=   61 Units/d

Appendix Table A-12. Calibration values of sources, storages, and flows for Coal2a, the model in Figure 4-33, with the calculated coefficients.

Item	Description	Symbol or Equation	Value	Units	Coeff.	Values
Sources						
1.	Natural yield	J0=	30	E15g/yr		
Storages						
2.	Coal resources	C=	5700	E15g		
3.	Coal mines	S=	6	E15g		
4.	Economic assets	E=	215	E15g		
Remainders						
5.	Unused yield	R=	2.1	E15g/yr		
6.	Unused coal	R2=	0.8	E15g/yr		
Flows						
7.	Tapped yield	J1=k1RR2E=	27.9	E15g/yr	k1=	7.72E-02
8.	Asset building	J2=k2RR2E=	4.8	E15g/yr	k2=	1.33E-02
9.	Asset decay	J3=k3E=	4.25	E15g/yr	k3=	1.98E-02
10.	Coal flow	J5=k5SC=	2.3	E15g/yr	k5=	6.73E-05
11.	Mine building	J6=k6RR2E=	1	E15g/yr	k6=	2.77E-03
12.	Mine decay	J7=k7S=	0.5	E15g/yr	k7=	8.33E-02
13.	Mine use	J8=k8SC=	0.5	E15g/yr	k8=	1.46E-05
14.	Coal flow	J9=k9SC=	2.3	E15g/yr	k9=	6.73E-05
15.	Coal consumption	J10=k10RR2E=	1.5	E15g/yr	k10=	4.15E-03

Notes to Appendix Table A-12

General: Items 3, 5, 6, 7, 10-14 : calibration values were adjusted so simulation matched historical trends.

1. Total plant growth = 130E15 g/yr (Dobrovolsky, 1994). Assuming 25% is used by the economic system then 0.25*130 $\sim=$
   30 E15g/yr

2. Total coal resources = 150,000 Quads (Fulkerson et al, 1990). Converting, 150,000 Quads *1.054E18 J/Quad / 27600 J/g $\sim=$
   5700 E15g

4. Present day industrial structure $\sim=$ 622E15g (See Table AS8, item 13). Then coal economy may be about a third that value $\sim=$
   215 E15g

8. With approximately 10% growth occurring, this will be 4.25*1.1=
   4.8 E15g/yr

9. Turnover time of economic structure assumed to be 50 years. Then 215/50 $\sim=$
   4.25 E15g/yr

15. Coal consumption in year 1925 (Clark, 1991) $\sim=$ 1.5 E15g/yr

Appendix Table A-13. Calibration values of sources, storages, and flows in Oiluse3, the model in Figure 4-38, with the calculated coefficients.

Item	Description	Symbol or Equation	Value	Units	Coeff.	Value
Sources						
1.	Natural yield	J0	30	E15g/yr		
Storages						
2.	Petro resources	O	318	E15g		
3.	Wells	S	5.7	E15g		
4.	Economic assets	E	555	E15g		
Flows						
5.	Unused yield	R	12.3	E15g/yr		
6.	Unused petro	R2	1.3	E15g/yr		
7.	Tapped yield	J1=k1RR2E=	87.7	E15g/yr	k1=	9.88E-03
8.	Asset building	J2=k2RR2E=	26.3	E15g/yr	k2=	2.96E-03
9.	Asset decay	J3=k3E=	11.1	E15g/yr	k3=	2.00E-02
10.	Well building	J4=k4SO=	1.2	E15g/yr	k4=	6.62E-04
11.	Well decay	J5=k5RR2E=	0.57	E15g/yr	k5=	6.42E-05
12.	Well use	J6=k6S=	0.52	E15g/yr	k6=	9.12E-02
13.	Petro flow	J7=k7SO=	6.25	E15g/yr	k7=	3.45E-03
14.	Petro flow	J8=k9SO=	6.25	E15g/yr	k8=	3.45E-03
15.	Petro consumption	J9=k9RR2E=	5	E15g/yr	k9=	5.63E-04

Notes to Appendix Table A-13

General: Items 3, 5, 6, 7, 10-14 : calibration values were adjusted so simulation matched historical trends.

1. Total plant growth = 130E15 g/yr (Dobrovolsky, 1994). Assuming 25% is used by the economic system then 0.25*130 ~=
   30 E15g/yr

2. Total petroleum resources = Crude Oil plus Natural Gas. Crude+Gas=1464E9 bbl (Masters et al, 1992) *140E3g/bbl + 6950E12 ft^3 (Cassedy, 1992) *20g/ft^3 ~= 318 E15g

4. Present day industrial structure ~= 622E15g (See Table AS8, item 13). For year 1990, estimate slightly less ~= 215 E15g

8. With approximately 3% growth occurring, and less losses in item 9:
   26.3 E15g/yr

9. Turnover time of economic structure assumed to be 50 years. Then 555/50 ~= 11.1 E15g/yr

15. Oil consumption in year 1990 (Energy Info. Admin., 1992) ~=
    5 E15g/yr

Appendix Table A-14. Calibration values of sources, storages, and flows in Coaloil, the model in Figure 4-41, with the calculated coefficients.

Item	Description	Symbol or Equation	Value Units	Coeff. Value
Sources				
1.	Natural sources	J0	1 Std/yr	
Storages				
2.	Natural assets	A	3720 E15g	
3.	Coal resources	C	5610 E15g	
4.	Petro resources	O	340 E15g	
5.	Coal mines	Sc	11.6 E15g	
6.	Oil wells	So	4.35 E15g	
7.	Economic assets	E	610 E15g	
Remainders				
8.	Unused natr. src.	R	0.076 Std/yr	
9.	Unused yield	R1	0.17 E15g/yr	
10.	Unused petro	R2	0.6 E15g/yr	
11.	Unused coal	R3	1.2 E15g/yr	
Flows				
12.	Nat src. to ecosys	J1=k1RA=	0.07 Std/yr	k1= 2.48E-04
13.	Nat src. to agric	J2=k2RAE=	0.85 Std/yr	k2= 4.93E-06
14.	Nat asset building	J3=k3RA=	160 E15g/yr	k3= 5.66E-01
15.	Agric. asset build	J4=k4RAE=	575 E15g/yr	k4= 3.33E-03
16.	Nat. asset decay	J5=k5A=	745 E15g/yr	k5= 2.00E-01
17.	Ecosys yield	J6=k6RA=	3.6 E15g/yr	k6= 7.33E+00
18.	Agric. yield	J7=k7RAE=	85 E15g/yr	k7= 4.93E-04
19.	Tapped yield: oil	J8=k8R1R2E=	13.6 E15g/yr	k8= 2.19E-01
20.	Tapped yield: coal	J9=k9R1R3E=	75 E15g/yr	k9= 6.03E-01
21.	Oil econ. build	J10=k10R1R2E=	36 E15g/yr	k10= 5.79E-01
22.	Coal econ. build	J11=k1R1R3E=	2.5 E15g/yr	k11= 2.01E-02
23.	Asset decay	J12=k12E=	24 E15g/yr	k12= 3.93E-02
24.	Ecosys mgmt.	J13=k13RAE=	0.88 E15g/yr	k13= 5.10E-06
25.	Well building	J14=k14R1R2E=	0.83 E15g/yr	k14= 1.33E-02
26.	Well decay	J15=k15So=	0.54 E15g/yr	k15= 1.24E-01
27.	Well Use	J16=k16OSo=	0.24 E15g/yr	k16= 1.62E-04
28.	Mine build	J17=k17R1R3E=	5.25 E15g/yr	k17= 4.22E-02
29.	Mine decay	J18=k18Sc=	2.5 E15g/yr	k18= 2.16E-01
30.	Mine Use	J19=k19CSc=	2.6 E15g/yr	k19= 4.00E-05
31.	Coal flow	J20=k20CSc=	5.23 E15g/yr	k20= 8.04E-05
32.	Petro flow	J21=k21OSo=	5.64 E15g/yr	k21= 3.81E-03
33.	Coal flow	J22=k22CSc=	4.75 E15g/yr	k22= 7.30E-05

Appendix Table A-14--continued

Item	Description	Symbol or Equation	Value Units	Coeff. Value
34.	Petro flow	J23=k23OSo=	5.64 E15g/yr	k23= 3.81E-03
35.	Coal consumption	J24=k24R1R3E=	3.57 E15g/yr	k24= 2.87E-02
36.	Petro consumption	J25=k25R1R2E=	5.05 E15g/yr	k25= 8.12E-02

Notes to Appendix Table A-14

General: Items 1, 5, 6, 8-15, 17-22, 24-34 : calibration values were adjusted so simulation matched historical trends.

2. Natural assets: total biomass dry wt. is presently 1880E15g (Dobrovolsky, 1990) Assuming dry wt fraction is half then 1880/0.5~= 3720 E15g/yr

3. Total coal resources = 150,000 Quads (Fulkerson et al, 1990). Converting, 150,000 Quads *1.054E18 J/Quad / 27600 J/g ~= 5610 E15g

4. Total petroleum resources = Crude Oil plus Natural Gas. Crude+Gas=1464E9 bbl (Masters et al, 1992) *140E3g/bbl + 6950E12 ft^3 (Cassedy, 1992) *20g/ft^3 ~= 340 E15g

7. Present day industrial structure ~= 610E15g (See Table AS8, item 13). 610 E15g

16. Assume about a 5 yr. turnover time for biomass, compared to 15 years given by Dobrovolsky. Then decay~= 745 E15g/yr

23. Turnover time of economic structure assumed to be 25 years. Then 215/25 ~= 24 E15g/yr

35. Coal consumption in year 1990 (Energy Info. Admin., 1991) ~= 3.6 E15g/yr

36. Oil consumption in year 1990 (Energy Info. Admin., 1992) ~= 5 E15g/yr

Appendix Table A-15. Calibration values for sources, storages, and flows for Pulse 2.0, the model in Figure 5-1, and the calculated coefficients.

Item Description	Symbol/Equation	Value	Units	Coefficient	Value
Sources					Turn. time
1. Energy Flow	S	10000	J		3
2. Leftover Energy	R	2000	J		6.67
Storages					
3. Producer	A	8000	J		
4. Consumer	B	100	J		
Flows					
5. Tapped energy	J0=k0*R*A	8000	J/yr	k0=	0.0005
6. Production	J1=k1*R*A	1600	J/yr	k1=	0.0001
7. Decay	J2=k2*A	100	J/yr	k2=	0.333
8. Consumption	J3=K3*A*B*B	48	J/yr	k3=	0.0000006
9. Growth	J4=k4*A*B*B	32	J/yr	k4=	0.0000004
10. Decay	J5=k5*B	10	J/yr	k5=	0.15
11. Linear feed	J6=k6*A	8	J/yr	k6=	0.001

Appendix Table A-16. Calibration values for sources , storages, and flows for Pulse 3.01, the model in Figure 5-5, and the calculated coefficients.

Item Description	Symbol/Equation	Value	Units		Coefficient Value
Sources					
1. Energy flow	S	10000	J		
2. Leftover energy	R	2000	J		
Storages					**Turn. time**
3. Producer	A	8000	J		3
4. Consumer	B	100	J		6.67
5. 2nd consumer	C	10			142.8
Flows					
6. Tapped energy	J0=k0*R*A	8000	J/yr	k1=	0.0005
7. Production	J1=k1*R*A	1600	J/yr	k2=	0.0001
8. Decay	J2=k2*A	2667	J/yr	k3=	0.33333333
9. Consumption	J3=K3*A*B*B	64	J/yr	k4=	0.0000008
10. Growth	J4=k4*A*B*B	32	J/yr	k5=	0.0000004
11. Decay	J5=k5*B	15	J/yr	k6=	0.15
12. Linear feed	J6=k6*A	8	J/yr	k7=	0.001
13. Linear feed	J7=k7*B	0.006	J/yr	k8=	0.00006
14. Consumption	J8=k8*B*C*C	0.05	J/yr	k9=	0.000005
15. Growth	J9=k9*B*C*C	0.02	J/yr	k10=	0.000002
16. Decay	J10=k10*C	0.07	J/yr	k11=	0.0070028

Appendix Table A-17. Calibration values for sources, storages, and flows for Pulse 3.1, the model in Figure 5-9, and the calculated coefficients.

Item	Description	Symbol/Equation	Value	Units	Coefficient Value	
Sources						
1.	Energy flow	S	10000	J		
2.	Leftover energy	R	2000	J		
Storages					**Turn. time**	
3.	Producer	A	8000	J		3
4.	Consumer	B	100	J		6.67
5.	2nd consumer	C	10	J		142.8
6.	Slow Storage	M	10000	J		
Flows						
7.	Tapped energy	J0=k0*R*A	8000	J/yr	k0=	0.0005
8.	Production	J1=k1*R*A	1600	J/yr	k1=	0.0001
9.	Decay	J2=k2*A	2667	J/yr	k2=	0.33333333
10.	Consumption	J3=K3*A*B*B	64	J/yr	k3=	0.0000008
11.	Growth	J4=k4*A*B*B	32	J/yr	k4=	0.0000004
12.	Decay	J5=k5*B	15	J/yr	k5=	0.15
13.	Linear feed	J6=k6*A	8	J/yr	k6=	0.001
14.	Slow buildup	J7=k7*R*A	12.8	J/yr	k7=	0.0000008
15.	Linear feed	J8=k8*B	0.004	J/yr	k8=	0.00004
16.	Consumption of B	J9=k9*B*C*C*M	0.8	J/yr	k9=	8E-09
17.	Growth	J10=k10*B*C*C*M	0.6	J/yr	k10=	6E-09
18.	Consumption of M	J11=k11*B*C*C*M	50	J/yr	k11=	0.0000005
19.	Decay	J12=k12*C	0.2	J/yr	k12=	0.02
20.	Decay	J13=k13*M	2.5	J/yr	k13=	0.00025

Appendix Table A-18. Calibration values for sources, storages, and flows for Pulse 4.0, the model in Figure 5-13, and the calculated coefficients.

Item	Description	Symbol/Equation	Value	Units	Coefficient	Value
Sources						
1.	Energy flow	S	10000	J		
2.	Leftover energy	R	2000	J		
Storages						**Turn. time**
3.	Producer	A	8000	J		3
4.	1st consumer	B	100	J		6.67
5.	2nd consumer	C	10	J		200.00
6.	3rd consumer	D	1	J		500.00
Flows						
7.	Tapped energy	J0=k0*R*A=	8000	J/yr	k0=	0.0005
8.	Production	J1=k1*R*A=	1600	J/yr	k1=	0.0001
9.	Decay	J2=k2*A=	2667	J/yr	k2=	0.333
10.	Consumption	J3=K3*A*B*B=	64	J/yr	k3=	0.0000008
11.	Growth	J4=k4*A*B*B=	32	J/yr	k4=	0.0000004
12.	Decay	J5=k5*B=	15	J/yr	k5=	0.15
13.	Linear feed	J6=k6*A=	8	J/yr	k6=	0.001
14.	Linear feed	J7=k7*B=	0.008	J/yr	k7=	0.00008
15.	Consumption	J8=k8*B*C*C=	0.05	J/yr	k8=	0.000005
16.	Growth	J9=k9*B*C*C=	0.02	J/yr	k9=	0.000002
17.	Decay	J10=k10*C=	0.05	J/yr	k10=	0.005
18.	Linear feed	J11=k11*C=	4E-04	J/yr	k11=	0.00004
19.	Consumption	J12=k12*C*D*D=	6E-04	J/yr	k12=	0.00006
20.	Growth	J13=k13*C*D*D=	3E-04	J/yr	k13=	0.00003
21.	Decay	J14=k14*D=	0.002	J/yr	k14=	0.002

Appendix Table A-19. Calibration values for sources , storages, and flows for the model in Figure 5-16, and the calculated coefficients.
Case1- Q=50% of T; case2- Q=75% of T

Item Description	Symbol/Equation	Value	Units	Coefficient	Value
CASE 1					
Sources					
1. Flow source	E	100	J/yr		
2. Pulse energy	Z	N/A			
Storages					
3. Raw material	D	50	g		
4. Product	Q	50	g		
Flows					
5. Unused energy	R	40	J/yr		
6. Power draw	J0=k0*R*D*Q	60	J/yr	k0=	6.00E-04
7. Production	J1=k1*R*D*Q	40	g/yr	k1=	4.00E-04
8. Recycle	J2=k2*Q	40	g/yr	k2=	8.00E-01
9. Uptake	J3=k3*R*D*Q	40	g/yr	k3=	4.00E-04
CASE 2					
Sources					
1. Flow source	E	100	J/yr		
2. Pulse energy	Z	N/A			
Storages					
3. Raw material	D	25	g		
4. Product	Q	75	g		
Flows					
5. Unused energy	R	40	J/yr		
6. Power draw	J0=k0*R*D*Q	60	J/yr	k0=	8.00E-04
7. Production	J1=k1*R*D*Q	40	g/yr	k1=	5.33E-04
8. Recycle	J2=k2*Q	40	g/yr	k2=	5.33E-01
9. Uptake	J3=k3*R*D*Q	40	g/yr	k3=	5.33E-04

Appendix Table A-20. Calibration values of storages, sources, and flows, and the calculated coefficients for the model of sedimentary pulsing in Figure 5-19.

Item	Description	Symbol or Equation	Value	Units	Coeff.	Value
Sources						
1.	Earth energies	D=	1	E30 sej/Ma		
Storages						
2.	Sediments	R=	2170	E21g		
3.	Uplifted sediments	L=	235	E21g		
4.	Mountains	M=	350	E21g		
Flows						
5.	Unused energies	R1=	0.2	E30 sej/Ma		
6.	Used energies	k0*R1*R*L=	0.8	E30 sej/Ma	k0=	7.84E-06
7.	Uplift	k1*R1*R*L=	10	E21g/Ma	k1=	9.80E-05
8.	Linear mtn build	k2*L=	0.5	E21g/Ma	k2=	2.13E-03
9.	Quad mtn build	k3*L*M*M=	11.2	E21g/Ma	k3=	3.89E-07
10.	Mtn erosion	k4*L=	13.2	E21g/Ma	k4=	3.77E-02
11.	Land erosion	k5*M=	3.5	E21g/Ma	k5=	1.00E-02

Notes to Table A-20.

1. Standardized to constant flow of 1 unit.   1 unit

2. Total sediments minus those uplifted on land.
   Total sediments=   2400 E21g   Dobrovolsky, 1994
   2400-230=   2170 E21g

3. Total sedimentary material above sea level, calculated as follows:
   Outcropping percentage of sedimentary rocks:
   Outcrop%sed: 66 %   Ronov, 1982
   Total land surface: 150 E6km^3   Dobrobolsky, 1994
   Mean land elev: 875 m   Ryabchikov, 1975
   Uplifted Seds= Outcrop%sed * Land area * mean elevation * density
   =66% * 150E6km^3 * 875m * 2.65kg/L * 1e6m^2/km^2 * 1000g/kg=
   230 E21g

4. Mountains: assuming mountains are any land above 1km in elevation, a hypsometric curve suggested percent of land surface is 8%, and average elevation of that land is 4.3km.
   (4.3-1)km *8% *510E6km^2 *2.65g/cm^3 *1E15cm^3/km^3 =
   357 E21g

5. Total energy not used in earth system, solar albedo is 30%, 0.2 used here.   0.2 unit

6. Used energies are those not lost to albedo in item 4.
   1-0.2=   0.8 unit

Notes to Appendix Table A-20--continued

7. Uplift= continental denudation in steady state, use pre-industrial value of Gregor, 1970   10 E21g/Ma

8. Linear mountain building representing the unreinforced contribution to mountains by land. Assume: 0.5 E21g/Ma

9. Quadratic mountain building representing the building of mountains in a process highly reinforced by their presence.
   Assume   11.2 E21g/Ma

10. Mountain erosion and land erosion combining to be larger than total land uplift in non steady-state condition. Assume total is about 17, and broken up into mostly mountain erosion because of their higher elevation.
   Mountain erosion=   13.2 E21g/Ma

11. Land erosion=   3.5 E21g/Ma

APPENDIX B
SIMULATION PROGRAM LISTINGS

This appendix contains the computer code used to simulate each of the models studied in this dissertation. All of the computer simulations used the QuickBasic® computer language, a compiled basic language that simulates faster than non-compiled versions. The simulations were carried out on IBM compatible microcomputers running DOS® version 6.22.

The symbols used as variables in these computer programs are those from the calibration tables of Appendix A, where sources were either constants or independently varying parameters, storages were the state variables calculated by difference equations, and flows were the "J" variables. In some of the shorter, simpler computer programs, the "J" flow variables appear only implicitly as terms in the difference equations for the storages.

Appendix Table B-1. Listing of computer simulation program for the hierarchical sedimentary cycle model in Figures 3-1 and 3-2.

```
10 ' ** PC Basic Simulation Program: Energy Circuit Model       **
20 ' ** Sedcycle: Overall Model of Sed. Cycle                   **
25 DEFDBL A-Z
30 CLS
40 SCREEN 9, 7: COLOR 7, 0
50 Xmax = 350: Ymax = 250    'Plot boundaries
60 Xoff = 25: Yoff = 25    'Plot offsets
70 LINE (Xoff, Yoff)-(Xoff + Xmax, Yoff + Ymax), 15, B
72 line (Xoff, Yoff+Ymax/3)-(Xoff+Xmax, Yoff+Ymax/3), 15
74 line (Xoff, Yoff+2*Ymax/3)-(Xoff+Xmax, Yoff+2*Ymax/3), 15
80 ' ** Next set the source constants                           **
90 G = 1
95 J = 1
96 O = 1322 'E21g
100 ' ** Next set the model coefficients                        **
102 k1 = 7.82e-4/(1800*20100)
103 k2 = .0265
104 k3 = 1.33e3/(1800*20100)
105 k4 = .339
106 k5 = 6.94e1
107 k6 = 9.72e-6
108 k7 = 7.58e-6
109 k8 = 6.39e-5
110 k9 = 0
111 k10 = 1.168e-2
112 k11 = 8.47e-5
113 k12 = 5.99E-11
114 k13 = 5.99E-11
115 k14 = 3.00e-13 '6.02E-09
116 k15 = 3.00e-13 '6.02E-09
117 k16 = 1.98e-8
118 k17 = 6.94e-6
119 k18 = 5.97e-13 '1.2e-8
150 ' ** Next set the time step                                 **
160 dt = .2' (million years)
170 ' ** Next set the plot scaling factors                      **
180 Sm = 620: Lm = 6000: Mm = 25000: Dmax = 80: Cm=24000
190 tm = 15000: totsedmax=12
200 ts = 0      'Starting year of simulation
210 ' ** Next set initial conditions                            **
220 S = 200 '600
222 L = 10 '1800
224 M = 1000 '20100
228 D = 10 '49.1
230 V = 300000 '415000
232 C = 1000 '5900
```

Appendix Table B-1--continued

```
234 R = .3
240 ' ** Start iterative loop here                                    **
250 X = t / tm * Xmax
255 totsed=k4*R*D +k11*C +k13*M*V +k15*L*V*M
260 PSET (X+Xoff, Yoff +2/3*Ymax -S/Sm*Ymax/3), 3   'Blue
270 PSET (X+Xoff, Yoff +1/3*Ymax -L/Lm*Ymax/3), 2   'Green
280 PSET (X+Xoff, Yoff +1/3*Ymax -M/Mm*Ymax/3), 4   'Red
282 PSET (X+Xoff, Yoff +2/3*Ymax -D/Dmax*Ymax/3), 1 'White
284 PSET (X+Xoff, Yoff +2/3*Ymax -C/Cm*Ymax/3), 6   'Brown
286 PSET (X+Xoff, Yoff +Ymax -totsed/totsedmax*Ymax/3), 15
290 R = J / (1 +k1*O*L*M +k2*D)
310 dS = k11*C +k4*R*D +k15*L*V*M +k13*M*V -k6*S*G*L
312 dL = k6*S*G*L +k17*S*G*L -k18*L*V*M -k14*L*V*M -k15*L*V*M
314 dM = k18*L*V*M -k16*M*M -k12*M*V -k13*M*V
316 dD = k12*M*V +k14*L*V*M -k4*R*D
318 dC = k5*G -k10*C*G -k11*C
320 L = L + dL * dt
322 M = M + dM * dt
326 S = S + dS * dt
330 D = D + dD * dt
335 C = C + dC * dt
340 t = t + dt
342 V = k3*R*O*L*M / (1 +k7*M +k8*L)
350 ' ** Repeat iteration if (t < tm)                                 **
360 IF t < tm GOTO 240
370 END
```

Appendix Table B-2. Listing of the computer program for simulating Bensed, the model in Figure 3-10.

```
10 '  ** PC Basic Simulation Program: Energy Circuit Model      **
30 '  ** Benard Earth Model, standard run                       **
40 CLS
50 SCREEN 9, 7: COLOR 7, 0
60 Xmax = 300: Ymax = 150   'Plot boundaries
70 Xoff = 25: Yoff = 25     'Plot offsets
90 LINE (Xoff, Yoff)-(Xoff + Xmax, Yoff + Ymax), , B
110 LINE (Xoff, Yoff + Ymax / 3)-(Xoff + Xmax, Yoff + Ymax / 3)
120 LINE (Xoff, Yoff + 2 * Ymax / 3)-(Xoff + Xmax, Yoff + 2 * Ymax / 3)
140 'LINE (Xoff + 1/2 * Xmax, Yoff + Ymax)-(Xoff + 1/2 * Xmax, Yoff + Ymax + 5)
150 'LINE (Xoff + 1/4 * Xmax, Yoff + Ymax)-(Xoff + 1/4 * Xmax, Yoff + Ymax + 5)
160 'LINE (Xoff + 3/4 * Xmax, Yoff + Ymax)-(Xoff + 3/4 * Xmax, Yoff + Ymax + 5)
170 '  ** Next set the source constants                         **
180 I = 5.6: H = 1
190 '** Next set the model coefficients                         **
199 k0 = .0017
200 k1 = .00231
203 k4 = 1.54E-04
207 k8 = 1.21e-3
208 k9 = 9.26e-6
209 k10 = 2.8e-5
210 k11 = 1.67e-5
211 k12 = 2.49e-7
213 k14 = 3.98e-4
214 k15 = 7.01e-5
240 '  ** Next set the time step                                **
250 dt = .5' (Ma)
260 '  ** Next set the plot scaling factors                     **
280 Sm = 1000: Cm = 30000: Mm = 15000
290 tm = 5000      'Time scale in million years
300 Ts = 0         'Starting year of simulation
305 t=0
310 '  ** Next set initial conditions for the model             **
320 S = 200: C = 2000: M = 500: W = 1350
380 ' ** Start iterated calculations here                       **
394 R = I / (1 + k0 * W)
395 Rr = k1*W*R / (1 + k4 * M)
398 Re = k4 * Rr * M / (1 + k10 * C)
401 J1 = k1 * R * W
404 J4 = k4 * Rr * M
408 J8 = k8 * Rr * M
409 J9 = k9 * S * H * M
410 J10 = k10 * Re * C
411 J11 = k11 * S * H * M
412 J12 = k12 * M * H * C
414 J14 = k14 * C
```

Appendix Table B-2--continued

```
415 J15 = k15 * Re * C
450 ' ** Next plot points to the screen                                    **
460 X = t / tm * Xmax
470 PSET (X + Xoff, Yoff + Ymax / 3 - S / Sm * Ymax / 3), 15' ** top
480 PSET (X + Xoff, Yoff + 2 / 3 * Ymax - M / Mm * Ymax / 3), 15' ** mid
490 PSET (X + Xoff, Yoff + Ymax - C / Cm * Ymax / 3), 15' ** bottom
600 ' ** Next update state variables, and increment time                   **
610 dC = J12 - J14 - J15
620 dM = J11 - J12 - J8
630 dS = J8 + J15 - J9
650 C = C + dC * dt: M = M + dM * dt
660 S = S + dS * dt
670 t = t + dt
680 ' ** Next repeat iteration if t < to                                   **
690 IF t < tm GOTO 380
700 END
```

Appendix Table B-3. Listing of the computer program for simulating Cogwheel, the model in Figure 3-13

```
10 ' ** PC Basic Simulation Program: Energy Circuit Model          **
20 ' **     model of cogwheel earth                                **
30 ' **
40 CLS
50 SCREEN 9, 7: COLOR 7, 0
60 Xmax = 300: Ymax = 200    'Plot boundaries
70 Xoff = 25: Yoff = 25      'Plot offsets
80 ' ** Next draw a box on the screen                              **
90 LINE (Xoff, Yoff)-(Xoff + Xmax, Yoff + Ymax),15 , B
100 ' ** Next separate the box into three parts                    **
110 LINE (Xoff, Yoff + Ymax / 3)-(Xoff + Xmax, Yoff + Ymax / 3),15
120 LINE (Xoff, Yoff + 2 * Ymax / 3)-(Xoff + Xmax, Yoff + 2 * Ymax / 3),15
170 ' ** Next set the source constants                             **
180 I0 = 526
182 Hr = 6.72
183 MT = 0
190 ' ** Next set the model coefficients                           **
200 k1 = 1.18e-3
210 k2 = 1.06e-4
220 k3 = 1.77e-5
230 k4 = 4.67e-4
232 k5 = 1.19e-4
233 k6 = 7.75e-5
234 k7 = 1
235 k8 = 2.34e-5
236 k9 = 1.48e-5
240 ' ** The following line sets the time step                     **
250 dt = .01' (million years)
260 ' ** Next set the plot scaling factors     **
280 Mm = 15: Dmax = 15000: Gm = 100: Sm=15: Hm=120
290 tm = 50     'Time scale in million years
300 ts = 0      'Starting year of simulation
310 ' ** Next set initial conditions for the storages             **
320 M=7.9: D=10600: G=31.5: S=7.2: H=53.2
330 R=415
380 ' ** Next do iterated calculations until  (t = tm)            **
400 R = I0 / (1 +k1*G*S)
410 J1 = k1*R*G*S)
420 J2 = k2*R*G*S
430 J3 = k3*D*H
440 J4 = k4*R*G*S
441 J5 = k5*M*D
442 J6 = k6*M*D
443 J7 = k7*Hr
444 J8 = k8*D*H
446 J9 = k9*R*G*S*S
```

Appendix Table B-3--continued

```
450 ' ** Next lines plot points to the screen                    **
460 X = t / tm * Xmax
470 PSET (X+Xoff, Yoff+Ymax/3 - S/Sm*Ymax/3), 2' ** top
480 PSET (X+Xoff, Yoff+1/3*Ymax - G/Gm*Ymax/3), 2' ** top
490 PSET (X+Xoff, Yoff+2/3*Ymax - M/Mm*Ymax/3), 2' ** mid
500 PSET (X+Xoff, Yoff+2/3*Ymax - D/Dmax*Ymax/3), 3' **mid
510 PSET (X+Xoff, Yoff+Ymax - H/Hm*Ymax/3),2 ' ** btm
600 ' ** Next update state variables, and increment time         **
610 dM = J9-J5
615 dD = J5-J3
620 dG = J3-J2
621 dS = J2-J9
622 dH = J6+J7-J8
650 M = M + dM*dt
652 D = D + dD*dt
654 G = G + dG*dt
656 S = S + dS*dt
660 H = H + dH*dt
670 t = t + dt
680 ' ** Next repeat loop if (t < tm)                            **
690 IF t < tm GOTO 400
700 END
```

Appendix Table B-4. Listing of computer program for simulating the model in Figure 3-18.

```
10 ' ** PC Basic Simulation Program: Energy Circuit Model        **
20 ' ** Sedimentary cycle and the global economy                 **
30 ' ** Short term simulation                                     **
40 CLS
50 SCREEN 9, 7: COLOR 7, 0
60 Xmax = 250: Ymax = 200    'Plot boundaries
70 Xoff = 25: Yoff = 25      'Plot offsets
80 ' ** Next draw a 4-part box on the screen                      **
90 LINE (Xoff, Yoff)-(Xoff + Xmax, Yoff + Ymax), , B
100 ' ** Next separate the box into three parts                   **
110 LINE (Xoff - 5, Yoff + Ymax / 3)-(Xoff + Xmax + 5, Yoff + Ymax / 3)
120 LINE (Xoff - 5, Yoff + 2 * Ymax / 3)-(Xoff + Xmax + 5, Yoff + 2 * Ymax / 3)
170 ' ** Next line sets the source constants                      **
180 So = 4: Sl = 1.64
185 Rl = 111000
188 G = 1
190 ' ** Next set the model coefficients                          **
200 k1 = 9.03E-14
210 k2 = 1.01E-16
220 k3 = 4.78E-08
230 k4 = .000132
240 k5 = 1.88E-06
250 k6 = 1.88E-06
260 k7 = 32
270 k8 = 1.29:          c8 = .537
280 k9 = 1.35E-11:      c9 = 1.06
290 k10 = 7.08e-15:     c10 = 10.425
300 k11 = .0688:        c11 = .237
310 k12 = .0000592:     c12 = .04
320 k13 = 9.42E-13:     c13 = 0 'was 1.48E-16
330 k14 = 3.95E-07:     c14 = .295
340 k15 = .00272:       c15 = .124
350 k16 = 0:            c16 = .000129
360 k17 = .0362:        c17 = .643
370 k18 = 5.32E-9:      c18 = .219
380 k19 = 1.02E-11:     c19 = .0000397
390 k20 = 4.71E-10:     c20 = .0000723
400 k21 = .1832:        c21 = .00197
410 k22 = 1.02E-08:     c22 = .458
420 k23 = 1.075e-3:     c23 = .981
430 k24 = 3.57E-13
440 k25 = 2.2558E-15
445 k26 = 1.21E-15
447 k27 = .6154
450 ' ** Next set time step and scales                            **
460 dt = .01' (years)
```

Appendix Table B-4--continued

```
480 Sm = 250000: Wm = 200000: J14m = 30: J12m = 30
490 Bm = 3000: Msm = 200
500 Om = 505: Cm = 6000: Rm = 1:    Ym = 100
510 Em = 1050: I22m = 7.5: I23m = 7.5: Ecm = 15: Eom = 15
520 tm = 400      'Time scale in years
530 ts = 1850     'Starting year of simulation
540 ' ** Next lines set initial conditions for the model        **
550 R1 = .49: R2 = 1.19: R3 = 5000
555 Ry = .03: Ro = .6: Rc = 1.2: Rl = 111000
560 O = 505: C = 6000: E = 15: Ec = 0.1: Eo = 0
570 B = 2500: S = 160000: W = 65000: Bo = 3.4
580 Md = 49300000: Ms = 25
590 ' ** Next lines plot X scale information        **
600 LOCATE 2 + INT((Yoff + Ymax) / 14), (Xmax + Xoff) / 8 - 4
610   PRINT (ts + tm)
620 LOCATE 2 + INT((Yoff + Ymax) / 14), (Xmax + Xoff) / 16 - 2
630   PRINT "Year"
640 LOCATE 2 + INT((Yoff + Ymax) / 14), 2 + INT(Xoff / 8)
650   PRINT ts
651
652 ' ** Next iterate calculations until t=tm        **
660 '** Initiate fossil growth at appropriate timein lieu of information tank    **
670 Flag = 0
680 IF ((t + ts) > 1920) THEN
690   IF Oilflag = 0 THEN
700     Eo = .075: 'IF E < 20 THEN E = 20
710     Oilflag = 1
720   END IF
730 ELSE
740   Eo = 0
750 END IF
760 IF ((t + ts) > 1870) THEN
770   IF Coalflag = 0 THEN
780     Ec = .05: 'IF E < .015 THEN E = .015
790     Coalflag = 1
800   END IF
810 ELSE
820   Ec = 0
830 END IF
860 R1 = Sl / (1 + k1 * W * S * B + k2 * W * S * B * E)
870 R2 = So / (1 + k3 * Md)
880 R3 = Rl / (1 + k4 * S)
890 J1 = k1 * R1 * W * S * B
900 J2 = k2 * R1 * W * S * B * E
910 J3 = k3 * R2 * Md
920 J4 = k4 * R3 * S
930 J5 = k5 * R2 * Md
```

Appendix Table B-4--continued

```
940 J6 = k6 * R2 * Md
950 J7 = k7 * Bo
960 J8 = k8 * Bo
970 J9 = k9 * R1 * W * S * B
980 J10 = k10 * R1 * W * S * B * E
990 J11 = k11 * B
1000 J12 = k12 * G * S
1010 J13 = k13 * R1 * W * S * B
1020 J14 = k14 * S * W * EXP(-k15 * B)
1030 J15 = 0
1040 J16 = k16 * E
1050 J17 = k17 * E
1060 J18 = k18 * R1 * W * S * B
1070 J19 = k19 * R1 * W * S * B * E
1080 J20 = k20 * S * W
1090 J21 = k21 * Ms
1110 J22 = k22 * Md
1120 J23 = k23 * S
1130 J24 = k24 * R1 * W * S * B
1140 J25 = k25 * R1 * W * S * B * E
1145 J26 = k26 * R1 * W * S * B * E
1147 J27 = k27 * W
1150 Y = J24 + J25
1160 Ry = Y / (1 + c8 * Ro * E + c9 * Rc * E)
1170 I8 = c8 * Ry * Ro * E
1180 I9 = c9 * Ry * Rc * E
1190 I10 = c10 * Ry * Ro * E
1200 I11 = c11 * Ry * Rc * E
1210 I12 = c12 * E
1220 I13 = c13 * R1 * S * W * B * E
1230 I14 = c14 * Ry * Ro * E
1240 I15 = c15 * Eo
1250 I16 = c16 * O * Eo
1260 I17 = c17 * Ry * Rc * E
1270 I18 = c18 * Ec
1280 I19 = c19 * C * Ec
1290 I20 = c20 * C * Ec
1300 I21 = c21 * O * Eo
1310 I22 = c22 * Ry * Rc * E
1320 I23 = c23 * Ry * Ro * E
1350 Ro = I21 / (1 + c23 * Ry * E)
1360 Rc = I20 / (1 + c22 * Ry * E)
1370 ' ** Next plot points to the screen                    **
1375 Ert=J14+J20 'Total erosion
1380 X = t / tm * Xmax
1390 PSET (X + Xoff, Yoff + Ymax / 3 - I22 / I22m * Ymax / 3)
1400 PSET (X + Xoff, Yoff + Ymax / 3 - I23 / I23m * Ymax / 3)
```

Appendix Table B-4--continued

```
1405 PSET (X + Xoff, Yoff + Ymax / 3 - E / Em * Ymax / 3)
1410 PSET (X + Xoff, Yoff + 2 / 3 * Ymax - B / Bm * Ymax / 3)
1420 PSET (X + Xoff, Yoff + 2 / 3 * Ymax - S / Sm * Ymax / 3)
1425 PSET (X + Xoff, Yoff + 2 / 3 * Ymax - W / Wm * Ymax / 3)
1430 PSET (X + Xoff, Yoff + Ymax - Ert / J14m * Ymax / 3)
1440 'PSET (X + Xoff, Yoff + Ymax - Ms / Msm * Ymax / 3)
1450 PSET (X + Xoff, Yoff + Ymax - J12 / J12m * Ymax / 3)

1540 ' ** Next update state variables, and increment time  **
1550 dB = J9 + J10 - J11: dBo = J6 - J7 - J8
1560 dMs = J14 - J21: dMd = J16 + J7 + J20 - J5 - J22
1570 dW = J4 - J27 - J18 - J19
1580 dS = J11 + J12 + J17 - J13 - J14 - J20 - J23 - J26
1590 B = B + dB * dt: Bo = Bo + dBo * dt
1600 Ms = Ms + dMs * dt: Md = Md + dMd * dt
1610 W = W + dW * dt: S = S + dS * dt
1620 dOil = -I21 '** "dO" is not allowed--BASIC keyword**
1630 dC = -I20
1640 dE = I10 + I11 - I12
1650 dEc = I17 - I18 - I19
1660 dEo = I14 - I15 - I16
1680 O = O + dOil * dt
1690 C = C + dC * dt
1700 Ec = Ec + dEc * dt
1710 Eo = Eo + dEo * dt
1720 E = E + dE * dt
1730 t = t + dt
1740 IF E < 15 THEN E = 15
1750 ' ** next  repeat iteration if (t < tm)                              **
1760 IF t < tm GOTO 680
1770 END
```

Appendix Table B-5. Listing of the computer program for simulating Hydro1.1, the model in Figure 4-3.

```
10 ' ** PC Basic Simulation Program: Energy Circuit Model        **
20 ' ** Generic Convectional Hydrology Model HYDRO 1.1           **
41 SCREEN 9, 7: COLOR 7, 0
42 Xmax = 500: Ymax = 300'Plot box size on screen
43 Xoff = 50' space on left of plot
45 ' ** Draw a divided box on the screen                         **
50 LINE (Xoff, 0)-(Xmax + Xoff, Ymax), 7, B
70 LINE (Xoff, Ymax / 2)-(Xmax + Xoff, Ymax / 2), 7
90 ' ** Next set source constants and coefficients               **
100 M = 1
110 H = 1
120 k1 = 1212.28
121 k2 = 72.117
122 k3 = 2.857
123  k6 = 5.568
130 k7 = .01425
131  k9 = .00315
132 k10 = 42.432
140 '** Next set the time step, scaling factors, and initial storages   **
150 dt = .01   'Days
170 Vm = 20: Cm = 4: Sm = 600: tm = 200
207 V = 16.8: C = .625: S = 200
210 ' ** Iterate calculations until the time is up.  (tmax=tm)   **
240 J1 = k1 * M
250 J2 = k2 * V
260 J3 = k3 * V * H * C
280 J5 = k5 * V * H * C
290 J6 = k6 * C
300 J7 = k7 * H * S
310 J8 = k8 * H * S
320 J9 = k9 * S
325 J10 = k10 * C
331 X = t / tm * Xmax' ** Horizontal scaling
340 PSET (X + Xoff, Ymax / 2 - (V / Vm * Ymax / 2))' ** top half of plot
344 PSET (X + Xoff, Ymax / 2 - (C / Cm * Ymax / 2))' ** top half of plot
346 PSET (X + Xoff, Ymax - (S / Sm * Ymax / 2))' ** bottom half of plot
370 dV = J1 + J7 + J10 - J2 - J3
380 dC = J3 - J6 - J10
385 dS = J6 - J7 - J9
390 V = V + dV * dt
400 C = C + dC * dt
405 S = S + dS * dt
410 t = t + dt
420 ' ** Next repeat iteration if t < tm                         **
430 IF t < tm GOTO 210
440 STOP
```

Appendix Table B-6 Listing of the computer program for simulating Hydro2.1, the model in Figure 4-7.

```
10 ' ** PC Basic Simulation Program: Energy Circuit Model         **
20 ' ** Generic Convectional Hydrology Model HYDRO 2.1            **
30 ' ** Includes effect of cloud albedo and limited heat source   **
40 SCREEN 9, 7: COLOR 7, 0
42 Xmax = 500: Ymax = 300'Plot box size on screen
43 Xoff = 50' space on left of plot
50 LINE (Xoff, 0)-(Xmax + Xoff, Ymax), 7, B
70 LINE (Xoff, Ymax / 2)-(Xmax + Xoff, Ymax / 2), 7
90 ' ** Next set source constants and coefficients               **
100 M = 1
110 I0 = 1
115 k0 = .520833
120 k1 = 288
121 k2 = 71.595
122 k3 = 720
123 k4 = .07156
124 k5 = 1.3608333
125 k6 = 5.8
130 k7 = .244
131 k8 = .244
132 k9 = .011
133 k10 = 138.2
140 '** Next set the time step, scaling factors, and initial storages  **
150 V = 4: C = .6: S = 150: dt = .01   'Days
170 Vm = 10: Cm = 3: Sm = 200: tm = 100: Im = 1.5: Rlm = .5: Rcm = .5
210 '** Iterate calculations until the time is up.  (tmax=tm)      **
225 Rc = k0 * I * C
230 I = I0 / (1 + k0 * C)
235 Rl = I / (1 + k4 * S + k5 * V * C)
240 J1 = k1 * M
250 J2 = k2 * V
260 J3 = k3 * V * Rl * C
270 J4 = k4 * Rl * S
280 J5 = k5 * Rl * V * C
290 J6 = k6 * C
300 J7 = k7 * Rl * S
310 J8 = k8 * Rl * S
320 J9 = k9 * S
325 J10 = k10 * C
331 X = t / tm * Xmax' ** Horizontal scaling
340 PSET (X + Xoff, Ymax - (V / Vm * Ymax / 2))' ** bottom half of plot
344 PSET (X + Xoff, Ymax - (C / Cm * Ymax / 2))' ** bottom half of plot
346 PSET (X + Xoff, Ymax - (S / Sm * Ymax / 2))' ** bottom half of plot
347 PSET (X + Xoff, Ymax / 2 - (I / Im * Ymax / 2))' ** top half of plot
348 PSET (X + Xoff, Ymax / 2 - (Rl / Rlm * Ymax / 2))' ** top half of plot
370 dV = J1 + J7 + J10 - J2 - J3
```

Appendix Table B-6--continued

```
380 dC = J3 - J6 - J10
385 dS = J6 - J7 - J9
390 V = V + dV * dt
400 C = C + dC * dt
405 S = S + dS * dt
410 t = t + dt
430 IF t < tm GOTO 210
440 STOP
```

Appendix Table B-7. Listing of computer program for simulating Dfrac, the model in Figure 4-10.

```
10 '  **  PC Basic Simulation Program: Energy Circuit Model        **
20 '  **  D/H Fractionation Model Dfrac                            **
54 Xmax = 500: Ymax = 300
55 Xoff = 75' space on left of plot
56 CLS
57 SCREEN 9, 7: COLOR 7, 0
58 '  **  Draw a three-section box on screen for plot area         **
59 LINE (Xoff, 0)-(Xmax + Xoff, Ymax), 15, B
70 LINE (Xoff, Ymax / 3)-(Xmax + Xoff, Ymax / 3), 15
75 LINE (Xoff, 2 / 3 * Ymax)-(Xmax + Xoff, 2 / 3 * Ymax), 15
80 LINE (Xoff - 10, 1 / 12 * Ymax)-(Xoff, 1 / 12 * Ymax), 15
85 LINE (Xoff - 10, 5 / 12 * Ymax)-(Xoff, 5 / 12 * Ymax), 15
86 LINE (Xoff - 10, 12 / 15 * Ymax)-(Xoff, 12 / 15 * Ymax), 15
90 '  **  Next set the sources and constants                       **
100 M = 1: I0 = 1: ALPHA = 1.074: Smow = .00019736#
110 '  **  Now set the rate coefficients                           **
115 k0 = .5
120 k2H = 72.117: k3H = 57.14286: k4 = .05367: k5 = .31105
125 k6H = 6.628: k7H = .285: k9H = .00315: k10H = 42.432
130 k2D = k2H: k3D = k3H * ALPHA: k6D = k6H
135 k7D = k7H / ALPHA: k9D = k9H: k10D = k10H / ALPHA
136 k1D = .446 * 1: k1H = 1212.2 - k1D
140 '  **  Next set time step, scale factors, and initial storages  **
150 dt = .01   '(Days)
170 Vm = 30: Cm = .8: Sm = 600: tm = 500: Im = 1.5: Rlm = .5: Rcm = .5
175 delDvm = 400: delDcm = 400: delDsm = 500
190 VH = 16.8: CH = .625: SH = 200
191 VD = 0: CD = 0: SD = 0
210 '  **  Start iterative calculation here                        **
225 Rc = k0 * I * (CH + CD)
230 I = I0 / (1 + k0 * (CH + CD))
235 Rl = I / (1 + k4 * (SH + SD) + k5 * (VH + VD) * (CH + CD))
240 J1D = k1D * M
245 J1H = k1H * M
250 J2D = k2D * VD
255 J2H = k2H * VH - J2D
260 J3D = k3D * VD * Rl * (CH + CD)
265 J3H = k3H * VH * Rl * (CH + CD)
270 J4 = k4 * Rl * (SH + SD)
280 J5 = k5 * Rl * (VH + VD) * (CH + CD)
290 J6D = k6D * (VH + VD) * CD * Rl
295 J6H = k6H * (VH + VD) * CH * Rl
300 J7D = k7D * Rl * SD
305 J7H = k7H * Rl * SH
320 J9D = k9D * SD
322 J9H = k9H * SH
```

Appendix Table B-7--continued

```
323 J10D = k10D * CD
325 J10H = k10H * CH
330 ' ** Next plot points to the screen                              **
331 X = t / tm * Xmax
347 PSET (X + Xoff, (1 / 12 * Ymax - delDv / delDvm * Ymax / 3))
348 PSET (X + Xoff, (5 / 12 * Ymax - delDc / delDcm * Ymax / 3))
349 PSET (X + Xoff, (12 / 15 * Ymax - delDs / delDsm * Ymax / 3))
378 ' ** Now update state variables, and increment time             **
379 dVH = J1H + J7H + J10H - J2H - J3H
380 dCH = J3H - J6H - J10H
381 dSH = J6H - J7H - J9H
382 dVD = J1D + J7D + J10D - J2D - J3D
383 dCD = J3D - J6D - J10D
384 dSD = J6D - J7D - J9D
390 VH = VH + dVH * dt
400 CH = CH + dCH * dt
405 SH = SH + dSH * dt
406 VD = VD + dVD * dt
407 CD = CD + dCD * dt
408 SD = SD + dSD * dt
500 t = t + dt
510 ' ** next return to start of loop until t=tm                     **
520 IF t < tm GOTO 210
540 STOP
```

Appendix Table B-8. Listing of the computer program for simulating Tempreg1, the model in Figure 4-16

```
10 ' ** PC Basic Simulation Program: Energy Circuit Model        **
20 ' ** Earth temperature regulation,   By Guy McGrane           **
30 ' **                                                          **
31 ' ** Tempreg1 6/16/97                                         **
35 DEFDBL A-Z
40 CLS
50 SCREEN 9, 7: COLOR 7, 0
60 Xmax = 300: Ymax = 250  'Plot boundaries
70 Xoff = 25: Yoff = 25    'Plot offsets
90 LINE (Xoff, Yoff)-(Xoff + Xmax, Yoff + Ymax), , B
110 LINE (Xoff, Yoff + Ymax / 3)-(Xoff + Xmax, Yoff + Ymax / 3)
120 LINE (Xoff, Yoff + 2 * Ymax / 3)-(Xoff + Xmax, Yoff + 2 * Ymax / 3)
130 ' ***  Next set model sources and constants                  **
140 It = 98: O = 1
145 Fs = .00097685#: Fa = .030626  'Conversion for heats to temps
190 ' ** Next set the model coefficients                         **
200 k1 = .0136
210 k2 = .00747
220 k3 = 4.67E-06
230 k4 = 1.710081
231 k5 = 2.35
232 k6 = 4.89E-06
233 k7 = .000257
234 k8 = 7.26E-10
235 k9 = .00226
236 k10 = 23.45
237 k11 = 1.17E-08
238 k12 = 4.19E-07
239 k13 = .000377
240 k14 = 142
241 k15 = .0000889
242 k16 = .0859
243 k17 = .00226
244 k18 = .0002525
245 k19 = .0000889
246 k20 = 4.44E-08
247 k21 = .00284
248 k22 = .0000425
249 k23 = .00118
250 k24 = .0166
251 k25 = .00143
252 k26 = 1.472E-06
253 k27 = .0000374
254 k28 = .000926
255 ' ** Next set up time step and scale factors                 **
259 dt = .05' (days)
```

Appendix Table B-8--continued

```
280 Tsm = 300: Tam = 300: Cm = 150
290 tm = 15000    'Time scale in days
300 Tst = 0       'Starting year of simulation
365 ' ** Next lines set initial conditions for the model          **
366 Ts = 288: Ta = 273: C = 55: B = 2500
367 Rs = 9: Rv = 75: Rr = 100: Isf = 56
368 Qs = Ts / Fs: Qa = Ta / Fa
370 t = 0
380 ' ** Next iterated calculations until t=tm                     **
382 Isf = It / (1 + k1 * C)
384 Rs = Isf / (1 + k3 * B * Rr + k4 + k5 * O)
388 Rr = k18 * Ts * Rv * C / (1 + k19 * Rs * B)
392 Rv = (k14 * Rs * O + k15 * Rs * Rr * B + k16 * C * Ta) / (1 + k17 * Ts * C)
396 Rc = k1 * Isf * C - k2 * Isf * C
400 J1 = k1 * Isf * C
402 J2 = k2 * Isf * C
404 J3 = k3 * Rs * Rr * B
406 J4 = k4 * Rs
408 J5 = k5 * Rs * O
410 J6 = k6 * Ts * Rv * C
412 If Ts>Ta then J7 = k7 * (Ts - Ta) ^ 4
414 If Ta>Ts then J7 = -k7 * (Ts - Ta) ^ 4
434 J8 = k8 * Ts ^ 4
435 J9 = k9 * Ts * Rv * C
436 J10 = k10 * C
437 J11 = k11 * Ta ^ 4
438 J12 = k12 * Rs * Rr * B
439 J13 = k13 * B
440 J14 = k14 * Rs * O
441 J15 = k15 * Rs * Rr * B
443 J16 = k16 * C * Ta
444 J17 = k17 * Ts * Rv * C
446 J18 = k18 * Ts * Rv * C
447 J19 = J15
448 J20 = k20 * Rs * Rr * B
449 J21 = k21 * B
450 J22 = k22 * Ts * Rv * C
451 J23 = k23 * Ts * Rv * C
452 J24 = k24 * Rv
453 J25 = k25 * C * Ta
454 J26 = k26 * Rs * Rr * B
455 J27 = k27 * Ts * Rv * C
456 J28 = J17 + J23 - J9 - J18
485 ' ** Still in the loop, the following lines plot points to the screen    **
486 X = t / tm * Xmax
487 PSET (X + Xoff, Yoff + Ymax / 3 - C / Cm * Ymax / 3), 15' ** top
489 PSET (X + Xoff, Yoff + 1 / 3 * Ymax + ((293 - Ta) / 50 * (Ymax / 3))), 15
```

Appendix Table B-8--continued

```
491 PSET (X + Xoff, Yoff + 2 / 3 * Ymax + ((313 - Ts) / 50 * (Ymax / 3))), 15
492 'PSET (X + Xoff, Yoff + 2/2*Ymax - Ta / Tam * Ymax / 2), 15' ** top
494 'PSET (X + Xoff, Yoff + 2/2*Ymax - Ts / Tsm * Ymax / 2), 15' ** top
600 ' ** The following lines update state variables, and increment time     **
610 dQs = J4 + J20 + J21 + J24 - J7 - J8
620 dQa = J7 + J2 + J22 - J11 - J25
630 dC = J9 - J16 - J23
640 dB = J12 - J13
650 Qs = Qs + dQs * dt: Qa = Qa + dQa * dt
655 Ts = Qs * Fs: Ta = Qa * Fa
660 B = B + dB * dt: C = C + dC * dt
670 t = t + dt
680 ' ** Next repeat loop if t < tm     **
690 IF t < tm GOTO 380
700 END
```

Appendix Table B-9. Listing of the computer program for simulating Tempreg2, the model in Figure 4-21

```
10 ' ** PC Basic Simulation Program: Energy Circuit Model        **
20 ' ** Tempreg2  6/23/97,  By Guy McGrane                       **
32 ' **                                                          **
35 DEFDBL A-Z
40 CLS
50 SCREEN 9, 7: COLOR 7, 0
60 Xmax = 300: Ymax = 200   'Plot boundaries
70 Xoff = 25: Yoff = 25     'Plot offsets
90 LINE (Xoff, Yoff)-(Xoff + Xmax, Yoff + Ymax), 15, B
110 LINE (Xoff, Yoff + Ymax / 2)-(Xoff + Xmax, Yoff + Ymax / 2), 15
130 ' ***  Next set model sources, constants, and flow coefficients  **
140 It = 98: W = 1: Cs = 1023.7: Ca = 32.64
195 K = 6.76E-2
200 k1 = .013636
210 k2 = .007468
220 k3 = 1.73E-08
230 k4 = 2.641653
231 k5 = .0000957
232 k6 = 2.8E-08
233 k7 = 1.66E-08
234 k8 = 4.65e-10
235 k9 = .0000131
236 k10 = 11.73
237 k11 = 2.9E-08
238 k12 = .0000068
239 k13 = .005769
240 k14 = 5.72e-7
241 k15 = 2.45E-07
242 k16 = .116364
243 k17 = .001185
244 k18 = .194548
245 k19 = 1.17E-08
246 k20 = 9.02e-9
247 k21 = 30.5
258       ' ** Next set time step and scale factors              **
259 dt = .025' (days)
280 Tsm = 315: Cm = 75: Tam = 300: Vm = 20000
290 tm = 7500   'Time scale in days
300 Tst = 0     'Starting year of simulation
365 ' ** Next set initial conditions for the model               **
366 Ts = 288: Ta = 273: C = 55: V = 13000: Qc = 2
367 Rs = 9: Rr = 5: Isf = 56
368 Qs = Ts * Cs: Qa = Ta * Ca
380 ' ** Do iterated calculations until t=tm                     **
395 Isf = It / (1 + k1 * C)
400 Rs = Isf / (1 + k4 + k20 * W * exp(K * Ts))
```

Appendix Table B-9--continued

```
410 Rr = k7 * Ts ^ 4 / (1 + k17 * V + k16 * C)
415 J1 = k1 * Isf * C
420 J2 = k2 * Isf * C
425 J3 = k3 * Ta ^ 4
430 J4 = k4 * Rs
432 J5 = k5 * V
434 J6 = k6 * Ts * V * C
441 J7 = k7 * Ts ^ 4
442 J8 = k8 * W * Rs * EXP(K * Ts)
443 J9 = k9 * Ts * V * C
444 J10 = k10 * C * Qc
445 J11 = k11 * Ta ^ 4
446 J12 = k12 * Ts * V * C
447 J13 = k13 * V
448 J14 = k14* W * Rs * EXP(K * Ts)
449 J15 = k15 * Ts * V * C
450 J16 = k16 * Rr * C
451 J17 = k17 * Rr * V
452 J18 = k18 * C * Qc
453 J19 = k19 * Ta ^ 4
455 J20 = k20 * W * Rs * EXP(K * Ts)
460 J21 = k21 * Qc
465 Rc = J1 - J2
468 ' ** Still in the loop, the following lines plot points to the screen        **
469 X = t / tm * Xmax + Xoff
470 PSET (X, Yoff + Ymax / 2 - C / Cm * Ymax / 2), 3' ** top
471 PSET (X, Yoff + Ymax / 2 - V / Vm * Ymax / 2), 15 ' ** top
475 PSET (X, Yoff + Ymax/2 + ((303 - Ta) / 50 * (Ymax / 2))), 15
476 PSET (X, Yoff + Ymax/2 + ((303 - Ts) / 50 * (Ymax / 2))), 4
600 ' ** Next update state variables, and increment time        **
610 dQs = J3 + J4 + J5 - J6 - J7 - J8
620 dC = J9 - J10 - J12
630 dQa = J2 + J17 + J21 - J11
640 dV = J10 + J14 - J9 - J13
641 dQc = J15 + J16 - J18 - J21
650 Qs = Qs + dQs * dt: Qa = Qa + dQa * dt
660 V = V + dV * dt: C = C + dC * dt
661 Qc = Qc + dQc * dt
670 t = t + dt
675 Ts = Qs / Cs: Ta = Qa / Ca
680 ' ** The next line causes loop to repeat if (t < to)
690 IF t < tm GOTO 380
700 END
```

Appendix Table B-10. Listing of the computer program for simulating Coal2a, the model in Figure 4-33.

```
10 ' ** PC Basic Simulation Program: Energy Circuit Model          **
20 ' ** Coal2a, By Guy McGrane                                      **
40 'CLS
50 SCREEN 12, 1 ': COLOR 7, 0
60 Xmax = 300: Ymax = 175   'Plot boundaries
70 Xoff = 50: Yoff = 50     'Plot offsets
75 H = Ymax / 3: W = Xmax / 4
80 ' ** Next draw graph box                                         **
90 LINE (Xoff, Yoff)-(Xoff + Xmax, Yoff + Ymax), , B
110 LINE (Xoff, Yoff + H)-(Xoff + Xmax, Yoff + H)
120 LINE (Xoff, Yoff + 2 * H)-(Xoff + Xmax, Yoff + 2 * H)
170 ' ** Next set the source constants and coefficients             **
180 J0 = 30
200 k1 = .0765
210 k2 = .0133
220 k3 = .02
230 k4 = 0
232 k5 = .00008
234 k6 = .00266
236 k7 = .0000145
240 k8 = .08
245 k9 = .0000691
250 k10 = .0042
255 ' ** Next set the time step, and scale factors                  **
260 dt = .1' (years)
280 Cm = 6000: R2m = 1: Rm = 30
281 Em = 250: J10m = 2: Sm = 20
282 tm = 200       'Time scale in years
283 ts = 1800      'Starting year of simulation
310 ' ** Next line sets Initial Conditions                          **
320 C = 6000: E = 20: R = 3: R2 = .00375: S = .35
380 ' ** Next iterate calculations until t=tm                       **
400 R = J0 / (1 + k1 * R2 * E)
410 J1 = k1 * R * R2 * E
420 J2 = k2 * R * R2 * E
430 J3 = k3 * E
440 J4 = 0
442 J5 = k5 * C * S
444 J6 = k6 * R * R2 * E
446 J7 = k7 * C * S
450 J8 = k8 * S
460 J9 = k9 * C * S
465 J10 = k10 * R * R2 * E
470 R2 = J9 / (1 + k10 * R * E)
475 ' ** Next plot points to the screen                             **
480 X = t / tm * Xmax + Xoff
```

Appendix Table B-10--continued

```
490 PSET (X, Yoff + H - E / Em * H), 15' ** top
500 PSET (X, Yoff + 2 * H - J10 / J10m * H), 15' ** mid
510 PSET (X, Yoff + 3 * H - (R2 / J9) / R2m * H), 15' ** bottom
600 ' **  Next update state variables, and increment time              **
630 dC = -J5
640 dE = J2 - J3
650 dS = J6 - J7 - J8
660 C = C + dC * dt
662 S = S + dS * dt
665 E = E + dE * dt
670 t = t + dt
690 IF t < tm GOTO 400
700 END
```

Appendix Table B-11. Listing of the computer program for simulating Oiluse3, the model in Figure 4-38.

```
10 ' ** PC Basic Simulation Program: Energy Circuit Model        **
20 ' ** Oiluse3, by Guy McGrane                                  **
40 CLS
50 SCREEN 9, 7: COLOR 7, 0
60 Xmax = 300: Ymax = 200   'Plot boundaries
70 Xoff = 25: Yoff = 25   'Plot offsets
75 H = Ymax / 3: W = Xmax / 4   'Plotting constants
80 ' ** Next draw the graph box                                  **
90 LINE (Xoff, Yoff)-(Xoff + Xmax, Yoff + Ymax), , B
110 LINE (Xoff, Yoff + H)-(Xoff + Xmax, Yoff + H)
120 LINE (Xoff, Yoff + 2 * H)-(Xoff + Xmax, Yoff + 2 * H)
170 ' ** Next set the source constants and coefficients          **
180 J0 = 100
200 k1 = .01
210 k2 = .003
220 k3 = .02
230 k4 = .0001333
232 k5 = .1
234 k6 = .000286
236 k7 = .00343
240 k8 = .00343
245 k9 = .000567
255 ' ** Next set the time step and scaling factors             **
260 dt = .1' (years)
280 Om = 505: R2m = 1: Rm = 1
285 Em = 1500: J9m = 5: Sm = 7.5
290 tm = 95       'Time scale in years
300 ts = 1900      'Starting year of simulation
310 ' ** Next set Initial Conditions                            **
320 O = 505: E = 32: S = .1: R = .01: R2 = .5
380 ' ** Next iterate calculations until t = tm                 **
400 R = J0 / (1 + k1 * R2 * E)
410 J1 = k1 * R * R2 * E
420 J2 = k2 * R * R2 * E
430 J3 = k3 * E
440 J4 = k4 * R * R2 * E
442 J5 = k5 * S
444 J6 = k6 * O * S
446 J7 = k7 * O * S
450 J8 = k8 * O * S
460 J9 = k9 * R * R2 * E
470 R2 = J8 / (1 + k9 * R * E)
475 ' ** Next plot points to the screen                         **
480 X = t / tm * Xmax + Xoff
490 PSET (X, Yoff + H - E / Em * H), 15' ** top
492 PSET (X, Yoff + H - S / Sm * H), 15'3' ** top
```

Appendix Table B-11--continued

```
495 PSET (X, Yoff + 2 * H - O / Om * H), 15'3' ** mid
500 PSET (X, Yoff + 2 * H - J9 / J9m * H), 15'3' ** mid
505 PSET (X, Yoff + 3 * H - R / J0 * H), 15'2' ** bottom
510 PSET (X, Yoff + 3 * H - (R2 / J8) / R2m * H), 15'3' ** bottom
600 '  ** Next update state variables, and increment time          **
630 dOil = -J7  '** "dO" not allowed--keyword in do-while loop **
640 dE = J2 - J3
650 dS = J4 - J5 - J6
660 O = O + dOil * dt
662 S = S + dS * dt
665 E = E + dE * dt
670 t = t + dt
690 IF t < tm GOTO 400
700 END
```

Appendix Table B-12. Listing of the computer program for simulating Coaloil, the model in Figure 4-41.

```
10 '  ** PC Basic Simulation Program: Energy Circuit Model      **
20 '  **Coaloil, By Guy McGrane                                 **
40 CLS
50 SCREEN 9, 7: COLOR 7, 0
60 Xmax = 300: Ymax = 200   'Plot boundaries
70 Xoff = 25: Yoff = 25   'Plot offsets
75 H = Ymax / 3: W = Xmax / 3
80 '  ** Next draw graph box                                    **
90 LINE (Xoff, Yoff)-(Xoff + Xmax, Yoff + Ymax), , B
110 LINE (Xoff, Yoff + H)-(Xoff + Xmax, Yoff + H)
120 LINE (Xoff, Yoff + 2 * H)-(Xoff + Xmax, Yoff + 2 * H)
170 '  ** Next line sets the source constants and coefficients  **
180 J0 = 1
200 k1 = .000256
205 k2 = 4.95E-06
210 k3 = .564
215 k4 = .00334
220 k5 = .2
225 k6 = .0128
230 k7 = .000495
232 k8 = .219
234 k9 = .608
236 k10 = .5824
238 k11 = .02
240 k12 = .04
242 k13 = 5.12E-06
244 k14 = .0133
245 k15 = .124
246 k16 = .00016
247 k17 = .0425
248 k18 = .22
249 k19 = .0000404
250 k20 = .00008
251 k21 = .0038
252 k22 = .0000727
253 k23 = .0038
254 k24 = .0289
255 k25 = .081
265 '  ** Next set the time stepand scaling factors            **
268 dt = .05' (years)
280 Om = 505: Cm = 6000: Rm = 1: Am = 8000: Ym = 100
285 Em = 750: J24m = 5: J25m = 5: Scm = 15: Som = 15
290 tm = 150      'Time scale in years
300 ts = 1850      'Starting year of simulation
310 '  ** Next line sets Initial Conditions                     **
320 O = 505: E = 10: R1 = 5: R2 = .11: R3 = .8
```

Appendix Table B-12--continued

```
330 C = 6000: Sc = 0: So = 0: A = 7000
335 Flag = 0
374 ' ** Next iterate calculations until t = tm.                    **
375 ' ** If statements start oil&coal at appropriate times          **
380 IF ((t + ts) > 1925) THEN
381   IF Oilflag = 0 THEN
382     So = .05: 'IF E < 20 THEN E = 20
383     Oilflag = 1
384   END IF
385 ELSE
386   So = 0
387 END IF
390 IF ((t + ts) > 1870) THEN
391   IF Coalflag = 0 THEN
392     Sc = .1: 'IF E < 10 THEN E = 10
393     Coalflag = 1
394   END IF
396 ELSE
397   Sc = 0
398 END IF
400 R = J0 / (1 + k1 * A + k2 * A * E)
402 J1 = k1 * A * R
404 J2 = k2 * A * R * E
406 J3 = k3 * A * R
408 J4 = k4 * A * R * E
410 J5 = k5 * A
412 J6 = k6 * A * R
413 J7 = k7 * A * R * E
414 J8 = k8 * R1 * R2 * E
415 J9 = k9 * R1 * R3 * E
416 J10 = k10 * R1 * R2 * E
417 J11 = k11 * R1 * R3 * E
418 J12 = k12 * E
420 J13 = k13 * A * R * E
422 J14 = k14 * R1 * R2 * E
424 J15 = k15 * So
426 J16 = k16 * O * So
428 J17 = k17 * R1 * R3 * E
430 J18 = k18 * Sc
432 J19 = k19 * C * Sc
434 J20 = k20 * C * Sc
436 J21 = k21 * O * So
438 J22 = k22 * C * Sc
440 J23 = k23 * O * So
442 J24 = k24 * R1 * R3 * E
444 J25 = k25 * R1 * R2 * E
466 R1 = (J6 + J7) / (1 + k8 * R2 * E + k9 * R3 * E)
```

Appendix Table B-12--continued

```
468 R2 = J23 / (1 + k25 * R1 * E)
470 R3 = (J22 + J27) / (1 + k24 * R1 * E)
472 Y = J6 + J7
475 ' ** Next plot points to the screen                          **
480 X = t / tm * Xmax + Xoff
490 PSET (X, Yoff + H - E / Em * H), 15' ** top
491 PSET (X, Yoff + H - A / Am * H), 15' ** top
500 PSET (X, Yoff + 2 * H - J24 / J24m * H), 15' ** mid
501 PSET (X, Yoff + 2 * H - J25 / J25m * H), 15' ** mid
507 PSET (X, Yoff + 3 * H - (R1 / (J6 + J7) / Rm * H)), 15' ** bottom
513 PSET (X, Yoff + 3 * H - Y / Ym * H), 15' ** bottom
600 ' ** Next update state variables, and increment time           **
630 dOil = -J21  '** "dO" not allowed--keyword in do-while loop
635 dC = -J20
640 dE = J10 + J11 - J12 - J13
645 dSc = J17 - J18 - J19
650 dSo = J14 - J15 - J16
655 dA = J3 + J4 - J5
660 O = O + dOil * dt
661 C = C + dC * dt
662 Sc = Sc + dSc * dt
663 So = So + dSo * dt
665 E = E + dE * dt
667 A = A + dA * dt
670 t = t + dt
675 IF E < 15 THEN E = 15
690 IF t < tm GOTO 380
700 END
```

Appendix Table B-13. Listing of computer program for simulating Pulse2.0, the model in Figure 5-1.

```
10 ' ** PC Basic Simulation Program: Energy Circuit Model        **
20 ' ** Pulse 2.0   Standard run    2 Module Pulsing Model        **
30 '
40 Xmax = 500: Ymax = 300  '(You can change these to fit your needs)
41 Xoff = 50 ' (space on left of plot)
42 SCREEN 9, 1
45 '** Following Line draws the graph box                         **
50 LINE (Xoff, 0)-(Xmax + Xoff, Ymax), 15, B
60 ' ** Following line divides box in 2                           **
70 LINE (Xoff, Ymax / 2)-(Xmax + Xoff, Ymax / 2), 15
90 ' ** Following line sets source values                        **
100 J = 10000
110 '** Following lines set coefficients                         **
115 k0 = .0005
120 k1 = .0001: k2 = .33: k3 = .0000006: k4 = .0000004#: k5 = .15: k6 = .001
140 '** Following line sets the time step                        **
150 dt = .01' (Years: ~ 3.65 d)
160 ' ** Following line sets the plot scaling factors            **
170 ' ** Input the actual scale desired for variables and time   **
171 A0 = 5000: B0 = 5000
172 t0 = 1000  '(Time scale in units you specified above)
180 ' ** Following line sets initial conditions                  **
190 A = 500: B = 50
195 REM ** Following lines print scale info                      **
200 LOCATE 2 + INT(Ymax / 14), (Xmax + Xoff) / 8: PRINT t0
202 LOCATE 2 + INT(Ymax / 14), (Xmax + Xoff) / 16: PRINT "Time (Yrs)"
205 LOCATE 2 + INT(Ymax / 14), INT(Xoff / 8): PRINT "0": 'time axis
203 LOCATE 1 + INT(Ymax / 14), 3: PRINT "0": REM Bottom half
204 LOCATE 2 + INT(Ymax / 2 / 14), 1: PRINT B0
206 LOCATE 1, 1: PRINT A0
207 LOCATE INT(Ymax / 2 / 14), 3: PRINT "0": REM top half
210 REM ** The loop starts here. Calculations are repeated       **
220 REM ** until the time is up. (tmax=t0)                        **
230 R = J / (1 + k0 * A)
240 J0 = k0 * R * A
245 J1 = k1 * R * A
250 J2 = k2 * A
260 J3 = k3 * A * B * B
270 J4 = k4 * A * B * B
280 J5 = k5 * B
290 J6 = k6 * A
330 '** Still in the loop, the following lines plot              **
331 '** points to the screen.                                    **
335 X = t / t0 * Xmax
```

Appendix Table B-13.--continued

```
339 PSET (X + Xoff, Ymax / 2 - A / A0 * Ymax / 2), 15
340 PSET (X + Xoff, Ymax - B / B0 * Ymax / 2), 15
353 IF t = 0 THEN ' Label the plotted curves
354    LOCATE Ymax / 4 / 14, 3: PRINT "A"
355    LOCATE Ymax * 3 / 4 / 14, 3: PRINT "B"
356 LOCATE 1, 1
361 END IF
362 REM ** Following lines update state variables, and increment time    **
370 dA = J1 - J2 - J3 - J6
380 dB = J4 - J5 + J6
390 A = A + dA * dt
400 B = B + dB * dt
410 t = t + dt
420 REM ** The next line causes loop to repeat if (t < to)               **
430 IF t < t0 GOTO 230
440 DO: LOOP UNTIL INKEY$ <> "": '(wait for printscreen)
450 END
```

Appendix Table B-14. Listing of the computer program for simulating
Pulse3.01, the model in Figure 5-5.

```
10 ' ** PC Basic Simulation Program: Energy Circuit Model          **
20 ' ** Pulse 3.01 --Test of simulating pulsing at three scales     **
30 ' **                                                             **
40 SCREEN 9, 1
41 Xmax = 500: Ymax = 300        'Plot size, Can be changed as needed
42 Xoff = 50              ' space on left of plot
45 ' ** The following line draws a box on the screen                **
50 LINE (Xoff, 0)-(Xmax + Xoff, Ymax), 15, B
60 ' ** Next separate the box into three parts                      **
70 LINE (Xoff, Ymax / 3)-(Xmax + Xoff, Ymax / 3), 15
80 LINE (Xoff, 2 * Ymax / 3)-(Xmax + Xoff, 2 * Ymax / 3), 15
90 ' ** The following line sets the source constant for the model   **
100 S = 10000
110 ' ** The following lines set the model coefficients             **
115 k0 = .0005
120 k1 = .0001
121 k2 = .33
122 k3 = .0000008
123 k4 = .0000004
124 k5 = .155
125 k6 = .001
130 k7 = .000006
131 k8 = .000005
132 k9 = .000002
133 k10 = .007
134 k11 = .00001
140 ' ** Next set the iteration time step and scale factors         **
150 dt = .01        'years, about 3.6 days
171 A0 = 8000: B0 = 5000: C0 = 100
172 t0 = 2500       'years
180 ' ** Next set the initial conditions of the storages            **
190 A = 500: B = 50: C = 5
210 ' ** Iterated calculations start here, and are                  **
220 ' ** repeated until the time is up. (tmax=t0)                   **
230 R = S / (1 + k0 * A)
240 J0 = k0 * R * A
245 J1 = k1 * R * A
250 J2 = k2 * A
260 J3 = k3 * A * B * B
270 J4 = k4 * A * B * B
280 J5 = k5 * B
290 J6 = k6 * A
291 J7 = k7 * B
292 J8 = k8 * B * C * C
293 J9 = k9 * B * C * C
294 J10 = k10 * C
```

Appendix Table B-14--continued

```
295 J11 = k11 * A
330 '  **  Still in the loop, the following lines plot points to the screen        **
331 '  **  First two plot to top half, rest to bottom half                         **
335 X = t / t0 * Xmax
339 PSET (X + Xoff, Ymax / 3 - A / A0 * Ymax / 3), 15
340 PSET (X + Xoff, 2 * Ymax / 3 - B / B0 * Ymax / 3), 15
350 PSET (X + Xoff, Ymax - C / C0 * Ymax / 3), 15
362 '  **  Next update state variables, and increment time                         **
370 dA = J1 - J2 - J3 - J6 - J11
380 dB = J4 - J5 + J6 - J7 - J8
385 dC = J7 + J9 + J11 - J10
390 A = A + dA * dt
400 B = B + dB * dt
405 C = C + dC * dt
410 t = t + dt
420 '  **  The next line causes loop to repeat if (t < to)                          **
430 IF t < t0 GOTO 230
440 DO: LOOP UNTIL INKEY$ <> ""
450 END
```

Appendix Table B-15. Listing of the computer program for simulating Pulse3.1, the model in Figure 5-9.

```
10 ' ** PC Basic Simulation Program: Energy Circuit Model          **
20 ' ** Pulse 3.1 --Test of simulating pulsing at three scales     **
25 ' **                 --Including Slow Storage M                  **
30 ' **                                                             **
35 SCREEN 9, 1
40 Xmax = 500: Ymax = 300:  'Size of graph box on screen
42 Xoff = 50              'space on left of plot
45 ' ** Draw a box on the screen                                    **
50 LINE (Xoff, 0)-(Xmax + Xoff, Ymax), 15, B
60 ' ** Next separate the box into four parts                       **
70 LINE (Xoff - 8, Ymax / 4)-(Xmax + Xoff, Ymax / 4), 15
80 LINE (Xoff - 8, 2 * Ymax / 4)-(Xmax + Xoff, 2 * Ymax / 4), 15
85 LINE (Xoff - 8, 3 * Ymax / 4)-(Xmax + Xoff, 3 * Ymax / 4), 15
90 ' ** Next set the source constants and coefficients              **
100 S = 10000
115 k0 = .0005
120 k1 = .0001
121 k2 = .333
122 k3 = .0000008
123 k4 = .0000004
124 k5 = .15
130 k6 = .001
131 k7 = .0000008
132 k8 = .00004
133 k9 = 8E-09
134 k10 = 6E-09
135 k11 = .0000005
136 k12 = .02
137 k13 = .00025
140 ' ** Next set the time step: units in the comment               **
150 dt = .01            'years
160 ' ** Next set the plot scaling factors                          **
171 A0 = 10000: B0 = 2000: C0 = 50: M0 = 12000
172 t0 = 5000  'Time scale in units you specified above
180 ' ** Next set the initial conditions                            **
190 A = 2000: B = 75: C = 1: D = 3000
210 ' ** Iterated calculations start here, and are                  **
220 ' ** repeated until the time is up.  (tmax=t0)                  **
230 R = S / (1 + k0 * A)
240 J0 = k0 * R * A
245 J1 = k1 * R * A
250 J2 = k2 * A
260 J3 = k3 * A * B * B
270 J4 = k4 * A * B * B
280 J5 = k5 * B
290 J6 = k6 * A
```

Appendix Table B-15--continued

```
291 J7 = k7 * R * A
292 J8 = k8 * B
293 J9 = k9 * B * C * C * M
294 J10 = k10 * B * C * C * M
295 J11 = k11 * B * C * C * M
296 J12 = k12 * C
297 J13 = k13 * M
330 ' ** Still in the loop, the following lines plot points to the screen     **
331 ' ** First two plot to top half, rest to bottom half                      **
335 X = t / t0 * Xmax
339 PSET (X + Xoff, Ymax / 4 - A / A0 * Ymax / 4), 15
340 PSET (X + Xoff, 2 * Ymax / 4 - B / B0 * Ymax / 4), 15
350 PSET (X + Xoff, 3 * Ymax / 4 - C / C0 * Ymax / 4), 15
351 PSET (X + Xoff, Ymax - M / M0 * Ymax / 4), 15
365 ' ** Next update storages, and increment time                             **
370 dA = J1 - J2 - J3 - J6
380 dB = J4 + J6 - J5 - J8 - J9
385 dC = J8 + J10 - J12
386 dM = J7 - J11 - J13
390 A = A + dA * dt
400 B = B + dB * dt
405 C = C + dC * dt
406 M = M + dM * dt
410 t = t + dt
420 ' ** Next repeat iteration if (t < to)
430 IF t < t0 GOTO 230
440 DO: LOOP UNTIL INKEY$ <> ""
450 END
```

Appendix Table B-16. Listing of the computer program for simulating Pulse4.0, the model in Figure 5-13.

```
10 ' ** PC Basic Simulation Program: Energy Circuit Model        **
20 ' ** Pulse 4.0 -- Test of simulating pulsing at four scales   **
30 ' **                                                          **
40 ' ** The following line draws a box on the screen             **
41 Xmax = 500: Ymax = 300 'Can be changed as needed to fit screen
42 Xoff = 50  'space on left of plot
43 CLS
44 SCREEN 9, 1
50 LINE (Xoff, 0)-(Xmax + Xoff, Ymax), 15, B
60 ' ** Next separate the box into four partitions               **
70 LINE (Xoff, Ymax / 4)-(Xmax + Xoff, Ymax / 4), 15
80 LINE (Xoff, 2 * Ymax / 4)-(Xmax + Xoff, 2 * Ymax / 4), 15
81 LINE (Xoff, 3 * Ymax / 4)-(Xmax + Xoff, 3 * Ymax / 4), 15
90 ' ** Next set the source constants and coefficients           **
100 S = 10000
115 k0 = .0005
120 k1 = .0001
121 k2 = .33
122 k3 = .0000008
123 k4 = .0000004
124 k5 = .155
125 k6 = .001
130 k7 = .00008
131 k8 = .000005
132 k9 = .00002
133 k10 = .005
134 k11 = .00004
135 k12 = .00006
136 k13 = .00003
137 k14 = .002
140 ' ** Next set the iteration time                             **
150 dt = .01        'years
160 ' ** Next set the plot scaling factors                       **
171 A0 = 5000#: B0 = 5000: C0 = 150: D0 = 150
172 t0 = 20000 'Time scale in units you specified above
180 ' ** Next set the initial conditions                         **
190 A = 500: B = 50: C = 5: D = .1
210 ' ** Iterated calculations start here, and are              **
220 ' ** repeated until the time is up.  (tmax=t0)              **
230 R = S / (1 + k0 * A)
240 J0 = k0 * R * A
245 J1 = k1 * R * A
250 J2 = k2 * A
260 J3 = k3 * A * B * B
270 J4 = k4 * A * B * B
280 J5 = k5 * B
```

Appendix Table B-16--continued

```
290 J6 = k6 * A
291 J7 = k7 * B
292 J8 = k8 * B * C * C
293 J9 = k9 * B * C * C
294 J10 = k10 * C
295 J11 = k11 * C
300 J12 = k12 * C * D * D
310 J13 = k13 * C * D * D
320 J14 = k14 * D
330 '  **  Still in the loop, the following lines plot points to the screen          **
331 '  **  First two plot to top half, rest to bottom half                           **
335 X = t / t0 * Xmax
339 PSET (X + Xoff, Ymax / 4 - A / A0 * Ymax / 4), 1
340 PSET (X + Xoff, Ymax / 2 - B / B0 * Ymax / 4), 2
350 PSET (X + Xoff, 3 * Ymax / 4 - C / C0 * Ymax / 4), 3
351 PSET (X + Xoff, Ymax - D / D0 * Ymax / 4), 4
362 '  **  Next update storages, and increment time  **
370 dA = J1 - J2 - J3 - J6
380 dB = J4 - J5 + J6 - J7 - J8
385 dC = J7 + J9 - J10 - J11 - J12
386 dD = J11 + J13 - J14
390 A = A + dA * dt
400 B = B + dB * dt
405 C = C + dC * dt
406 D = D + dD * dt
410 t = t + dt
420 '  **  Next line repeat iteration if (t < t0)
430 IF t < t0 GOTO 230
440 DO: LOOP UNTIL INKEY$ <> ""
450 END
```

Appendix Table B-17. Listing of computer program for simulating the model in Figure 5-16.

```
10 ' ** PC QuickBasic Simulation Program: Energy Circuit Model      **
20 ' ** Test model for optimum Q for max power                      **
40 Xmax = 300: Ymax = 150  '(You can change these to fit your needs)
41 Xoff = 50: Yoff = 50' (space on left of plot)
42 SCREEN 9, 1
45 '** Next draw the graph box                                      **
50 LINE (Xoff, Yoff)-(Xmax + Xoff, Ymax + Yoff), 15, B
60 LINE (Xoff, Yoff + Ymax / 2)-(Xoff + Xmax, Yoff + Ymax / 2)
90 ' ** Next set sources, coefficients, initial storages, scale factors **
100 E = 100: Tint = 2: Q0 = 30
115 k0 = .0008
120 k1 = .000533
122 k2 = .533
124 k3 = .000533
150 dt = .01' (Years: ~ 3.65 d)
171 Qm = 80: Pm = 100: MT = 100:tm = 40
190 Q = Q0: D = MT - Q
200 '** Next iterate calculations until t=tm                        **
230 R = E / (1 + k0 * D * Q)
240 J0 = k0 * R * D * Q: P = J0
245 J1 = k1 * R * D * Q
250 J2 = k2 * Q
260 J3 = k3 * R * D * Q
330 '** Next plot points to the screen.                            **
335 X = t / tm * Xmax
340 PSET (X + Xoff, Yoff + Ymax / 2 - Q / Qm * Ymax / 2), 15'White
345 PSET (X + Xoff, Yoff + Ymax - P / Pm * Ymax / 2), 4'Red
362 REM ** Following lines update state variables, and increment time **
370 dQ = J1 - J2
390 Q = Q + dQ * dt
392 '** Next pulse at certain times                                **
396 'IF ABS(10 - t) < dt THEN Q = Q0
397 'IF ABS(15 - t) < dt THEN Q = Q0
398 'IF ABS(20 - t) < dt THEN Q = Q0
399 'IF ABS(25 - t) < dt THEN Q = Q0
400 'IF ABS(30 - t) < dt THEN Q = Q0
401 'IF ABS(35 - t) < dt THEN Q = Q0
404 D = MT - Q
405 Ptot = Ptot + P
410 t = t + dt
420 REM ** Next loop if (t < tm)                                    **
430 IF t < tm GOTO 230
440 LOCATE 10, 30: PRINT Ptot
450 END
```

Appendix Table B-17. Listing of the computer program for simulating the sedimentary cycle pulsing model in Figure 5-19.

```
10 ' ** PC Basic Simulation Program: Energy Circuit Model         **
20 ' ** Generic pulsing w/ sed cycle numbers                      **
50 SCREEN 9, 7: COLOR 7, 0
60 Xmax = 250: Ymax = 200   'Plot boundaries
70 Xoff = 25: Yoff = 25   'Plot offsets
80 ' ** Next lines draw a box on the screen                       **
90 LINE (Xoff, Yoff)-(Xoff + Xmax, Yoff + Ymax), , B
100 LINE (Xoff, Yoff + Ymax / 3)-(Xoff + Xmax, Yoff + Ymax / 3)
110 LINE (Xoff, Yoff + 2 * Ymax / 3)-(Xoff + Xmax, Yoff + 2 * Ymax / 3)
120 '** Next set sources, coefficients, initial storages, scale values  **
121 E = 1: L = 230: M = 357: MT = 2755
125 k0 = 8.01E-06
126 k1 = .0001002
127 k2 = .00217
128 k3 = 3.89E-07
129 k4 = .0377
130 k5 = .01
140 F2 = 1
150 Lm = 1000: Mm = 1000: Rm = 2500
165 R0 = .04
170 tm = 2000: ts = 0
190 dt = .5
200 R = MT - L - M
205 R1 = E / (1 + k0 * R * L)
210 dL = k1 * R1 * R * L - k2 * L - k3 * M * M * L - k5 * L
220 DM = k2 * L + k3 * M * M * M - k4 * M
230 L = L + dL * dt
240 M = M + DM * dt
246 X = t / tm * Xmax
248 '** Next plot the points                                      **
250 PSET (X + Xoff, Yoff + 1 / 3 * Ymax - L / Lm * Ymax / 3), 2 ' ** top
260 PSET (X + Xoff, Yoff + 2 / 3 * Ymax - M / Mm * Ymax / 3), 3' ** mid
265 PSET (X + Xoff, Yoff + Ymax - R / Rm * Ymax / 3), 15' ** bottom
270 t = t + dt
280 IF t < tm GOTO 200
290 END
```

THERMODYNAMICS OF THE OVERALL
SEDIMENTARY CYCLE REACTION

In the cogwheels model of the overall sedimentary cycle (Figure 3-13),
movement of sedimentary material to a deep Earth location contributes energy
to the deep crust. This energy may be in the form of chemical potentials and
compression heating. In addition, the horizontal displacement of large
quantities of sediments via erosion and river transport, causes uplift and
subsidence in areas of erosion and deposition, respectively. This action
deforms the crust, and can generate deep heat which is related to surface
energies.

In order to evaluate possible thermodynamic properties of these
processes, enthalpy and Gibbs' free energy was calculated for an overall
sedimentary reaction proposed by Li, 1972. Appendix Table C-1 lists the
products and reactants, their chemical formulae, and the number of moles
involved per 100kg of hard rock formed.

Thermodynamic properties of the reaction were calculated with the
computer program Supercrt92®, as described in Johnson et al. (1992). The
program lacked data on organic matter and hydrochloric acid, so these values
are missing from the evaluation.

Appendix Figure C-1 shows the Gibbs' free energy of the reaction in
graphical form, for temperatures from 0 to 1000°C, and for pressures from 0 to 5
kbar. For any pressure, the free energy became negative at around 150°C. So
the reaction tended to proceed to the hard rock constituents at any pressure

with temperature higher than 150°C. This result supports the contention that the reaction is an appropriate representation of the overall sedimentary cycle process, because the Gibbs' free energy is a direct indicator of chemical reactions' tendency to proceed.

Appendix Figure C-2 shows the enthalpy of the reaction in graphical form, for temperatures from 0 to 1000C, and for pressures from 0 to 5 kbar. Positive values for enthalpy mean the reaction is exothermic, and this reaction was exothermic for all tested conditions of temperature and pressure. So direct contribution to deep crustal heat by the reaction may be negative. Perhaps compression potentials and deformation energy contribute the bulk of the heat not produced radiogenically or flowing from the deep Earth (Odum, 1996).

Appendix Table C-1. Minerals in the overall surface sedimentary cycle reaction given by Li, 1973. Numbers of moles referring to 100kg of hard rock, combining with 13 kg of acid volatiles, to make 113 kg of sediments.

Mineral	Moles produced	Chemical Formula	Description
Reactants			
Microcline	42	KAlSi3O8	Framework Silicate
Albite	94	NaAlSi3O8	Framework Silicate
Anorthite	82	CaAl2Si2O8	Framework Silicate
Enstatite	129	MgSiO3	Chain Silicate
Wollastonite	78	CaSiO3	Chain Silicate
Ferrosilite	81	FeSiO3	Chain Silicate
HCl	56	HCl	Gas
CO2	219	CO2	Gas
H2S	20	H2S	Gas
Water	160	H2O	Liquid
H2	16	H2	Gas
Products			
Clinochlore	-25.8	Mg5Al2Si3O10(OH)8	Clay
Daphnite	-4.6	Fe5Al2Si3O10(OH)8	Clay
Muscovite	-42	KAl3Si3O10(OH)2	Clay
Paragonite	-38	NaAl3Si3O10(OH)2	Clay
Quartz	-536	SiO2	Framework Silicate
Hematite	-29	Fe2O3	Oxide
Pyrite	-5.5	FeS2	Sulfide
Anhydrite	-7	CaSO4	Sulfate
Calcite	-153	CaCO3	Carbonate
Magnesite	-22	MgCO3	Carbonate
Halite	-18	NaCl	Salt
Na+	-34	Na+	Ion
Mg+2	-4	Mg+2	Ion
Cl-	-38	Cl-	Ion
SO4-2	-2	SO4-2	Ion
CH2O	-44	CH2O	Organic
O2	-1.75	O2	Gas
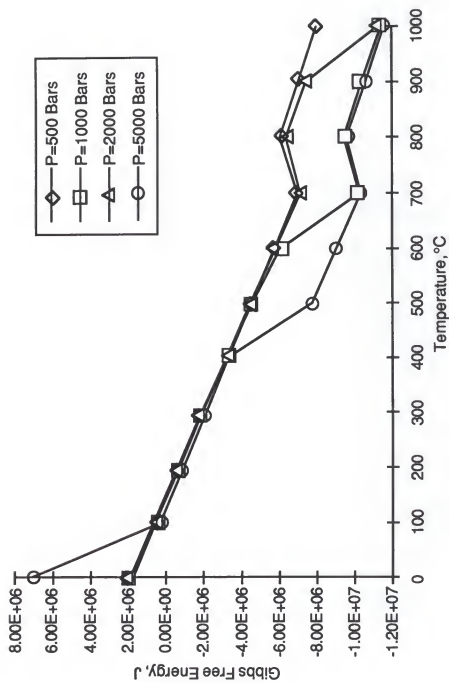
Appendix Figure C-1. Gibbs Free Energy of the reaction that converts sediments into hard rock, reaction adapted from Li, 1973. Temperature is the main trend variable, while pressure induces phase transitions that give rise to discontinuous jumps in energy. The reaction tends to proceed at temperatures higher than150°C.
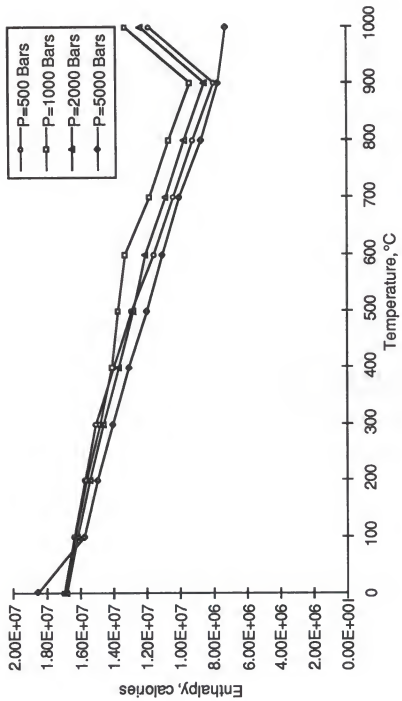
Appendix Figure C-2. Enthalpy of the overall sedimentary cycle reaction listed in Appendix Table C-1, not including HCl and CH₂O, which were unknown.

LIST OF REFERENCES

Alexander, J.F., 1978, Energy Basis of disaster and Cycles of Order and Disorder, Ph.D. Dissertation, University of Florida, Gainesville.

Anderson, D.L., 1989, Where on Earth is the crust, Physics Today, March 1989, p38(9).

Armstrong, R.L., 1981, Radiogenic isotopes: the case for crustal recycling on a near steady state no continental growth earth, in Moorbath, S., and B.F. Windley, eds., 1981, The origin and evolution of the Earth's continental crust, Philosophical Transactions of the Royal Society of London, v301, n461, p183(305).

Arndt, N.T. , and S.L. Goldstein, 1989, An open boundary between lower continental crust and mantle: its role in crust formation and crustal recycling, Tectonophysics, v161, p201(12).

Baker, R.S., G.W. Gee, C. Rosenzweig, and D Hillel, 1994, Soil and water Science: the Key to Understanding Our Global Environment, Soil Science Society of America, Madison, Wisconsin.

Barker, F., J.G. Arth, and T. Hudson, 1981, Tonalites in crustal evolution, in Moorbath, S., and B.F. Windley, eds., 1981, The origin and evolution of the Earth's continental crust, Philosophical Transactions of the Royal Society of London, v301, n461, p183(305).

Barry, R.C., and R.J. Chorley, 1976, Atmosphere, Weather and Climate, Methuen, London.

Barth, T.F.W., 1962, Theoretical Petrology, Wiley, New York.

Bekki, S., R. Toumi, and J.A. Pyle, 1993, Role of sulphur photochemistry in tropical ozone depletion after the eruption of Mount Pinatubo, Nature, v362, n6418, p331(4).

Benard, H., 1900, Review of General Science Pure and Applied, v11, n1261.

Berman, R.G., 1988, Internally consistent thermodynamic data for minerals in the system $Na_2O-K_2O-CaO-MgO-FeO-Fe_2O_3-Al_2O_3-SiO_2-TiO_2-H_2O-CO_2$, Journal of Petrology 29:2:445(78).

Berner, E.K., and R.A. Berner, 1987, The Global Water Cycle, Prentice-Hall, Englewood Cliffs, New Jersey.

Berner, R.A., A.C. Lasaga, and R.M. Garrels, 1983, The carbonate-silicate geochemical and its effect on carbon dioxide over the past 100 million years, American Journal of Science, v283, p641(43).

Berner, R.A., and K. Caldeira, 1997, The need for mass balance and feedback in the geochemical carbon cycle, Geology, v25, n10, p955(2).

Beyers, R.J., and H.T. Odum, 1993, Ecological Microcosms, Springer-Verlag, New York.

Black, P.E., 1996, Watershed Hydrology, Ann Arbor Press, Chelsea, MI.

Boggs, Sam, 1987, Principles of Sedimentology and Stratigraphy, MacMillan, New York.

Bott, M.H.P., 1993, Modeling the plate driving mechanism, Journal of the Geological society, v150, p941(12).

Braat, L.C., and W.F.J. Van Lierop (eds.), 1987, Economic-Ecological Modeling, Elsevier, New York.

Bridges, E.M., 1978, World Soils, Cambridge University Press, Cambridge.

Broecker, W.S., 1991, The great ocean conveyor, Oceanography, v4, n2, p79(11).

Broecker, W.S., and G. Denton, 1990, What drives glacial cycles?, Scientific American v262, n2, p51(3).

Broecker, W.S., and T. Peng, 1982, Tracers in the Sea, Lamont-Doherty Geological Observatory, Palisades, New York.

Brown, G.C., 1981, Space and time in granite plutonism, in Moorbath, S., and B.F. Windley, eds., 1981, The origin and evolution of the Earth's continental crust, Philosophical Transactions of the Royal Society of London, v301, n461, p183(305).

Brown, L.R., 1994, State of the World 1994, Norton, New York.

Budyko, M.I., 1969, The effect of solar radiation variations on the climate of the Earth, Tellus, v21, p611(9).

Bureau of Mines, 1991, 1990 Minerals Yearbook, U.S. Government, Washington, D.C.

Butcher, S.S., R.J. Charlson, G. H. Orians, and G.V. Wolfe (eds.), 1992, Global Biogeochemical Cycles, Academic Press, London.

Campbell, C.J., 1997, Estimates of future oil and gas production, Oil and Gas Journal, Dec 29, 1997, p33(4).

Cartwright, T.J., 1993, Modeling the World in a Spreadsheet, Johns Hopkins University Press, Baltimore.

Cassedy, E.S., and P.Z. Grossman, 1990, Introduction to Energy, Cambridge University Press, Cambridge.

Central Intelligence Agency, International Energy Statistical Review, CIA, Washington, DC.

Chahine, M.T., 1995, Observation of local cloud and moisture feedbacks over high ocean and desert surface temperatures, Journal of Geophysical Research, v100, p8919(6).

Clark, J.G., 1991, The political economy of world energy: a twentieth-century perspective, University of North Carolina Press, Chapel Hill.

Clarke, F.W., 1908, Data of Geochemistry, U.S. Government Printing Office, Washington, D.C.

Cloud, P., 1983, The biosphere, Scientific American, Sept. 1983, v249, p176(12).

Colinvaux, Paul, 1986, Ecology, Wiley, New York.

Condie, K.C., 1973, Bulletin of the Geological Society of America, v84, p2981(12).

Craig, H., 1961, Isotopic variations in meteoric waters, Science, v173, p1702(2).

Culp, A., 1979, Principles of Energy Conversion, McGraw-Hill, New York.

Cummings, D., and Schiller, G.I., 1971, Earth Science Reviews, v7, p97(29).

Davies, G.F., 1979, Earth and Planetary Science Letters, v26, p125(8).

Davies, G.F., 1995, Punctuated tectonic evolution of the Earth, Earth and Planetary Science Letters, v136, p363(17).

Davis, G.R., Energy for Planet Earth, Scientific American, Sept. 1990, p55(8).

Deardorff, J., 1978, Efficient prediction of ground temperature and moisture with inclusion of a layer of vegetation, Journal of Geophysical Research, v83, p1889(14).

Decker, W.L., 1988, The use of statistical climate-cropland models for simulating yield to project the effects of CO2 induced climate change, US Department of Energy, Washington, DC.

Dewey, J.F., and B.F. Windley, 1981, Growth and differentiation of continental crust, in Moorbath, S., and B.F. Windley, eds., 1981, The origin and evolution of the Earth's continental crust, Philosophical Transactions of the Royal Society of London, v301, n461, p183(305).

Dickinson, R.E., 1984, Modeling evapotranspiration for three dimensional global climate models, In J.E. Hansen and T. Takahashi (eds.), Climate Processes and Climate Sensitivity, Geophysical Monograph 29, Maurice Ewing V5, American Geophysical Union, Washington D.C., p58(14).

Dickinson, W.R., 1981, Plate tectonics through geological time, in Moorbath, S., and B.F. Windley, eds., 1981, The origin and evolution of the Earth's continental crust, Philosophical Transactions of the Royal Society of London, v301, n461, p183(305).

Dobrovolsky, V.V.,1994, Biogeochemistry of the World's Land, CRC Press, Boca Raton.

Duncan, Christopher C., and Donald L. Turcotte, 1994, On the breakup and coalescence of continents, Geology, v22, p103(4).

Dunlop, D.J., 1981, Paleomagnetic evidence for Proterozoic continental development, in Moorbath, S., and B.F. Windley, eds.,1981, The origin and evolution of the Earth's continental crust, Philosophical Transactions of the Royal Society of London, v301, n461, p183(305).

Eagleson, P.S. , 1982 (ed.), Land Surface Processes in Atmospheric General Circulation Models, Cambridge University Press, Cambridge.

Energy Information Administration, 1976, World Natural Gas, Supt. of Docs., U.S. G.P.O., Washington, D.C.

Energy Information Administration, 1982-95, Annual Energy Outlook, The Office, Washington, D.C.

Energy Information Administration, 1982-95, Annual Energy Review, The Office, Washington, D.C.

Eyre, S.R., 1963, Vegetation and Soils: a World Picture, Aldine, Chicago.

FAO, 1995, Facts on Agricultural Production, United Nations, New York.

Faure, G., 1986, Principles of Isotope Geology, Wiley, New York.

Fetter, C.W., 1988, Applied Hydrogeology, Merrill, Columbus.

Few, A., 1992, Global Energy Balance Models: The Training Exercise, USRA-ESSE workshop on modeling in the classroom, Boulder, Colorado.

Fisher, D.A., C.H. Hales, and D.L. Filkin, 1990, Model calculations on the relative effects of CFC's and their replacements on stratospheric ozone, Nature, v344, n6266, p508(4).

Forrester, J.W. ,1971, World Dynamics, Wright-Allen Press, Cambridge, Massachusetts.

Francoise, L.M., J.C.G. Walker, and B.N. Opdyke, 1993, The history of global weathering and the chemical evolution of the ocean-atmosphere system, in Evolution of the Earth and Planets, Geophysical Monograph 74, IUGG Volume 14, International Union of Geodesy and Geophysics and the American Geophysical Union.

Friend, 1992, Achieving soil sustainability, Journal of Soil and Water Conservation, v47, p156(2).

Fulkerson, W., 1996, World's energy appetite may crave nuclear power, Forum for Applied Research and Public Policy, Spring 1996, v11, n1, p96(5).

Fulkerson, W., R.R. Judkins, and M.K. Sanghui, 1990, Energy from fossil fuels, Scientific American v263, n3, p128(8).

Garrels, R.M., 1988, Sediment cycling during earth history, in A. Lerman and M. Meybeck, eds., Physical and Chemical Weathering in Geochemical Cycles, Kluwer, Boston.

Garrels, R.M., and F. T. MacKenzie, 1971, Evolution of Sedimentary Rocks, Norton, NY.

Garrels, R.M., F.T. MacKenzie, and C. Hunt, 1975, Chemical Cycles and the Global Environment, William Kaufman, Los Altos, CA.

Gasperini, Marco,1993, Global forces on the lithosphere, Journal of Geodynamics, v17, n3, p121-132.

Geiger, 1965, The Climate Near the Ground, Harvard Press, Cambridge, Mass.

Goldberg, E.D., 1971, Atmospheric transport, in D.W. Hood (ed.), The Impingement of Man on the Oceans, Wiley, New York.

Goldberg, E.D., 1972, Man's role in the major sedimentary cycle, in D. Dyrssen and D Jagner (eds.), The Changing Chemistry of the Oceans, Wiley, New York.

Goldschmidt, V.M., 1933, Grundlagen der quantitaven geochemie, Fontsch. Mineral. Krist. Petrog, v17, p112 (44).

Goldschmidt, V.M., 1937, The principals of chemical distribution of elements in minerals and rocks, Journal of the Chemical Society, p655.

Gordon, C.T., and W.F. Stern, 1982, A description of the GFDL global spectral model, Monthly Weather Review, v110, p625(20).

Green, J.S.A., 1970, Transfer properties of the large scale eddies and the general circulation of the atmosphere, Quarterly Royal Meteorological Society, v90, p157(27).

Gregor, B., 1970, Denudation of the continents, Nature, v228, p273-5.

Gremilion, P.T., 1994, Separation of Streamflow Components in the Econlockhatchee River System Using Stable Isotope Tracers, Ph.D. Dissertation, University of Central Florida, Orlando.

Griffiths, G.A., 1993, Estimation of landform life expectancy, Geology, v21, p403(4).

Gulf Pub. Co., 1947-1994, World oil, Houston, Tex.

Hall, C.A.S., C.J. Cleveland, and R. Kaufman, 1986, Energy and Resource Quality, Wiley, New York.

Hall, R.P., and D.J. Hughes, 1993, Early Precambrian crustal development: changing styles of mafic magmatism, Journal of the Geologic Society v150, p625(11).

Hamilton, W., 1981, Crustal evolution by arc magmatism, in Moorbath, S., and B.F. Windley, eds., 1981, The origin and evolution of the Earth's continental crust, Philosophical Transactions of the Royal Society of London, v301, n461, p183(305).

Hansen, J.D., and A. A. Lacis, 1990, Sun and dust versus greenhouse gases: an assessment of their relative roles in global climate change, Nature v346, p713(9).

Hansen, J.D., J. Rind, I.S. Lebedeff, G. Russell, I. Funf, A. Laics, and S. Ruedy, 1981, Global climate change as forecast by Goddard Institute for Space Studies three-dimensional model, Journal of Geophysical Research, v93, p9341(23).

Hansen, J., G. Russell, D. Rind, P. Stone, A. Lacis, S. Lebedeff, R. Ruedy, and L. Travis, 1983, Efficient three-dimensional global models for climate studies: models I and II, Monthly Weather Review, v111, p609(13).

Hanson, N., 1981, Geochemical constraints on the evolution of the early continental crust, in Moorbath, S., and B.F. Windley, eds., 1981, The origin and evolution of the Earth's continental crust, Philosophical Transactions of the Royal Society of London, v301, n461, p183(305).

Hart, Stanley R., and L. Gulen (eds.), 1989, Crust/Mantle Recycling at Convergence Zones, Kluwer, Boston.

Harwood and Pyle, 1975, A two-dimensional mean circulation model for the atmosphere below 80km, Quarterly Journal of the Royal Meteorological Society, v101, p723

Hays, J.D., J. Imbrie, and N.J. Shackleton, 1976, Variations in the earth's orbit: pacemaker of the ice ages, Science v195, n4270, p1121(11).

Henderson-Sellers, A., 1987, Effects of change in land use on climate in the humid tropics, In R.E. Dickinson (ed.), The Geophysiology of Amazonia, Wiley, New York, p 463(30).

Henderson-Sellers, A., and K. McGuffie, 1987, A Climate Modeling Primer, Wiley, Chichester.

Hoeller, P. and J. Coppel, 1992, Energy Taxation and Price Distortions in Fossil Fuel Markets: Some Implications for Climate Change Policy, Organization for Economic Cooperation and Development, Paris.

Holdren, J., 1990, Energy in transition, Scientific American, Sept. 1990 p157(7).

Holland, H.D., 1978, The chemistry of the atmosphere and oceans, Wiley, New York.

Holland, H.D., 1981, The role of the atmosphere and the hydrosphere in crustal evolution, in Moorbath, S., and B.F. Windley, eds., 1981, The origin and evolution of the Earth's continental crust, Philosophical Transactions of the Royal Society of London, v301, n461, p183(305).

Holland, H.D., B. Lazar, and M. McCaffrey, 1986, Evolution of the atmosphere and oceans, Nature v320, p27(7).

Holling, C.S., 1995, Cross Scale Ecology Lecture Notes, University of Florida, Gainesville.

Holmen, K., 1992, The Global Carbon Cycle, in Butcher, S.S., R.J. Charlson, G. H. Orians, and G.V. Wolfe (eds.), 1992, Global Biogeochemical Cycles, Academic Press, London.

Hubbert, M.L.K., 1972, Energy from fossil fuels, Science v109, p103(6).

Jacobs, G.K. and D.M. Kerrick, 1981, APL and FORTRAN programs for a new equation of state for H_2O, CO_2, and their mixtures at supercritical conditions, Computers and Geosciences v7, p131(13).

Jenny, H., 1980, The Soil Resource: Origin and Behavior, Springer-Verlag, New York.

Johnson, J. W., Oelkers, E. H., and Helgeson, H. C., 1992, SUPCRT92: A software package for calculating the standard molal thermodynamic properties of minerals, gases, aqueous species, and reactions from 1 to 5000 Bar and 0 to 1000 C, Computer & Geosciences, v18, p899(48).

Jordan, T.H., 1981, continents as a chemical boundary layer, in Moorbath, S., and B.F. Windley, eds., 1981, The origin and evolution of the Earth's continental crust, Philosophical Transactions of the Royal Society of London, v301, n461, p183(305).

Karig, D.E., and R.W. Kay, 1981, Fate of sediments on the descending plate at convergent margins, in Moorbath, S., and B.F. Windley, eds., 1981, The origin and evolution of the Earth's continental crust, Philosophical Transactions of the Royal Society of London, v301, n461, p183(305).

Kerrick, D. M., and K. Caldeira, 1996, Metamorphic CO2 degassing and early Cenozoic paleoclimate, GSA Today, v4, n3, p62(3).

Kerrick, D.M., and G.K. Jacobs, 1981, A modified Redlich-Kwong equation for H_2O, CO_2, and H_2O-CO_2 mixtures at elevated pressures and temperatures, American Journal of Science v281, p735(33)

Kiehl, J.T., and K.E. Trenberth, 1997, Earth's Global Mean Energy Budget, Bulletin of the American Meteorological Society, v78, n2, p197(11).

Kleinbach, M.H., and C.E. Salvagin, 1986, Energy Technologies and conversion systems, Prentice-Hall, New Jersey.

Kroner, A., and P.W. Layer, 1992, Crust formation and plate motion in the early Archaean, Science, v256, p1405(7).

Lal, R. J. Kimble, E. Levine, and B.A. Stewart , eds., Soils and Global Change, Lewis, Boca Raton.

Lerman, A., and M. Meybeck, eds., 1988, Physical and Chemical Weathering in Geochemical Cycles, Kluwer, Boston.

Li, Y.H., 1972, Geochemical mass balance among listhosphere, hydrosphere, and atmosphere, American Journal of Science, v272, p119(18).

Loftness, R.L., 1978, Energy Handbook, Van Nostrand, New York.

Lotka, A.J., 1925, Physical Biology, Williams and Wilkins, Baltimore.

Lovelock, J. E., 1979, Gaia, a new look at life on earth, Oxford University Press, New York.

Lowman, P.D. 1989, Comparative planetology and the origin of continental crust, Precambrian Research, v44, p171(25).

MacCracken, M.C., and S. J. Ghan, 1988, Design and use of zonally averaged climate models, in M.E. Schlesinger (ed.), Physically Based Modeling and Simulation of Climate and Climate Change, Kluwer, Boston.

Malley, J.R. 1990, The specification, estimation, and simulation of a small global macroeconomic model, US Department of Agriculture, Washington, DC.

Manabe, S., and K. Bryan, 1985, CO2 induced changes in a coupled ocean-atmosphere model and its palaeoclimatic implications, Journal of Geophysical Research, v90, p1689(18).

Manabe, S., and R.F. Strickler, 1964, Thermal equilibrium of the atmosphere with a convective adjustment, Journal of Atmospheric Science, v21, p361(24).

Manabe, S., and R.T. Wetherald, 1967, Thermal equilibrium of the atmosphere with a given distribution of relative humidity, Journal of Atmospheric Science, v21, p361(24).

Manabe, S., and R.T. Wetherald, 1975, The effect of doubling CO2 concentration on the climate of a GCM, Journal of Atmospheric Science, v32, p3(12).

Marchetti, C., 1977, Primary energy substitution models: on the interaction between energy and society, in D.W. Jorgenson, and J. Waelbroeck, (eds.) Contributions to Economic Analysis, North-Holland, Amsterdam.

Marchetti, C., 1980, Society as a learning system: Discovery, invention, and innovation cycles revisited, Technological Forecasting and Social Change, v18, p267(15).

Marchetti, C., and N. Nakicenovic, 1979, The Dynamics of Energy Systems and the Logistic Substitution Model, RR 79-13, International Institute for Applied Systems Analysis, Laxenburg Austria.

Masters, C.D., and D.H. Root, and E.D. Athanasi, 1990, World Oil and Gas Resources, in Annual Review of Energy 1990, Annual Review Press, Palo Alto, CA.

McBirney, A.R., 1993, Igneous Petrology, Jones and Bartlett, Boston.

McCracken, M.C., and S.J. Gann, 1988, Design and use of zonally averaged climate models, in Schlesinger, M.E. (ed.), Physically Based Modeling and Simulation of Climate and Climatic Change, Kluwer, Boston.

McGovern, P.J., and G. Schubert, 1989, Thermal evolution of the Earth: effects of volatile exchange between atmospher and interior, Earth and Planetary Science Letters, v96, p27(11).

McIntyre, Andrew, Nilva G. Kipp, A.W.H. Be, Thomas Crowley, Thomas Kellogg, James V. Gardner, Warren Prell, and William F. Ruddiman, 1976, Glacial North Atlantic 18,000 Years Ago: a CLIMAP Reconstruction, Geological Society of America Memoir 145, Geological Society of America.

McLennan, S.M., and S.R. Taylor, 1982, Geochemical constraints on the growth of the continental crust, The Journal of Geology, v90, n4, p347(15).

Meadows, D.H., D.L. Meadows, and J. Randers, 1972, The Limits to Growth: a Report for the Club of Rome's Project on the Predicament of Mankind, Universe Books, New York.

Meadows, D.H., D.L. Meadows, and J. Randers, 1992, Beyond the Limits, Chelsea Green, Post Hills, Vermont.

Milankovitch, M.M., 1941, Kanon dez Erdbestrahlung und Seine Anwendung auf das Eiszeitproblem, Belgrade.

Miller, D.H. 1977, Water at the Surface of the Earth, Academic Press New York.

Mintz, Y., 1984, The sensitivity of numerically simulated climates to land surface boundary conditions, In J.T. Houghton (ed.), The Global Climate, Cambridge University Press, Cambridge, p79(27).

Molnar, Peter, 1992, Crust in mantle overdrive, Nature, v358, p105(2).

Monteith, J.L., 1957, Dew, Quarterly Journal of the Royal Meteorological Society, V 83, p 322(20).

Moorbath, S., and B.F. Windley, eds., 1981, The origin and evolution of the Earth's continental crust, Philosophical Transactions of the Royal Society of London, v301, n461, p183(305).

Moores, E.M., 1993, Neoproterozoic oceanic crustal thinning, emergence of continents, and origin of the Phanerozoic ecosystem: a model, Geology, v21, p5(4).

Mudelsee, M., and M. Schultz, 1997, The Mid-Pleistocene climate transition: onset of 100ka cycle lags ice volum build-up by 280 ka, Earth and Planetary Science Letters, v151, p117(7).

Neumann, G., and W.H. Pierson, 1966, Principles of Physical Oceanography, Prentice-Hall, Englewood cliffs, NJ.

Nordhaus, W.D., 1994, Managing the Global Commons: the Economics of Climate Change, MIT Press, Cambridge, Massachusetts.

O'Nions, and P.J. Hamilton, 1981, Isotope and trace element models of crustal evolution, in Moorbath, S., and B.F. Windley, eds., 1981, The origin and evolution of the Earth's continental crust, Philosophical Transactions of the Royal Society of London, v301, n461, p183(305).

Odum, H.T., 1951, The stability of the world's strontium cycle, Science, v114, n2964, p407(4).

Odum, H.T., 1972a, An energy circuit language for ecological and social systems: its physical basis, in B. Patten (ed.), Systems Analysis and Simulation in Ecology, Volume II, Academic Pres, New York.

Odum, H.T., 1972b, Chemical cycles with energy circuit models, in in D. Dyrssen and D Jagner (eds.), The Changing Chemistry of the Oceans, Wiley, New York.

Odum, H.T., 1983, Systems Ecology, Wiley, New York.

Odum, H.T., 1987, Models for national, international, and global systems policy, in Braat, L.C., and W.F.J. Van Lierop (eds.), Economic-Ecological Modeling, Elsevier, New York.

Odum, H.T., 1995, Tropical forest ecosystems and the human economy, in A.E. Lugo and C. Lowe (eds.), Ecological Studies 112, Tropical Forest Management and Ecology, Springer-Verlag, New York.

Odum, H.T., 1996, Environmental Accounting, Wiley, New York.

Organisation for Economic Co-operation and Development, 1971-1987-1985-1988, World energy statistics and balances, Paris.

Organization for Economic Cooperation and Development, 1992, Climate Change: Designing a practical tax system, Organization for Economic Cooperation and Development, Paris.

Osburgh, E.R., 1981, Heat flow and differences in lithospheric thickness, in Moorbath, S., and B.F. Windley, eds., 1981, The origin and evolution of the Earth's continental crust, Philosophical Transactions of the Royal Society of London, v301, n461, p183(305).

Owen, T., R.D. Cess, and V Ramanathan, 1979, Enhanced greenhouse to compensate for reduced solar luminosity on early earth, Nature, v277, p640(1).

Pachauri, R. K.1985 The Political Economy of Global Energy, Johns Hopkins University Press, Baltimore.

Paton, T.R., 1995, Soils: a New Global View, UCL Press, Bristol, PA.

Perfit, M., 1995, Lecture notes, Igneous Petrology, University of Florida, Gainsesville, FL.

Pernetta, J. (ed.), 1995, The Impact of Climate Change on Ecosystems and Species, IUCN, Gland, Switzerland.

Potter, G.L., H.W. ElSaesser, M.C. MacCracken, and F.M. Luther, 1979, Performance of the Lawrence Livermore Laboratory total atmospheric model, In Proceedings GARP J6C Study Conference on Climate Models, Garp Publications Series No. 22.

Ramanathan, V., 1981, The role of ocean-atmosphere interactions in the CO2 climate problem, Journal of Atmospheric Science, v38, p918(13).

Ramanathan, V., B.R. Barkstrom, and E.F. Harrison, 1989, Climate and the Earth's radiation budget, Physics Today, May 1989, p22.

Rankama, K., and T.G. Sahama, 1950, Geochemistry, University of Chicago Press, Chicago.

Raymo, M.E., and W.F. Ruddiman, 1992, Tectonic forcing of late Cenozoic climate, Nature, v359, p117 (8).

Raymo, M.E., W. F. Ruddiman, and Philip N. Froelich, 1988, Influence of late Cenozoic mountain building on ocean geochemical cycles, Geology v16, p649(5).

Raymo, M.E., W.F. Ruddiman, N.J. Shackleton, and D.W. Oppo, 1990, Evolution of Atlantic-Pacific del 13C gradients over the last 2.5 million years., Earth and Planetary Science Letters, v97, p353(16).

Rea, D.K., & Ruff, L.J., 1996, Composition and mass flux of sediment entering the world's subduction zones: Implications for global sediment budgets, great earthquakes, and volcanism, Earth and Planetary Science Letters v140, p1(12).

Reymer, A., and G. Schubert, 1984, Phanerozoic addition rates to the continental crust and crustal growth, Tectonics, v3, n1, p63 (15).

Reymer, A., and G. Schubert, 1986, Rapid growth of some major segments of continental crust, Geology, v14, p299 (4).

Roningen, V., 1992, Documentation of the dynamic world policy simulation model, Department of Agriculture, Washington, DC.

Ronov, A.B., 1982, The Earth's sedimentary shell (quantitative patterns of its structure, compositions, and evolution), International Geology Review, v24, n11, p1313(76).

Ronov, A.B., and A.A. Yaroshevskiy, 1976, A new model of the chemical structure of the Earth's crust, Geokhymia (aka Geochemistry International), n12, p1761(34).

Rubey, W.W., 1951, Geologic history of sea water: an attempt to state the problem, Geological Society of America Bulletin, v62, p 1111 (36).

Russell, A.G. 1990, D. St. Pierre, and J.B. Milford, Ozone control and methanol fuel use, Science, v247, n4939, p201(5).

Ryabchikov, A. 1975, The Changing Face of the Earth, Progress, Moscow.

Sagan, C., and G. Mullen, 1972, Earth and Mars: Evolution of atmospheres and temperatures, Science, v177, p52(4).

Saltzmann, B., and M.Y. Verbitsky, 1993, Multiple instabilities and modes of glacial rhythmicity in the Plio-Plesitocene: a general theory of late Cenozoic climatic change, Climate Cynamics, v9, p1(15).

Sandiford, M., and D. Coblentz, 1994, Plate-scale potential energy distributions and the fragmentation of aging plates, Earth and Planetary Science Letters, v126, p143 (16).

Schlesinger, W.H., 1992, Biogeochemistry: an Analysis of Global Change, Academic, San Diego.

Schlesinger, W.H., 1995, An overview of the carbon cycle, in R. Lal, John Kimble, Elissa Levine, and B.A. Stewart , eds., Soils and Global Change, Lewis Boca Raton.

Schneider, S.H., and R. Londer, 1984, The coevolution of Climate and Life, Sierra Club Books, San Francisco.

Schubert, G., 1991, The lost continents, Nature v354, p358 (2).

Schubert, G., and A.P.S. Reymer, 1985, Continental volume and freeboard through geological time, Nature, v316, p339 (3).

Schwartzman, D.W., and Tyler Volk, 1989, Biotic enhancement of weathering and the habitability of the earth, Nature, v340, p457 (3).

Sclater, J.F., C. Jaupart, and D. Galson, 1980, The heat flow through the oceanic and continental crust and the heat loss of the earth, Reviews of Geophysics and Space Physics, v18, n1, p269(42).

Scott, S.K., 1991, Chemical Chaos, Clarendon, Oxford.

Sellers, A.M., and A.J. Meadows, 1975, Long-term variations in albedo and surface temperatures of the Earth, Nature v254, p44.

Sellers, P.J., Y. Mintz, Y.C. Sud, and A. Dalcher, 1986, A Simple Biosphere (SiB) model for use with general circulation models, Journal of Atmospheric Science, v43, p505(26).

Sellers, W.D., 1969, A global climate model based on the energy balance of the earth-atmosphere system, Journal of Applied Meteorology, v8, p392(8).

Selley, R.C., 1985, Elements of Petroleum Geology, Freeman, New York.

Sergin, B.Ya., 1979, Numerical modeling of the glaciers-ocean-atmosphere global system, Journal of Geophysical Research, v84, p3191(13).

Siever, 1968, Sedimentological conxequences of a steady-state ocean-atmosphere: Sedimentology, v11, p5(25).

Smil, V., 1987, Energy, Food, and Environment, Clarendon, Oxford.

Smith, J.V., 1981, The first 800 million years of Earth's history, in Moorbath, S., and B.F. Windley, eds., 1981, The origin and evolution of the Earth's continental crust, Philosophical Transactions of the Royal Society of London, v301, n461, p183(305).

Solomon, A.H. and H.H. Shugart, 1993, Vegetation Dynamics and Global Change, Chapman and Hall, New York.

Somerville, R.C.J., 1995, Atmospheric physics, Handout, Seminar Series on Global Change, Pasadena CA, August, 1995.

Spohn, T., and Breuer, D, 1993, Mantle differentiation through continental growth and recycling and the thermal evolution of the Earth, in Evolution of the Earth and Planets, Geophysical Monograph 74, IUGG Volume 14, International Union of Geodesy and Geophysics and the American Geophysical Union.

Stallard, R. F., 1988, Weathering and erosion in the humid tropics, in Lerman, A. and M. Meybeck (eds.), Physical and Chemical Weathering in Geochemical Cycles, p225(22), Kluwer, Boston.

Stallard, R.F., and J.M. Edmond, 1983, Geochemistry of the Amazon 2. The influence of geology and weathering environment on the dissolved load, Journal of Geophysical research, v88, n14, p9671(17).

Staudigel, H., R.a. Chastain, A. Mayans, and W. Bouncier, 1995, Biologically mediated dissolution of glass, Chemical Geology, v126, p147 (7).

Stouffer, R.J. , S. Manabe, and K. Bryan, 1989, Interhemispheric asymmetry in climate response to a gradual increase in atmospheric CO_2, Nature v342, p660(2).

Tarney, J. and B.F. Windley, 1981, Marginal basins through geological time, in Moorbath, S., and B.F. Windley, eds., 1981, The origin and evolution of the Earth's continental crust, Philosophical Transactions of the Royal Society of London, v301, n461, p183(305).

Taylor, R.S., and S.M. McLennan, 1981, The composition and evolution of the continental crust: rare earth element evidence form sedimentary rocks, in Moorbath, S., and B.F. Windley, eds., 1981, The origin and evolution of the Earth's continental crust, Philosophical Transactions of the Royal Society of London, v301, n461, p183(305).

Taylor, S.R., and S. M. McLennan, 1985, The Continental Crust: its Composition and Evolution, Blackwell Scientific, Oxford.

Taylor, S.R., and S. M. McLennan, 1996, The evolution of the continental crust, Scientific American, January 1996.

Thorpe, R.S., P.W. Francis, and R.S. Harmon, Andean andesites and crustal growth, in Moorbath, S., and B.F. Windley, eds., 1981, The origin and evolution of the Earth's continental crust, Philosophical Transactions of the Royal Society of London, v301, n461, p183(305).

Thorseth, I.H., T. Torsvik, H. Furnes, and K. Muehlenbachs, 1995, Microbes play an important role in the alteration of oceanic crust, Chemical Geology v126, p137(10).

Trenberth, K.E., 1992, Climate System Modeling, Cambridge University Press, Cambridge, Massachusetts.

Turekian, K.K., 1968, Oceans: Foundations of Earth Science Series, Prentice-Hall, Englewood Cliffs, New Jersey.

United Nations, 1948, Statistical Yearbook, United Nations, New York.

United Nations, 1975, World Energy Supplies 1950-1974, United Nations, New York.

United Nations, 1993, World Statistics, 1993, United Nations, New York.

United Nations, 1994, World Statistics, United Nations, New York.

United Nations, Energy Statistics Yearbook 19xx, United Nations, New York.

Veissman, W., 1989, G.L. Lewis, and J.W. Knapp, Introduction to Hydrology, Harper and Row, New York.

Veizer, J., and S.L. Jansen, 1979, Basement and sedimentary recycling and continental evolution, Journal of Geology, v87, n4, p341(30).

Veizer, J., and S.L. Jansen, 1985, Basement and sedimentary recycling-2:time dimension to global tectonics, Journal of Geology, v93, n6, p625(23).

Veizer, J.M., 1988a, The Earth and its life: systems perspective, Origins of Life and Evolution of the Biosphere v18, p13 (26).

Veizer, J.M., 1988b, The evolving exogenic cycle, in Gregor, C. Bryan, Robert M. Garrels, Fred T. MacKenzie, and J. Barry Maynard, Chemical Cycles in the Evolution of the Earth, Wiley, New York.

Veizer, J.M., Jochen Hoefs, D.R. Low, and P.C. Thurston, 1989a, Geochemistry of Precambrian carbonates: II. Archaean greenstone belts and Archaean sea water., Geochimica et Cosmochimica Acta, v53, p859(12).

Veizer, J.M., P. Laznicka, and S.L. Jansen, 1989b, Mineralization through geologic time, American Journal of Science v289, p484(41).

Von Bertalanffy, L., 1968, General Systems Theory, Brazillier, New York.

Walker, J., and J.F. Kasting, 1992, Effects of fuel and forest conservation on future levels of atmospheric CO_2, Global and Planetary Change, v5, n3, p15(38).

Walker, J.C.G., P.B. Hays, and J.F. Kasting, 1981, A negative feedback mechanism for the long term stabilization of the earth's surface temperature, Journal of Geophysical Research, v86, p9776(6).

Wallace, J.M., and P.V. Hobbs, 1977, Atmospheric Science, an Introductory Survey, Academic, New York.

Washington, W.M., and G.A. Meehl, 1989, Climate sensitivity due to increased CO_2 experiments with a coupled atmosphere and ocean general circulation model, Climate Dynamics v4, p1(38).

Watson, A.J., and J.E. Lovelock, 1983, Biological homeostasis of the global environment: the parable of Daisyworld, Tellus v35B, p284(6).

Webster, P.J., 1994, The role of hydrological processes in ocean-atmosphere interactions, Reviews of Geophysics, v32, n4, p427(49).

Wells, P.R.A., 1981, Accretion of continental crust: thermal and geochemical consequences, in Moorbath, S., and B.F. Windley, eds., 1981, The origin and evolution of the Earth's continental crust, Philosophical Transactions of the Royal Society of London, v301, n461, p183(305).

Yakir, D. and X.F. Wang. 1996. Fluxes of CO_2 and water between terrestrial vegetation and the atmosphere estimated from isotope measurements. Nature, v380, p515(3).

Zhang, Y., and A. Zindler, 1993, Distribution and evolution of carbon and nitrogen in earth, Earth and Planetary Science Letters, v117, p331(14).

Ziegler, A.M., S.F. Barrett, and C.R. Scotese, 1981, Paleoclimate, sedimentation and continental accretion, in Moorbath, S., and B.F. Windley, eds., 1981, The origin and evolution of the Earth's continental crust, Philosophical Transactions of the Royal Society of London, v301, n461, p183(305).

BIOGRAPHICAL SKETCH

Guy McGrane was raised in Daytona Beach, Florida, and graduated from Father Lopez high school in 1981. He attended Florida State University and the University of Florida, from which he obtained the bachelor's degree in electrical engineering in 1986. He then worked in the electric power industry for six years, specializing in design of power transmission facilities, both underground and overhead.

In 1992, he pursued graduate study in environmental engineering, again at the University of Florida, where he evaluated personal transportation alternatives as part of a contract with the Florida Department of Transportation, and he obtained the master's degree in 1994. He subsequently worked at the Center for Environmental Policy as a graduate research assistant, and continued studies in systems ecology with an emphasis on Earth systems. In May, 1998, he obtained the doctoral degree in environmental engineering sciences, with a minor in geology.

I certify that I have read this study and that in my opinion it conforms to acceptable standards of scholarly presentation and is fully adequate, in scope and quality, as a dissertation for the degree of Doctor of Philosophy.

Howard T. Odum, Chair
Graduate Research Professor
Emeritus of Environmental
Engineering Sciences

I certify that I have read this study and that in my opinion it conforms to acceptable standards of scholarly presentation and is fully adequate, in scope and quality, as a dissertation for the degree of Doctor of Philosophy.
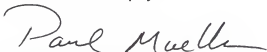
Paul A. Mueller, Cochair
Professor of Geology

I certify that I have read this study and that in my opinion it conforms to acceptable standards of scholarly presentation and is fully adequate, in scope and quality, as a dissertation for the degree of Doctor of Philosophy.

Clay L. Montague
Associate Professor of
Environmental Engineering
Sciences

I certify that I have read this study and that in my opinion it conforms to acceptable standards of scholarly presentation and is fully adequate, in scope and quality, as a dissertation for the degree of Doctor of Philosophy.

Ellen E. Martin
Assistant Professor of Geology

I certify that I have read this study and that in my opinion it conforms to acceptable standards of scholarly presentation and is fully adequate, in scope and quality, as a dissertation for the degree of Doctor of Philosophy.

Michael W. Binford
Associate Professor of
Geography

This dissertation was submitted to the Graduate Faculty of the College of Engineering, to the College of Liberal Arts and Sciences, and to the Graduate School and was accepted as partial fulfillment of the requirements for the degree of Doctor of Philosophy.

May, 1998
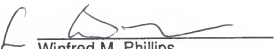
Winfred M. Phillips
Dean, College of Engineering

Karen A. Holbrook
Dean, Graduate School